Construction and characterizations of new perylenediimide based molecular assemblies derived from nitro or amino bay-substituted derivatives

Rayane El Berjawi

UNIVERSITE MATIERE BRETAGNE MOLECULES LOIRE ET MATERIAUX

université angers

THESE DE DOCTORAT

DE L'UNIVERSITE D'ANGERS
COMUE UNIVERSITE BRETAGNE LOIRE

ECOLE DOCTORALE N° 596
Matière, Molécules, Matériaux
Spécialité : Chimie Moléculaire et Matériaux

Rayane EL BERJAWI

Construction and characterizations of new perylenediimide based molecular assemblies derived from nitro or amino bay-substituted derivatives

Thèse présentée et soutenue à Angers, le 22 Novembre 2019
Unité de recherche : Laboratoire MOLTECH-Anjou - CNRS UMR 6200
Thèse N° :

Composition du Jury :

Rapporteurs :	**Isabelle Chataigner**, Professeure des Universités, Université de Rouen Normandie
	Nicolas Leclerc, Chargé de Recherche, ICPEES-ECPM Strasbourg
Examinateurs :	**Françoise Le Guen**, Professeure des Universités, Université de Rennes 1
	Stéphanie Lhez, Maître de Conférences, Université de Limoges
	Pierre Frère, Professeur des Universités, Université d'Angers
Directeur de Thèse :	**Piétrick Hudhomme**, Professeur des Universités, Université d'Angers

‘’We are limited by our thoughts, not our feelings’’

“Smoking oxygen’’

‘’Feel my words and let them land safely, if I am to speak to a wall, I’d rather do scarcely.’’

When I write, Rayane EL BERJAWI

‘’Anyone who believes that a second is faster than a decade did not live my life.’’

Extremely loud & incredibly close, Jonathan S. FOER

‘’Flee, my friend, into your solitude - and there, where a rough strong breeze blows. It is not your lot to shoo flies.”

Thus spoke Zarathustra, Friedrich NIETZSCHE

ACKNOWLEDGEMENTS

To **M**arc **S**allé, for welcoming me to the laboratory of MOLTECH-Anjou during these three years, thank you!

To **I**sabelle **C**hataigner and **N**icolas **L**eclerc for agreeing to be the reviewers of this thesis and also to **P**ierre **F**rère**, F**rançoise **L**e **G**uen and **S**téphane **L**hez for accepting to be the examiners, thank you!

To **P**hilippe **B**lanchard and **Y**ann **P**ellegrin for being members of my thesis supervision committee, thank you!

To **E**ric **L**evillain and **O**livier **A**leveque, for the discussions on electrochemistry, thank you!

To **S**onia **J**erjir and **I**ngrid **F**reuze, for mass spectrometry analysis, thank you!

To **S**ébastien **G**oeb, for your helpful advices on UV-vis spectroscopy, thank you!

To **J**érémie **G**rolleau, the 'coffee-wake-up call', thank you!

To **C**lément **D**rou, good luck with your remaining thesis years! And thank you!

To **P**hilippe **B**lanchard that was always there when I needed, thank you!

To my friend, **T**homas **C**hoisnet, to whom I wish but happiness, thank you!

To the great supervisor that invited me to his lab in Canada, **G**regory **W**elch, simply and impossibly, thank you! And, to the chemists, **E**di **C**ieplechowicz, **T**om **W**elsh, **A**udrey **L**aventure and **F**rancesco **T**intori, thank you!

To my sense of relief, **D**avid **C**anevet, Thank you!

To my friend, **A**ntoine **B**usseau, I've been blessed having you there! Thank you!

To my sanity and strength,

إلى أمي، دائماً وأبداً

Lina

Table of Contents

List of Abbreviations

A (Acceptor)

AFM (Atomic force microscopy)

Ar (Aromatic)

BHJ (Bulk heterojunction)

CAN (Cerium (IV) ammonium nitrate)

CV (Cyclic voltammetry)

D (Donor)

D/A (Donor/Acceptor)

d (Doublet)

dd (Doublet of doublets)

DFT (Density functional theory)

DME (Dimethoxyethane)

DMF (Dimethylformamide)

DMSO (Dimethyl sulfoxide)

DSC (Differential Scanning Calorimetry)

ET (Energy transfer)

FF (Fill Factor)

FQY (Fluorescence Quantum Yield)

HOMO (Highest Occupied Molecular Orbital)

HPLC (High-Performance Liquid Chromatography)

HRMS (High Resolution-Mass Spectrometry)

ICT (Intramolecular Charge Transfer)

ITO (Indium-tin-oxide)

J$_{SC}$ (Short-Circuit Current)

LUMO (Lowest Unoccupied Molecular Orbital)

M (Molarité in mol.L^{-1})

m (multiplet)

MALDI-TOF (MS) (Matrix-assisted laser desorption/ionization - time-of-flight mass spectrometer)

***m*-NBA** (3-nitrobenzyl alcohol)

NFA (Non Fullerene Acceptor)

NIR (Near Infrared Region)

NMP (1-methyl-2-pyrrolidinone)

NMR (Nuclear magnetic resonance)

ODCB (*ortho*-Dichlorobenzene)

OFET (Organic Field-Effect Transistor)

OLED (Organic light-emitting diode)

OPV (Organic photovoltaic)

OSC (Organic solar cell)

PCE (Power conversion efficiency)

PCET (Proton coupled electron transfer)

PDC (Pyridinium dichromate)

PEDOT:PSS (Poly(3,4-ethylenedioxythiophene):poly(styrenesulfonate)

PDI (Perylenediimide)

PDT (Photodynamic therapy)

PL (Photoluminescence)

PTCDA (Perylene tetracarboxylic dianhydride)

PV (Photovoltaic)

s (singlet)

SMC (Suzuki–Miyaura coupling)

t (Triplet)

TBABr (Tetra-n-butylammonium bromide)

TBAF (Tetra-n-butylammonium fluoride)

TFA (Trifluoroacetic acid)

TGA (Thermogravimetric analysis*)*

THF (Tetrahydrofuran)

TLC (Thin layer chromatography)

TM (Transition metal)

UV/Vis (Ultraviolet/Visible)

$\mathbf{V_{oc}}$ (Open Circuit Voltage)

General Introduction

*P*erylene-3,4,9,10-tetracarboxylic acid di(*bis*)imide derivatives, usually named perylenediimides (PDIs) or perylene*bis*imides (PBIs), have been extensively studied as industrial colorants, both as dyes (soluble) and pigments (insoluble).[1] Since the first member of the family was discovered in 1913,[2] PDIs are today one of the most important heterocyclic pigments.[3] Moreover, the combination of a large aromatic perylene core and strong electron-withdrawing carbonyl groups on the *peri* positions allows PDIs to form stable radical anions, making them well suited as precursors for electron transport materials.[4] Hence, they find applications as n-type materials in organic field-effect transistors (OFETs),[5–9] organic light-emitting diodes (OLEDs), [10–12] organic photovoltaic cells (OPVs),[9,13,14] dye sensitizers in solar cells,[15,16] and quantum dots.[17] This wide range of applications is also due to their unique combination of optical and redox properties, high extinction coefficients, high fluorescence quantum yields (FQYs), strong light absorption in the visible region between 400 nm and 650 nm, low lying LUMO levels, high electron mobilities, as well as outstanding chemical, thermal, and photochemical stability in organic solvents.[18,19]

Since this thesis focuses on studying the reactivity of PDIs at the *bay* region and developing their chemistry, reaching different original assemblies, some of them are presented with their applications in organic solar cells (OSCs), a review of mono and bis *bay* region functionalization of PDI derivatives and their applications in OPV is presented in the first chapter.

The development of new reactivity in the PDI series through the *bay*-substituted mono and dinitro PDI for the synthesis and characterization of new target PDI derivatives is presented in the second chapter.

The application of PDIs used as powerful acceptors in solar cells will be presented in the third chapter. The effect of side chain substituents on self-assembly of PDI dimers and their solar cell performance are investigated.

In the last chapter, the use of mono-amino PDI as starting building block is described, for the synthesis and characterization of the target PDI derivatives. In addition to an initial study of some of these acceptors obtained in organic solar cells.

Chapter I: State of the art- '*Bay'* region functionalization of perylenediimides

The functionalization of PDI (Figure I-1) through organic synthesis can first occur upon introducing different substituents at the imide N,N'-positions. However, this chemistry has no significant impact over the geometrical features of the core and do not allow tuning the optical and electronic properties. This phenomenon results from the nodes present in the HOMO and LUMO orbitals at the imide nitrogen atom, which explains the moderate effect on the frontier orbitals.

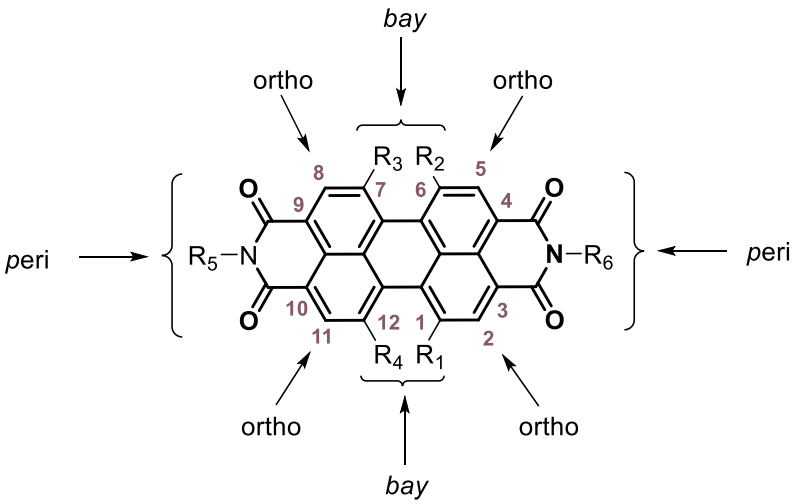

Figure I-1 General structure of perylenediimides.

Secondly, synthetic procedures related to the substitution at the 2,5,8,11 positions (*ortho* region) have been available only until the last decade.[20,21,3] Introduction of alkyl groups at these positions significantly enhances their solid-state emission as well as their solubility in organic solvents without causing any serious distortion of the PDI core.

Finally, PDIs can be conveniently modified through substitution in the aromatic core at the positions 1, 6, 7, 12 (*bay* region) via halogenation and successive straightforward nucleophilic substitution[22–24] or coupling reaction[25]. Introducing substituents on the bay region of PDIs allows the rational fine tuning of their solubility, HOMO-LUMO levels, as well as their optoelectronic and self-assembling properties.[1,26] Indeed, such functionalization leads to non-planar PDI derivatives, which form weaker aggregates and hence, display higher solubilities.

I.1 Symmetrical imidization of perylenetetracarboxylic dianhydride (PTCDA)

Introduction of different substituents at the imide N,N'-positions of PDIs to control solubility in organic solvents, using a bulky alkyl or aryl substituent, or in water, by the introduction of carboxylates or quaternary ammonium cations via ionic bond formation are reported. Table I-1 shows some R amine groups that are introduced to PTCDA via symmetrical imidization reactions reported till day. The synthesis starts with the commercially available PTCDA (Figure I-2), which is commonly considered as the parent compound of this class of dyes, described first in 1912,[27] and its condensation with the corresponding amine. General reaction scheme is shown in Figure I-3.

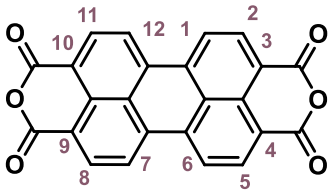

Figure I-2 Chemical structure of PTCDA.

I.1.1 Controlling PDI solubility in organic solvents

PDIs possessing the R amine groups **1-29** were synthesized according to the described procedure of S. Demmig and H. Langhals, [28–30] by heating the anhydride and a primary amine in molten imidazole with a Lewis acid catalyst. They noted that long-chain alkyl groups do not increase, but diminish solubility.

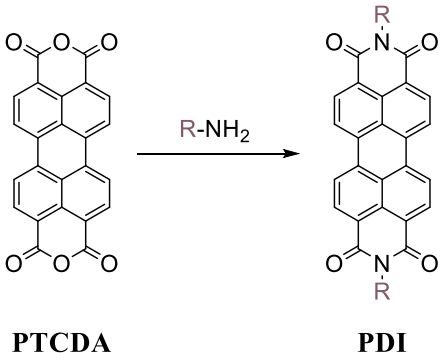

Figure I-3 Conversion of PTCDA to PDI.

Cycloalkyl substituents give a minimum of solubility with medium sized rings and a maximum with the cyclotetradecyl derivative **16**. Very high solubility in organic solvents is attained by substitution with secondary alkyl residues having two long chains.[28] V. Percec *et al*. reported the reaction of PTCDA with two equivalents of 1-ethylpropylamine **30** in pyridine in the presence of $Zn(OAc)_2$ that produced the symmetrical PDI in 55% yield.[31]

Table I-1 R amine groups that are introduced to PTCDA through imidization reaction.

1: n-Hexyl	2: Dodecyl	3: Octadecyl	4: Allyl	5: Cyclopropyl
6: Cyclobutyl	7: Cyclopentyl	8: Cyclohexyl	9: Cycloheptyl	10: Cyclooctyl
11: Cyclononyl	12: Cyclodecyl	13: Cycloundecyl	14: Cyclododecyl	15: Cyclotridecyl
16: Cyclotetradecyl	17: Cyclopentadecyl	18: 1-Ethylpropyl	19: 1-Propylbutyl	20: 1-Butylpentyl
21: 1-Pentylhexyl	22: 1-Hexylheptyl	23: Heptyl	24: Dodecyl	25: Octadecyl
26: 1-Isobutyl-3-methylbutyl	27: 1-Butylhexyl	28: Tert-butyl-1,3,4-thiadiazole-2-yl	29: 3-(N,N-dibutyl)propyl	30: 1-Ethylpropyl
31: n-Butyl	32: 2-Ethyl-hexyl	33: 2-Decyl-tetradecyl	34: Nonadecyl	35: 1,8-Nonadien-5-yl
36: 1,12-Tridecadien-7-yl	37: 3,4,5-Tridodecyloxyl	38: Aminotricosanyl	39: Nonyldecyl	40: 1-Undecyldodecyl
41: 1-Pentylbutyl	42: 1-Hexylpentyl	43: Pentyl	44: 2,4,6-Triphenyl	45: 4-Tritylphenyl
46: aminoethyl	47: Heptafluorobutyl	48: Pentafluorophenyl	49: Nonafluoropentyl	50: Pentafluorophenylethyl

Condensation of PTCDA and the corresponding amines in quinoline and zinc acetate as a Lewis acid catalyst gave PDIs with the imide substituents **31-37**.[32–37] In 2007, M. J. Ahrens *et al.* reported the condensation reaction between PTCDA and 12-aminotricosane **38** to give the bis substituted PDI, without the use of a Lewis acid as described before, where both starting materials were heated in imidazole at 180°C.[38] Following the same procedure, symmetrical PDIs with imide group **1**, **24**, **25**, **32**, **39**, **40**, **41**, **42 and 43** were also synthesized.[39–45] Other procedures for introducing 2-ethylhexylamine, **32**, onto PTCDA included refluxing both compounds only in DMF or in N,N-dimethylacetamide (DMAC) and $Zn(OAc)_2$ to give the

yields 97% and 93% respectively.[46,47] Also, **1** and **24** were introduced to the PTCDA with a fivefold excess of the corresponding primary amine in refluxing DMF with 92% and 95% yield respectively, in addition to **25** and **43** with 100% yield for each .[48,49]

The selection of the solvent is based on several experiments consisting in dispersing PTCDA in sulfolane, water, THF and even neat conditions (no solvent). DMF is the only medium that gives sufficiently high yields and reproducible results for the amines studied by F. Rigodanza *et al,* noting that the imidization using DMF as solvent was firstly studied by Y. Nagao *et al* in 1996.[50,51]

Condensation of an aliphatic or aromatic amine is also reported to be carried out with core substituted PTCDAs such as of 1,7-dibromoperylene tetracarboxylic acid anhydride and 1,6,7,12-tetrachloroperylene dianhydride in refluxing propionic acid, each imidized respectively with the R amine groups **25**-**43**,[35,49] general reaction scheme is depicted in Figure I-4. It is noteworthy that H. Langhals, R Ismael and O. Yuruk tried to prepare symmetrical PDIs with the R groups **44** and **45** in imidazole. They succeeded only in preparing PDI with **45** without **44**, even in the presence of zinc acetate dihydrate, since the bulky 4-aminotetraphenylmethane is less shielded at the amino group than 2,4,6-triphenylaniline and hence can be condensed with PTCDA successfully.[52]

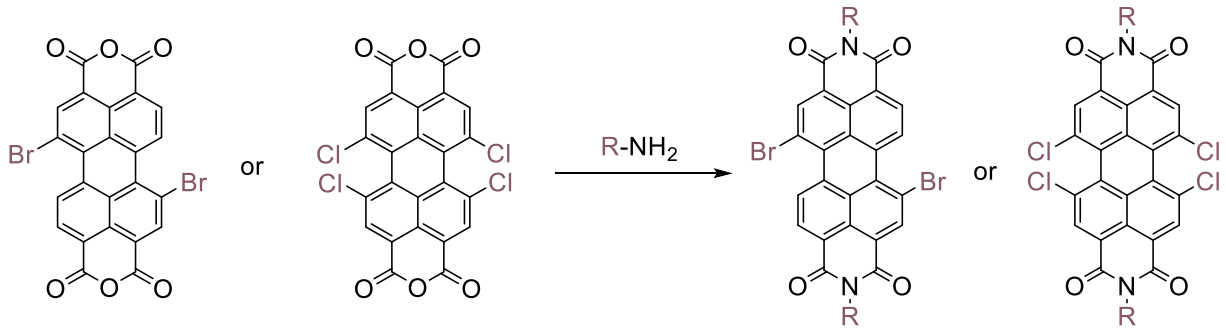

Figure I-4 Conversion of 1,7-dibromo substituted PTCDA or 1,6,7,12-tetrachloro substituted PTCDA to 1,7-dibromo or 1,6,7,12-tetrachloro perylene diimides.

Another method for symmetrical PDI synthesis is treating PTCDA with reactive amines in hot mixture of alcohol (such as propanol) and water, as in the case with n-butylamine **31**.[53] In addition, the respective *o*-phenylenediamine derivatives could be isolated in good to excellent yields. Generally, a mixture of two regioisomers can be obtained in the synthesis of benzoimidazole derivatives and the separation of the isomers is challenging.[54] Besides

alcohols, catalytic amounts of acetic acid could also be employed in imidization reaction, using 1-methyl-2-pyrrolidinone (NMP) as solvent, as with **47** and **48**. [5,59]

Introduction of other fluorinated amines into the PTCDA is also possible, however, their low reactivity and the poor solubility of monoimidized intermediate products, afforded in some cases low yields, as with nonafluoropentylamine **49**, and pentafluorophenylethylamine **50**, as described by R.Schmidt *et al*.[5]

Little is known about PTCDA with tertiary substituents where synthesis by the condensation of *tert*-alkylamines proved to be difficult, because standard syntheses with dilute solutions in quinoline or imidazole were not successful, as reported by H. Langhals *et al*.[55] Moreover, the condensation of PTCDA with aromatic amines and amino acids requires long reaction times, up to 48 hours at reflux in non-common solvents, such as quinoline and imidazole, while it gives quantitative yields with aliphatic amines and need a simpler work-up to remove the excess of amines.[50]

I.2 Introducing various substituents on the *bay* region of PDI

I.2.1 Mono-substitution of PDI on the bay region

I.2.1.1 C-Br bond formation

I.2.1.1.1 Bromination

In 2007, P. Rajasingh *et al*.[56] reported the first PDI bromination methodology that employs mild conditions (organic solvent, room temperature) resulting in facile formation of mono- and dibrominated PDIs. Bromination was applied on three different known PDI derivatives, bearing 2,4-dimethylpent-3-yl, ethylpropyl, and cyclohexyl substituents respectively. Each of the three derivatives was stirred with excess of bromine in CH_2Cl_2 as shown in Figure I-5. Mono-brominated PDIs **I-1a** and **I-1b** were isolated in 57% and 50% yield respectively. However, no evidence was shown for mono-brominated PDI **I-1c** bearing cyclohexyl imide substituent where the corresponding reaction gave exclusively the dibromoPDI derivative. Using the same procedure described before, compound **I-1d** was also obtained, however the solvent used was $CHCl_3$ instead of CH_2Cl_2,[57] or concentrated sulfuric acid, which is the case for **I-1e** and **I-1f** with the corresponding yields 75% and 71% respectively.[58,59] A large excess of bromine and the presence of potassium carbonate were required to prepare the mono-brominated PDI **I-1g**, **I-1h** and **I-1i** with 86% yield.[60] Clearly this strategy of PDI bromination suffers from a lack of

selectivity and the necessity of fastidious column chromatography for separating mono from dibrominated compounds.

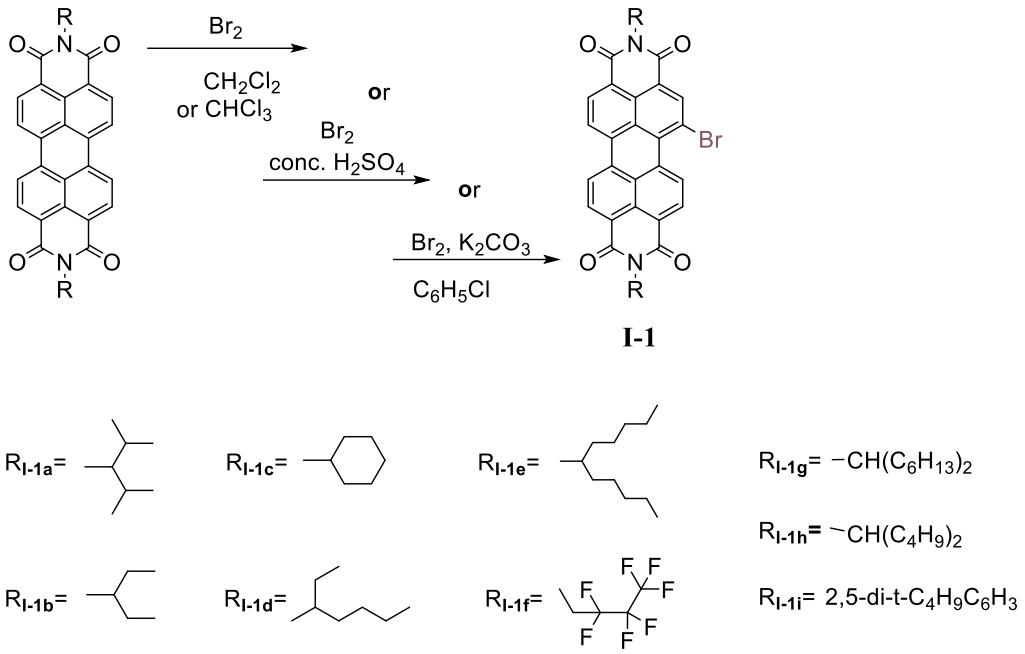

Figure I-5 Different synthetic pathways for the monobromination of PDIs bearing different imide substituents.

I.2.1.2 C-N bond formation

I.2.1.2.1 Nitration

The introduction of strong electron-withdrawing nitro groups on PDIs was first studied by K. Chen and T.J Chow (Figure I-6).[61]

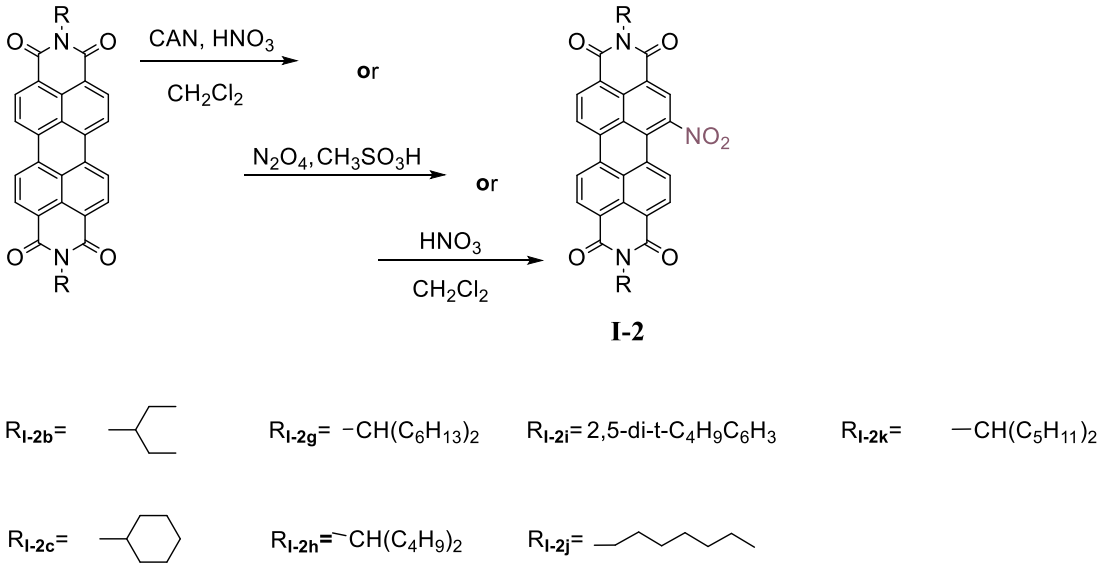

Figure I-6 Different synthetic pathways for the mononitration of PDIs bearing different imide substituents.

The mononitration can be achieved in high yields ca. 90% (**I-2c** and **I-2j**) by a reaction of unsubstituted PDIs, bearing either cyclohexyl or octyl imide substituents, using cerium (IV) ammonium nitrate (CAN) and HNO_3 (with or without H_2SO_4) in CH_2Cl_2 under ambient temperature, or at 0°C for **I-2k**.[62,63] Compared to the difficulties of controlling the monobromination reaction of PDI core, the introduction of an electron-withdrawing group such as the nitro group can proceed with excellent selectivity to form the mono-nitro PDI, in agreement with Holleman rules for electrophilic aromatic substitution. Nevertheless, the reaction time plays an important role[64,65] as both mono- and di-substituted nitroPDIs could be obtained. Hence, it must be well controlled to obtain selectively the desired mono-nitro PDI. Another mono nitration procedure proceeds with excess of N_2O_4 in CH_2Cl_2, where the addition of a catalytic amount of methanesulfonic acid further increases the yield of mono-nitro PDIs **I-2g-i** to 90%, 98% and 93% respectively.[60]

According to P. Singh *et al.* nitration of PDI bearing cyclohexyl substituent could only take 10 min instead of 2h,[65] where PDI was treated with ceric ammonium nitrate (CAN) followed by immediate addition of H_2SO_4–HNO_3 mixture at room temperature to give **I-2c**.[66] The synthesis of mono-nitro PDI can also be led without the use of CAN .This electrophilic aromatic nitration of the PDI core in CH_2Cl_2 with excess of nitric acid at room temperature gave the desired products **I-2b** and **I-2c** in 96% and 93% yields, respectively.[45,67]

I.2.1.2.2 Reduction of nitro-group

In 2011, K. Chen *et al*. reported the conversion of the nitro group to the corresponding amino group by using tin (II) chloride dihydrate ($SnCl_2.2H_2O$) in refluxing THF. This procedure yielded the corresponding mono-amino PDIs **I-3c**, **I-3j** and **I-3m** in 80% yield (Figure I-7). The products obtained were purified by chromatography using silica gel.[68]

Mono-amino PDIs **I-3c** and **I-3l** were obtained by the employment of zinc dust with acetic acid in THF at room temperature, where no further purification of the products by chromatography was indicated.[64,66,69] Another procedure used to prepare amino-PDI **I-3c** consists of introducing palladium on activated charcoal into a sealed reaction system containing hydrogen gas.[70]

Despite the fact that K. Chen *et al*. reported the purification of the amino-PDI by chromatography using silica gel, some reports that were published later,[70,71] mentioned the use of the crude product obtained from the reduction reaction directly in the next step reaction,

without any further purification. The purification of the amino-PDI was displayed unresolved, regardless of the R groups added at the imide positions.

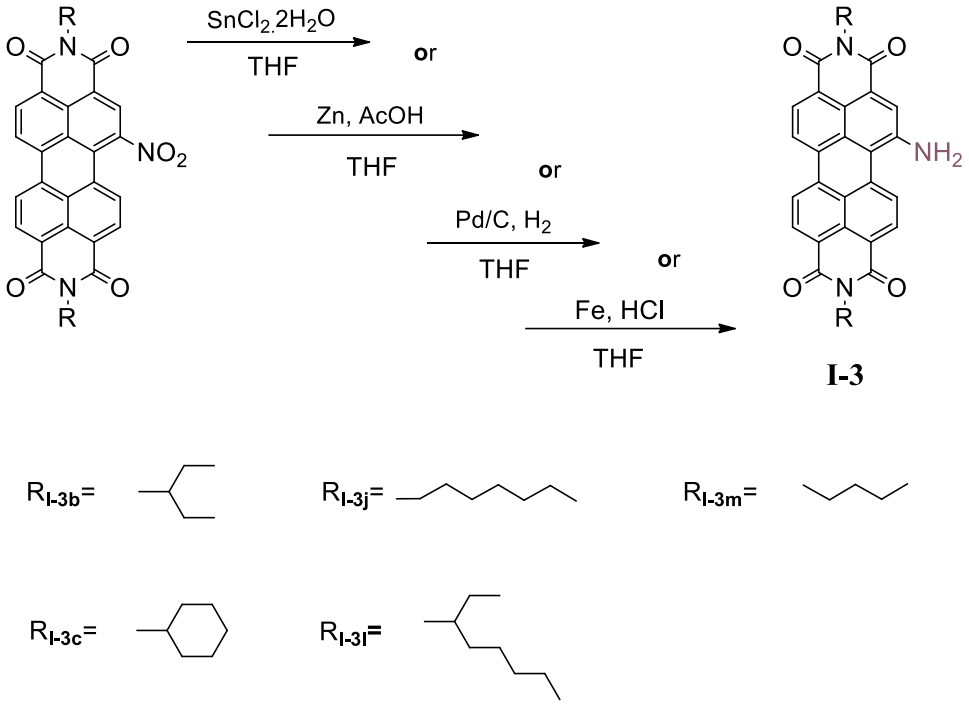

Figure I-7 Different synthetic pathways for the reduction of mono-nitro PDIs bearing different imide substituents.

The reason for this was reported as the 'instability of the amino-PDI in air'. Recently, C. Domínguez *et al*. reported the reaction of mono-nitro PDI with metallic iron in acidic medium at 65°C, to produce the desired product **I-3b** in 70% yield, where the product was purified by chromatography using alumina.[72]

I.2.1.2.3 Nucleophilic displacement reactions

It was reported by M. Franceschin *et al*. that partial dehalogenation of the dibromoPDI occurred during its reaction with excess of 3-dimethylamino-1-propylamine at 110°C, yielding 14% of **I-4n** as a by-product (Figure I-8).[73] The product of dehalogenation increased with temperature and it was suggested that this reaction may involve a free radical mechanism. V. Casagrande *et al*.[74] also discovered that the presence of an increasing number of amine groups had an influence on reaction yields, favoring the dehalogenation side reactions.

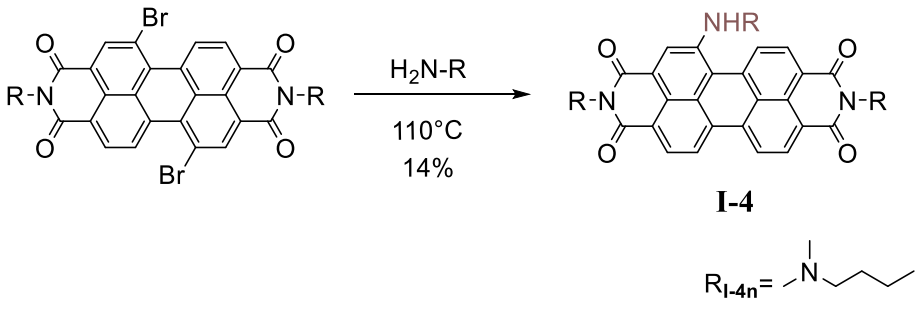

Figure I-8 Nucleophilic substitution on the bay region of PDI.

For example, treatment of dibromo PDI with excess of piperidine at 95°C gave three products, one of which being **I-5o** as shown in Figure I-9.

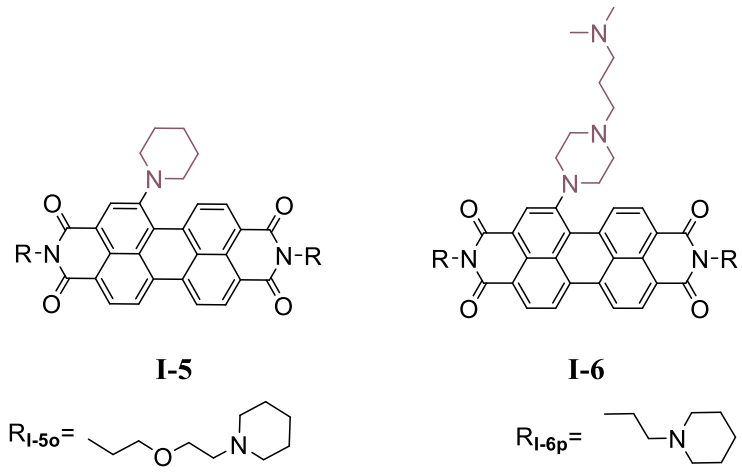

Figure I-9 Nucleophilic substitution on the bay region of PDI.

Compound **I-5o** could also be obtained from the nucleophilic substitution of mono-bromo PDIs with piperidine.[22,56] Importantly, treatment of PDI with an excess of 1-(3-dimethylaminopropyl) piperazine in anhydrous dioxane as solvent, enabled the reaction to take place at a higher temperature, giving only the mono-substituted derivative, **I-6p**.

Side reactions also occurred, giving both the mono and the di-substituted PDI when the same reaction was performed at room temperature. This result is distinct from what was observed in all other reported cases. C. Huang et al.[75] reported the nucleophilic displacement of the bromo substituent on the PDI *bay* position with 2-(piperazin-1-yl)ethanol in NMP, giving PDI derivative **I-7q** (Figure I-10). Importantly, this product could be further functionalized at the hydroxyl group.

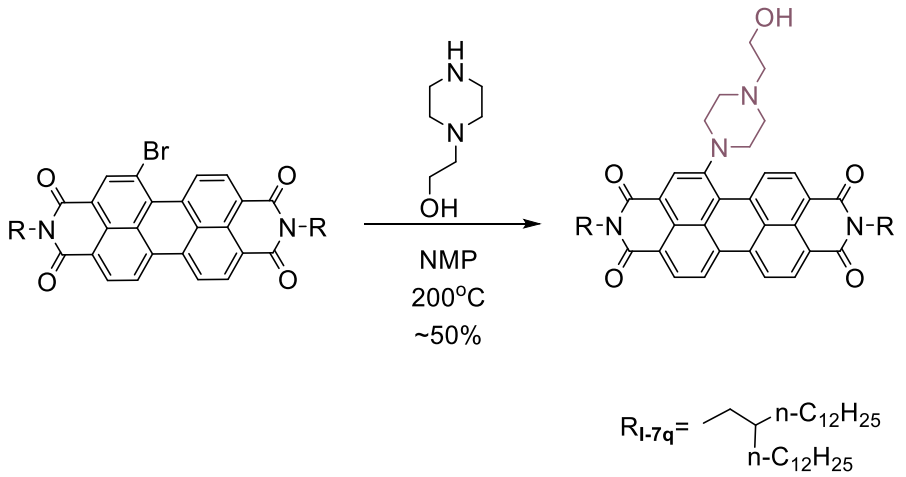

Figure I-10 Nucleophilic reactions of PDI and hydroxyl-functionalized amine compounds.

A similar reaction was reported by L. Martín-Gomis *et al.*[76] employing (*R*)-prolinol on the *bay* region of PDI **I-8d** (Figure I-11). The product was obtained in 51% yield.

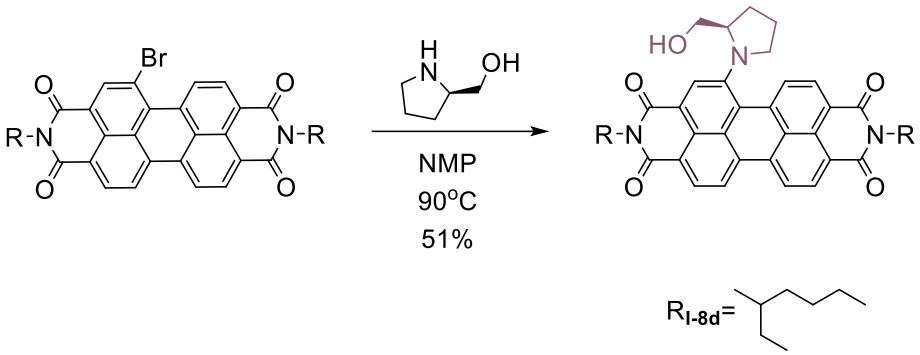

Figure I-11 Nucleophilic reactions of PDI and hydroxyl-functionalized amine compounds.

I.2.1.2.4 Direct amination

A pivotal discovery was made by G. Rauch and S. Hoger[77] when stirring unsubstituted PDIs in the presence of a primary amine with copper(II) salts as catalysts and oxygen (air) as an oxidant provided the N-alkylated and N,N-dialkylated 1-amino and 1,6-diamino PDIs. The reaction were carried out with other metal salts to analyse their catalysis effect on the reaction, such as iron ($Fe(acac)_3$) and palladium ($Pd(PPh_3)_2Cl_2$) salts, however, best results were only achieved with Cu (II) salts. Different Cu (II) salts gave similar yields, which implied that the counter ion has no effect on the reaction. Intriguingly, L. George et al.[78] reported after the conversion of unsubstituted perylenes to mono substituted PDIs without the use of a catalyst.

The reaction of PDI with pyrrolidine, and a pyridinium dichromate (PDC) for a subsequent oxidation, yielded 20-70% of **I-9t** and only 15% of it when PDC was combined with $AgNO_3$. Surprisingly, Cu (II) catalyzed amination reaction did not take place with pyrrolidine, even with the three studied substrates R_g, R_r and R_s (Figure I-12, Table I-2).

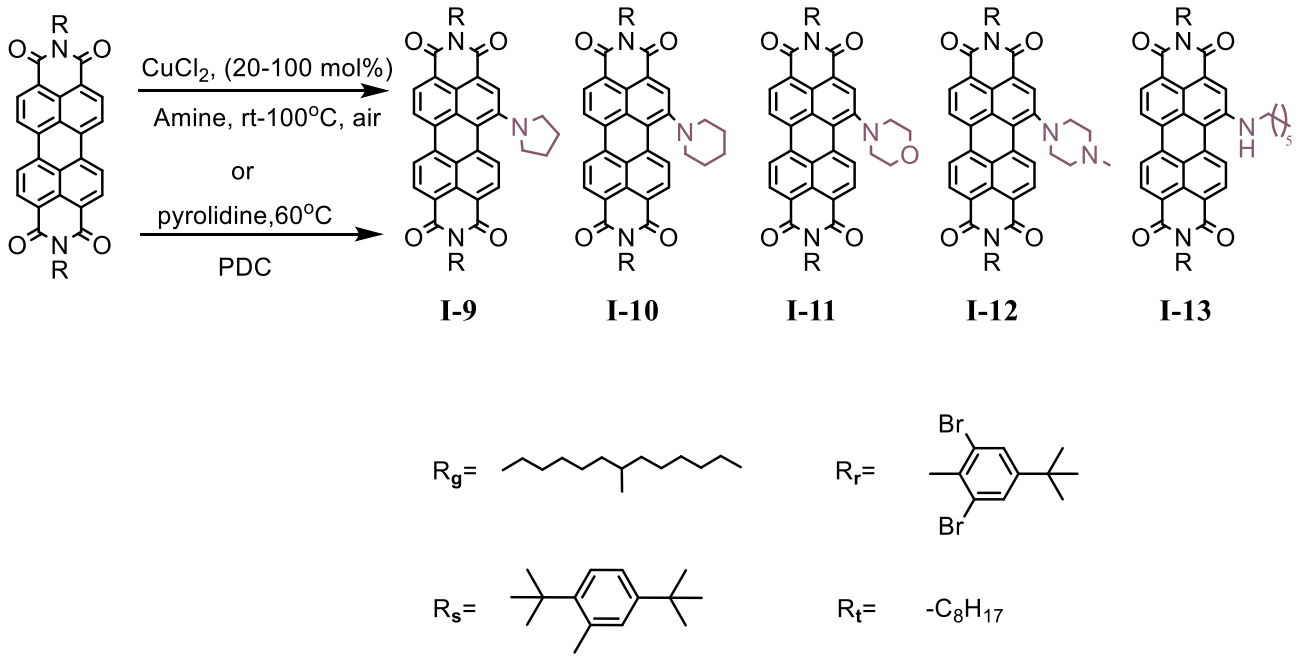

Figure I-12 Amination reactions of PDI bearing different imide substituents.

Table I-2 Amination reaction yields of the corresponding PDI derivatives.

	I-9	I-10	I-11	I-12	I-13
R_g	0%	60%	18%	25%	9%
R_r	0%	0%	-	-	-
R_s	0%	56%	-	-	-
R_t	20-70%		-	-	-

The authors noted that the formation of the mono derivative depends on the reacting amine and the PDI imide substrate which means that the reactivity of PDI depends strongly on their solubility in the amine used as reagent and solvent. For example, the amination reaction of PDIs (with R_g, R_s or R_t) and piperidine gave mainly the mono substituted derivatives **I-10g** or **I-10s** however, **I-10t** was not formed. Similarly, compounds **I-11g**, **I-12g** and **I-13g** were obtained only in moderate yields from the reactions of PDI with morpholine (18% yield), N-methylpiperazine (25% yield) and 1-hexylamine (9% yield). The proposed mechanism for the reaction of PDI with pyrrolidine and PDC proceeds through the radical anion, and since the generated radical anion is sensitive to air, the yield varied greatly.[78]

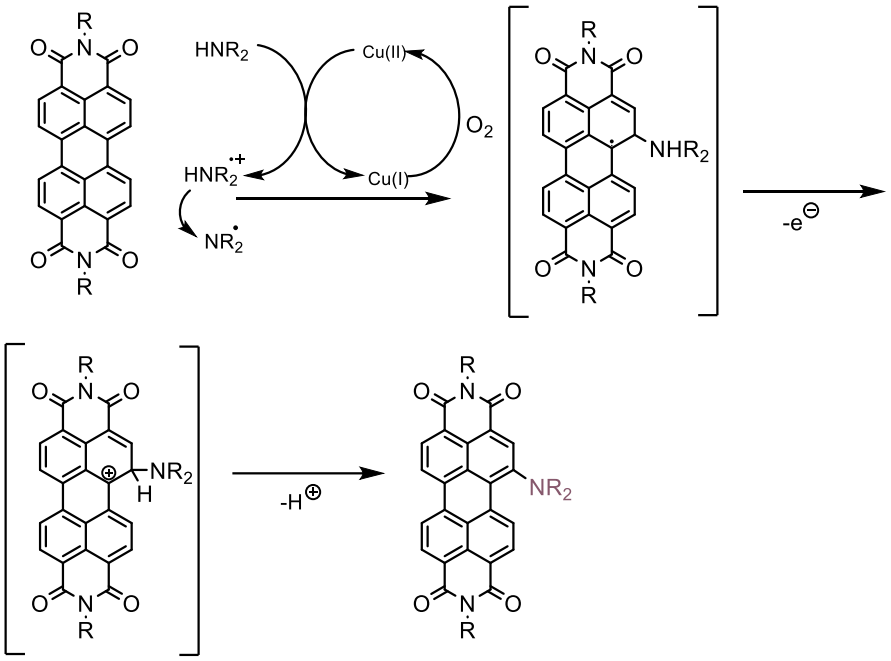

Figure I-13 Proposed mechanism for PDI amination.

For the Cu (II) catalyzed amination, the proposed mechanism (Figure I-13) starts with the coordination of the amine with Cu (II) and its oxidation to the ammonium radical, which is acidic enough to be deprotonated in the amine solvent. Finally, the addition of the amino radical to the PDI followed by a proton coupled electron transfer (PCET) leads to the amino PDI. Re-oxidation of the Cu(I) to Cu(II) is performed by oxygen.[77]

I.2.1.2.5 Introduction of Isocyanides

The versatile use of isocyanide metal complexes such as polymerization catalyst and precursors of carbene complexes led C. Domínguez *et al.*[79] to focus on introducing isocyanide to the core of PDI. This isocyanide donor group can act as a ligand that forms stable organometallic complexes with most transition metals. The reaction requires the formylation of amino-PDI with formic acid followed by dehydration with bis(trichloromethyl)carbonate (triphosgene) and triethylamine (Figure I-14).

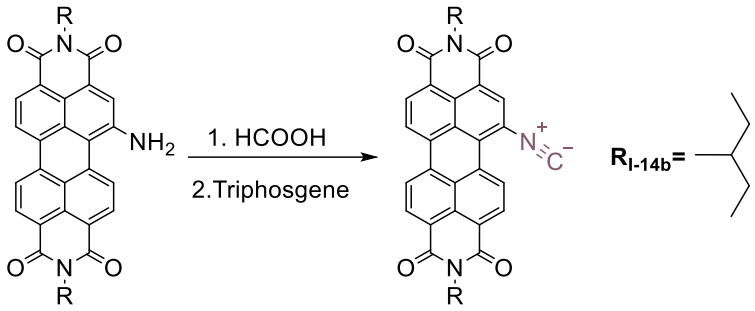

I-14

Figure I-14 Introducing isocyanide to position 1 of PDI.

I.2.1.3 C-O bond formation

I.2.1.3.1 Nucleophilic substitution reactions

Nucleophilic substitution reactions including monobromo-PDI and aryl-alcohols is reported by J. Choi *et al.*[80] The use of anhydrous K_2CO_3 as a base and NMP as a solvent achieved the desired products **I-15u**, **I-16u** and **I-18u** from monobromo-PDI and each of 4-*tert*-butylphenol, phenol, and 4-*tert*-octylphenol with 85%, 86% 87% yield, respectively. Following the same procedure, J. Yun Kim *et al* [81] reported the synthesis of **I-17u** and **I-19u** in 78% and 73% yields, respectively (Figure I-15).

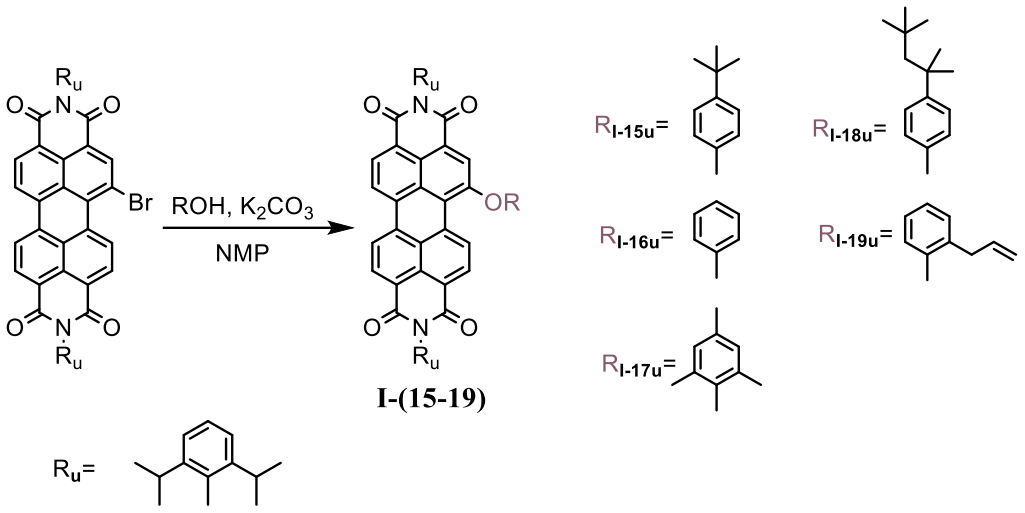

Figure I-15 Nucleophilic reaction between PDI-Br and aryl-alcohols.

The use of hydroquinone and each of catechol, resorcinol and hydroquinone (*o*-, *m*- and *p*-substituted dihydroxybenzenes) in a 1:5 ratio in the presence of 18-crown-6 as a catalyst and K_2CO_3 as a base in toluene for the reaction of monobromo PDI did not lead to useful yields as reported by L. C. Kasi Viswanath *et al.*[82] Hence, to achieve effective nucleophilic substitution, the increase of the solubility of the monobromo PDI with ethylpropyl groups at the imide positions, and a mixture of toluene/DMF (4:1) were employed. The reaction mixture was heated to 120°C to obtain mono-substituted PDI with *ortho*, *meta* and *para* substituted dihydroxybenzene derivatives **I-20b, I-21b** and **I-22b** in 54%, 54% and 48% yield, respectively (Figure I-16).[82]

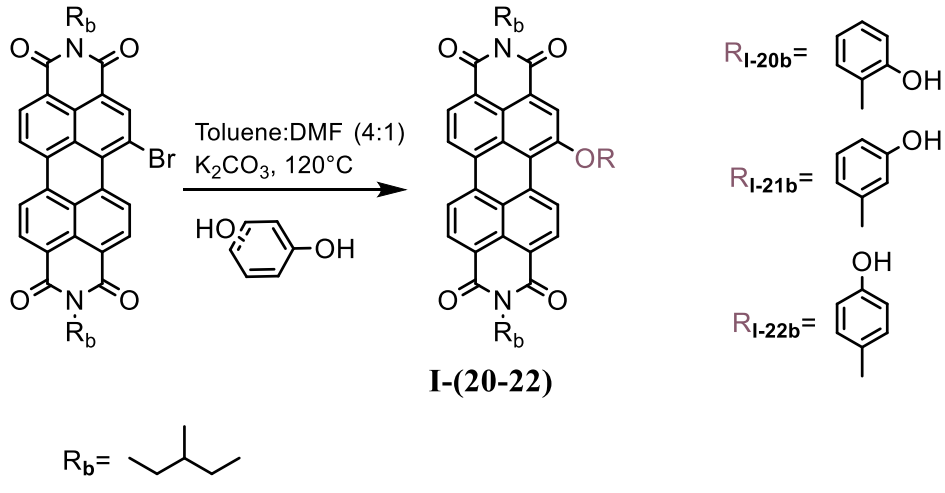

Figure I-16 Nucleophilic substitution of o-, m- and p-substituted dihydroxybenzenes on monobromo PDI.

The aromatic nucleophilic substitution using K_2CO_3 and 18-crown-6-ether with the reaction of monobromo PDI (R_g) and *N*-Boc-4-hydroxyaniline in toluene at 80°C, yielded the product **I-23g** in 40% yield (Figure I-17) as reported by M. Barrejon *et al*.[83]

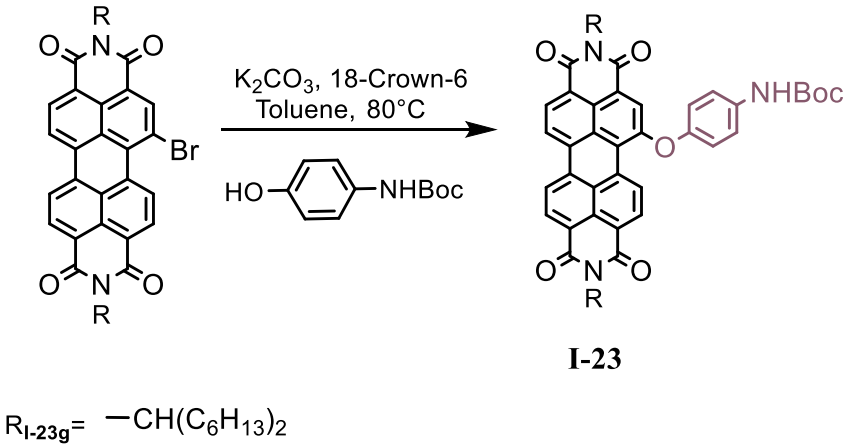

Figure I-17 Synthesis of N,N'-di(1-hexylheptyl)-1-(4-(N-Boc)aminophenoxy)PDI.

Figure I-18 shows different electron-donating alkoxy groups introduced on the *bay* region of PDI. Since the mono-bromination step which precedes the displacement with alcohol affords a mixture of mono-bromo, dibromo PDIs and unreacted materials, N. Zink-Lorre *et al*[84] discovered that it is possible to perform the alkoxylation process directly in one step, avoiding the bromine intermediate compound by treatment of PDI with the corresponding alcohol in the presence of fluoride ions source (such as TBAF) in THF.

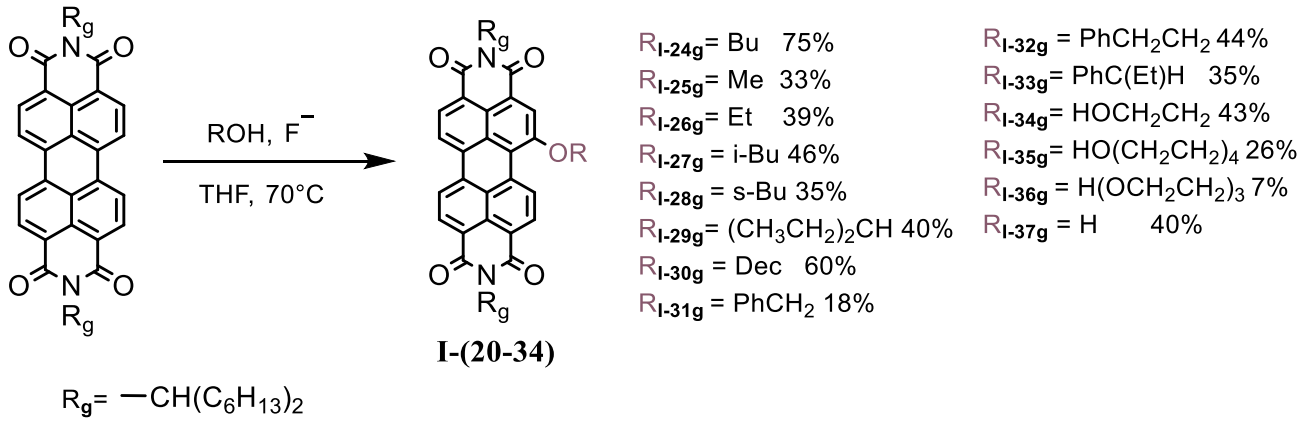

Figure I-18 Fluoride-mediated alkoxylation of PDI.

The choice of THF was justified by higher conversions compared to other solvents, such as acetonitrile and CH_2Cl_2 that failed completely to allow the reaction to proceed, as reported.

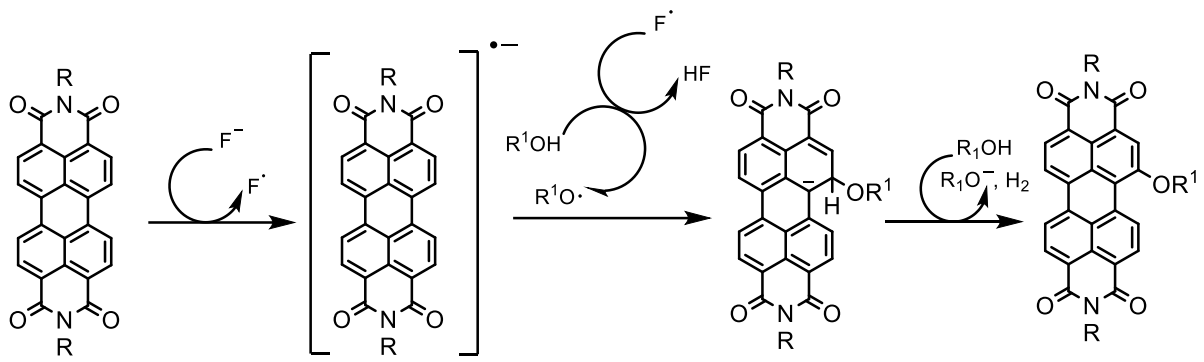

Figure I-19 Proposed mechanism of the Fluoride-mediated alkoxylation of PDI.

However, carrying the reaction at higher temperatures decomposes the TBAF. CsF/18-crown-6 could also be used instead of TBAF, but not the mixture KF/18-crown-6, which means that the cation has an influence on the reaction. Finally, using TBABr did not allow the reaction to proceed at all, pointing out to the crucial role played by the fluoride anion. The proposed mechanism of the reaction is showed in Figure I-19.

I.2.1.4 C-S bond formation

I.2.1.4.1 Nucleophilic substitution reactions

A conceptually similar strategy was also employed by this group[85] during their synthesis of monoalkylthio-PDIs, shown in Figure I-20. The choice of THF as a solvent gave also the best results where hexane and DMF failed to dissolve the reaction mixture. The couple potassium fluoride/18-crown-6 gave the best results this time, suggesting a possible potassium–sulfur stabilizing interaction.

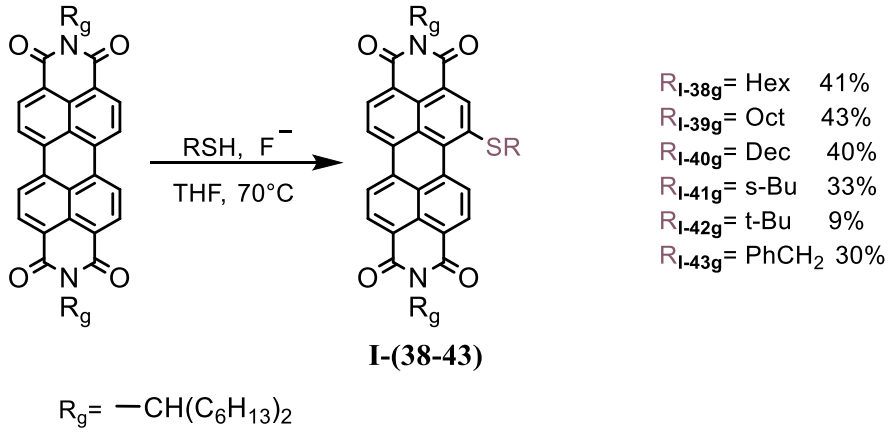

Figure I-20 Alkylthio-functionalization of PDIs.

It is noteworthy that the reaction procedure worked with tertiobutylthiol, while it did not work with tertiobutanol. The reaction of PDI and 2-mercaptoethanol in the presence of TBAF did not take place, probably due to the proximity of both functional groups. Hence PDI was treated with 6-mercaptohexan-1-ol in the presence of KF and yielded 18% of **I-44g**, as shown in Figure I-21. When a large excess of KF was used, the reaction yield increased to 38%. However, by using TBAF instead of KF, **I-44g** was obtained in 6% yield, in addition to the mono-hydroxy PDI, **I-45g**, obtained in 13% yield.

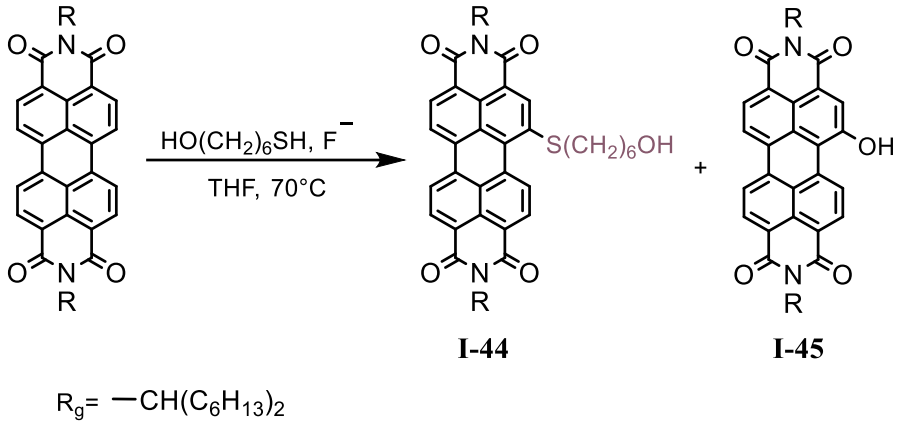

Figure I-21 Reaction of PDI with RSH-ROH.

I.2.1.5 C-C bond formation

I.2.1.5.1 Cross-coupling reactions

Examples of substituted PDIs prepared following Sonogashira cross-coupling reaction are presented in Figure I-22. PDIs **I-46a**, **I-46b**, **I-46v** and **I-47v** are obtained by treatment of monobromo PDIs with trimethylsilyl acetylene and triphenylsilylacetylene respectively. The cross-coupling reaction could also work with phenylacetylene having different groups at positions 'a' and 'b'.[56,86,87]

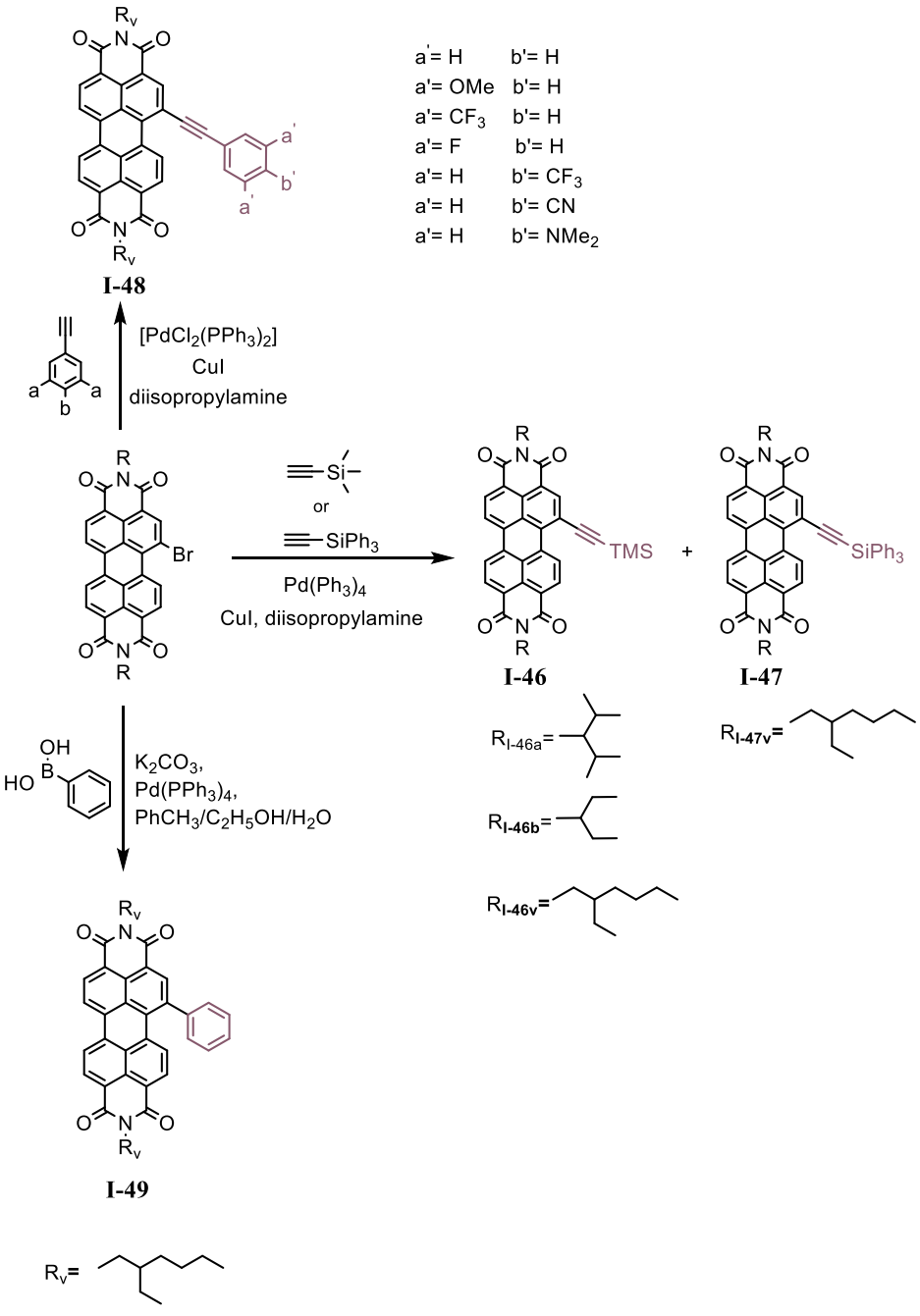

Figure I-22 C-C cross coupling reactions.

Introducing phenyl ring to the *bay* region of PDI following Suzuki-Miyaura coupling (SMC) is reported by Z. Mahmood *et al*. using phenylboronic acid, K_2CO_3 as the base and $Pd(Ph_3)_4$ as the catalyst, producing **I-49v** (Figure I-22).[88] In 2009, W. Yue *et al.*[89] reported an original palladium catalyzed meta-selective alkylation process for the generation of monoalkylated PDI on the *bay* region.

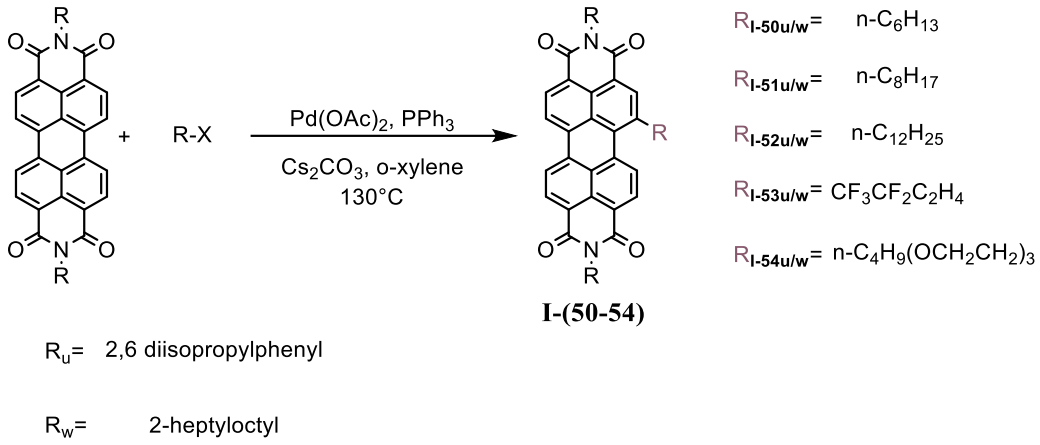

Figure I-23 Palladium catalyzed direct alkylation of PDI.

PDI was observed to form C-C bond directly with alkyl halides on the meta position, due to the higher meta C-H bond reactivity of electron deficient arenes.[90] The reaction employs $Pd(OAc)_2$ as the catalyst, PPh_3 as the ligand, and excess of Cs_2CO_3 as the base in o-xylene (Figure I-23). Using stronger base such as t-BuOK would keep the starting material unchanged. In addition to alkylbromide, alkyliodide would also lead to good yields, unlike alkyl chloride due to its low reactivity.

I.2.2 Di-substitution of PDI on the bay region

I.2.2.1 C-Br bond formation

I.2.2.1.1 Di-Bromination

It is known that obtaining halogenated derivatives of PDI is important for subsequent substitution and expansion of the PDI core. Bromination reaction can be achieved following either the BASF patent,[24,91–98] procedure where PTCDA is treated with concentrated H_2SO_4, elemental iodine and subsequent addition of bromine upon heating, followed by imidization with amines (Figure I-24). F. Würthner *et al* showed by ^{1}H NMR (600 MHz) that 1,7 and 1,6 and 1,6,7 regioisomers **I-55** were formed in a 76:20:4 ratio, however, remained non-purified due to the insolubility of the product in organic solvents.[24] The other strategy consists of treating PDI derivatives with an excess of bromine at room temperature , where 1,7 and 1,6 di-bromo PDIs **I-56a** and **I-56b** are obtained in 26% and 25% yields, respectively (Figure I-25).

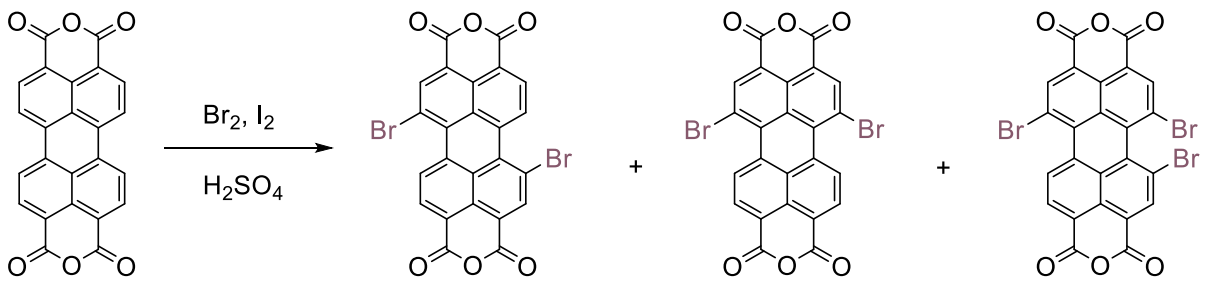

Figure I-24 Di-bromination of perylene dianhydride.

Compound **I-56c** was obtained in 85% yield after increasing the temperature to 50°C where the reaction did not undergo at room temperature as reported by P. Rajasingh *et al*.[56] F. Würthner *et al*[24] revealed that the major regioisomer **1,7-I-56c** can be obtained in pure form by repetitive recrystallization, confirmed by X-ray crystal structure of the compound. It is noteworthy that the yields of di-bromo PDIs **I-56a** and **I-56b** increased to 92% and 89%, respectively, when the reaction was heated under reflux.

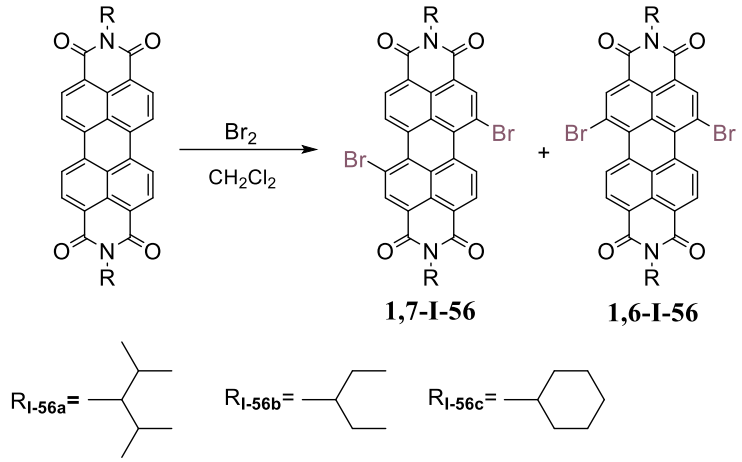

Figure I-25 Di-bromination of perylenediimides.

I.2.2.2 C-N bond formation

I.2.2.2.1 Di-Nitration

As mentioned earlier, the reaction time for the production of mono-nitro PDI plays an important role.[64,65] For example, by using the same reagents (cerium (IV) ammonium nitrate (CAN) and HNO_3 in CH_2Cl_2 under ambient temperature), di-nitro PDI is also obtained when the reaction time is increased to 48h (Figure I-26).[61,99–103]

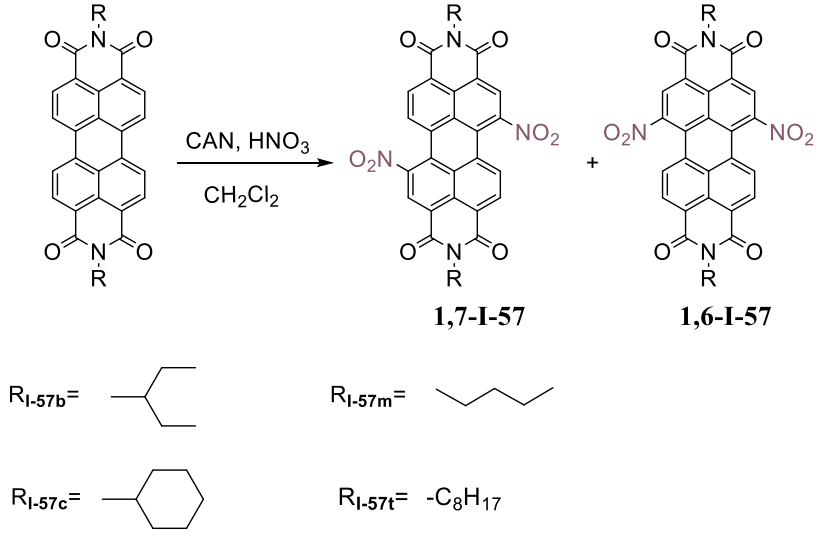

Figure I-26 Di-nitration of perylenediimides.

Similar to dibromo PDIs, the dinitro PDIs are obtained as a mixture of 1,6 and 1,7 regioisomers, where repetitive crystallizations[61,99,102] could ensure the purification of 1,7 di-nitro PDI.

Separation of the 1,6 and 1,7 regioisomers could be also performed on a preparative HPLC system, as reported by H-Y Tsai *et al.*[100,104]

Di-nitro PDI could also be obtained from the reaction of PTCDA with fuming nitric acid in $CHCl_3$ at room temperature, followed by imidization with 2,6-diisopropylaniline, as reported by L. Hao *et al.*, where only the 1,7 di-nitro PDI was observed.[71]

I.2.2.2.2 Reduction of nitro-groups

L. Hao *et al.* also reported the catalytic hydrogenation using hydrazine and Pd/C in DME to further reduce the dinitro PDI into diamino PDI. However, the product was used in the next step without further purification.[71] Another procedure was applied on di-nitro PDIs employing tin chloride dihydrate in THF, this reaction gave 82% yield of the PDIs bearing R_c, R_m or R_t.[99,101]

I.2.2.3 Boron-Nitrogen (B-N) annulation

A formidable challenge of fusing BN fragment to the highly electron-deficient PDI was reported by G. Li *et al.*[70] Importantly, the difference in electronegativities between boron (B, 2.0) and nitrogen elements (N, 3.0) in the BN unit contributes largely to the molecular frontier orbitals and intermolecular interactions of PDIs. Figure I-27 shows the BN-annulation by reacting amino-PDI with dichlorophenylborane, using toluene as solvent and triethylamine as a base. It is noteworthy that the product is soluble in CH_2Cl_2, $CHCl_3$, THF, and toluene, but slightly soluble in DMF and DMSO.

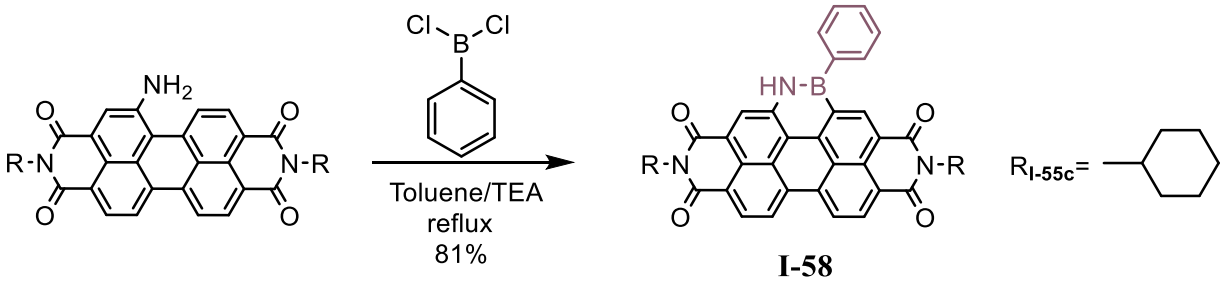

Figure I-27 Introduction of azaborine into perylenediimides.

I.2.2.4 Heterocyclic annulation

Significant electronic coupling between the nitrogen heteroatom and the PDI core could occur upon incorporating a nitrogen containing ring at the *bay* positions of the PDI chromophore. Welch *et al.* reported the reaction of mono-nitro PDI with triphenylphosphine, to obtain the *N*-heterocyclic annulated PDI (Figure I-28). [45,105] The discovery of this reductive cyclization, also known as Cadogan cyclization, started as early as 2000 with Langhals and S. Kirner,[106] using triethylphosphite as the reducing agent. However, this resulted in low yields, due to the production of an unwanted N-ethyl by-product during the course of the reaction. Moreover, *S*-heterocyclic and *O*-heterocyclic annulated PDI were also prepared.[59,106,107] The electronic structures and photochemical properties of these heterocyclic annulated perylenes could be highly changed as a result of the inclusion of these heteroatoms into the perylene skeleton. Furthermore, the presence of these heteroatoms can induce inter- and intramolecular interactions responsible for excellent OSCs device performance.

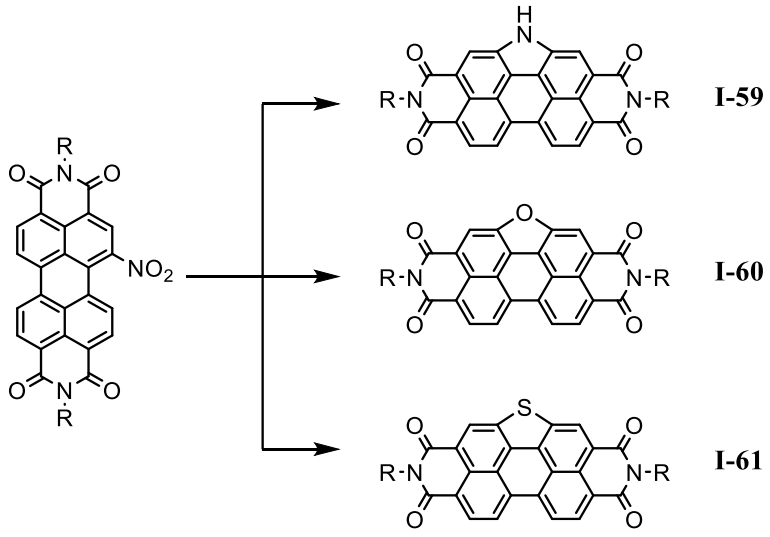

Figure I-28 Reductive cyclization of perylenediimides.

I.2.2.5 Incorporation of Nitrogen atom into coronenes

A new synthetic endeavor toward the development of *N*-decorated coronene bisimides is reported by L. Hao *et al*,[71] following Pictet-Spengler reaction procedure, after which oxidative aromatization is accompanied in one pot, to yield the corresponding *N*-decorated PDIs (Figure I-29). The reaction employs the highly electron-deficient aminoPDI and corresponding aldehydes, in the presence of TfOH or TFA as the catalyst. A conceptually similar procedure is

reported by M. Schulze *et al*.[108] However, to facilitate the oxidative rearomatization, the inert atmosphere was exchanged by pure oxygen after the completion of the iminium ion formation, in addition to using molecular sieves to remove the released water. This modified procedure protocol, despite the consistency of moderate yields, was essential to deal with the reported less reactive aldehydes shown in the Figure I-29.[108] The reaction mechanism is initiated by an iminium ion formation followed by an intramolecular electrophilic aromatic substitution of the aromatic system by the iminium ion, known as Mannich-type transformation. After annulation of the perylene core, an oxidative rearomatization takes place to generate the fully π-coordinating pyridyl subunits.

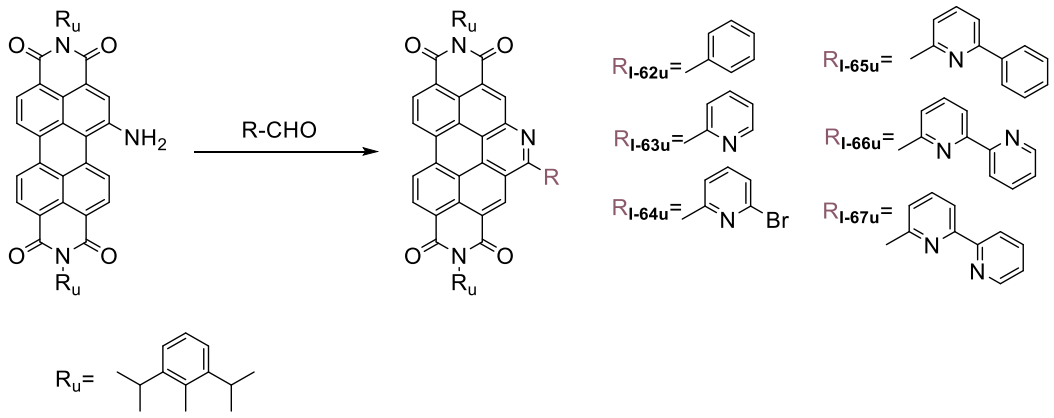

Figure I-29 Synthesis of coronene bisimides containing nitrogen atom.

I.2.2.6 Replacement of di-bromo PDI with various substituents

Replacement of the halogen atoms in aromatic cores via nucleophilic substitution on dibromo-*bay*-substituted PDI with amine,[22] phenol,[109] thiol,[110] cyanide[6] and fluoride[5] based nucleophiles are reported (Figure I-30).

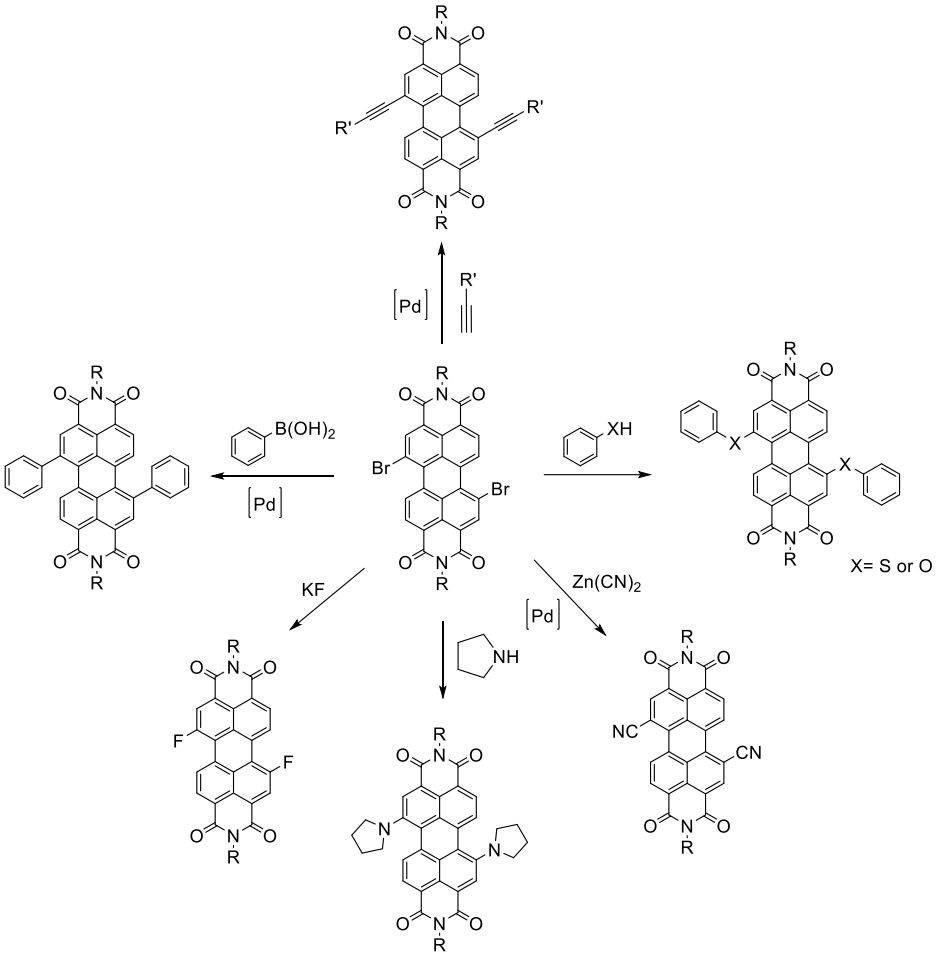

Figure I-30 Nucleophilic substitution on dibromo-*bay*-substituted PDI with various substituents.

The various PDIs obtained represent interesting optical and electronic features, because of the direct electronic coupling between the new substituents and the PDI cores.[111,112] Y. Zhao *et al*. indicated that the selective formation of the di-substituted adduct is temperature and solvent dependent when secondary cyclic amines such as pyrrolidine, piperidine, and morpholine are used. In addition to nucleophilic displacement reactions, dibromo-*bay*-substituted PDI were also employed in transition-metal catalytic C-C coupling reactions, such as Suzuki-Miyaura coupling,[88,113,114] Stille,[14,115] and Sonogashira couplings,[86,116] to further functionalize PDIs.

I.3 Physical properties of PDIs

PDI derivatives present remarkable absorption, emission, redox, and other physical properties. These advantages had led to significant results upon research on these materials applied in various applications, including OPVs and OFETs. [9,128] A brief discussion about some of these physical properties, is given as follows.

I.3.1 Optical properties

The diverse properties of PDI chromophores including strong light absorption with high molar extinction coefficients in the visible region (400 nm - 650 nm), high fluorescence quantum yields close to unity and long-lived singlet-excited state life-times, made them important chromophores in dyes and pigments chemistry as well as in the field of electronic materials.[23]

PDI-based chromophores are mostly known to exist as red solids, having high melting points with excellent thermal and photochemical stabilities. However, in some cases, the very pronounced aggregation effects of these chromophores lead to the variation in the solid absorption spectra.[23,27,118] Thereby, PDI-based pigments appear also in orange, green, brown, and even black color.

In general, PDIs are characterized by a vibronically structured band with strong absorption in the visible region between 400 to 550 nm, and they exhibit a strong yellow-green mirror image fluorescence in common solvents.[119] Würthner *et al*.[120] have proposed a typical UV/vis and fluorescence spectrum of the parent PDI, shown in Figure I-31. The spectrum of unsubstituted PDI solution shows three peaks, characteristic of the π–π* electronic transition of PDI. These electronic transitions are reported to be predominantly HOMO to LUMO transition. The peak at ~525 nm corresponds to the 0–0 vibronic transition while the other two bands at ~490 and ~460 nm correspond to the 0–1 and 0–2 vibronic transitions, respectively.[120,121]

The effect of 'solubilizing' substituents introduced at the imide position of PDI on absorption and emission properties stays insignificant. This is due to the nodes in the HOMO and the LUMO at the imide nitrogen, reducing the coupling between the perylene units and the imide substituents. For example, PDI with cyclohexyl group at the imide position shows maximum of absorption at 526 nm in $CHCl_3$, this reported value is similar to PDIs substituted with hexylheptyl group, other examples are shown in Table I-3.[23,71,122]

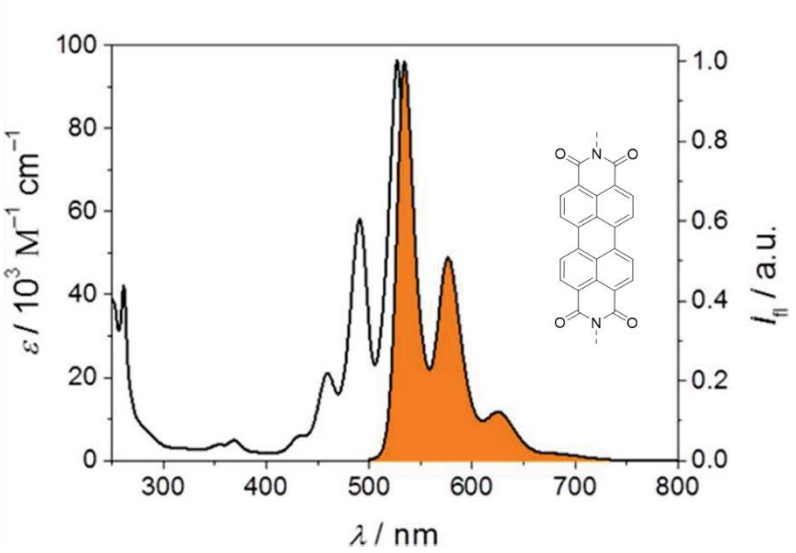

Figure I-31 Typical UV/vis (white) and fluorescence (orange) spectrum of PDI.

Generally, a change of less than 5 nm in the absorption and emission maximum could be observed upon changing the *N*-terminal group.[23,71] However, studies made on the aggregation effect of these material has been reported to have considerable effect on solid state absorption spectra and hence leading to important changes of their colors when modifying the imide substituents.[118]

Table I-3 Optical properties of some unsubstituted PDI dyes in chloroform.

R	λ_{abs}^{max}(nm)	ε ($M^{-1}cm^{-1}$)	λ_{em}^{max}(nm)	Φ_f
	526	78700	534	1.00
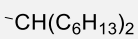	526	88000	533	1.00
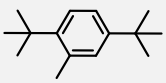	526	95000	537	1.00
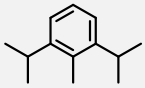	527	80,900	534	1.00

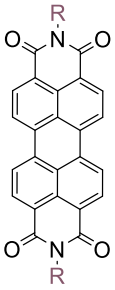

In contrast, it is well-known that substituents on the aromatic core *bay*-positions show a considerable effect on the absorption and emission spectra of PDIs due to the stronger electronic coupling between the π-orbital of the perylene chromophore and the substituents on the aromatic *bay* region. For example, introduction of a mono nitro group, **I-1c** (Table I-4), shows a slight blue-shift of about 4 nm in the absorption spectra compared to that of the unsubstituted PDI, this phenomenon is increased with di-substituted nitro perylenes, and the reason could be attributed to the steric hindrance induced by the nitro-groups which reduces the molecular rigidity. In addition, very weak emission is observed for both mono-nitro and di-nitro PDIs.[61,99,122]

Incorporating other electron withdrawing groups at the *bay* region of the PDI (such as F, Cl, Br and CN) has led to a limited spectral change and solvatochromism effect. Examples are **I-56c** and **I-68c** that have been reported to have almost identical photophysical properties to those of the unsubstituted PDI. Generally, the inductive effect of such σ-acceptors lowers both the LUMO and the HOMO energy levels in a similar manner without obvious intramolecular charge transfer (ICT) present in these systems. The several nanometer red-shifts in the absorption and emission maxima observed for these compounds are usually attributed to the σ-acceptors stabilizing the LUMO slightly more than the HOMO, consequently narrowing the energy gap, probably due to the pronounced coupling between the PDI LUMO and the acceptors.

A systematic red-shift in the absorption and emission peaks, compared to the non-substituted PDI is observed when a mono-*p*-*tert*-butylphenoxy group was introduced at the *bay* position, **I-15c**,[123] due to the enlargement of the conjugation system of PDI core. More pronounced spectral changes occur upon the *bay*-inclusion of electron donors, such as amino groups, **I-3c**, where the mono-amino PDI shows a broad absorption band which is red-shifted relative to the unsubstituted PDI. This phenomenon is also observed for the emission spectra, where in both cases, the red-shifts increase with the solvent polarity.[68] The bathochromic shifts in the absorption and emission maximum become more important upon the inclusion of another amino group at the *bay* position, **I-69c**.[99] Both mono and di amino PDI exhibit very weak emission in the near infrared (NIR) region, which indicates strong ICT characteristics for the excited states of such compounds. Another significant example is the introduction of pyrrolidinyl groups, with **I-9c** and **I-70c**, which shifted drastically the absorption spectra to longer wavelength region, 118 nm and 156 nm respectively.[134] The absorption spectra of mono pyrrolidinyl PDI is less red-shifted compared to the disubstituted pyrrolidinyl derivatives, as expected for lower electron-donating ability of one pyrrolidinyl group *vs.* two such groups.

Table I-4 Optical properties of bay-substituted PDIs.

n°	R_1	R_2	Solvent	λ_{abs}^{max}(nm)	ε ($M^{-1}cm^{-1}$)	λ_{em}^{max}(nm)	Φ_f
I-1c	NO_2	-	$CHCl_3$	522	31000	-	-
I-3c	NH_2	-	CH_2Cl_2	578	41200	677	0.10
I-9c	pyrrolidinyl	-	$CHCl_3$	644	31300	-	-
I-15c	p-tert-butylphenoxy	-	$CHCl_3$	539	34700	564	
I-56c*	Br	Br	$CHCl_3$	526	57300	547	
I-57c**	NO_2	NO_2	THF	515	54200	-	-
I-68c*	CN	CN	$CHCl_3$	530	47000	545	1.00
I-69c	NH_2	NH_2	CH_2Cl_2	620	42500	693	0.09
I-70c	pyrrolidinyl	pyrrolidinyl	$CHCl_3$	682	31600	-	-

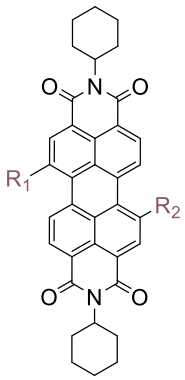

* Values determined for mixtures of 1,6- and 1,7-substituted isomers. ** Values determined for 1,7-substituted isomer.

Other significant examples are the heterocyclic annulated PDIs, where both **I-60c** and **I-61c**, shown again in Figure I-32, present a blue-shift in their maximum absorption bands compared to that of the unsubstituted PDI (Table I-3). This slight blue shift is due to the extended aromatic core along the short molecular axis. Compared to *S*-PDI, the maximum absorption of *O*-PDI is bathochromically shifted of about 10nm.

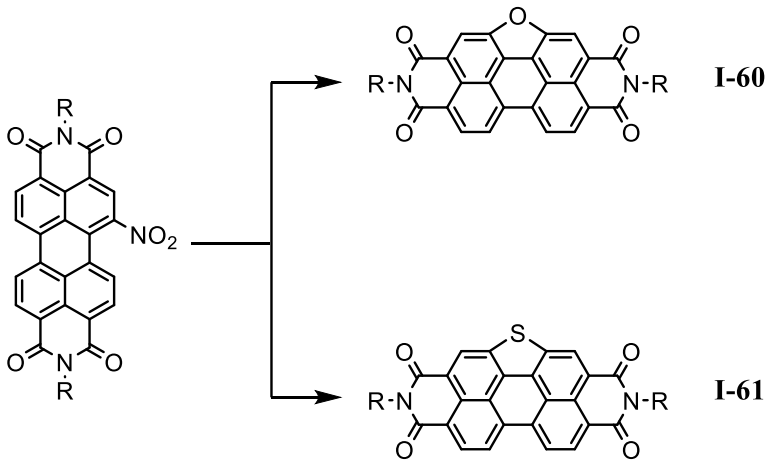

Figure I-32 Reductive cyclization of perylenediimides.

Moreover, the emission spectra of **I-60c** and **I-61c** are also hypsochromically shifted relative to the unsubstituted PDI. This reflects the interesting effect of the corresponding annulated PDIs on the energy gap between the electronic excited state and the ground state.

I.3.2 Electrochemical properties

As mentioned earlier, PDIs are electron deficient molecules and have been highly investigated as electron acceptor materials. Würthner *et al*.[120] has also represented a general look of the cyclic voltammetry usually seen for such PDIs, which reflects their n-type character (Figure I-33). PDIs are readily reduced and difficult to oxidize in solution. Usually two reversible redox couples are observed, which are located at around -1.0 and -1.2 V vs. Fc/Fc^+. The electrochemical data being surely dependent on the conditions, with which, accordingly, an irreversible oxidation wave is also sometimes observed at values close to that of solvent oxidation, that is above 1.2 V vs. Fc/Fc^+.

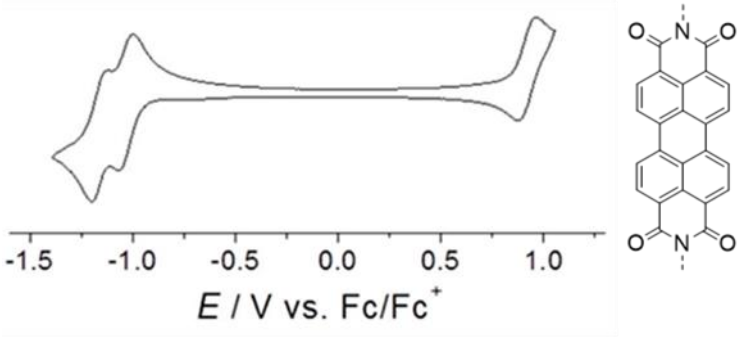

Figure I-33 Typical cyclic voltammogram of PDI.

The redox properties of PDIs in solution are slightly affected by the variation of the substituents at their imide positions, of which case seen also for their optical behavior.[124] However, pronounced effect on the redox potentials is resulted out of introducing different substituents on the *bay* position of the PDI.[6,125] Some of the electrochemical data are shown in Table I-5.[57,71,95,126,127] For example, *bay*-substituted PDIs with cyano groups have more positive reduction potentials than unsubstituted PDI compounds. The introduction of such electron withdrawing groups stabilizes the PDI core by lowering both HOMO and LUMO energy levels. In contrast, PDI *bay*-substituted with electron donating groups, such as pyrrolidine, are more difficult to reduce and hence, their reduction potentials become more negative. Moreover, the extension of the conjugation of PDIs by incorporating conjugated substituents on their core position result in more positive reduction potentials compared to the non-substituted PDIs. This

result is to some extent unaffected by the nature (π-donor or π-acceptor) of the corresponding groups attached.[116]

Table I-5 Reduction potentials vs. Fc/Fc^+.

R	R_a	R_b	E^1_{red}(V)	E^2_{red} (V)
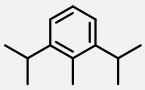	-	-	-0.96	-1.22
	-	-	-1.07	-1.28
—C_5H_{11}	-	-	-1.04	-1.22
	CN	CN	-0.67	-0.98
	pyrrolidinyl	pyrrolidinyl	-1.40	-1.52

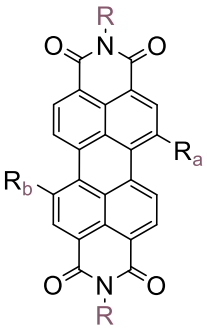

While varying the imide substituents on the PDIs serves for tuning their solubility and molecular packing, introducing different functional groups at their *bay*-positions allows the control of their optical and electrical properties.[6,22,95,107,128–130] Indeed, the reported results made to date prove the effectiveness of both approaches, for example, in improving the device performance of PDI-based OPVs.

I.4 Perylenediimides in organic solar cells

The growing demand for replacing fossil fuels with clean energy has caused the emergence of photovoltaic science and technology. Organic photovoltaics (OPVs) is a type solar technology that can be fabricated by solution processing techniques, using organic semiconductors as active materials (light-harvesting and charge-transport materials). Organic solar cells (OSCs) have the potential of being light-weight, semi-transparent and even flexible, which makes them attractive

compared to heavy and bulky traditional inorganic PV. Research in new organic semi-conductors is necessary to develop efficient, stable and easy to produce materials that can be solution processed using industrial large-area manufacturing processes, like roll-to-roll printing technologies.[131–134] A single active layer made up of intermixed π-conjugated p-type donor and n-type acceptor materials, to create internal interpenetrating networks of both components, called bulk heterojunctions (BHJs), is employed in the fabrication of bulk heterojunction (BHJ) solar cell devices. Within this active layer occur the light absorption, exciton formation, charge dissociation and charge transport.[135]

The process of converting solar light into electricity in OPV cells begins by photoexcitation of the donor semiconductor (Figure I-34). This creates an electrically neutral and coulombically bound electron–hole pair, called exciton. This exciton diffuses (diffusion length is typically on the order of 10 nm) to a near D/A interface, where it can dissociate into a free hole and electron, which can then migrate towards the anode and the cathode, respectively. These collected charges at the electrodes will generate electrical power.[131,136]

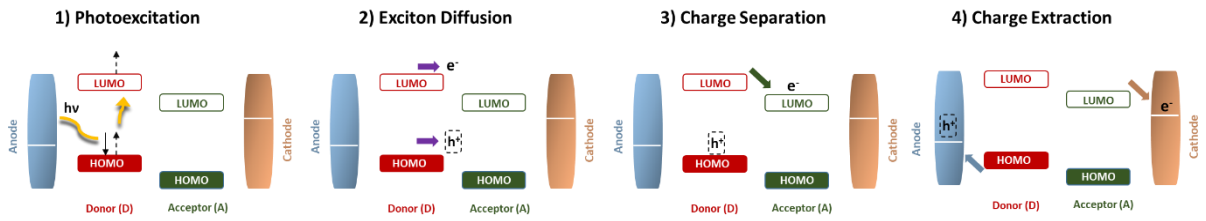

Figure I-34 General working mechanism for organic solar cells.

Power conversion efficiency (PCE) determines how much electrical power is effectively generated from an OSC. PCE is defined as the ratio of maximum power output (P_{max}) to power input (P_{in}). The electrical power output is the product of the current and the voltage at which a given device's electrical output is the maximum, P_{max} ($P_{max} = I_{max}.V_{max}$) and is constituted of three parameters essential for determining the photovoltaic performance,[137] open-circuit voltage (V_{OC}), short-circuit current (J_{SC}) and fill factor (FF). Tailoring a connection between the molecular structure of the active layer and these physical parameters is critical for designing strategies suitable for enhancing the efficiency of OPVs.[138] V_{OC} corresponds to the voltage at zero current density, it depends mainly on the energy difference of the HOMO level of the donor (D) and the LUMO level of the acceptor (A). J_{sc} corresponds to the maximum current when the voltage across the device is zero, it depends on absorption profiles of the donor and acceptor materials, surface area of the active layer, device thickness and also on the charge transport properties of the organic semiconductors. The maximum area within the J–V curve, (Figure I-

35), determines the Fill Factor (FF) (FF= $I_{max}.V_{max}/V_{oc}.J_{sc}$) which represents the quality of the solar cell. This depends on the morphology of the active layer where a nanostructured bicontinuous phase maximizes the charge transport processes (therefore, increasing the FF) and decreases the possibility of charge carrier recombination.[136,139–141]

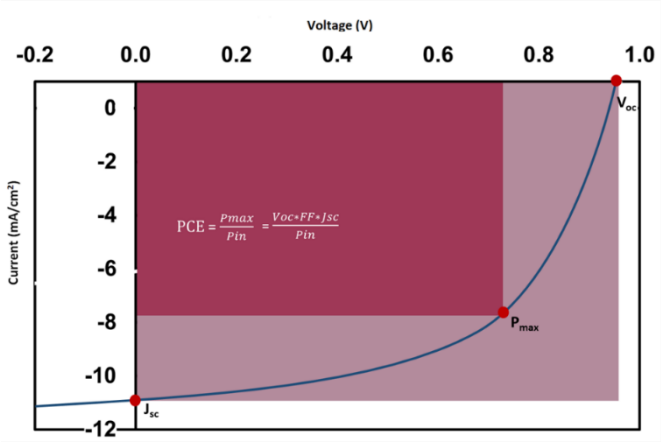

Figure I-35 Illustration of Current-voltage (I-V) curve of a BHJ solar cell under illumination. Essential parameters for organic solar cell device performance are shown: V_{OC} and J_{SC} and FF.

BHJ solar cells devices exist in two general anode/BHJ/cathode architectures (Figure I-36), - *i*) the 'conventional' architecture',[142] in which the device structure consists of a metal (Ca or Al) contact, as the cathode, on the surface of the active layer on a glass substrate, coated with transparent indium-tin-oxide (ITO), as the anode, - *ii*) the 'inverted' architecture, in which the top electrode is a metal anode and the transparent conductive electrode, ITO, is the cathode, thereby, the electrons and holes generated in the active layer exit the device in the opposite direction compared to the conventional BHJ solar cells.

Research on inverted BHJ solar cells, [143–146] has been recently augmenting, since inverted device structure implies various important aspects such as, enhanced efficient energy conversion, more facile device fabrication and better long-term ambient stability, in which the use of the hygroscopic hole transporting layer PEDOT:PSS and low-work-function metal cathode employed in conventional architectures are replaced. Furthermore, the fabricated OPV device with an inverted geometry benefits from the vertical phase separation and concentration gradient in the active layer, in addition to the collecting nature of the electrodes being reversed and hence, granting the use of air-stable and high work function metal anode (Ag, Au) deposited as the top electrode to collect holes, and metal oxide (TiO_2, ZnO), as an interlayer between the ITO and active layer, to collect electrons. Such crucial properties make the inverted device structure an ideal configuration for all types of OSCs.

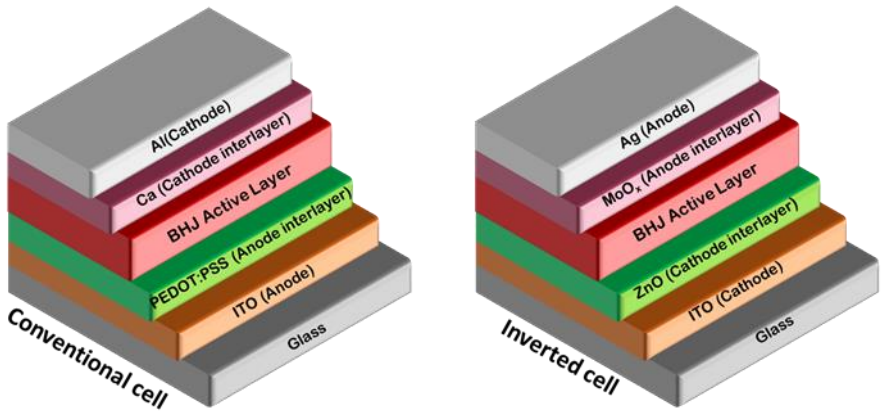

Figure I-36 Device architectures of the conventional and inverted type organic solar cells.

As mentioned earlier, PDIs are among the most important classes of electron acceptor materials investigated in OSCs,[63,147] their excellent structural stability, low lying LUMO levels, small optical band-gaps, high molar absorption coefficients, strong electron accepting ability and high electron mobility, made them potential non-fullerene acceptor (NFA) candidates.[54,128,148] However, their high crystallinity and ability to strongly aggregate in the solid state due to their coplanar molecular structures lead to micrometer sized phase separation between the donor and acceptor materials, which is detrimental to OPVs efficiency.[133,149] Therefore, understanding of the materials and device fundamentals, such as charge generation and transport, and better control of materials' structure and blend morphology is required for the improvement of BHJ OPV device performance.[150,151] For this, many strategies have been developed to disrupt the planarity to minimize the intermolecular interactions and excessive domain sizes of PDI based acceptor materials, knowing that exciton diffusion length in organic semiconductors are typically within ~15-20 nm. [149,152] These strategies include, introducing large bulky groups at the imide and/or *bay* position of PDI monomers, and developing twisted PDI dimers,[45,59,153,154] trimers [155–157] and tetramers,[149,158,159] where PDI chromophores are directly linked via *bay* position, or through central cores. Figure I-37 shows the first and the recent examples of PDIs used as electron acceptor materials in OSCs. In 1986, Tang first fabricated a double-junction OSCs in which the perylene derivative (PV) was the acceptor layer and copper phthalocyanine (CuPc) was the donor layer.[160] These photovoltaic devices achieved a PCE of 1%. The self-aggregation of the perylenes contributed to the low efficiency obtained. Whereas, H. Yan *et al*.[149] recently reported PCE beyond 10% employing the PDI tetramer FTTB-PDI_4 in inverted BHJ OSCs. This PDI tetramer is one of the efficient models signifying the importance of

controlling the intermolecular twisting and domain sizes for obtaining considerable photovoltaic performances.

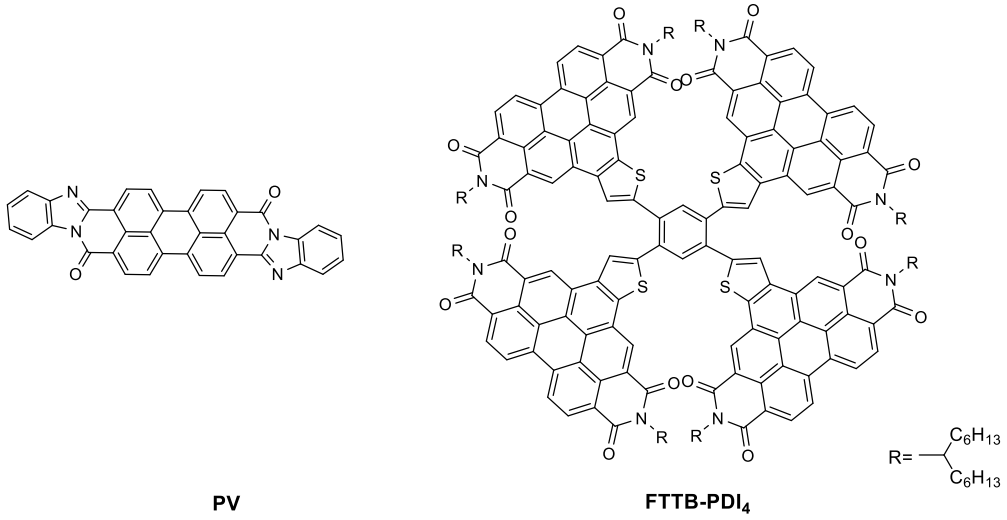

Figure I-37 Chemical structures of perylene tetracarboxylic derivative (PV) and PDI tetramer FTTB-PDI4.

The expanded attention and research advances in the field of OSCs have shown that the photovoltaic technology is of constant progress with the increased PCEs obtained (>10%) till date. Major investment in device engineering and developing of new materials as into new more efficient, long-lasting organic materials, with controlled thickness and morphology as well as more robust, light-weight and low-cost large-area solution processing techniques, are substantial for increasing OPV devices efficiencies.

I.5 Presentation of our work

Following this state-of -the-art, we will present our work devoted to the development of new reactivity of nitro and aminoPDI derivatives. The remainder of the thesis manuscript will be centered on the following three chapters:

Chapter II concerns research on *bay*-substituted mono and dinitro PDI as starting building blocks for the development of new reactivity in the PDI series with the design and synthesis of new target PDI derivatives. It includes literature overviews of the different synthetic pathways undertaken, the developed synthesis, optical and electrochemical properties of the compounds obtained.

Chapter III concerns the effect of side chain substituents on self-assembly of PDI dimers and their solar cell performance. It includes a literature overview of PDI dimers used in organic solar cells, the design and synthesis of the target PDI dimer, comparative studies of their physical properties, thin film morphologies, and solar cell performance.

Chapter IV describes the use of mono-amino PDI as starting building block for the design and synthesis of the target PDI derivatives. It covers a discussion of the amino-PDI reactivity, optical and electrochemical analysis as well as an initial study of solar cell performance of some PDI derivatives.

By developing this chemistry around *bay* substituted PDI, we have reached different original acceptor systems, some of which were applied in organic solar cells. Therefore, synthesis of new PDI derivatives, discussion about their optical and electronic properties, in addition to their application as n-type materials in organic solar cells will be given in the following chapters.

I.6 References

[1] C. Huang, S. Barlow, S. R. Marder, *The Journal of Organic Chemistry* **2011**, *76*, 2386–2407.

[2] M. Kardos, *Ber. Dtsch. Chem. Ges.* **1913**, *46*, 2086–2091.

[3] G. Battagliarin, C. Li, V. Enkelmann, K. Müllen, *Organic Letters* **2011**, *13*, 3012–3015.

[4] J. E. Anthony, A. Facchetti, M. Heeney, S. R. Marder, X. Zhan, *Advanced Materials* **2010**, *22*, 3876–3892.

[5] R. Schmidt, J. H. Oh, Y.-S. Sun, M. Deppisch, A.-M. Krause, K. Radacki, H. Braunschweig, M. Könemann, P. Erk, Z. Bao, et al., *Journal of the American Chemical Society* **2009**, *131*, 6215–6228.

[6] B. A. Jones, M. J. Ahrens, M.-H. Yoon, A. Facchetti, T. J. Marks, M. R. Wasielewski, *Angewandte Chemie* **2004**, *116*, 6523–6526.

[7] B. J. Jung, N. J. Tremblay, M.-L. Yeh, H. E. Katz, *Chem. Mater.* **2011**, *23*, 568–582.

[8] C. d. Dimitrakopoulos, P. r. l. Malenfant, *Adv. Mater.* **2002**, *14*, 99–117.

[9] X. Zhan, A. Facchetti, S. Barlow, T. J. Marks, M. A. Ratner, M. R. Wasielewski, S. R. Marder, *Adv. Mater.* **2011**, *23*, 268–284.

[10] P. Ranke, I. Bleyl, J. Simmerer, D. Haarer, A. Bacher, H. W. Schmidt, *Appl. Phys. Lett.* **1997**, *71*, 1332–1334.

[11] A. Kraft, A. C. Grimsdale, A. B. Holmes, *Angew. Chem. Int. End Engl* **1998**, *37*, 402–428.

[12] M. A. Angadi, D. Gosztola, M. R. Wasielewski, *Materials Science and Engineering: B* **1999**, *63*, 191–194.

[13] D. Sun, D. Meng, Y. Cai, B. Fan, Y. Li, W. Jiang, L. Huo, Y. Sun, Z. Wang, *J. Am. Chem. Soc.* **2015**, *137*, 11156–11162.

[14] X. Zhan, Z. Tan, B. Domercq, Z. An, X. Zhang, S. Barlow, Y. Li, D. Zhu, B. Kippelen, S. R. Marder, *Journal of the American Chemical Society* **2007**, *129*, 7246–7247.

[15] L. Schmidt-Mende, *Science* **2001**, *293*, 1119–1122.

[16] C. Li, H. Wonneberger, *Adv. Mater.* **2012**, *24*, 613–636.

[17] E. Rusen, A. Mocanu, L. C. Nistor, P. Hudhomme, A. Diacon, *RSC Adv.* **2015**, *5*, 28228–28232.

[18] M. Sun, K. Müllen, M. Yin, *Chem. Soc. Rev.* **2016**, *45*, 1513–1528.

[19] M. Yi, J. Yi, J. Wang, L. Wang, W. Gao, Y. Lin, Q. Luo, H. Tan, C.-Q. Ma, H. Wang, *Dyes and Pigments* **2017**, *139*, 498–508.

[20] S. Nakazono, S. Easwaramoorthi, D. Kim, H. Shinokubo, A. Osuka, *Organic Letters* **2009**, *11*, 5426–5429.

[21] M.-X. Zhang, G.-J. Zhao, *ChemSusChem* **2012**, *5*, 879–887.

[22] Y. Zhao, M. R. Wasielewski, *Tetrahedron Letters* **1999**, *40*, 7047–7050.

[23] F. Würthner, *Chem. Commun.* **2004**, 1564–1579.

[24] F. Würthner, V. Stepanenko, Z. Chen, C. R. Saha-Möller, N. Kocher, D. Stalke, *J. Org. Chem.* **2004**, *69*, 7933–7939.

[25] Y. Avlasevich, C. Li, K. Müllen, *Journal of Materials Chemistry* **2010**, *20*, 3814.

[26] C. Li, H. Wonneberger, *Advanced Materials* **2012**, *24*, 613–636.

[27] W. Herbst, K. Hunger, *Industrial Organic Pigments: Production, Properties, Applications*, John Wiley & Sons, **2006**.

[28] S. Demmig, H. Langhals, *Chemische Berichte* **1988**, *121*, 225–230.

[29] C. W. Struijk, A. B. Sieval, J. E. J. Dakhorst, M. van Dijk, P. Kimkes, R. B. M. Koehorst, H. Donker, T. J. Schaafsma, S. J. Picken, A. M. van de Craats, et al., *Journal of the American Chemical Society* **2000**, *122*, 11057–11066.

[30] G. Türkmen, S. Erten-Ela, S. Icli, *Dyes and Pigments* **2009**, *83*, 297–303.

[31] V. Percec, E. Aqad, M. Peterca, M. Imam, M. Glodde, T. Bera, Y. Miura, V. K. Balagurusamy, P. Ewbank, F. Würthner, et al., *Chemistry - A European Journal* **2007**, *13*, 3330–3345.

[32] M.-C. Yuan, M.-H. Su, M.-Y. Chiu, K.-H. Wei, *Journal of Polymer Science Part A: Polymer Chemistry* **2010**, *48*, 1298–1309.

[33] J. H. Hurenkamp, W. R. Browne, R. Augulis, A. Pugžlys, P. H. M. van Loosdrecht, J. H. van Esch, B. L. Feringa, *Organic & Biomolecular Chemistry* **2007**, *5*, 3354.

[34] F. Würthner, C. Thalacker, S. Diele, C. Tschierske, *Chem. Eur. J.* **2001**, *7*, 2245–2253.

[35] S. Chen, Y. Liu, W. Qiu, X. Sun, Y. Ma, D. Zhu, *Chemistry of Materials* **2005**, *17*, 2208–2215.

[36] E. Kozma, F. Munno, D. Kotowski, F. Bertini, S. Luzzati, M. Catellani, *Synthetic Metals* **2010**, *160*, 996–1001.

[37] M. Funahashi, M. Yamaoka, K. Takenami, A. Sonoda, *Journal of Materials Chemistry C* **2013**, *1*, 7872.

[38] M. J. Ahrens, R. F. Kelley, Z. E. X. Dance, M. R. Wasielewski, *Physical Chemistry Chemical Physics* **2007**, *9*, 1469.

[39] F. Donati, A. Pucci, C. Cappelli, B. Mennucci, G. Ruggeri, *The Journal of Physical Chemistry B* **2008**, *112*, 3668–3679.

[40] S. H. Oh, B. G. Kim, S. J. Yun, M. Maheswara, K. Kim, J. Y. Do, *Dyes and Pigments* **2010**, *85*, 37–42.

[41] D. K. Mohamad, A. Fischereder, H. Yi, A. J. Cadby, D. G. Lidzey, A. Iraqi, *J. Mater. Chem.* **2011**, *21*, 851–862.

[42] Y. Huang, L. Fu, W. Zou, F. Zhang, *New Journal of Chemistry* **2012**, *36*, 1080.

[43] G. Boobalan, P. M. Imran, S. Nagarajan, *Superlattices and Microstructures* **2012**, *51*, 921–932.

[44] A. Senthilraja, B. Krishnakumar, M. Swaminathan, S. Nagarajan, *New J. Chem.* **2014**, *38*, 1573–1580.

[45] A. D. Hendsbee, J.-P. Sun, W. K. Law, H. Yan, I. G. Hill, D. M. Spasyuk, G. C. Welch, *Chem. Mater.* **2016**, *28*, 7098–7109.

[46] L. Zhang, L. Wang, G. Zhang, J. Yu, X. Cai, M. Teng, Y. Wu, *Chinese Journal of Chemistry* **2012**, *30*, 2823–2826.

[47] R. Narayan, P. Kumar, K. S. Narayan, S. K. Asha, *Advanced Functional Materials* **2013**, *23*, 2033–2043.

[48] M.-A. Tehfe, F. Dumur, B. Graff, D. Gigmes, J.-P. Fouassier, J. Lalevée, *Macromolecular Chemistry and Physics* **2013**, *214*, 1052–1060.

[49] L. Perrin, P. Hudhomme, *European Journal of Organic Chemistry* **2011**, *2011*, 5427–5440.

[50] F. Rigodanza, E. Tenori, A. Bonasera, Z. Syrgiannis, M. Prato, *European Journal of Organic Chemistry* **2015**, *2015*, 5060–5063.

[51] Y. Nagao, T. Naito, Y. Abe, T. Misono, *Dyes and pigments* **1996**, *32*, 71–83.

[52] H. Langhals, R. Ismael, O. Yürük, *Tetrahedron* **2000**, *56*, 5435–5441.

[53] H. Lee, B. Moon, H. C. Ko, W. Choi, S. Kim, *Pyrrole Derivative and Photosensitive Film Using the Same*, **2008**, US7446166B2.

[54] Y. Nagao, *Progress in Organic Coatings* **1997**, *31*, 43–49.

[55] H. Langhals, C. Dietl, A. Zimpel, P. Mayer, *The Journal of Organic Chemistry* **2012**, *77*, 5965–5970.

[56] P. Rajasingh, R. Cohen, E. Shirman, L. J. W. Shimon, B. Rybtchinski, *J. Org. Chem.* **2007**, *72*, 5973–5979.

[57] B. Dhokale, T. Jadhav, Y. Patil, R. Misra, *Dyes and Pigments* **2016**, *134*, 164–170.

[58] D. Meng, H. Fu, C. Xiao, X. Meng, T. Winands, W. Ma, W. Wei, B. Fan, L. Huo, N. L. Doltsinis, et al., *J. Am. Chem. Soc.* **2016**, *138*, 10184–10190.

[59] D. Sun, D. Meng, Y. Cai, B. Fan, Y. Li, W. Jiang, L. Huo, Y. Sun, Z. Wang, *Journal of the American Chemical Society* **2015**, *137*, 11156–11162.

[60] H. Langhals, S. Kirner, *Eur. J. Org. Chem.* **2000**, *2000*, 365–380.

[61] K.-Y. Chen, T. J. Chow, *Tetrahedron Letters* **2010**, *51*, 5959–5963.

[62] J. M. Mellor, S. Mittoo, R. Parkes, R. W. Millar, *Tetrahedron* **2000**, *56*, 8019–8024.

[63] D. Meng, D. Sun, C. Zhong, T. Liu, B. Fan, L. Huo, Y. Li, W. Jiang, H. Choi, T. Kim, et al., *Journal of the American Chemical Society* **2016**, *138*, 375–380.

[64] L. Zhang, Y. Wang, J. Yu, G. Zhang, X. Cai, Y. Wu, L. Wang, *Tetrahedron Letters* **2013**, *54*, 4019–4022.

[65] P. Singh, L. S. Mittal, V. Vanita, K. Kumar, A. Walia, G. Bhargava, S. Kumar, *J. Mater. Chem. B* **2016**, *4*, 3750–3759.

[66] P. Singh, K. Kumar, G. Bhargava, S. Kumar, *J. Mater. Chem. C* **2016**, *4*, 2488–2497.

[67] R. El-Berjawi, P. Hudhomme, *Dyes and Pigments* **2018**, *159*, 551–556.

[68] K.-Y. Chen, T.-C. Fang, M.-J. Chang, *Dyes and Pigments* **2012**, *92*, 517–523.

[69] Z. J. Chen, L. M. Wang, G. Zou, L. Zhang, G. J. Zhang, X. F. Cai, M. S. Teng, *Dyes and Pigments* **2012**, *94*, 410–415.

[70] G. Li, Y. Zhao, J. Li, J. Cao, J. Zhu, X. W. Sun, Q. Zhang, *The Journal of Organic Chemistry* **2015**, *80*, 196–203.

[71] L. Hao, W. Jiang, Z. Wang, *Tetrahedron* **2012**, *68*, 9234–9239.

[72] C. Domínguez, M. J. Baena, S. Coco, P. Espinet, *Dyes and Pigments* **2017**, *140*, 375–383.

[73] M. Franceschin, E. Pascucci, A. Alvino, D. D'Ambrosio, A. Bianco, G. Ortaggi, M. Savino, *Bioorganic & Medicinal Chemistry Letters* **2007**, *17*, 2515–2522.

[74] V. Casagrande, E. Salvati, A. Alvino, A. Bianco, A. Ciammaichella, C. D'Angelo, L. Ginnari-Satriani, A. M. Serrilli, S. Iachettini, C. Leonetti, et al., *J. Med. Chem.* **2011**, *54*, 1140–1156.

[75] C. Huang, W. J. Potscavage, S. P. Tiwari, S. Sutcu, S. Barlow, B. Kippelen, S. R. Marder, *Polymer Chemistry* **2012**, *3*, 2996.

[76] L. Martín-Gomis, G. Rotas, K. Ohkubo, F. Fernández-Lázaro, S. Fukuzumi, N. Tagmatarchis, Á. Sastre-Santos, *Nanoscale* **2015**, *7*, 7437–7444.

[77] G. Rauch, S. Höger, *Chemical Communications* **2014**, *50*, 5659.

[78] L. George, Z. Ahmed, H. Lemmetyinen, A. Efimov, *European Journal of Organic Chemistry* **2015**, *2015*, 584–590.

[79] C. Domínguez, M. J. Baena, S. Coco, P. Espinet, *Dyes and Pigments* **2017**, *140*, 375–383.

[80] J. Choi, C. Sakong, J.-H. Choi, C. Yoon, J. P. Kim, *Dyes and Pigments* **2011**, *90*, 82–88.

[81] J. Y. Kim, C. Sakong, S. Choi, H. Jang, S. H. Kim, K. S. Chang, M. S. Han, J. S. Lee, J. P. Kim, *Dyes and Pigments* **2016**, *131*, 293–300.

[82] L. C. Kasi Viswanath, L. D. Shirtcliff, S. Krishnan, N. V. Handa, K. Darrell Berlin, *Tetrahedron Letters* **2014**, *55*, 4199–4202.

[83] M. Barrejón, S. Pla, I. Berlanga, M. J. Gómez-Escalonilla, L. Martín-Gomis, J. L. G. Fierro, M. Zhang, M. Yudasaka, S. Iijima, H. B. Gobeze, et al., *J. Mater. Chem. C* **2015**, *3*, 4960–4969.

[84] N. Zink-Lorre, E. Font-Sanchis, Á. Sastre-Santos, F. Fernández-Lázaro, *Dyes and Pigments* **2016**, *127*, 9–17.

[85] N. Zink-Lorre, E. Font-Sanchis, Ángela Sastre-Santos, F. Fernández-Lázaro, *Org. Biomol. Chem.* **2016**, *14*, 9375–9383.

[86] Á. J. Jiménez, M. Sekita, E. Caballero, M. L. Marcos, M. S. Rodríguez-Morgade, D. M. Guldi, T. Torres, *Chemistry - A European Journal* **2013**, *19*, 14506–14514.

[87] R. Mishra, J. M. Lim, M. Son, P. Panini, D. Kim, J. Sankar, *Chem. Eur. J.* **2014**, *20*, 5776–5786.

[88] Z. Mahmood, K. Xu, B. Küçüköz, X. Cui, J. Zhao, Z. Wang, A. Karatay, H. G. Yaglioglu, M. Hayvali, A. Elmali, *The Journal of Organic Chemistry* **2015**, *80*, 3036–3049.

[89] W. Yue, Y. Li, W. Jiang, Y. Zhen, Z. Wang, *Org. Lett.* **2009**, *11*, 5430–5433.

[90] Y.-H. Zhang, B.-F. Shi, J.-Q. Yu, *Journal of the American Chemical Society* **2009**, *131*, 5072–5074.

[91] M. Franceschin, A. Alvino, G. Ortaggi, A. Bianco, *Tetrahedron Letters* **2004**, *45*, 9015–9020.

[92] Á. J. Jiménez, F. Spänig, M. S. Rodríguez-Morgade, K. Ohkubo, S. Fukuzumi, D. M. Guldi, T. Torres, *Organic Letters* **2007**, *9*, 2481–2484.

[93] S. Vajiravelu, L. Ramunas, G. Juozas Vidas, G. Valentas, J. Vygintas, S. Valiyaveettil, *Journal of Materials Chemistry* **2009**, *19*, 4268.

[94] J. A. Mikroyannidis, K. Y. Cheung, M. K. Fung, A. B. Djurišić, *Reactive and Functional Polymers* **2010**, *70*, 426–432.

[95] M. Queste, C. Cadiou, B. Pagoaga, L. Giraudet, N. Hoffmann, *New Journal of Chemistry* **2010**, *34*, 2537.

[96] M. Supur, M. E. El-Khouly, J. H. Seok, J. H. Kim, K.-Y. Kay, S. Fukuzumi, *The Journal of Physical Chemistry C* **2010**, *114*, 10969–10977.

[97] M. L. Keshtov, D. Yu. Parashchuk, V. S. Kochurov, D. V. Marochkin, V. P. Perevalov, A. R. Khokhlov, *Doklady Chemistry* **2011**, *440*, 257–262.

[98] G. Balaji, T. S. Kale, A. Keerthi, A. M. Della Pelle, S. Thayumanavan, S. Valiyaveettil, *Organic Letters* **2011**, *13*, 18–21.

[99] H.-Y. Tsai, K.-Y. Chen, *Dyes and Pigments* **2013**, *96*, 319–327.

[100] H.-Y. Tsai, C.-W. Chang, K.-Y. Chen, *Tetrahedron Letters* **2014**, *55*, 884–888.

[101] H.-Y. Tsai, C.-W. Chang, K.-Y. Chen, *Molecules* **2013**, *19*, 327–341.

[102] H.-Y. Tsai, K.-Y. Chen, *Journal of Luminescence* **2014**, *149*, 103–111.

[103] X. Zhang, X. Hao, L. Liu, A.-T. Pham, J. López-Andarias, A. Frontera, N. Sakai, S. Matile, *Journal of the American Chemical Society* **2018**, *140*, 17867–17871.

[104] C.-W. Chang, H.-Y. Tsai, K.-Y. Chen, *Journal of the Chinese Chemical Society* **2014**, *61*, 415–419.

[105] A. W. Freeman, M. Urvoy, M. E. Criswell, *J. Org. Chem.* **2005**, *70*, 5014–5019.

[106] H. Langhals, S. Kirner, *Eur. J. Org. Chem.* **2000**, *2000*, 365–380.

[107] Y. Ma, Z. Shi, A. Zhang, J. Li, X. Wei, T. Jiang, Y. Li, X. Wang, *Dyes and Pigments* **2016**, *135*, 41–48.

[108] M. Schulze, M. Philipp, W. Waigel, D. Schmidt, F. Würthner, *The Journal of Organic Chemistry* **2016**, *81*, 8394–8405.

[109] B. Liang, Y. Zhang, Y. Wang, W. Xu, X. Li, *Journal of Molecular Structure* **2009**, *917*, 133–141.

[110] C. Zhao, Y. Zhang, R. Li, X. Li, J. Jiang, *The Journal of Organic Chemistry* **2007**, *72*, 2402–2410.

[111] H. Langhals, *Heterocycles* **1995**, *1*, 477–500.

[112] M. J. Ahrens, M. J. Fuller, M. R. Wasielewski, *Chemistry of Materials* **2003**, *15*, 2684–2686.

[113] K. Khokhlov, N. J. Schuster, F. Ng, C. Nuckolls, *Organic Letters* **2018**, *20*, 1991–1994.

[114] V. Sivamurugan, K. Kazlauskas, S. Jursenas, A. Gruodis, J. Simokaitiene, J. V. Grazulevicius, S. Valiyaveettil, *J. Phys. Chem. B* **2010**, *114*, 1782–1789.

[115] X. Zhan, Z. Tan, E. Zhou, Y. Li, R. Misra, A. Grant, B. Domercq, X.-H. Zhang, Z. An, X. Zhang, et al., *Journal of Materials Chemistry* **2009**, *19*, 5794.

[116] Z. An, S. A. Odom, R. F. Kelley, C. Huang, X. Zhang, S. Barlow, L. A. Padilha, J. Fu, S. Webster, D. J. Hagan, et al., *J. Phys. Chem. A* **2009**, *113*, 5585–5593.

[117] R. Xin, J. Feng, C. Zeng, W. Jiang, L. Zhang, D. Meng, Z. Ren, Z. Wang, S. Yan, *ACS Applied Materials & Interfaces* **2017**, *9*, 2739–2746.

[118] P. M. Kazmaier, R. Hoffmann, *Journal of the American Chemical Society* **1994**, *116*, 9684–9691.

[119] Y. Acikbas, M. Erdogan, R. Capan, F. Yukruk, *Sensors and Actuators B: Chemical* **2014**, *200*, 61–68.

[120] F. Würthner, C. R. Saha-Möller, B. Fimmel, S. Ogi, P. Leowanawat, D. Schmidt, *Chemical Reviews* **2016**, *116*, 962–1052.

[121] W. Huang, D. Yan, Q. Lu, Y. Huang, *European Polymer Journal* **2003**, *39*, 1099–1104.

[122] X. Kong, J. Gao, T. Ma, M. Wang, A. Zhang, Z. Shi, Y. Wei, *Dyes and Pigments* **2012**, *95*, 450–454.

[123] X. Kong, J. Gao, T. Ma, M. Wang, A. Zhang, Z. Shi, Y. Wei, *Dyes and Pigments* **2012**, *95*, 450–454.

[124] H. Z. Chen, M. M. Ling, X. Mo, M. M. Shi, M. Wang, Z. Bao, *Chem. Mater.* **2007**, *19*, 816–824.

[125] B. A. Jones, A. Facchetti, M. R. Wasielewski, T. J. Marks, *J. Am. Chem. Soc.* **2007**, *129*, 15259–15278.

[126] L. Perrin, P. Hudhomme, *European Journal of Organic Chemistry* **2011**, *2011*, 5427–5440.

[127] W. Suk Shin, H.-H. Jeong, M.-K. Kim, S.-H. Jin, M.-R. Kim, J.-K. Lee, J. Wook Lee, Y.-S. Gal, *Journal of Materials Chemistry* **2006**, *16*, 384–390.

[128] F. Würthner, *Chemical Communications* **2004**, *0*, 1564–1579.

[129] Y. Shibano, H. Imahori, C. Adachi, *J. Phys. Chem. C* **2009**, *113*, 15454–15466.

[130] A. Nowak-Król, F. Würthner, *Org. Chem. Front.* **2019**, *6*, 1272–1318.

[131] Y. Lin, X. Zhan, *Materials Horizons* **2014**, *1*, 470.

[132] J. C. Bernede, *Journal of the Chilean Chemical Society* **2008**, *53*, 1549–1564.

[133] Y. Duan, X. Xu, Y. Li, Q. Peng, *Chinese Chemical Letters* **2017**, *28*, 2105–2115.

[134] B. Kippelen, J.-L. Brédas, *Energy & Environmental Science* **2009**, *2*, 251–261.

[135] C. J. Brabec, N. S. Sariciftci, J. C. Hummelen, *Advanced Functional Materials* **2001**, *11*, 15–26.

[136] A. F. Eftaiha, J.-P. Sun, I. G. Hill, G. C. Welch, *J. Mater. Chem. A* **2014**, *2*, 1201–1213.

[137] Z. He, C. Zhong, X. Huang, W.-Y. Wong, H. Wu, L. Chen, S. Su, Y. Cao, *Advanced Materials* **2011**, *23*, 4636–4643.

[138] W. J. Potscavage, A. Sharma, B. Kippelen, *Acc. Chem. Res.* **2009**, *42*, 1758–1767.

[139] A. Mishra, P. Bäuerle, *Angewandte Chemie International Edition* **2012**, *51*, 2020–2067.

[140] C. Nicolet, D. Deribew, C. Renaud, G. Fleury, C. Brochon, E. Cloutet, L. Vignau, G. Wantz, H. Cramail, M. Geoghegan, et al., *J. Phys. Chem. B* **2011**, *115*, 12717–12727.

[141] B. C. Thompson, J. M. J. Fréchet, *Angewandte Chemie International Edition* **2008**, *47*, 58–77.

[142] G. Yu, J. Gao, J. C. Hummelen, F. Wudl, A. J. Heeger, *Science* **1995**, *270*, 1789–1791.

[143] Z. He, C. Zhong, S. Su, M. Xu, H. Wu, Y. Cao, *Nature Photonics* **2012**, *6*, 591–595.

[144] M. S. White, D. C. Olson, S. E. Shaheen, N. Kopidakis, D. S. Ginley, *Applied Physics Letters* **2006**, *89*, 143517.

[145] S. K. Hau, H.-L. Yip, J. Zou, A. K.-Y. Jen, *Organic Electronics* **2009**, *10*, 1401–1407.

[146] Z. Xu, L.-M. Chen, G. Yang, C.-H. Huang, J. Hou, Y. Wu, G. Li, C.-S. Hsu, Y. Yang, *Advanced Functional Materials* **2009**, *19*, 1227–1234.

[147] Y. Zhong, M. T. Trinh, R. Chen, G. E. Purdum, P. P. Khlyabich, M. Sezen, S. Oh, H. Zhu, B. Fowler, B. Zhang, et al., *Nature Communications* **2015**, *6*, DOI 10.1038/ncomms9242.

[148] C. Li, H. Wonneberger, *Advanced Materials* **2012**, *24*, 613–636.

[149] J. Zhang, Y. Li, J. Huang, H. Hu, G. Zhang, T. Ma, P. C. Y. Chow, H. Ade, D. Pan, H. Yan, *J. Am. Chem. Soc.* **2017**, *139*, 16092–16095.

[150] P. M. Beaujuge, J. M. J. Fréchet, *J. Am. Chem. Soc.* **2011**, *133*, 20009–20029.

[151] S. Günes, H. Neugebauer, N. S. Sariciftci, *Chem. Rev.* **2007**, *107*, 1324–1338.

[152] Y. Sun, G. C. Welch, W. L. Leong, C. J. Takacs, G. C. Bazan, A. J. Heeger, *Nature Mater* **2012**, *11*, 44–48.

[153] W. Jiang, L. Ye, X. Li, C. Xiao, F. Tan, W. Zhao, J. Hou, Z. Wang, *Chemical Communications* **2014**, *50*, 1024–1026.

[154] L. Ye, W. Jiang, W. Zhao, S. Zhang, D. Qian, Z. Wang, J. Hou, *Small* **2014**, *10*, 4658–4663.

[155] Y. Lin, Y. Wang, J. Wang, J. Hou, Y. Li, D. Zhu, X. Zhan, *Adv. Mater.* **2014**, *26*, 5137–5142.

[156] H. Fu, D. Meng, X. Meng, X. Sun, L. Huo, Y. Fan, Y. Li, W. Ma, Y. Sun, Z. Wang, *J. Mater. Chem. A* **2017**, *5*, 3475–3482.

[157] B. Wang, W. Liu, H. Li, J. Mai, S. Liu, X. Lu, H. Li, M. Shi, C.-Z. Li, H. Chen, *Journal of Materials Chemistry A* **2017**, *5*, 9396–9401.

[158] Q. Wu, D. Zhao, J. Yang, V. Sharapov, Z. Cai, L. Li, N. Zhang, A. Neshchadin, W. Chen, L. Yu, *Chem. Mater.* **2017**, *29*, 1127–1133.

[159] R. Singh, J. Lee, M. Kim, P. E. Keivanidis, K. Cho, *Journal of Materials Chemistry A* **2017**, *5*, 210–220.

[160] C. W. Tang, *Appl. Phys. Lett.* **1986**, *48*, 183–185.

Chapter II : New reactivities of nitro-*bay* substituted PDI

II.1 Suzuki-Miyaura reaction employing mono bromo-*bay* PDI

II.1.1 Cross-coupling reactions: General overview

Synthesis in organic chemistry is based mostly on the creation of carbon-carbon (C-C) bond to produce π-conjugated systems of alkenes, styrenes, or biaryl compounds, in which the corresponding reactions are catalyzed by the presence of a transition metal. Transition metal (TM)- catalyzed cross-coupling reactions have been an important contributing factor to the advances reached in organic electronics as efficient synthetic methods for coupling aromatic π-conjugated systems. Among the various utilized methodologies centered on Pd-catalyzed reactions between aryl or alkenyl halides and organometallic compounds (Negishi coupling (Zn), Stille coupling (Sn), Hiyama coupling (Si), Heck coupling (terminal alkenes and Sonogashira coupling (alkynes)), palladium-catalyzed Suzuki–Miyaura (SM) is particularly valued for the huge impact it caused in organic synthesis since 1981.[1]

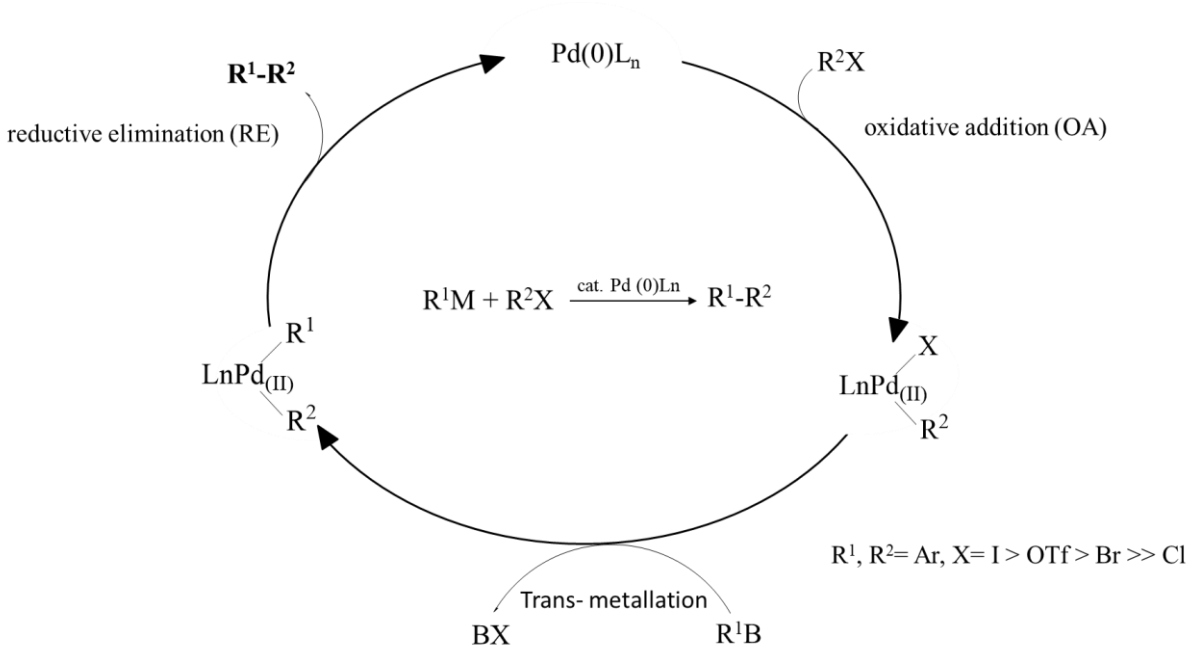

Figure II-1 General mechanism of Suzuki-Miyaura cross coupling reaction.

Main advantages are the mild reaction conditions, commercial availability of diverse boronic acids and esters that are less toxic than other organometallic reagents, ease of by-products removal and product isolation. SMC reactions conventionally employ boron nucleophiles and aryl electrophiles. It proceeds in the presence of base and a palladium catalyst. A general reaction mechanism is shown in Figure II-1,[2] where it consists of three steps: (i) oxidative

addition (OA) of R^2X to $Pd(0)L_n$ species, where L_n represents a shell of coordinating ligands, (ii) trans-metallation between $R^2Pd(II)L_nX$ and R^1M, and (iii) reductive elimination (RE) of $R^1R^2Pd(II)L_n$ to give $\mathbf{R^1R^2}$ via C-C bond formation.

Commonly, the use of a base is known to accelerate the transmetallation step. Among the most suitable bases used for SMC, are Na_2CO_3, K_3PO_4, K_2CO_3 and Cs_2CO_3. As for the catalyst, the most frequently used is the $Pd(PPh_3)_4$, others catalysts such as $PdCl_2(dppf)$, $PdCl_2(PPh_3)_2$ and $Pd(OAc)_2$ could be also seen in such reactions. The solvent employed also plays an important role in the rate of the cross-coupling, generally, THF, DMF, DMSO, dioxane and toluene are employed.[3]

II.1.1 Preparing PDI derivatives starting from mono bromo PDI

A wide range of PDI derivatives were reported following SMC reaction employing mono-bromo *bay* substituted PDI with various nucleophilic derivatives. The selection of the catalyst, $Pd(PPh_3)_4$, is repeatedly reported to be constant. However, the choice of solvent and base employed are reported to be different even with the same starting materials.

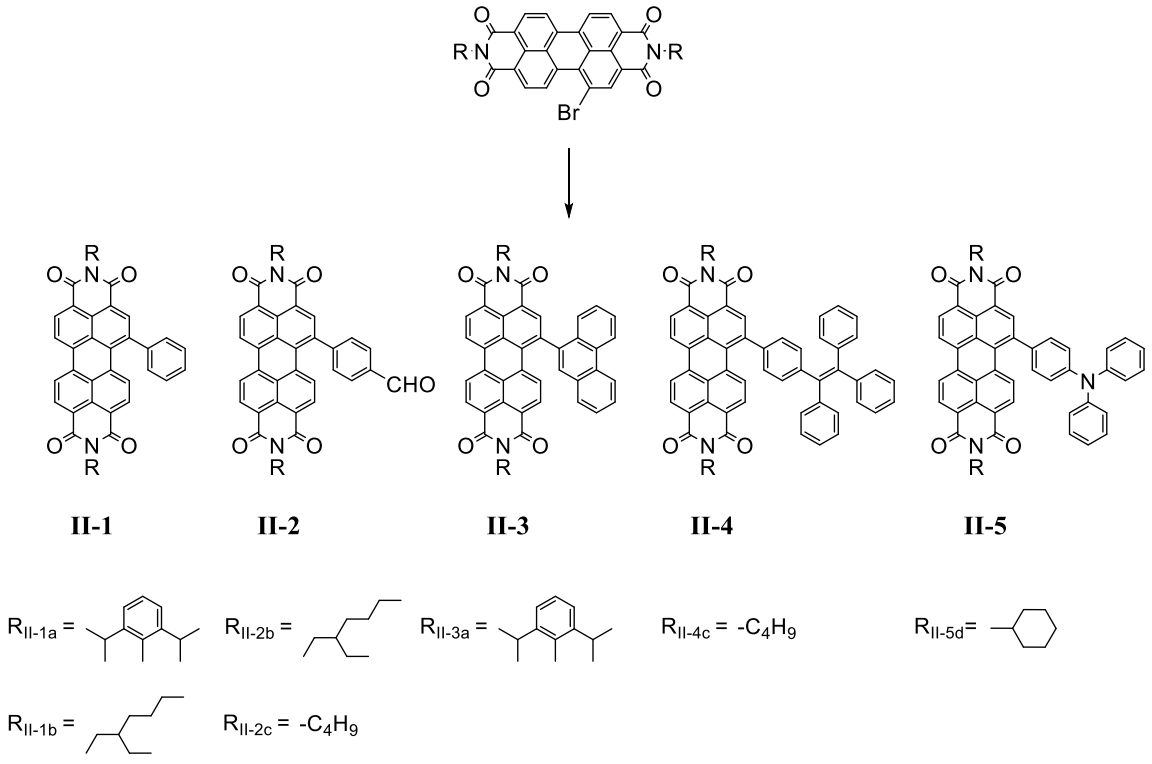

Figure II-2 Suzuki-Miyaura cross coupling reaction starting from mono bromo PDI.

This might have small or large effect on the yields obtained. For example, the yield of **II-1b** is reported to be 41% using phenylboronic acid,[4] in the presence of Na_2CO_3 as the base and 2-

methoxyethanol/H_2O as solvent and 56% when the base and solvents employed where respectively K_2CO_3 and Toluene/EtOH/H_2O.[5]

Performing the reaction under the same conditions, while excluding water, compound **II-1a** is obtained in 82% yield.[6] Comparable yields were obtained for **II-2b** (72%) and **II-2c** (78%) upon carrying both reactions with 4-boronic acid benzaldehyde, in the presence of CsF, Ag_2O in THF and Na_2CO_3 in 2-methoxyethanol/H_2O, respectively.[4,7] This is also observed for **II-3a** (50%) and **II-5d** (49%), with 9-phenanthreneboronic acid and triphenylamine boronic acid respectively.[8,9] However, the base (K_2CO_3) and the solvent (THF) employed are the same, except the additional use of water as co-solvent to obtain **II-3a**.

Compound **II-4c** was obtained with tetraphenylethene boronic acid in 51% yields, in the presence Na_2CO_3 in THF.[10] The products obtained (Figure II-2) were studied either as final compounds or as intermediates for the preparation of PDI dyads or dimers,[4,7,11–15] applied in different domains.

As mentioned earlier, the general procedure for the formation of mono-brominated PDI includes stirring the unsubstituted PDI with excess of bromine in CH_2Cl_2 or $CHCl_3$ for several hours. The reaction success depends to an important degree on the *N,N'* imide substituents and the solubility of the forming product, as PDIs have generally low reactivity towards electrophiles. This was firstly demonstrated by H. Langhals *and coll*,[16] in addition to the lack of selectivity of such reactions where in many cases, a concomitant introduction of a second bromine atom occurs during the course of the reaction leading to a mixture of 1,6 and 1,7 dibrominated PDI.[17,18]

II.2 Suzuki-Miyaura reaction employing mono nitro-*bay* PDI

II.2.1 Cross-coupling reaction using nitroarenes as electrophiles: An overview

In 2017, M.Yadav *et al*.[19] have reported the first pallado-catalyzed Suzuki-Miyaura reaction using nitroarene as electrophiles instead of arylhalides, in which the nitro group (NO_2) acts as the leaving group. Nitroarenes are known to be widely used in organic synthesis reactions, such as nucleophilic substitution reactions, in which the NO_2 group also plays the same role. Compared to halogenated aromatics, the preparation of nitroarenes is direct and more selective toward the monofunctionalization, where in some cases, a mixture of mono- and dihalogenated aromatics is obtained upon halogenation of the respective arenes. The selection of reaction parameters, such as metal catalysts, ligands, solvents and bases had an important effect on the

yield of the compounds obtained. For example, BrettPhos was found to be the most effective ligand among others employed, such as Buchwald's ligands, SPhos, RuPhos, and CPhos. The use of 18-crown-6 is reported to be essential for increasing the yields of the reactions. Concerning the catalyst, $Pd(PPh_3)_4$ showed to be ineffective, in contrast to using $Pd(acac)_2$. Studies of the impact of bases used onto the progress of the reaction showed that Cs_2CO_3 and K_2CO_3 did not yield the desired compound, while CsF and K_3PO_4 afforded the targeted biaryl. However, the presence of water with dried K_3PO_4 seemed more important, as its presence recaptured the reactivity. As for the solvent, toluene or THF resulted in a diminished yield, as reported. Hence, the optimized conditions for the reported SMC reaction of nitroarenes with arylboronic acids were using $Pd(acac)_2$, BrettPhos, 18-crown-6 and K_3PO_4. nH_2O in 1,4-dioxane at 130 °C for 24 h. The mechanism for this reaction was also proposed (Figure II-3), in which the catalytic cycle is initiated by the formation of a nitroarene−Pd complex, from which the oxidative addition of the Ar−NO_2 bond occurs. Transmetalation between the resulting Pd(II) intermediate and the arylboronic acid, followed by reductive elimination, generates the biaryl.

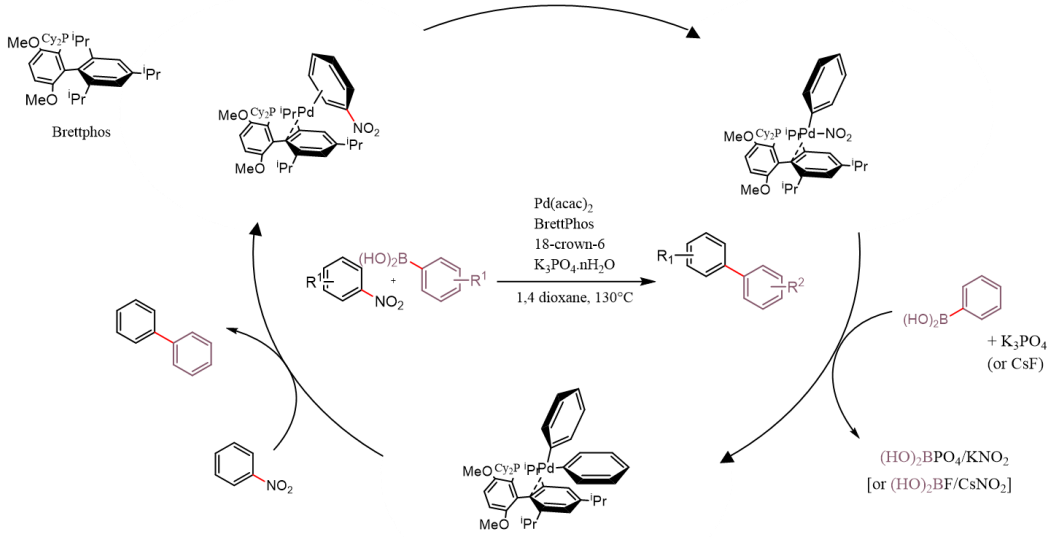

Figure II-3 Proposed mechanism of Suzuki-Miyaura cross coupling reaction employing nitroarenes.[19]

II.2.2 Preparing PDI derivatives starting from mono nitro PDI

Subsequently, we were interested in the construction of C-C bond starting from the mono-nitro PDI to study their potential in SMC reactions. As mentioned earlier, monohalogenation reaction

in the PDI series is considered difficult to control due to the ease of access to dibromo derivatives. The poor selectivity of bromination reaction causes, in some cases, the concomitant introduction of a second bromine atom yielding a mixture of 1,6- and 1,7-dibrominated PDI. Indeed, the reaction dependence on the imide substituents incorporated, and therefore the solubility of the PDI determines the difficulty level for obtaining the mono-bromo compound. For example, PDIs with cyclohexyl groups at the imide positions was shown to be not accessible even upon reflux in CH_2Cl_2 for 4 days, where only a mixture of 1,6- and 1,7-dibrominated regioisomers was obtained. Some other reports indicated the use of the corresponding mono-bromo PDI as starting material, however its preparation was not described.[9]

In contrast, the mononitration reaction was effectively expected to be easier to control compared to the monobromination, due to the inductive and mesomeric electron-withdrawing effects of the nitro group which sufficiently deactivates the PDI core towards the second electrophilic substitution. Moreover, the advantage of the nitro group results in an interesting better atom economy process. Discussion about the preparation of some PDI series (with *N,N'* dicyclohexyl imide groups) using the Suzuki-Miyaura coupling reaction carried out on mono-nitro PDI as electrophile is given as follows with the aim of reaching PDI-C_{60} dyad as a target molecule.

II.2.2.1 Preparation of the starting material: Mono-nitro PDI

First, starting material PTCDA **1** was transformed in 98% yield into compound **2** by an imidization reaction using cyclohexylamine in refluxing DMF as a more simplified and modified procedure than those reported.[20–22] Concerning the electrophilic aromatic nitration reaction, following the procedure described[23] (HNO_3 0.1M in the presence of cerium ammonium nitrate (CAN)) did not afford the desired molecule. On the contrary, we have shown that the nitration reaction could be done using fuming nitric acid where the addition of CAN was not improving the yield or favoring the kinetic of the reaction.[24] Mono-nitroPDI **3** was prepared in 93% yield (at room temperature and in short time) in a multigram scale without the need of purification using chromatographic techniques as a new simplified procedure (Figure II-5).[25,26]

To gain insight into the molecular structures and electronic properties of the starting material mono-nitro PDI **3** and to compare it with mono-bromo PDI, quantum chemical calculations were performed using density functional theory (DFT) at the PBE0/6-311+G(2df,2pd) level. The highest occupied molecular orbitals (HOMOs) and the lowest unoccupied molecular orbitals (LUMOs) of both compounds are equal, -6.69 eV and -3.90 eV respectively (Figure II-4). The

HOMO of PDI **3** is delocalized mainly on the perylene core, while the LUMO is extended from the central perylene core to the peripheral nitro and the bisimide groups. In the case of mono-bromo PDI, the HOMO is delocalized mainly on the perylene core and the LUMO is extended from the central perylene core to the bisimide groups.

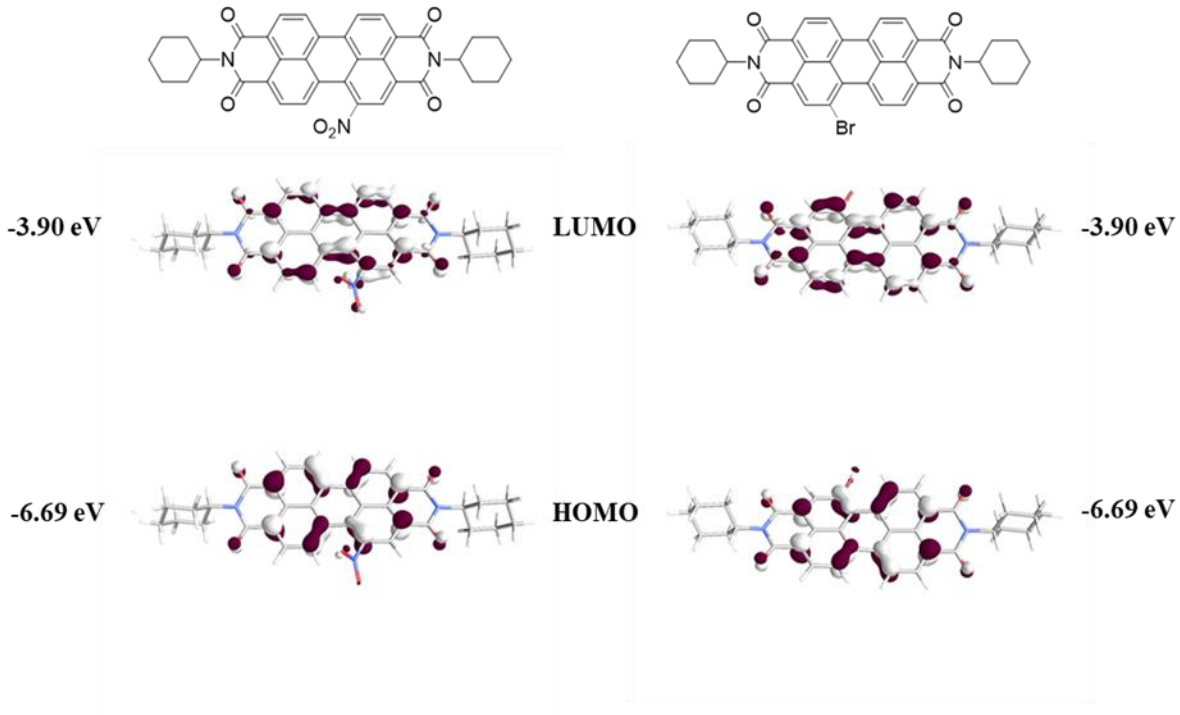

Figure II-4 PBE0/6-311+G(2df,2pd) computed FOs of mono-nitro PDI **3** and mono-bromo PDI. HOMOs (bottom) and LUMOs (top).

II.2.2.2 Synthesis of PDI derivatives

A straightforward and more simplified procedure than the one reported for the nitroarenes was employed for the synthesis of the PDI derivatives.[26] The reaction with 3-formylphenylboronic acid in the presence of $Pd(PPh_3)_4$ and K_3PO_4 as a base in refluxing THF gave, after column chromatography and crystallization, compound **4** in 81% yield (Figure II-5). This reaction corresponds to the first example of SMC reaction using an electron-deficient arene system such as PDI possessing a nitro group as the electrophilic coupling partner. The result obtained indicates that the experimental conditions using mono-nitro PDI and $Pd(PPh_3)_4$ as catalyst (which is also selected in SMC reactions starting from mono-bromo PDI) give good results, in a simplified procedure compared to the case described for other nitroarenes. The reaction was also carried out using different solvents to study their effect on the rate of the reaction. Hence,

CH_2Cl_2 and toluene were employed with which the yields obtained where 9% and 20% respectively, indicating the greatest efficiency of the solvent THF used.

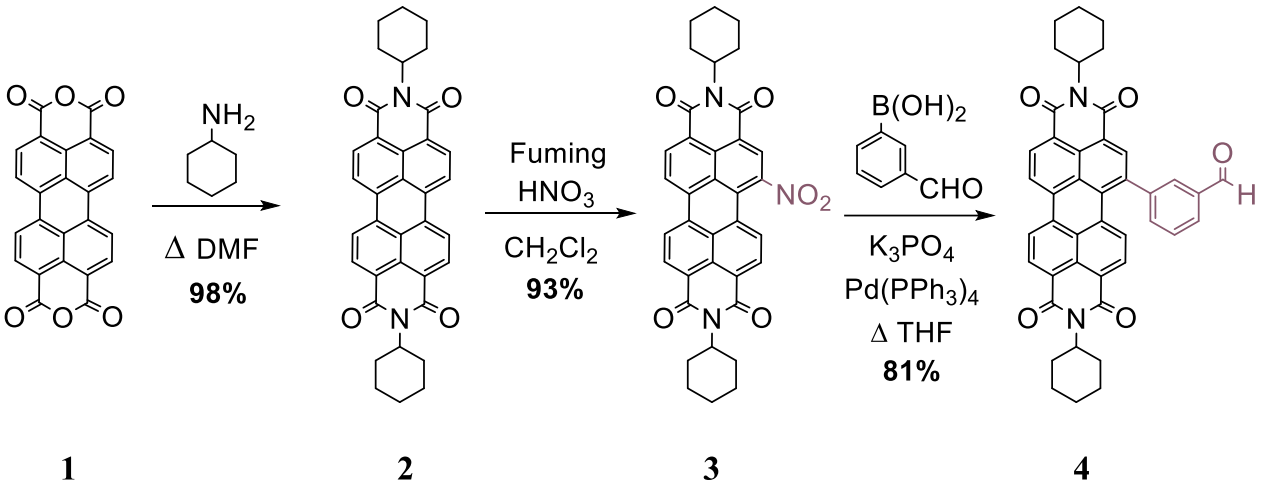

Figure II-5 Suzuki-Miyaura cross coupling reaction starting from mononitro PDI.

Single crystals were obtained by slow evaporation of a solution containing compound **4** in a mixture of $CHCl_3$ and petroleum ether then analyzed by X-ray diffraction (Figure II-6).[26] The crystallographic analysis revealed that the central six-membered ring is slightly twisted with a torsion angle of 11.74 (4)° associated with bay carbons C7-C8-C13-C22 and C9-C10-C15-C14, respectively. On the other hand, the deviation of the phenyl group with respect to the PDI core is equal to 61.03 (9)°.

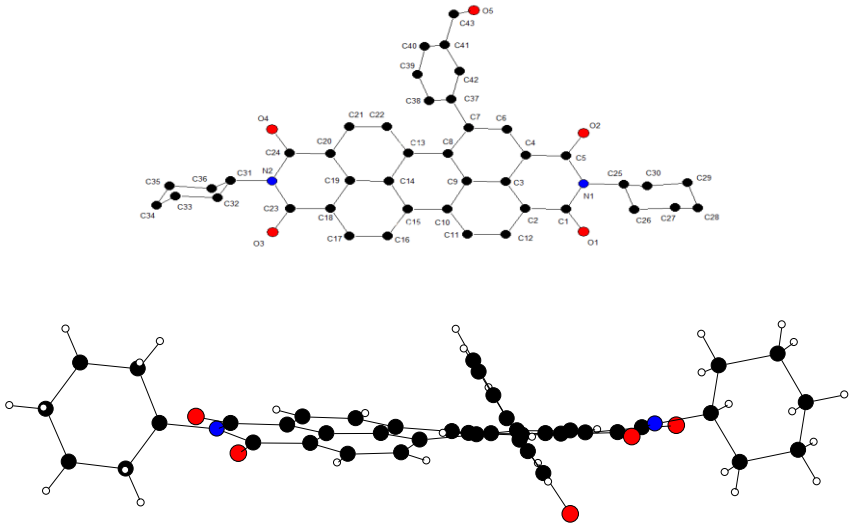

Figure II-6 View of the crystal structure of PDI derivative **4** (top) for determining the twist and distortion angles (down).

Considering that in compound **4** the formyl group in meta position presents only an electron-withdrawing inductive effect, we have investigated the extension of this SMC reaction using a phenyl boronic acid substituted in para position either by an electron-withdrawing group or -donating group by mesomeric effect.

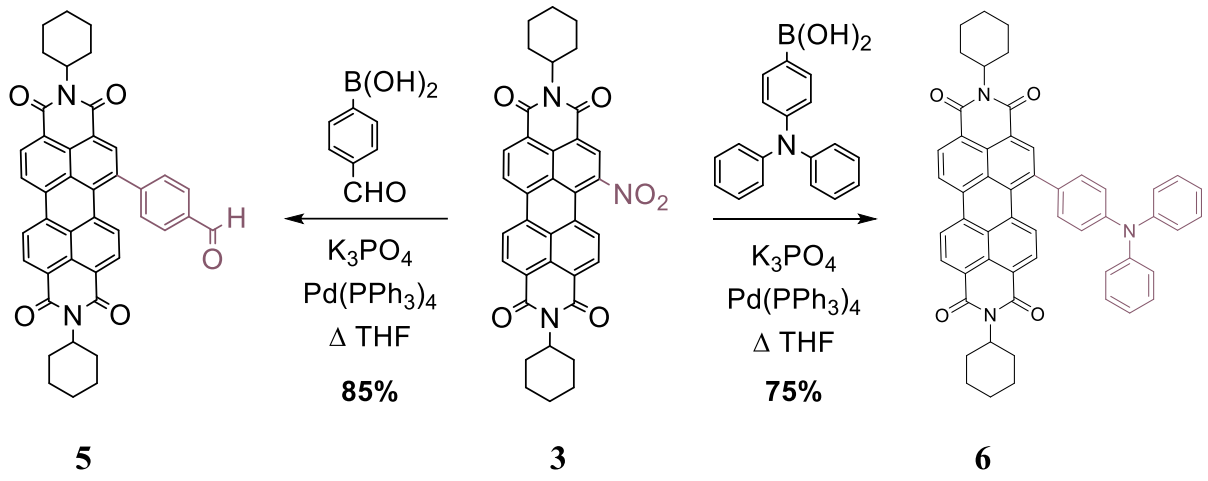

Figure II-7 Other examples of SMC reaction with phenylboronic acid substituted by electron-withdrawing or -donating group.

Reaction with 4-formylphenylboronic acid or (4-diphenylamino)phenylboronic acid gave compound **5** and **6** in 85% and 75% yield, respectively (Figure II-7). In the case of compound **5**, the yield is slightly higher than the one obtained starting from mono-bromo PDI (**II-2c** (78%) and **II-2b** (72%)). This is more pronounced in the case of PDI **6**, which shows more important yield than **II-5 (**49%), obtained from mono-bromoPDI. This demonstrates the versatility of this original SMC reaction which could be used with varied substituted phenylboronic acid derivatives.

II.3 Application to the synthesis of C_{60}-PDI dyad

II.3.1 C_{60}-PDI dyads and applications

In order to take advantage of the solar spectrum coverage of PDIs, intensive efforts have been devoted towards the synthesis of C_{60}-PDI dyads in the search of photoinduced electron and/or energy transfer processes. Fullerene C_{60} derivatives, which absorbs light in the UV/Vis range, have shown excellent three-dimensional electron acceptors, due to their various intrinsic advantages, such as a relatively low-lying LUMO energy level which is thermodynamically favorable to accepting electrons from an excited donor material, and unique stabilization of negative charges reflected by their ability to be reduced up to six electrons.

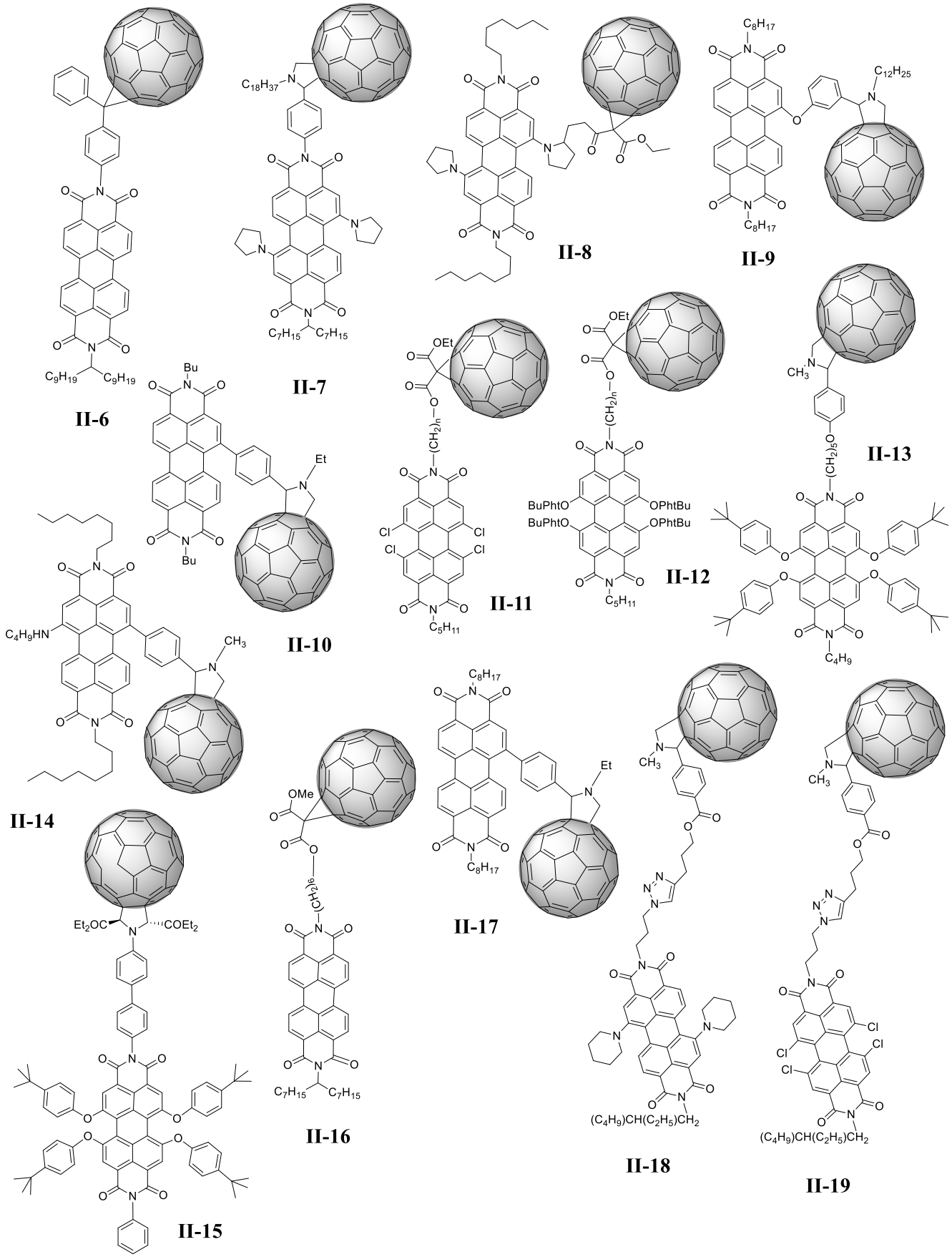

Figure II-8 Examples of PDI-C_{60} dyad where the fullerene is introduced either on the imide or the bay position of PDI.

Their rigid aromatic structures evoke low reorganization energies in electron transfer reactions (similar to the case of the PDI systems), which lead to remarkable acceleration of photo-induced charge separation and charge shift and deceleration of charge recombination. Furthermore, when the two electron acceptor parts are included within the same dyad, both moieties start to compete for the incoming electrons, making it more difficult to predict their location. This may result in an unpaired electron taken by each of the acceptor-acceptor dyad, giving rise to species with a high total electron spin that is essential for molecular electronics and magnetic applications. In most of the described examples, fullerene C_{60} was attached at the imide position of the PDI, [27–34] as shown in Figure II-8. In few examples, C_{60} unit has been linked at the *bay* region of the PDI core,[7,35–38] also shown in Figure II-8, to provide light-harvesting skeleton and solar-energy conversion systems.

Other potential applications include photocatalysis, photooxidation and photodynamic therapy, in which the light-harvesting PDI-C_{60} dyads were prepared as organic triplet photosensitizers,[4,37] replacing the high cost transition metal complex triplet photosensitizers that on contrary absorb weakly in the visible region. It is known that for triplet photosensitizers, efficient intersystem crossing (ISC) occurs with which the triplet excited states of the chromophores are populated upon photoexcitation. This could be achieved by C_{60} in which triplet excited state quantum yield can reach beyond 95%. Having PDI in the same system compensate for C_{60} weak absorption in the visible range. As a result, PDI should play the role of visible light-harvesting antenna, from which the singlet energy transfer (ET) to C_{60} will occur. Then the singlet excited state, and in turn the T_1 excited state of C_{60} will be populated via ISC. From this point, PDI-C_{60}, was prepared as singlet oxygen ($^1O_2$) photosensitizer for photooxidation of 1,5-dihydroxy-naphthalene Figure II-9. J. Zhao *and coll*.[4] reported the synthesis starting from **II-2b**, described above, in which it undergoes a modified Prato reaction using creatine and C_{60} in refluxing toluene. The product **II-20** was obtained in 12% yield, which is lower than the similar dyad **II-10**, previously reported by N.R. Champness *and coll*.,[7] in which Prato reaction on **II-2c** using C_{60} and N-ethylglycine in refluxing toluene afforded the corresponding product in 42% yield.

Studies on **II-20** showed efficient singlet intramolecular energy transfer from PDI to C_{60}, with long-lived triplet excited state, however, T_1 state of the dyad is deduced to be localized on the PDI moiety, instead of C_{60} unit, where upon photoexcitation, backward triplet ET from C_{60} to the PDI moiety occurs producing the PDI localized T_1 state.

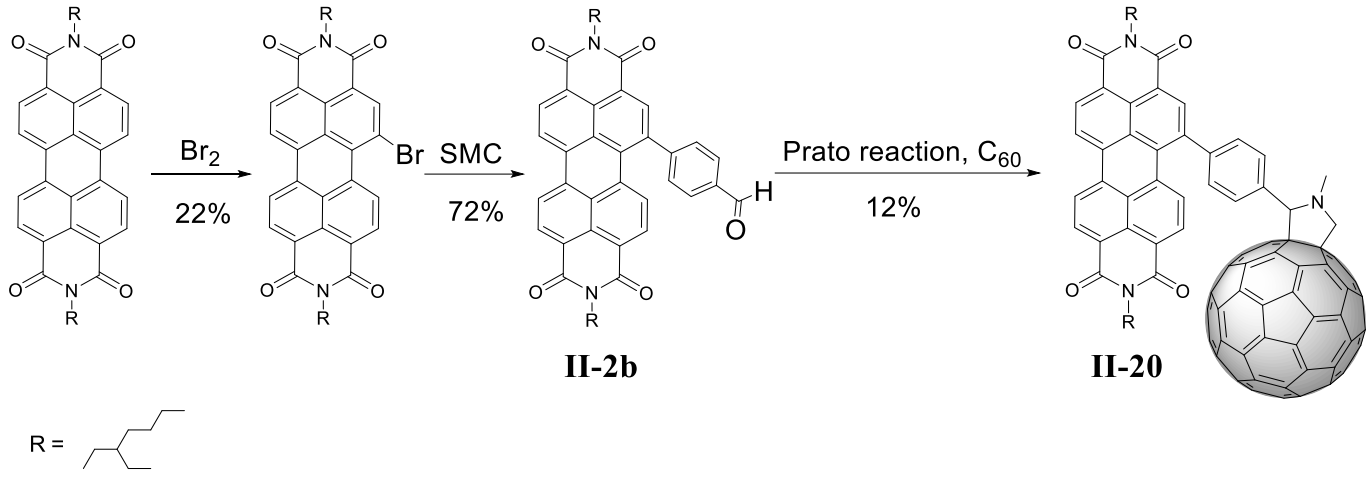

Figure II-9 Reported synthesis of Dyad **II-20**.

Consequently, this visible light harvesting antenna PDI-C_{60} is effective organic triplet photosensitizer, confirming their ability to be used in photocatalysis, photooxidation, and photodynamic therapy (PDT).

II.3.2 Synthesis of PDI-C_{60} Dyad

From all these considerations, we were interested in the synthesis of a PDI-C_{60} dyad using as an intermediate reaction, the efficient and easy SMC reaction using the mono-nitroPDI as described above. The full reaction scheme is shown in Figure II-10.[26] Starting from compound **4**, the subsequent 1,3-dipolar cycloaddition was carried out using C_{60} and N-methylglycine (sarcosine) in o-dichlorobenzene (o-DCB) at 180 °C affording, after purification by silica gel column chromatography, dyad **7** in 20% yield.

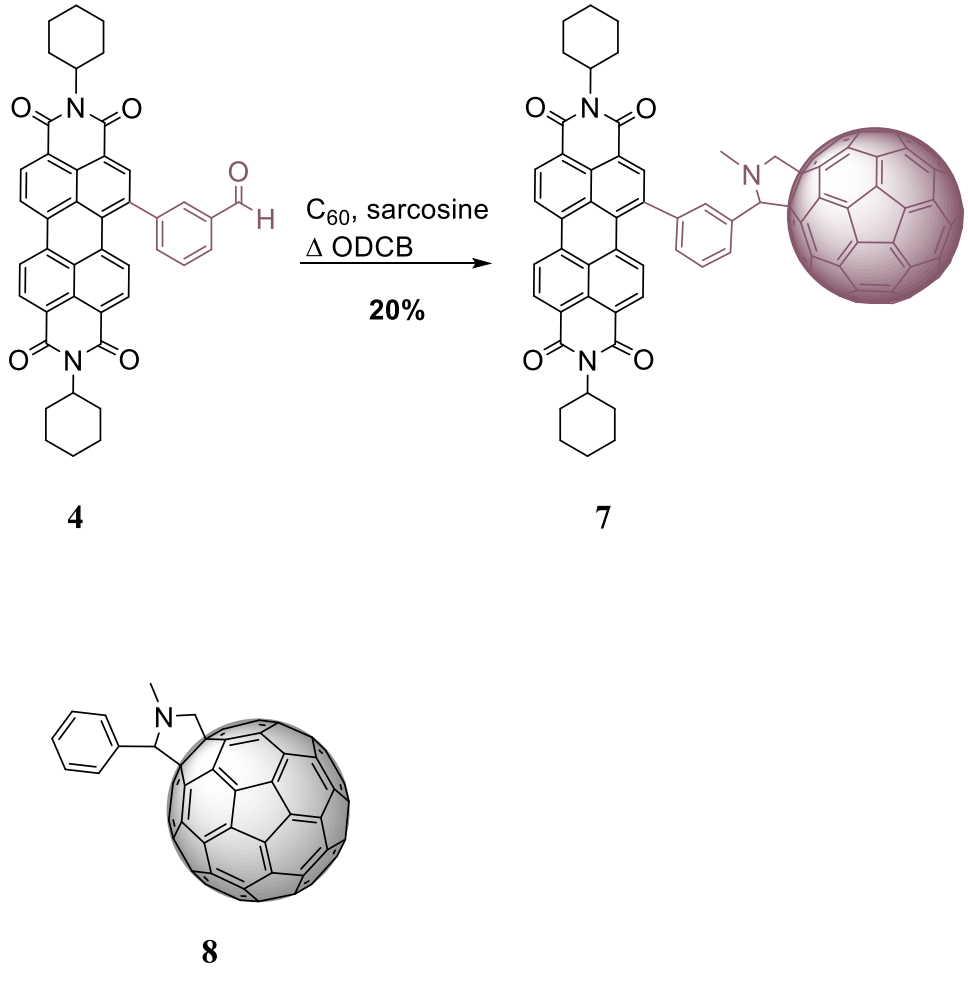

Figure II-10 Synthesis of dyad PDI-C_{60} **7**.

The structure of PDI-C_{60} dyad **7** has been fully characterized through ^{1}H (Figure II-11) and ^{13}C NMR, mass spectrometry (MALDI-TOF and HRMS), and HPLC chromatography (Figure II-12).

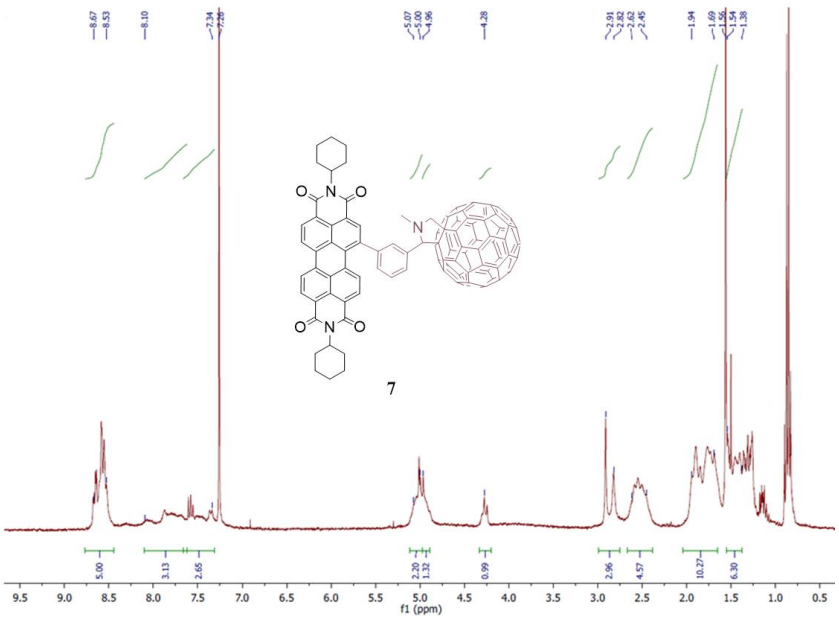

Figure II-11 ^{1}H NMR spectrum of the dyad PDI-C_{60} **7**.

From this technique, the purity of dyad **7** could be estimated to be high up to 99.8%. As a further reference for electrochemical and optical studies, fulleropyrrolidine **8** was prepared using benzaldehyde as the starting material to generate the azomethine ylide **8**.[26]

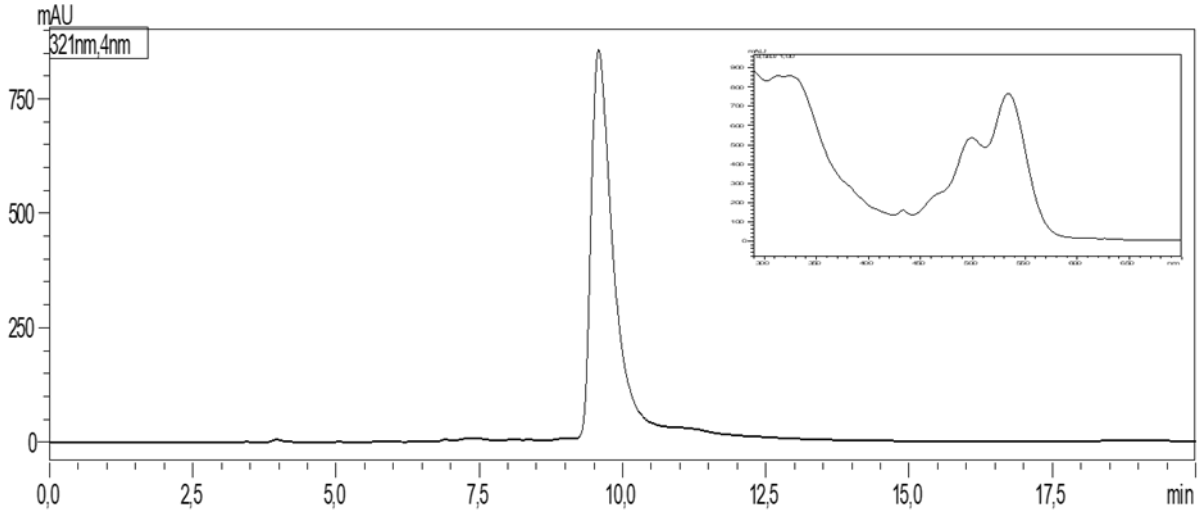

Figure II-12 HPLC chromatogram of compound **7**. Retention time: 9.58 min (eluent: toluene, flow rate: 1ml/min, λ=320nm) the UV spectrum corresponds to the peak.

II.3.2.1 Optical Properties

The optical properties of dyad **7** and PDI derivatives **3** and **4** have been analyzed in diluted CH_2Cl_2 solutions by UV–vis absorption (ca. 10^{-5} M) and photoluminescence emission (ca. 10^{-6}

M) spectroscopy, data are summarized in Table II-1.[26] The UV–Vis spectrum of these three compounds, shown in Figure II-13, shows strong absorption in the visible region between 400 to 550 nm, characteristic of the π–π* electronic transition of PDI derivatives. A first peak with a maximum (λ_{max}) at 520~530 nm corresponds to the 0–0 vibrionic transition, and a weaker peak (490–500 nm) which corresponds to 0–1 vibronic transitions of PDI oriented along the long axis. A third peak (440–450 nm) is attributed to the 0–2 vibronic transitions oriented perpendicular to the long axis.

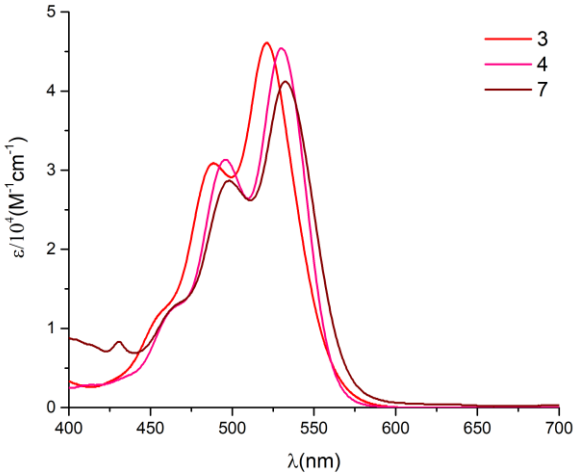

Figure II-13 UV/vis absorption spectra of compounds **3**, **4** and **7** (CH_2Cl_2, 298K).

The UV–Vis spectrum of PDI-C_{60} dyad **7** corresponds to the superimposition of the optical signature of PDI with that of C_{60} derivative suggesting the absence of electronic coupling in the ground state between the acceptor PDI and the fullerene moiety. This result was also observed in the case of dyad **II-10** where its absorption showed to be superimposed on the sum of the absorption spectra of C_{60} and PDI indicating as well, weak electronic interaction of C_{60} and PDI moieties in PDI-C_{60} at the ground state.

The photoluminescence studies of the three compounds, show that mono-nitroPDI **3** does not exhibit any emission, which is in agreement with the previously reported data.[39,40] PDI derivative **4** emits strongly at 566 nm, normalized absorption and emission spectra is shown in Figure II-14. The quantum yield was calculated for compound **4** (Φ_f= 0.66) determined from N,N′-diphenylperylenediimide[41] as standard for fluorescence quantum yield measurements.

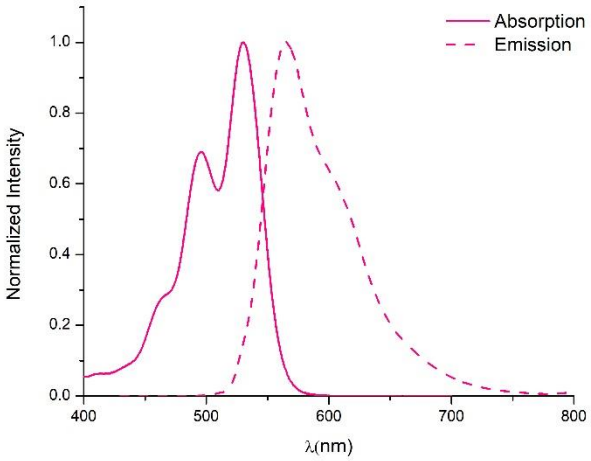

Figure II-14 Normalized steady-state absorption (full line) and emission spectra (Dotted line; λ_{ex}=530 nm) of compound **4** in CH_2Cl_2.

However, this emission was quenched (Φ_f= 0.01%) with PDI-C_{60} **7**, in which a quasi-quantitative quenching (ca. 98.5%) was observed. This fluorescence quantum yield decrease suggested the occurrence of either a photo-induced electron transfer or an energy transfer in solution from the photo-excited PDI chromophore to the electron-accepting fullerene unit.

Table II-1 UV-Vis absorption (10^{-5} M in CH_2Cl_2) and emission data (10^{-6} M in CH_2Cl_2) of PDI derivatives **3**, **4** and dyad **7**.

Compound	λ_1 (nm)	ε_1 ($M^{-1}cm^{-1}$)	λ_2 (nm)	ε_2 ($M^{-1}cm^{-1}$)	Φ^a	$E_g{}^b$	E^{LUMO} (eV)^c	E^{HOMO} (eV)^d
3	488	30 900	521	46 100	-	2.19	- 4.0	- 6.2
4	496	31 400	530	45 400	0.66[a]	2.27	- 3.8	- 6.1
7	497	28 900	533	41 200	0.01	2.16	- 3.8	- 5.9

[a] Standard N,N'-diphenylperylenediimide (Φ_{fl}= 0.96 in CH_3CN);[41] λ_{ex}=530 nm.[b] From the intersection of the absorption and emission spectra or onset of absorption.[c] $E^{LUMO} = -(E^1_{red} + 4.8)$. [d] $E^{HOMO} = [E_{LUMO}-E_g]$.

These results are also in accordance with dyad **II-20** where an estimated 98% quenching of fluorescence observed was attributed to an efficient intramolecular energy transfer (ET) from PDI to C_{60} and nanosecond time-resolved transient absorption and spin density analysis confirmed that the triplet state of dyad **II-20** is localized on the PDI unit, as mentioned above.

II.3.2.2 Electrochemical Properties

The electrochemical properties of PDI derivatives **3** and **4**, dyad **7** and fulleropyrrolidine **8** were investigated by cyclic voltammetry (CV) in CH_2Cl_2 in the presence of 0.1 M Bu_4NPF_6 as

supporting electrolyte. While PDI derivatives show the expected two reversible one-electron reduction waves, we could detect four reversible reduction processes for dyad **7**, for which the cyclic voltammogram and those of the three reference compounds are illustrated in Figure II-15.

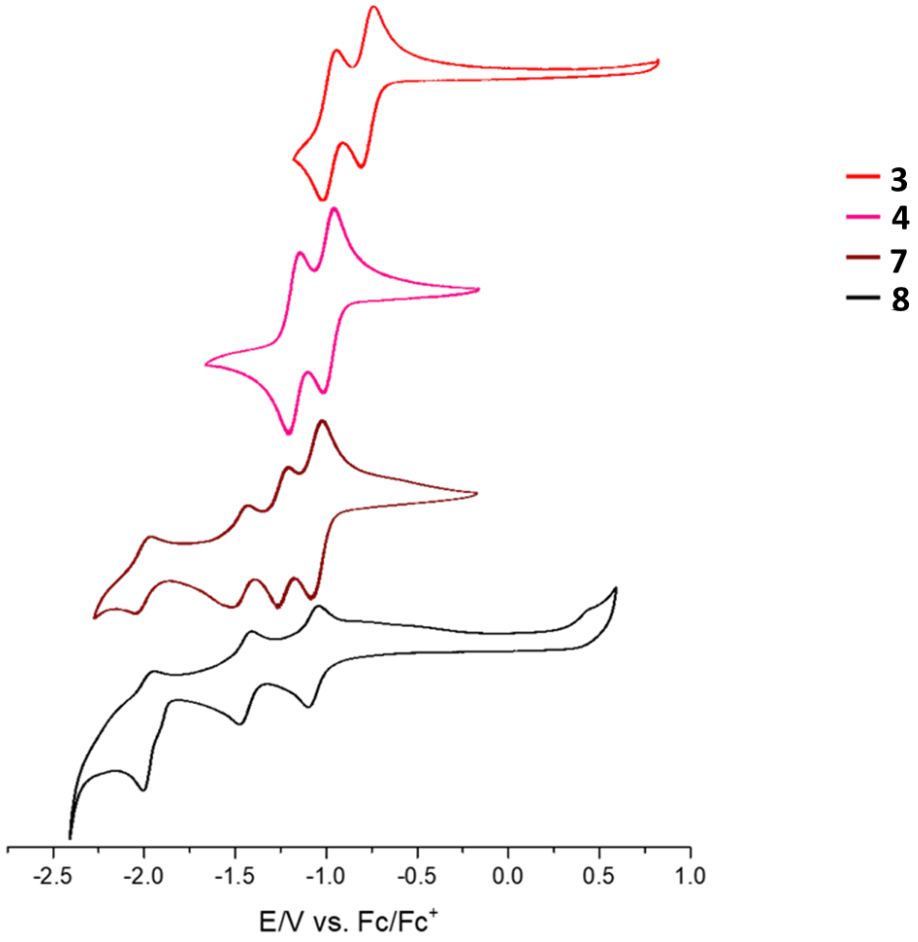

Figure II-15 Cyclic voltammogram of **3** (red), **4** (pink), **7** (wine) and **8** (black) (V vs Fc/Fc^+; Pt as a working electrode; Bu_4NPF_6 0.1 M, 100 mV/s, CH_2Cl_2 for **3**, **4** and **7**; o-DCB/CH_2Cl_2 (1:1.2) for **8**).

From the deconvoluated cyclic voltammogram of dyad **7**, shown in Figure II-16, and its comparison with voltammograms of PDI **4** and reference C_{60} derivative **8**, we could assign the first wave to a two-electron process at E^1_{red} = – 1.05 V *vs* Fc/Fc^+, suggesting that the first reduction process of C_{60} and the first reduction process of PDI are overlapping. Consequently this process was assigned to a simultaneous reduction of C_{60} and PDI leading to dianion-diradical $C_{60}^{\cdot-}$-PDI^{-} species. This allow dyad **7** to accept more than one electron in the initial reduction step due to the overlap happening in the first reduction potentials. The second (E^2_{red} = – 1.23 V), third (E^3_{red} = – 1.46 V) and fourth (E^4_{red} = –1.99 V) waves were assigned to one-electron processes corresponding to the successive formation of $C_{60}^{\cdot-}$ - PDI^{2-}, then C_{60}^{2-} - PDI^{2-},

and at the end $C_{60}^{3.-}$ - PDI^{2-} species. Moreover, comparison of these different values for dyad **7** with reference compounds **4** and **8** suggests that there is no significant interaction taking place between both electroactive moieties in the ground state.

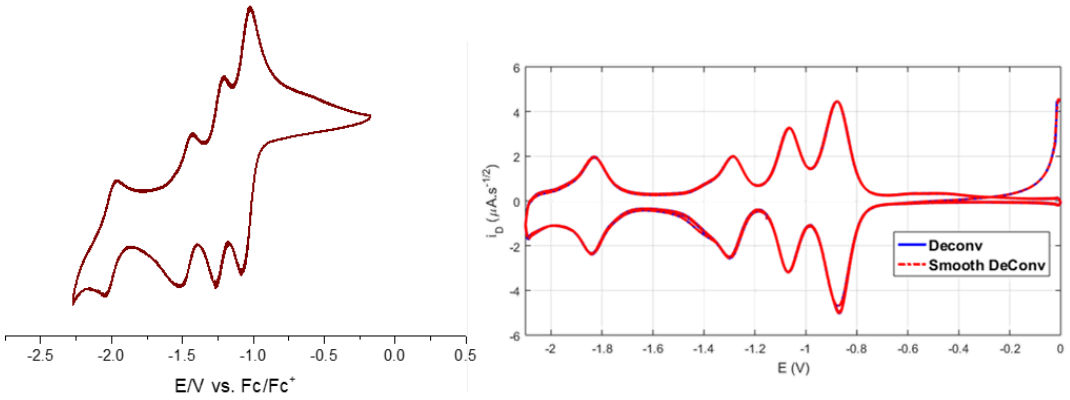

Figure II-16 Cyclic voltammogram (CV) and deconvoluted CV of PDI-C_{60} dyad **7**.

Table II-2 Redox potential values (V vs. Fc/Fc^+) of PDI-C_{60} dyad **7** and reference compounds **3**, **4** and **8**. Values recorded in a CH_2Cl_2 solution (0.5 mM) for **3**, **4** and **7** and o-DCB/CH_2Cl_2 (1:1.2) for **8**, using Bu_4NPF_6 0.1M as the supporting electrolyte, platinum wires as counter and working electrodes. Scan rate: 100 mV/s.

COMPOUND	E^1_{red}	E^2_{red}	E^3_{red}	E^4_{red}
3	- 0.77	- 0.98		
4	- 0.98	- 1.17		
7	- 1.05	- 1.23	- 1.46	- 1.99
8	- 1.07	- 1.44	- 1.97	

These results are also in agreement with the electrochemical studies of dyad **II-10** reported by N.R. Champness *and coll.*, in which an overlap of the first reduction potentials of C_{60} and PDI moieties was observed confirming that the initial reduction step was leading to the simultaneous formation of the $C_{60}^{\cdot-}$-$PDI^{\cdot-}$ species. It was also demonstrated by complementary spectroelectrochemical studies that this two-electron step was followed by two one-electron processes leading to the successive formation of $C_{60}^{\cdot-}$ - PDI^{2-}, then C_{60}^{2-} - PDI^{2-} species.

HOMO and LUMO energy levels of the three compounds are also estimated from cyclic voltammetry (CV). It appears that the first reduction potential of dyad **7** is less positive than that

of compound **4**. This can be explained by the fact that compound **4** has more electron-withdrawing ability (and expectedly less than compound **3**), and hence easier to reduce than dyad **7** upon which increase of the electronic density in the PDI core occurs with the attachment of C_{60}. The HOMO/LUMO energy levels of **4** and **7** are estimated to be -6.1/-3.8 eV and -5.9/-3.8 eV, respectively.[26]

II.4 Bay-Phosphinimine PDI

II.4.1 Heterocyclic Annulation of mono nitro-PDI: General Overview

The *N*-heterocyclic annulation reaction of mono-nitro PDI was described by Welch *et al*.[25] The incorporation of a nitrogen heteroatom at the *bay* position of the PDI was obtained using triphenylphosphine as the reducing agent gave compound **II-21** in quantitative yields (Figure II-17).

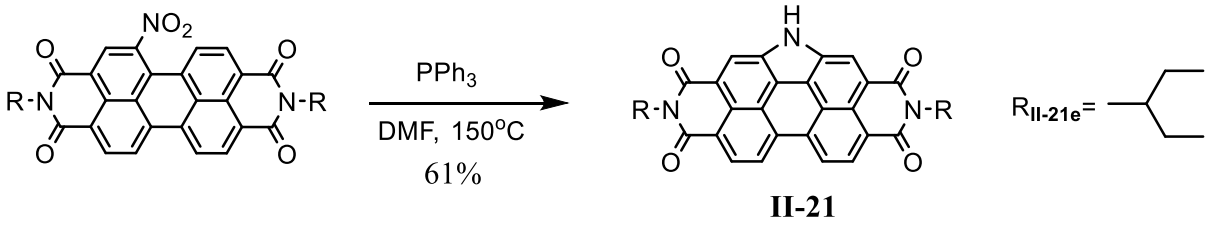

Figure II-17 N-heterocyclic annulation reaction of mono-nitro PDI.

This reductive cyclization, known as Cadogan reaction, is a common method for deoxygenating the aromatic nitro groups by means of reducing agents, such as trialkyl and triaryl phosphines and trialkyl phosphites.[16,42,43] This leads to the formation of more reactive nitrogen functions of lower oxidation state that would likely undergo intramolecular reactions accomplishing heteroannulation of the starting system, giving a variety of fused nitrogen heterocyclic systems, such as for compound **II-21**. In 2000 Langhals and S. Kirner reported such Cadogan cyclization.[16] However, the mono-nitro PDI was treated with triethylphosphite instead of triphenylphosphine which led to poor yields with unnecessary by-products.

The proposed mechanism of this reaction is shown in Figure II-18, illustrated from Freeman *et al.*[43] where they reported the synthesis of carbazoles from reductive cyclization of 2-nitroso biphenyl derivatives. The cyclization is preceded with nucleophilic attack on the nitro groups by PPh_3 or reductive deoxygenation, which plays an important role in determining the rate of the reaction. Removing oxygen atoms from the nitro group is reported to proceed stepwise through a formation of a nitroso group and a nitrene intermediate after which intramolecular reactions achieve the desired carbazole or fused nitrogen heterocyclic systems.

The inclusion of *N*-heteroatom into the perylene skeleton is important as it can modify the optoelectronic properties of these heterocyclic annulated perylenes. Moreover, the *pyrrolic* nitrogen provides an additional site to be functionalized by side chain engineering. This can

allow to tune the morphology and consequently the OSCs device performance obtained from these different compounds.[44]

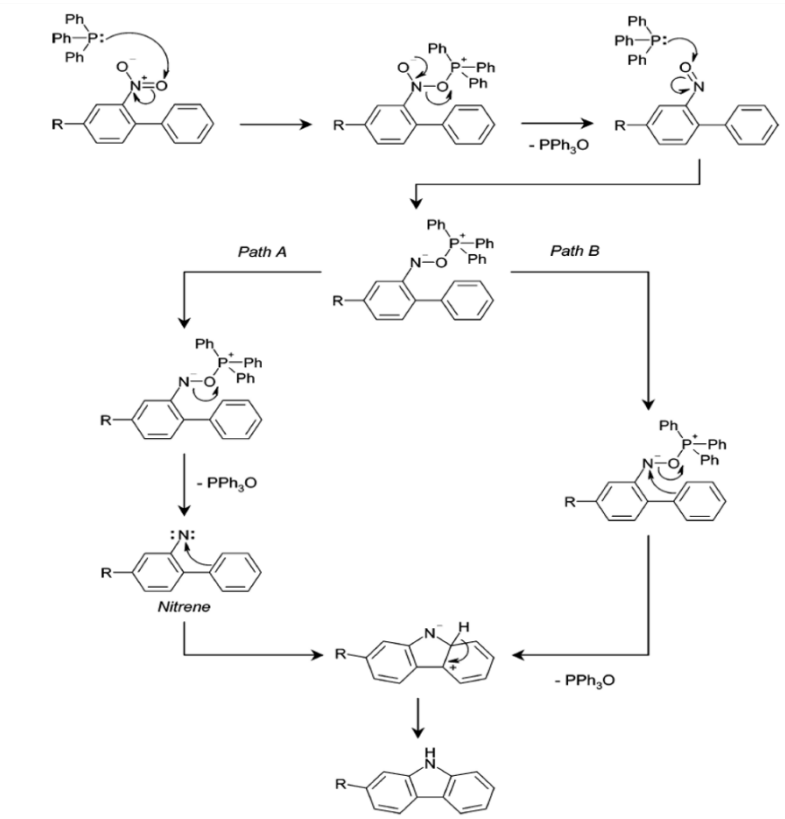

Figure II-18 Proposed reaction mechanism for reductive cyclization.[43]

In a similar manner, *N*-heterocyclic annulation of PDI was carried out, starting from di-nitro PDI to include two *N*-heteroatoms into the perylene skeleton leading to di-carbazole based PDI. Having *N*-heterocyclic annelated in two *bay* regions would allow us to study and compare with the mono-carbazole based PDI the effect of introducing another *pyrrolic* ring on the physical properties of PDI.

II.4.2 Heterocyclic Annulation of di-nitro-PDI

II.4.2.1 Synthesis of starting material: Di-nitro PDI

The electrophilic aromatic di-nitration reaction of compound **2** was carried out following the mono-nitration procedure using only fuming nitric acid without the need of the addition of CAN.[39,45,46] However, the reaction time was increased to allow for the formation of the di-nitro PDI since, as mentioned before, the formation of the mono and di-nitro PDI are time dependent.

Di-nitroPDI **9** (Figure II-19), was obtained in 88% yield as a mixture of 1,6 and 1,7 regioisomers in a 50:50 ratio.

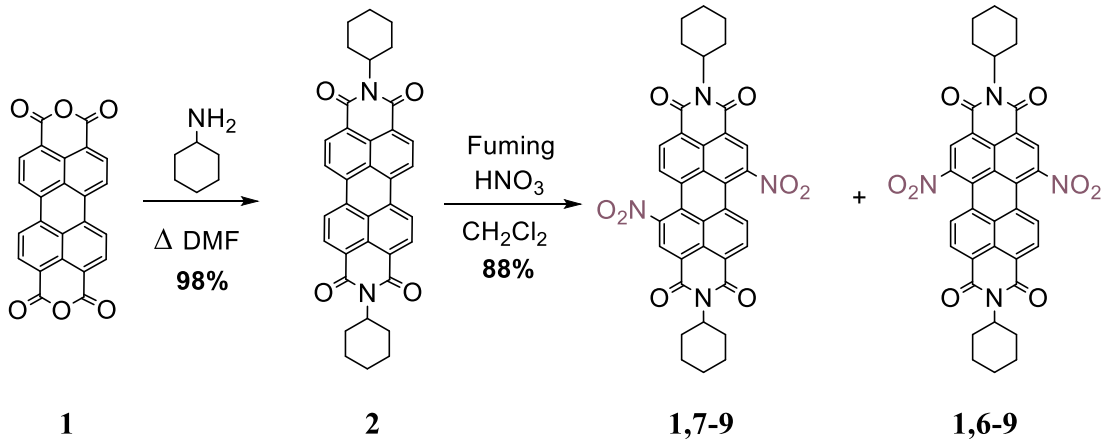

Figure II-19 Di-nitration reaction of PDI.

II.4.2.2 Formation of phosphinimine functional group

The obtained mixture of regioisomers of di-nitro PDI **9** (**1,6** and **1,7**) was treated with excess of PPh_3 in distilled THF, chosen to be the solvent for this reaction mixture that was heated under reflux for 96h, after which TLC showed the formation of new product and remaining starting material **9**. After successive purification of the crude product, compound **10** was isolated. However, characterization by ^1H NMR, and mass spectrometry (MALDI-TOF), did not show the expected di-annulated PDI product (Figure II-20).

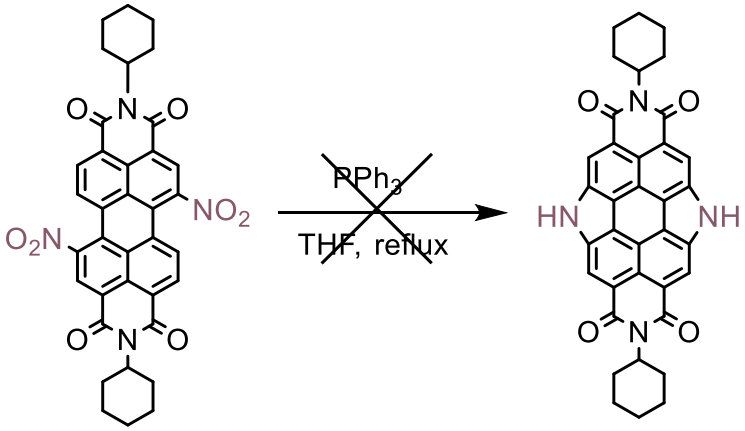

Figure II-20 N-Heterocyclic annulation of di-nitro PDI.

The reason behind the reaction failure could be explained by the inclusion of the first nitrogen heterocycle on the PDI skeleton which renders the molecule having a ‘’bowed’’ shape, as studied by Welch *et al*. that provided the single crystal structure of the alkylated NH-PDI **II-21** shown in Figure II-21. A shortening of the central C_2−C_{19} aromatic bonds in the structure occurs (bond distance = 1.37 Å), hence making the possibility of including another nitrogen heterocyclic on PDI more difficult. The other central C_4-C_{21} aromatic bonds become larger in distance (bond distance = 1.48 Å) compared to the one bearing the *pyrrolic* N-atom.[25] It is noteworthy that this non-planar PDI **II-21** is very poorly soluble in organic solvents, due to possible intermolecular hydrogen bonding interactions. This could also be another reason for the difficulty in performing di-reductive cyclization, where the insolubility of the wanted compound and therefore the increased of PDI aggregation propensity, controlled by π-π stacking could have led to such undesirable results.

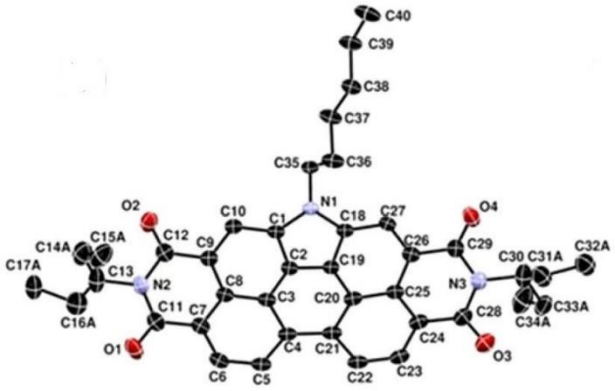

Figure II-21 Single crystal structure of compound **II-21**.[25]

Single crystals of one of the two isomers of compound **10** (Figure II-22) were obtained by slow evaporation of a solution containing PDI **10** in a mixture of CH_2Cl_2 and hexane then analyzed by X-ray diffraction (Figure II-23). The X-ray crystal structure of **10-*1,6*** clearly shows the formation of a phosphinimine functional group, and the presence of both one nitro and one hydroxyl functional groups. This isomer corresponds effectively to the starting material on which both nitro groups were present in the relative 1,6 positions of PDI. These results were also confirmed by ^{1}H NMR spectra (Figure II-24) and ^{31}P spectra that confirms the presence of a phosphorous atom with a singlet at 21.20 ppm and an -*OH* group with a singlet at 12.54 ppm.

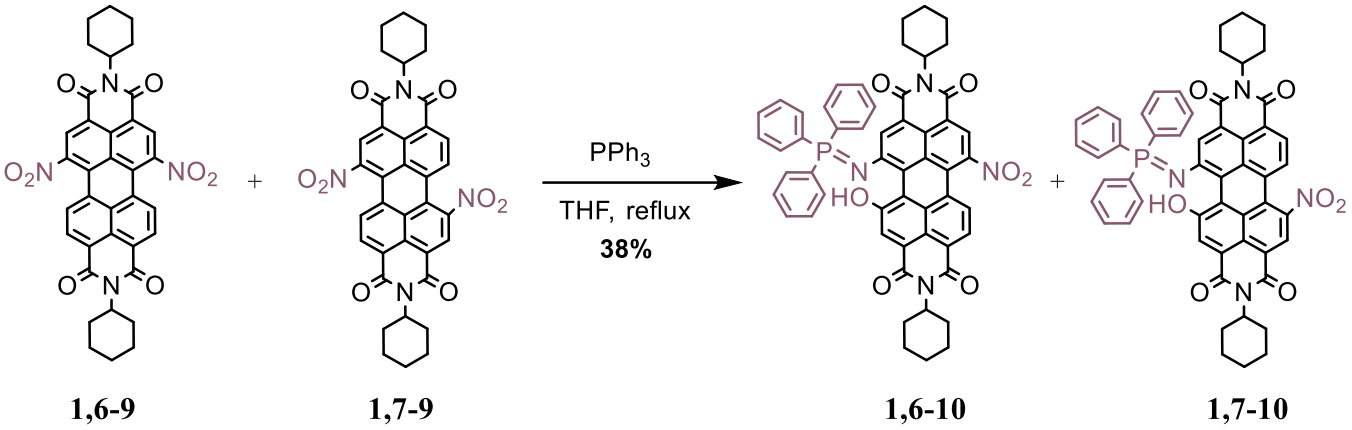

Figure II-22 Formation of phosphinimine functional group starting from di-nitro PDI.

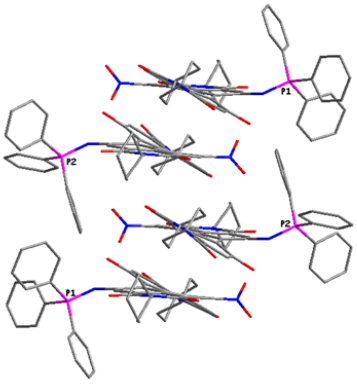

Arrangements of molecules in the unit cell

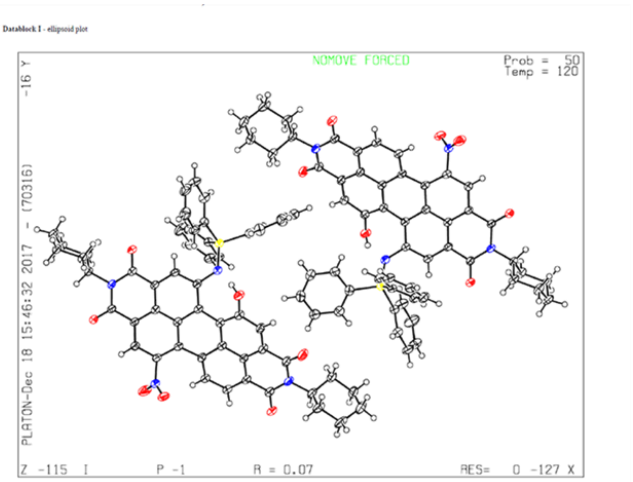

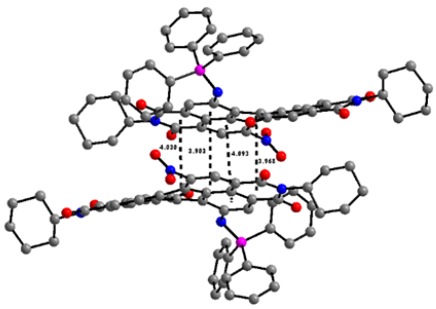

π-π interaction

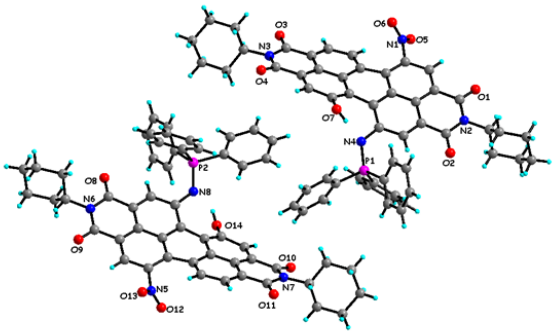

Figure II-23 Crystal structure of PDI derivative **10.**

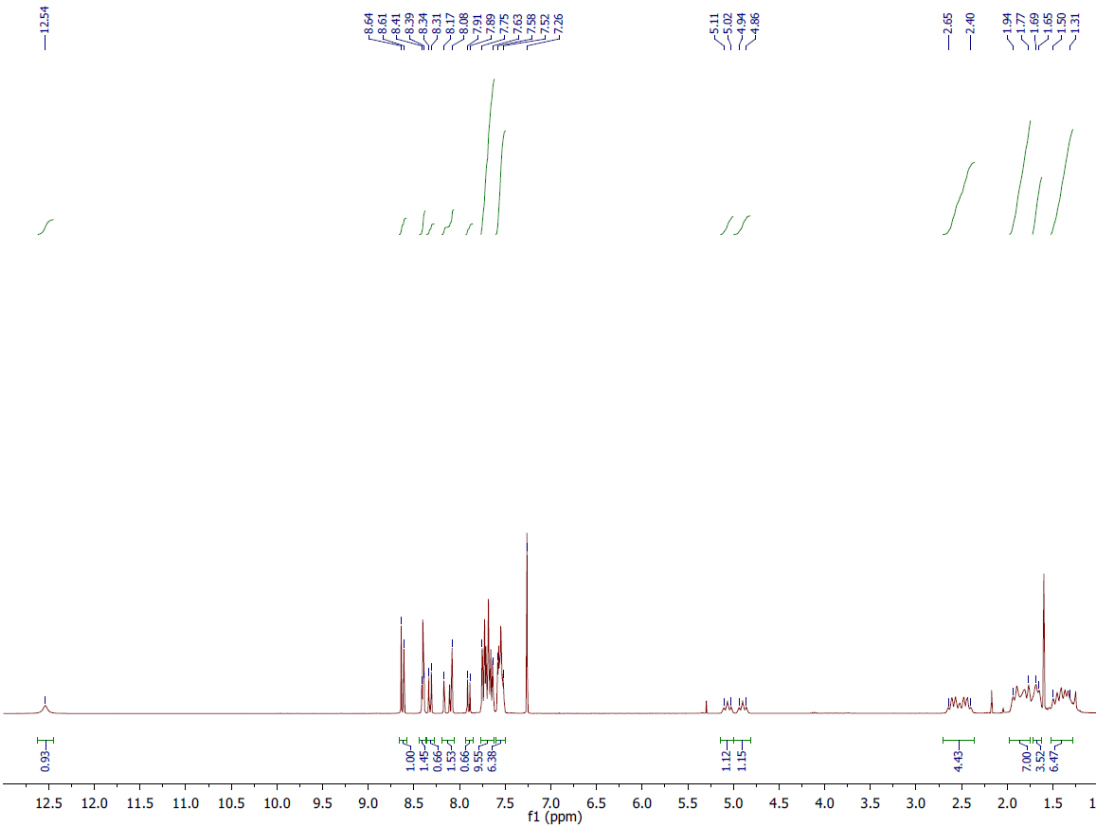

Figure II-24 ^{1}H NMR spectrum of PDI derivative **10**.

II.4.2.2.1 Phosphinimine formation from nitro group: Overview

The first example of phosphinimine or iminophosphorane compound $PhN{=}PPh_3$ was introduced by Staudinger and Meyer in 1919.[47] This phosphorus-nitrogen containing compound was prepared as the nitrogen analogue of a Wittig reagent for its subsequent use in aza-Wittig reaction,[48] in which phosphinimines are employed in the construction of C=N double bonds through their reaction with carbonyl compounds, in a similar fashion to phosphorus ylides in the Wittig reaction. In general, phosphinimine compounds are known to be used as reagents, ligands or intermediates in organic synthesis. Their ability to play the role of ylides in the formation of C=N is of valuable importance, especially when the reacting groups are in the same molecule and therefore new heterocyclic rings could be formed. Their preparation could be done following various methods,[49] in which the oldest known as Staudinger and Meyer' method involves reaction of a tertiary phosphine (R_3P) with an organic azide ($R'N_3$) with the formation of dinitrogen. Staudinger reaction remains an effective common method for the production of

phosphinimine that has been widely used till day.[50] Other methods include the reaction of primary arylamines with dibromotriphenylphosphorane in the presence of triethylamine or sodium amide as the base. The reaction of triphenylphosphine and hydroxylamine-O-sulphonic acid gave a phosphonium salt as reported which could be deprotonated in liquid ammonia to also give the phosphinimine product. In addition to the reactions involving the use of oxidants such as halogenating agents, azodicarboxylates or ethylenedicarboxylates with phosphines and amines. Recently, formation of aryliminophosphoranes or phosphinimines from 2-nitrodiarylamines was reported,[51,52] although the reaction of Staudinger is more dominating as practical method for phosphinimine formation. The deoxygenation of nitroarenes employed for this purpose is described as unpredictable as such processes with nitro and nitroso groups are generally more complex and less selective with dominating subsequent reactions of intermediate nitrenes such as cyclizations and rearrangements (Figure II-25). Best results described were obtained when the corresponding reaction was carried out without a solvent in a melted mixture of the nitroarene and excess of PPh_3 at 150°C. High temperature and excess of PPh_3 are required for the deoxygenation of nitroarenes and trapping of the intermediates 2-nitrosodiarylamines, respectively. These reported results, and other similar reported cases, further explain the formation of compound **10** from the di-nitro PDI when it was treated with PPh_3 and its deviation from the wanted cyclization results, where instead, deoxygenation of nitroarenes led to the production of phosphinimine function.

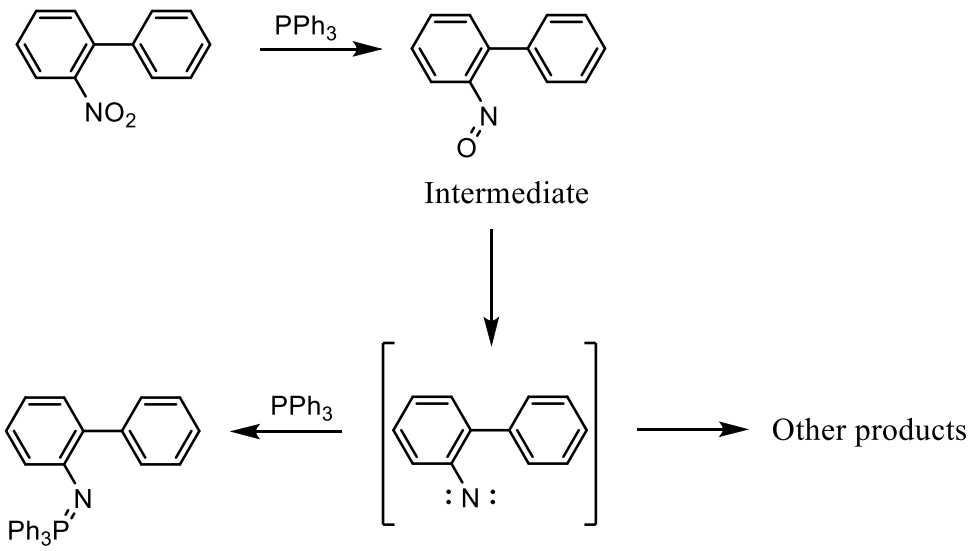

Figure II-25 General reaction pathways of nitroarenes with triphenylphosphine.

II.4.3 Proposed mechanism

The proposed mechanism for the formation of compound **10** is depicted in Figure II-26, where it starts with the nucleophilic attack of PPh_3 on the nitro-groups followed by the formation of nitroso groups as intermediates. Instead of the formation of nitrenes as seen in the case of carbazole or fused rings reaction mechanism, a sequential intramolecular cyclization – ring opening occurs, using a second equivalent of PPh_3, leading to this 2'-phosphinimine-1,1'biphenyl-2-ol functionality not yet described.

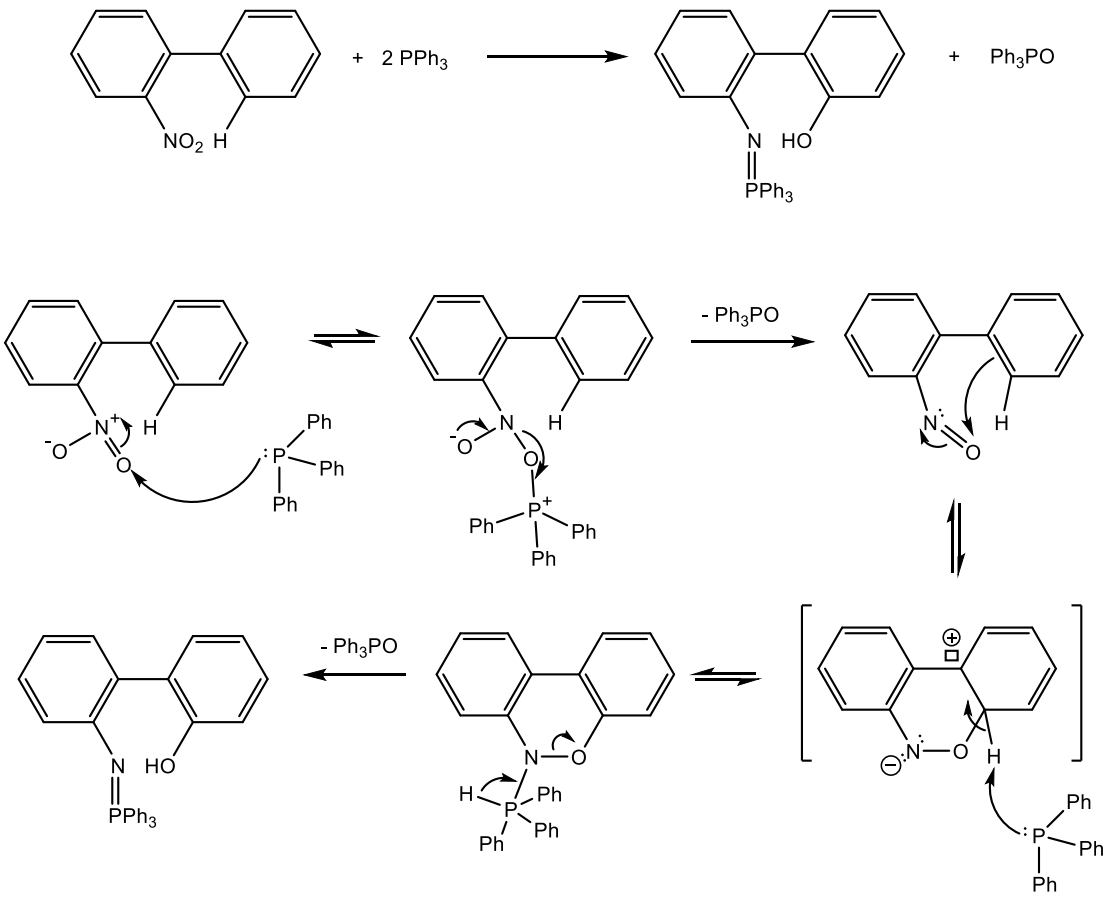

Figure II-26 Proposed mechanism for the formation of compound **10**.

II.4.4 Study of the solvent effect on phosphinimine formation

In addition to the temperature effect on the reaction path and the necessity to employ rational excess of triphenylphosphine, it has been shown, that for carbazole or phosphinimine formation, solvent plays also an important role in determining the yield obtained or even the product

formed. Hence, the reaction of di-nitro with PPh_3 was carried out in different solvents to study its influence on the reaction pathway.

Reactions carried out in refluxing DMF or Toluene as solvents gave after purification, product **10** in 30% and 13% yields, respectively (Figure II-27). In the case where toluene was employed, another product **11** was isolated in 8% yield. Its subsequent characterizations by ^{1}H, ^{31}P NMR (in which a singlet at 9.8 ppm appears) and MS spectra showed that both phophinimine formation and N-heterocyclic annulation of PDI (in which a singlet corresponding to N-H proton appears at 9.6ppm) are present. This result is in agreement with the different competitive processes which can occur according to the described mechanism.

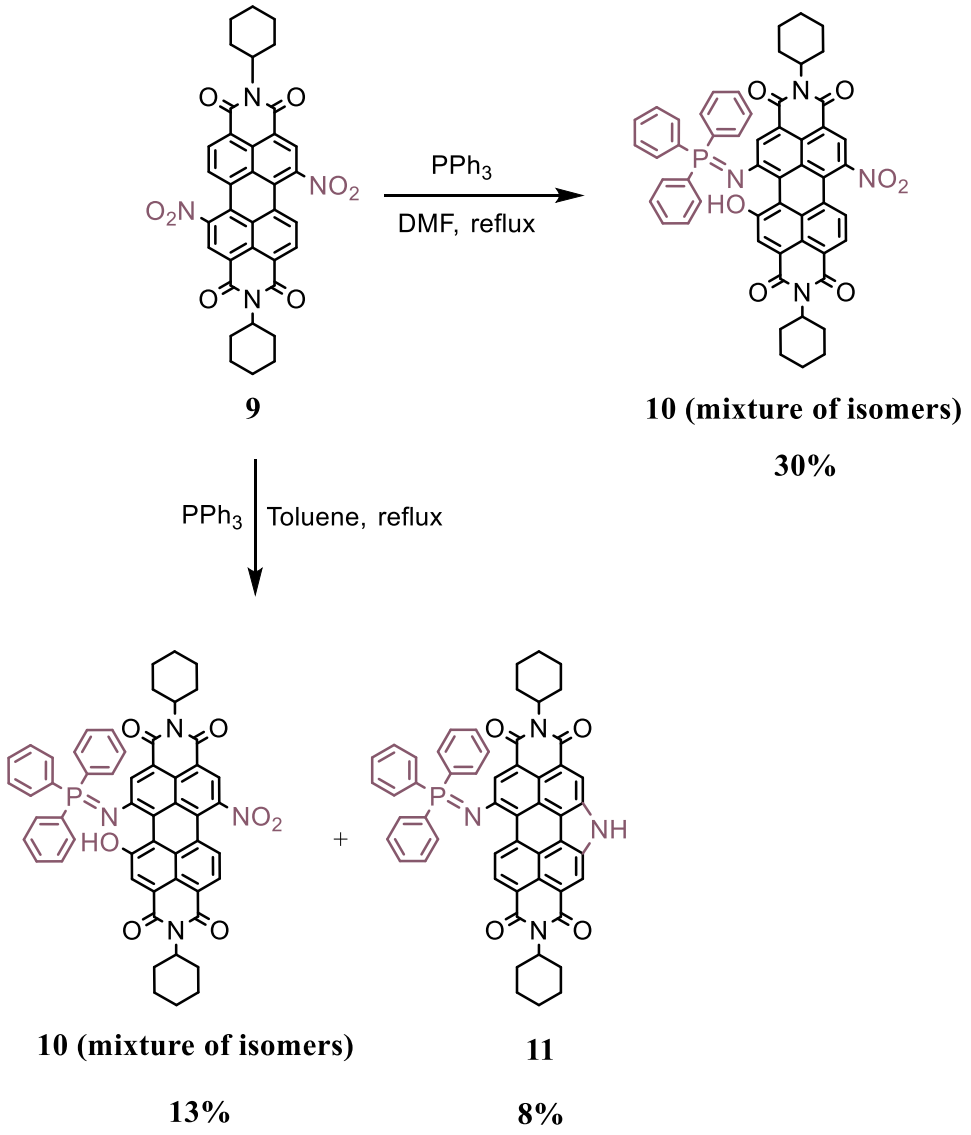

Figure II-27 Phosphinimine functional group formation.

II.4.5 Phosphinimine formation from mono-nitro PDI.

Reaction using mono-nitro PDI **3** was carried out with an excess of PPh_3 in distilled THF, chosen to be the solvent since it gave the best yields in the case of di-nitro PDI. The reaction mixture was heated under reflux for around four days, after which TLC showed the formation of new product. Successive purification of the crude product and characterization by ^{1}H NMR, ^{31}P (in which a singlet at 20.28 ppm appears) and mass spectrometry (MALDI-TOF), gave **12** in 30% yield (Figure II-28).

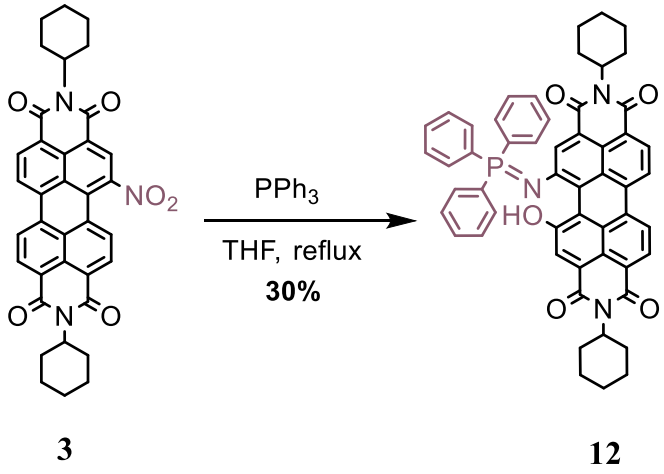

Figure II-28 Formation of phosphinimine functional group starting from mono-nitro PDI.

II.4.6 Subsequent Reactions

II.4.6.1 Aza-Wittig reactions

As mentioned above, phosphinimine compounds have been found to have great significance in organic synthesis, mainly due to their ylide character where they could be used as powerful reagents for the construction of C=N double bonds in reactions with carbonyl compounds. Based on that, attempts to carry out subsequent aza-Wittig reaction as one pot synthesis were tested. Mono-nitro PDI **3** was treated with excess of PPh_3 and 4-formyltriphenylamine used as the carbonyl compound reagent. The reaction mixture was heated in microwave at 150°C for 30 min after which TLC showed compound **12** without the appearance of any new formed compound. Increasing the reaction time did not help in obtaining the expected product, where the formation of compound **12** was persistent (Figure II-29). However, increasing the time of the reaction, from 30 min to 1h, increased slightly the yield of compound **12** from 16% to 20%. The failure of the corresponding aza-Wittig reaction could be due to the proximity of both hydroxyl and

phosphinimine group in compound **12**, suggesting a steric hindrance. Moreover, the absence of reaction is in agreement with the poor nucleophilicity of the phosphinimine group.

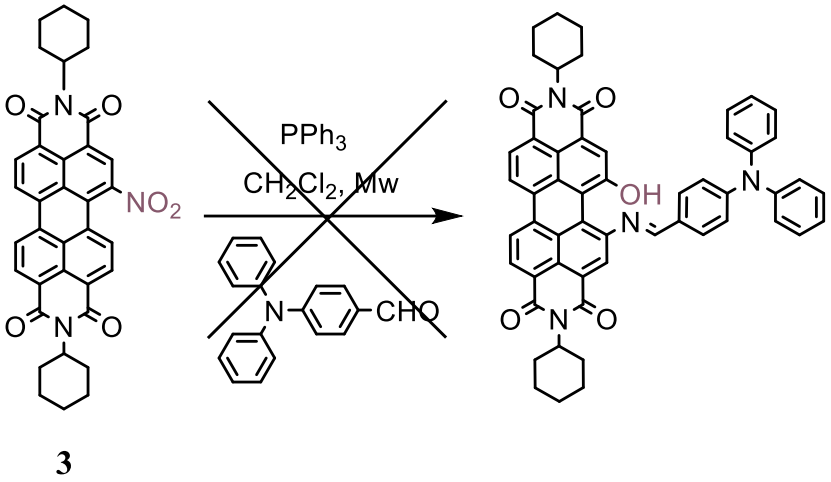

Figure II-29 Attempts to perform one pot aza-Wittig reaction.

II.4.6.2 Bromination reactions

Having compound **10** with three different substituents at PDI *bay* region we were interested to substitute the one *bay* empty position, in order to obtain tetrasubstituted PDI derivatives with four different substituents. Bromination reaction was carried out so that the bromine fulfills the requirement of being the fourth substituent (Figure II-30). Compound **10** was dissolved in CH_2Cl_2 and treated with only one equivalent of bromine, to avoid side reactions, such as bromination of the phenyl groups of the phosphinimine. The reaction mixture was stirred at room temperature for three successive days, however, TLC showed unreactive starting material. Increasing to three equivalents of bromine, or reaction time, did not yield the expected product. This could be due to the nitro group, being a deactivating electron-withdrawing group by inductive and resonance effect. Better understanding of the reactivity and selectivity of compound **10** that could be affected by the three different substituents present at the *bay* position is hence required.

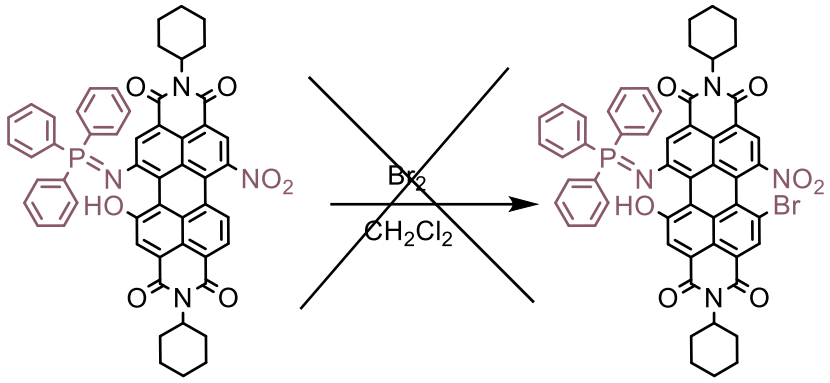

10

Figure II-30 Bromination reaction of compound **10**.

II.4.7 Optical Properties

The optical properties of compound **10** and **11** have been analyzed in diluted CH_2Cl_2 solutions by UV–vis absorption (ca. 10^{-5} M) and photoluminescence emission (ca. 10^{-6} M) spectroscopy, as shown in Figure II-31 and Figure II-32. The UV-vis absorption spectra show compound **11** exhibit more well-defined vibronic π- π* transition absorption bands, with the longest maximum at 602 nm. This has to be compared to compound **10** that shows very broad band and nearly structureless absorption bands that span a large part of the visible spectrum, with the longest maximum at 617 nm. These broad bands could be explained by the photoinduced charge transfer occurring due to the presence of electron-donor group -*OH* at the *bay* region of PDI. In comparison with compound **11**, the maximum absorption of compound **10** is bathochromically shifted about 15 nm.

The fluorescence spectra of compound **10** and **11**, excited respectively at 617 nm and 602 nm, show that PDI **10** does not exhibit any emission, which suggests intramolecular charge transfer (ICT) characteristics for the excited states of compound **10**. On the other hand, compound **11** exhibit strong emission with maximum emission peak at 637 nm.

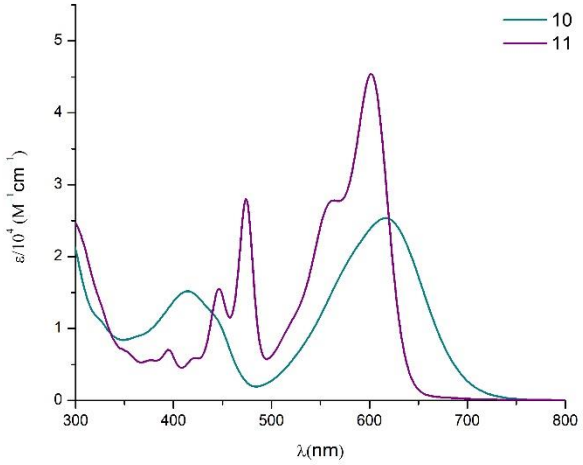

Figure II-31 UV/vis absorption spectra of compounds **10** and **11** (CH_2Cl_2, 298K).

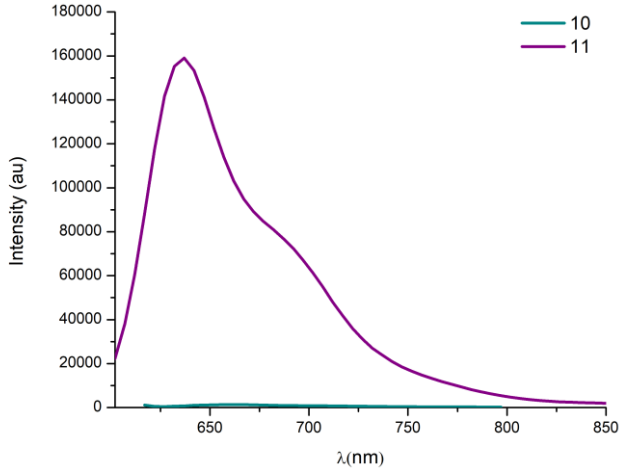

Figure II-32 Emission spectra of compounds **10** and **11** (CH_2Cl_2, 298K).

II.4.8 Electronic Properties

General study on the electrochemical properties of PDI derivatives **10** and **11** were investigated by cyclic voltammetry (CV) in CH_2Cl_2 in the presence of 0.1 M Bu_4NPF_6 as supporting electrolyte, illustrated in Figure II-33. Both compounds are able to be reduced and oxidized, where they both show two reversible reduction waves. These reduction processes originate from successive reduction of PDI to give a radical anion (**10**-$PDI^{\cdot-}$ or **11**-$PDI^{\cdot-}$) in the first reduction step and a dianion (**10**-PDI^{2-} or **11**-PDI^{2-}) in the second step. Compound **10** exhibit quasi-reversible oxidation wave due to -*OH* group, whereas compound **11** shows a reversible oxidation

wave due to the N-heterocyclic ring at the *bay* position that induces the reversibility of the oxidation process. It appears that the first reduction of compound **10** is more positive than that of compound **11**, which could be explained by the presence of an electron-withdrawing group at the *bay* region that is the nitro-group.

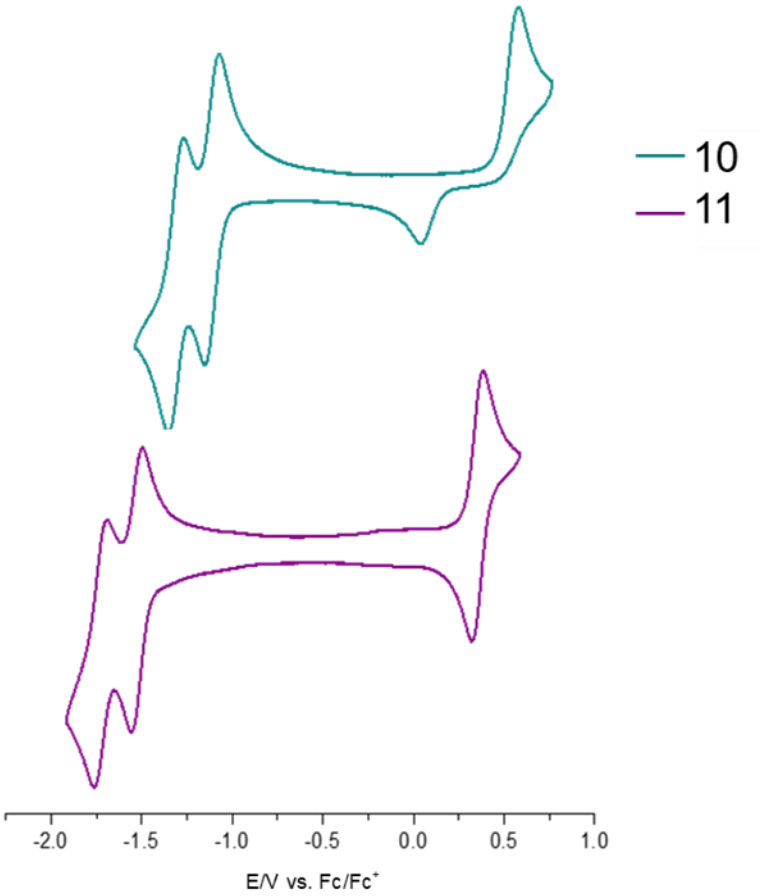

Figure II-33 Cyclic voltammogram of **10** (Cyan) and **11**(purple) (V vs Fc/Fc^+; Pt as a working electrode; Bu_4NPF_6 0.1 M, 100 mV/s, CH_2Cl_2.

II.5 Conclusion

In this chapter, we have carried out original Suzuki-Miyaura coupling (SMC) reactions using an electron deficient arene system possessing a nitro group as the electrophilic coupling partner. From this mono-nitro *bay* substituted PDI **3**, compound **4**, **5**, **6** were synthesized and obtained in quantitative yields. Compounds structures were confirmed by using ^{1}H and ^{13}C NMR, in addition to mass spectrometry (MALDI-TOF and HRMS). This new reaction in PDI chemistry is of particular interest because it allows to avoid the fastidious preparation of corresponding monobromoPDI as starting material for this organometallic coupling reaction. Subsequently, we adopted this reaction to construct a PDI-C_{60} dyad **7** for which C_{60} is connected at the *bay* region of the PDI core. From HPLC chromatography technique, the purity of dyad **7** was estimated to be high up to 99.8%. Optical and electrochemical properties were studied using compound **3**, **4** and fulleropyrrolidine **8** as references.

Attempts to synthesize di-carbazole based PDI starting from di-nitro PDI **9** through reductive cyclization method, afforded an unprecedented phosphinimine derivative with compound **10** for which the structure was mainly confirmed by analysis of single crystal X-ray diffraction. The reaction was carried out again from mono-nitro *bay* PDI **3** where compound **12** was obtained and characterized by ^{1}H, ^{31}P NMR and mass spectrometry (MALDI-TOF). We employed these compounds as starting materials in aza-Wittig or bromination reactions, however the compounds wanted were not obtained.

II.6 References

[1] N. Miyaura, T. Yanagi, A. Suzuki, *Synthetic Communications* **1981**, *11*, 513–519.

[2] S. Xu, E. H. Kim, A. Wei, E. Negishi, *Sci. Technol. Adv. Mater.* **2014**, *15*, 044201.

[3] T. Ishiyama, M. Murata, N. Miyaura, *J. Org. Chem.* **1995**, *60*, 7508–7510.

[4] Y. Liu, J. Zhao, *Chemical Communications* **2012**, *48*, 3751.

[5] Z. Mahmood, K. Xu, B. Küçüköz, X. Cui, J. Zhao, Z. Wang, A. Karatay, H. G. Yaglioglu, M. Hayvali, A. Elmali, *The Journal of Organic Chemistry* **2015**, *80*, 3036–3049.

[6] Y. Li, H. Zheng, Y. Li, S. Wang, Z. Wu, P. Liu, Z. Gao, H. Liu, D. Zhu, *J. Org. Chem.* **2007**, *72*, 2878–2885.

[7] T. W. Chamberlain, E. S. Davies, A. N. Khlobystov, N. R. Champness, *Chemistry - A European Journal* **2011**, *17*, 3759–3767.

[8] K. Nagarajan, A. R. Mallia, K. Muraleedharan, M. Hariharan, *Chem. Sci.* **2017**, *8*, 1776–1782.

[9] L. Cao, L. Xu, D. Zhang, Y. Zhou, Y. Zheng, Q. Fu, X.-F. Jiang, F. Lu, *Chemical Physics Letters* **2017**, *682*, 133–139.

[10] Q. Zhao, X. A. Zhang, Q. Wei, J. Wang, X. Y. Shen, A. Qin, J. Z. Sun, B. Z. Tang, *Chem. Commun.* **2012**, *48*, 11671–11673.

[11] H. Horinouchi, H. Sakai, Y. Araki, T. Sakanoue, T. Takenobu, T. Wada, N. V. Tkachenko, T. Hasobe, *Chemistry - A European Journal* **2016**, *22*, 9631–9641.

[12] Y. Yang, Y. Wang, Y. Xie, T. Xiong, Z. Yuan, Y. Zhang, S. Qian, Y. Xiao, *Chem. Commun.* **2011**, *47*, 10749–10751.

[13] J. Yi, Y. Ma, J. Dou, Y. Lin, Y. Wang, C.-Q. Ma, H. Wang, *Dyes and Pigments* **2016**, *126*, 86–95.

[14] J. Yi, J. Wang, Y. Lin, W. Gao, Y. Ma, H. Tan, H. Wang, C.-Q. Ma, *Dyes and Pigments* **2017**, *136*, 335–346.

[15] P. E. Hartnett, H. S. S. Ramakrishna Matte, N. D. Eastham, N. E. Jackson, Y. Wu, L. X. Chen, M. A. Ratner, R. P. H. Chang, M. C. Hersam, M. R. Wasielewski, et al., *Chemical Science* **2016**, *7*, 3543–3555.

[16] H. Langhals, S. Kirner, *Eur. J. Org. Chem.* **2000**, *2000*, 365–380.

[17] B. Dhokale, T. Jadhav, Y. Patil, R. Misra, *Dyes and Pigments* **2016**, *134*, 164–170.

[18] P. Rajasingh, R. Cohen, E. Shirman, L. J. W. Shimon, B. Rybtchinski, *J. Org. Chem.* **2007**, *72*, 5973–5979.

[19] M. R. Yadav, M. Nagaoka, M. Kashihara, R.-L. Zhong, T. Miyazaki, S. Sakaki, Y. Nakao, *Journal of the American Chemical Society* **2017**, *139*, 9423–9426.

[20] M.-J. Lin, Á. J. Jiménez, C. Burschka, F. Würthner, *Chemical Communications* **2012**, *48*, 12050.

[21] Á. J. Jiménez, M.-J. Lin, C. Burschka, J. Becker, V. Settels, B. Engels, F. Würthner, *Chem. Sci.* **2014**, *5*, 608–619.

[22] P. Singh, L. S. Mittal, V. Vanita, K. Kumar, A. Walia, G. Bhargava, S. Kumar, *J. Mater. Chem. B* **2016**, *4*, 3750–3759.

[23] C.-W. Chang, H.-Y. Tsai, K.-Y. Chen, *Materials* **2014**, *7*, 5488–5506.

[24] K.-Y. Chen, T.-C. Fang, M.-J. Chang, *Dyes and Pigments* **2012**, *92*, 517–523.

[25] A. D. Hendsbee, J.-P. Sun, W. K. Law, H. Yan, I. G. Hill, D. M. Spasyuk, G. C. Welch, *Chem. Mater.* **2016**, *28*, 7098–7109.

[26] R. El-Berjawi, P. Hudhomme, *Dyes and Pigments* **2018**, *159*, 551–556.

[27] R. Gómez, J. L. Segura, N. Martín, *Org. Lett.* **2005**, *7*, 717–720.

[28] Y. Shibano, T. Umeyama, Y. Matano, N. V. Tkachenko, H. Lemmetyinen, H. Imahori, *Org. Lett.* **2006**, *8*, 4425–4428.

[29] J. Hua, F. Meng, F. Ding, F. Li, H. Tian, *Journal of Materials Chemistry* **2004**, *14*, 1849.

[30] J. Baffreau, L. Perrin, S. Leroy-Lhez, P. Hudhomme, *Tetrahedron Letters* **2005**, *46*, 4599–4603.

[31] Y. Shibano, T. Umeyama, Y. Matano, N. V. Tkachenko, H. Lemmetyinen, Y. Araki, O. Ito, H. Imahori, *J. Phys. Chem. C* **2007**, *111*, 6133–6142.

[32] J. Baffreau, S. Leroy-Lhez, N. Vân Anh, R. M. Williams, P. Hudhomme, *Chemistry - A European Journal* **2008**, *14*, 4974–4992.

[33] S. Pla, L. Martín-Gomis, K. Ohkubo, S. Fukuzumi, F. Fernández-Lázaro, Á. Sastre-Santos, *Asian Journal of Organic Chemistry* **2014**, *3*, 185–197.

[34] S.-E. Zhu, K.-Q. Liu, X.-F. Wang, A.-D. Xia, G.-W. Wang, *The Journal of Organic Chemistry* **2016**, *81*, 12223–12231.

[35] K. M. Kaunisto, P. Vivo, R. K. Dubey, V. I. Chukharev, A. Efimov, N. V. Tkachenko, H. J. Lemmetyinen, *The Journal of Physical Chemistry C* **2014**, *118*, 10625–10630.

[36] S. Pla, M. Niemi, L. Martín-Gomis, F. Fernández-Lázaro, H. Lemmetyinen, N. V. Tkachenko, á. Sastre-Santos, *Physical Chemistry Chemical Physics* **2016**, *18*, 3598–3605.

[37] Y. Li, N. Wang, X. He, S. Wang, H. Liu, Y. Li, X. Li, J. Zhuang, D. Zhu, *Tetrahedron* **2005**, *61*, 1563–1569.

[38] S. Xiao, Y. Li, Y. Li, J. Zhuang, N. Wang, H. Liu, B. Ning, Y. Liu, F. Lu, L. Fan, et al., *J. Phys. Chem. B* **2004**, *108*, 16677–16685.

[39] K.-Y. Chen, T. J. Chow, *Tetrahedron Letters* **2010**, *51*, 5959–5963.

[40] X. Kong, J. Gao, T. Ma, M. Wang, A. Zhang, Z. Shi, Y. Wei, *Dyes and Pigments* **2012**, *95*, 450–454.

[41] S. Içli, H. İcil**, *Spectroscopy Letters* **1994**, *27*, 323–332.

[42] J. I. G. Cadogan, *Q. Rev., Chem. Soc.* **1968**, *22*, 222.

[43] A. W. Freeman, M. Urvoy, M. E. Criswell, *J. Org. Chem.* **2005**, *70*, 5014–5019.

[44] S. V. Dayneko, A. D. Hendsbee, G. C. Welch, *Small Methods* **2018**, *2*, 1800081.

[45] H.-Y. Tsai, C.-W. Chang, K.-Y. Chen, *Tetrahedron Letters* **2014**, *55*, 884–888.

[46] H.-Y. Tsai, K.-Y. Chen, *Dyes and Pigments* **2013**, *96*, 319–327.

[47] H. Staudinger, J. Meyer, *Helvetica Chimica Acta* **1919**, *2*, 635–646.

[48] F. Palacios, C. Alonso, D. Aparicio, G. Rubiales, J. M. de los Santos, *Tetrahedron* **2007**, *63*, 523–575.

[49] E. W. Abel, S. A. Mucklejohn, *Phosphorus and Sulfur and the Related Elements* **1981**, *9*, 235–266.

[50] C. G. Martínez-De-León, A. Rodríguez-Álvarez, A. Flores-Parra, J.-M. Grévy, *Inorganica Chimica Acta* **2019**, *495*, 118945.

[51] M. Tryniszewski, R. Bujok, P. Cmoch, R. Gańczarczyk, I. Kulszewicz-Bajer, Z. Wróbel, *J. Org. Chem.* **2019**, *84*, 2277–2286.

[52] E. Łukasik, Z. Wróbel, *Heteroatom Chem* **2016**, *27*, 372–380.

Chapter III：N-annulated perylenediimide dimers in organic solar cells

III.1 From N-annulated PDI monomer to PDI dimer

III.1.1 General overview

III.1.1.1 PDI dimers for solar cell applications

Over the last decades, efficient results were obtained from OPVs based upon solution processed PDI active layers. As mentioned earlier, PDIs are powerful electron acceptors that have been widely investigated as electron transport materials. Their low lying LUMO levels, small optical band-gaps, strong electron accepting ability, photochemical stability and high electron mobility made them potential non-fullerene acceptor (NFA) candidates. However, it is still of great importance to understand and control their structure by introducing different functional groups, which affects their self-assembly and optoelectronic properties, hence the device performance of organic electronics devices. To achieve this, Welch *et al.*[1] reported a series of N-annulated PDI dimers, with which the planarity is disrupted and aggregation formation is decreased compared to the monomeric PDIs that tend to strongly aggregate in solid state leading to poor OPV performances. Figure III-1 shows the reported PDI dimers, developed through side-chain engineering approach on the *pyrrolic* position for fine-tuning of molecular packing and BHJ morphology. Eco-friendly solvents were employed for the fabrication of solution-processed OSC devices based on these PDI dimers and the donor polymer **PTB7-Th** using inverted BHJ structure. The recorded PCEs for the corresponding OSCs reached up to 6.6% (**III-9a**).

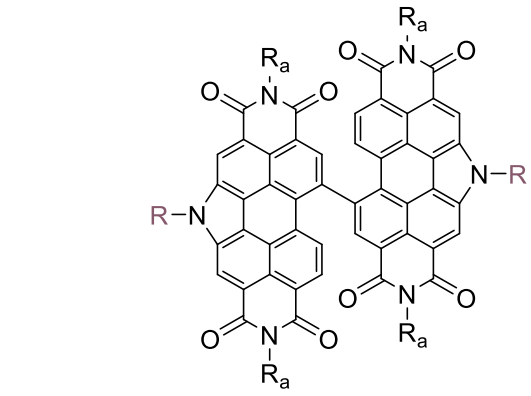

III-(1-9)

R_a= 

$R_{III\text{-}1a}$ = —CH_3

$R_{III\text{-}2a}$ = —CH_2CH_3

$R_{III\text{-}3a}$ = —$CH_2CH_2CH_3$

$R_{III\text{-}4a}$ = —$CH_2CH_2CH_2CH_3$

$R_{III\text{-}5a}$ = —$CH_2CH_2CH_2CH_2CH_3$

$R_{III\text{-}6a}$ = —$CH_2CH_2CH_2CH_2CH_2CH_3$

$R_{III\text{-}7a}$ = —$CH_2CH_2CH_2CH_2CH_2CH_2CH_3$

$R_{III\text{-}8a}$ = —$CH_2CH_2CH_2CH_2CH_2CH_2CH_2CH_3$

$R_{III\text{-}9a}$ = —$CH_2CH(CH_2CH_3)$-$CH_2CH_2CH_2CH_3$

Figure III-1 Reported N-annulated PDI dimers.

III.1.2 Synthesis of N-annulated PDI dimer

While the purpose of the study described above was to study the impact of including different side chains on the *pyrrolic* position of the PDI, we wanted to investigate through side-chain engineering approach the impact of introducing other substituents on the *imide* positions (i.e. cyclohexyl groups) of the PDI. Study of the change that could occur upon the incorporation of the corresponding imide substituents was performed, correlating it to the PDI dimer device performance. This in comparison to the PDI-EPD dimer **III-6a** having ethylpropyl imide substituents, in which both possessing hexyl linear alkyl chains at the *pyrrolic* N-positions.

The synthesis, shown in Figure III-2, starts with the formation of a *pyrrolic* nitrogen at the *bay* position of the PDI, in which mono-nitro PDI **3** was dissolved in o-DCB and treated with triphenylphosphine, followed by microwave heating of the reaction mixture at 180°C for 2h. The product was purified by stirring the mixture in methanol for 1h at room temperature, after which filtration and isolation gave compound **13** in 97% yield. It should be noted that under these experimental conditions, any trace of phosphinimine reported in the previous chapter could be detected.

Due to the low solubility of NH-PDI **13**, it was only characterized by MS spectrometry and used directly in the next step. The low solubility of the N-annulated PDI monomer could be explained by the possible intermolecular hydrogen bonding interactions of adjacent perylene molecules in solution between the N-H and C=O functional groups.[2] Alkylation of NH-PDI **13**, was also carried out using microwave synthesis techniques, in the presence of 1-bromohexane and K_2CO_3 heated in DMF at 170°C for 1h. After purification of the crude product using silica gel chromatography, compound **14** was obtained in 87% yield. Bromination of PDI **14** was achieved in the presence of excess bromine, the reaction mixture was stirred at room temperature in CH_2Cl_2 for 4h after which TLC indicated the complete consumption of PDI **14**. After purification, compound **15** was obtained in 65% yield. Dimerization of PDI was done following a homocoupling reaction in which compound **15** was treated with $Pd_2(dba)_3$ and zinc powder as the catalyst in DMF at 100°C for 6h. The reaction mixture was then passed through a silica plug to remove solid contaminants from the reaction followed by purification using neutral alumina column chromatography. Compound **16** was further purified via recrystallization in methanol and obtained after filtration in 21% yield.

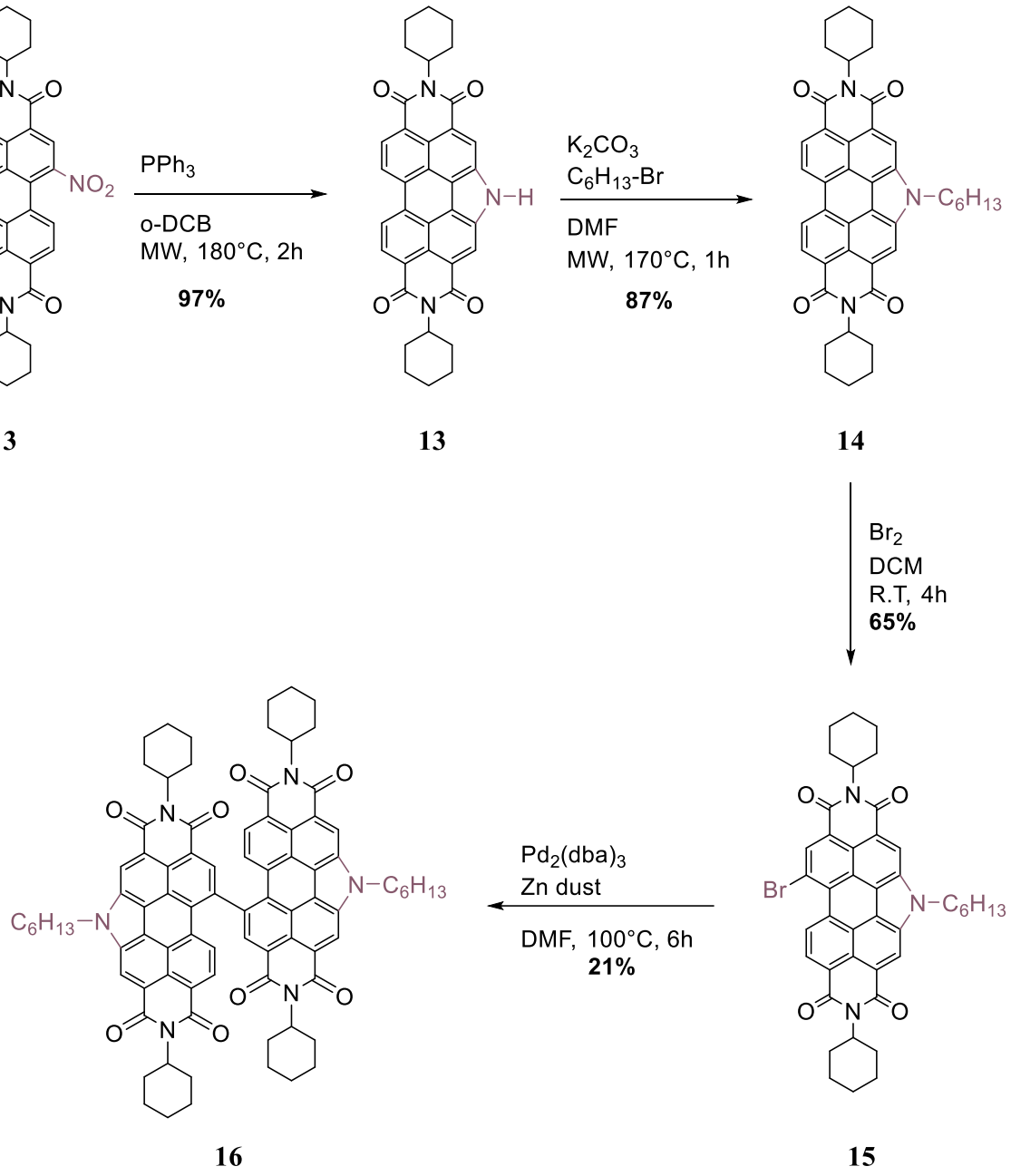

Figure III-2 Synthetic route of N-annulated PDI dimer **16**.

III.1.3 Electronic properties

The electrochemical properties of PDI-Cy dimer **16** were studied by cyclic voltammetry (CV) and differential pulse voltammetry (DPV) in CH_2Cl_2 in the presence of ~0.1 M Bu_4NPF_6 as supporting electrolyte, illustrated in Figure III-3. The study was performed in collaboration with Dr. G. C. Welch research group at the University of Calgary, AB, Canada.

The compound shows clean reversible and oxidation waves, similar to the CV obtained for PDI-EPD dimer and other bay-linked PDI materials.[2] The PDI-EPD dimer differs from PDI-Cy dimer only at the imide *N*-positions, in which ethylpropyl substituents are incorporated instead of cyclohexyl substituents.

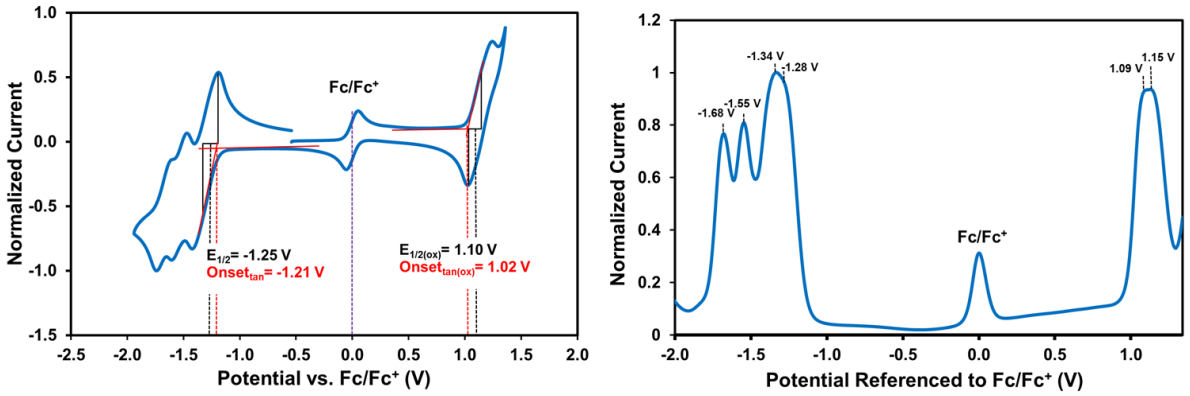

Figure III-3 Cyclic voltammogram and Differential pulse voltammetry of PDI dimer **16** (V vs Fc/Fc^+; Pt as a working electrode; Bu_4NPF_6 ~0.1 M, 100 mV/s, CH_2Cl_2)

The reversibility of the oxidation waves is due to the electron rich N-heterocyclic unit incorporated at the *bay* position of the PDI.[2] The first two reduction processes of both PDIs in the dimer are overlapping, which is also observed in differential pulse voltammogram, leading to $PDI^{\cdot-}$-$PDI^{\cdot-}$ species. Following this two-electron process were observed two one-electron reduction waves at – 1.55 and – 1.68 V corresponding to the generation of PDI^{2-}-$PDI^{\cdot-}$ and PDI^{2-}—PDI^{2-} species, respectively. The HOMO and LUMO energy levels of both PDI dimers were estimated to be -5.9 eV and -3.6 eV.

III.2 Solar cells applications

To assess the photovoltaic performance of PDI-Cy dimer **16**, solution-processed BHJ solar cell devices were fabricated using the inverted device architecture (Glass/ITO/ZnO/BHJ/MoOx/Ag). Experiments were also performed in collaboration with Dr. G. C. Welch research group at the Department of Chemistry at the University of Calgary. The first electron donor chosen was **PTB7-Th** (chemical structure shown in Figure III-4) which has already been reported to achieve good OPV device performances with PDI dimers.[2,3] This allowed for a direct comparison of a 1:1 **PTB7-Th: PDI-Cy dimer active layer** with a **PTB7-Th: PDI-EPD dimer** which has been previously reported.[2]

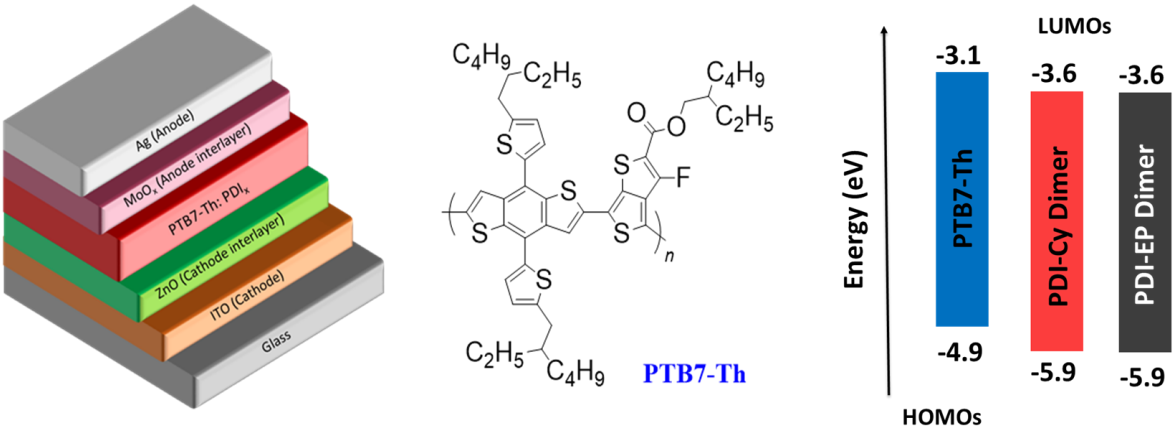

Figure III-4 Device Architecture, chemical structure of **PTB7-Th** and energy level diagram of active layer materials.

Active layer BHJ blends were spin-cast using o-xylene as the processing solvent that readily dissolves both donor and acceptor, at 10 mg/mL concentrations and cast at 1000 rpm. In general, the donor: acceptor blends were cast onto glass/indium tin oxide (ITO) substrates coated with a thermally annealed sol-gel ZnO preparation, acting as the electron transport layer. The anode interlayer MoO_x (10 nm) was then thermally evaporated onto the organic films followed by the evaporation of 100 nm of Ag as the anode. The resulting PCEs were 3.2% for PDI-Cy dimer and 4.7% for PDI-EPD dimer, with similar high open-circuit voltages (V_{OC}) of 0.96 and 0.97 V and similar fill factors (FF) of 47 %. The main gap in performance is related to the short circuit current (J_{SC}), which is 7.3mA/cm^2 for PDI-Cy dimer and 10.3 mA/cm^2 for PDI-EPD dimer (Table III-1 and Figure III-5).

The photovoltaic performance was also investigated using a different donor, the **PPDT2FBT** (Figure III-6). The noncovalent coulomb interactions occurring between neighboring moieties of the donor structure is responsible for minimizing the torsional angle, therefore maximizing the planarity and ordering of the polymer chain which leads to highly ordered film morphologies, deep HOMO level and devices with high level of stability.[4] The HOMO (-5.5 eV) level of this donor was estimated from cyclic voltammetry (~10mg/mL, ~0.1 M Bu_4NPF_6, 100 mV/s, o-xylene) and the LUMO (-3.7eV) level calculated from the HOMO value and the optical band gap of the film which was determined to be 1.82 eV.

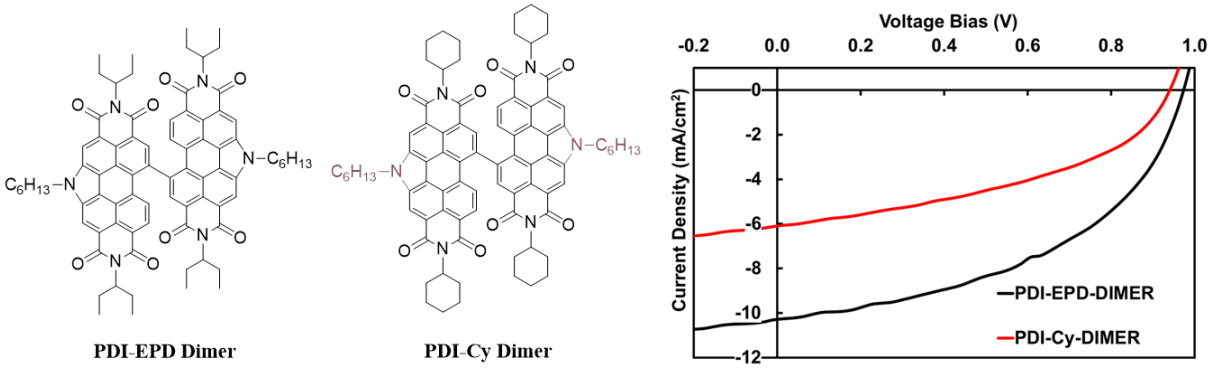

Figure III-5 Chemical structure of the acceptors used. J-V curves for the active layer blends **PTB7-Th: PDI-EPD** dimer (black) and **PTB7-Th: PDI-Cy dimer** (red).

Table III-1 OPV devices performance parameters and statistics for **PTB7-Th: PDI$_x$** active layer blend, cast from a 1:1 ratio at 10 mg/mL in o-xylene.

Acceptor	Voc (V)	Jsc (mA/cm^2)	FF (%)	PCE (%)
PDI-Cy dimer	0.94 (0.96)	6.7 (7.3)	44 (46)	2.8 (3.2)
PDI-EPD dimer	0.96 (0.97)	10.2 (10.3)	47 (47)	4.6 (4.7)

Average (Best) device.

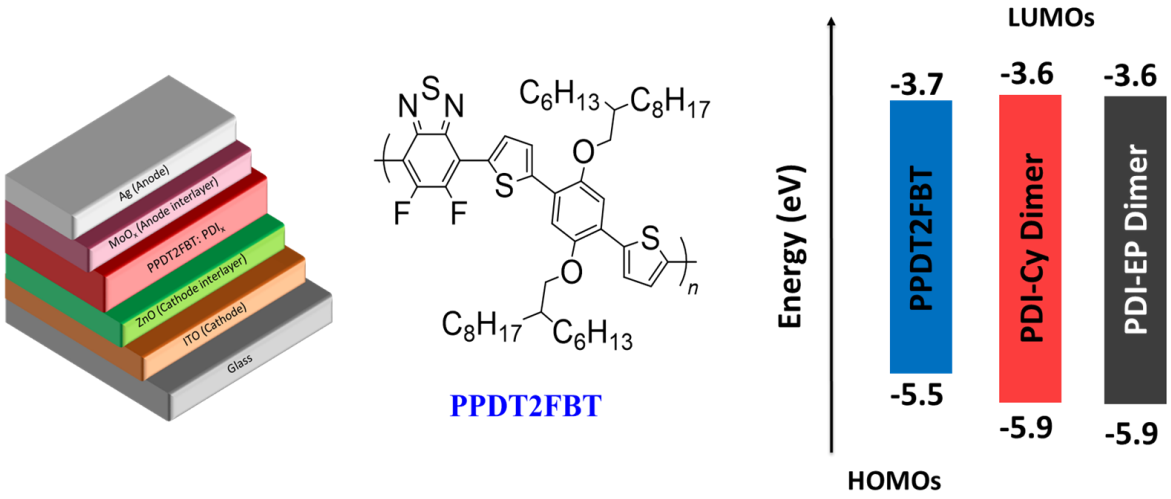

Figure III-6 Device Architecture, chemical structure of **PPDT2FBT** and energy level diagram of active layer materials.

Active layer BHJ blends were spin-cast using also o-xylene as the processing solvent at 20 mg/mL and cast at 2000 rpm.

Table III-2 OPV devices performance parameters and statistics for **PPDT2FBT: PDI-Cy dimer** active layer blend, cast from a 1:1 ratio at 20 mg/mL in o-xylene with various concentrations of DPE.

Processing	Voc (V)	Jsc (mA/cm^2)	FF (%)	PCE (%)
0.0 % v/v DPE	0.99 (1.00)	4.4 (4.6)	37 (37)	1.6 (1.7)
0.25% v/v DPE	1.00 (1.00)	5.0 (5.2)	38 (38)	1.9 (2.0)
0.5% v/v DPE	0.99 (1.00)	5.5 (5.9)	38(39)	2.1(2.3)
0.75% v/v DPE	0.99 (1.00)	5.9 (6.2)	38 (39)	2.2(2.4)
1.0% v/v DPE	0.98 (0.98)	5.7 (5.7)	39 (39)	2.1 (2.2)
3.0% v/v DPE	1.00 (0.99)	6.4 (6.9)	41 (42)	2.6 (2.8)
5.0% v/v DPE	0.99 (1.01)	6.8 (6.8)	40 (41)	2.7 (2.8)
8.0% v/v DPE	1.00 (1.01)	6.7 (6.6)	41(42)	2.8 (2.8)
10% v/v DPE	1.01(1.01)	6.1(6.1)	44 (42)	2.7 (2.7)

Average (Best) device.

The best device efficiencies were 1.7% for PDI-Cy dimer and 2.0% for PDI-EPD dimer with high V_{OC} at 1.00 V, FF at 37 % with J_{SC} being the only difference between these three parameters, 4.6 mA/cm^2 for PDI-Cy dimer and 5.3 mA/cm^2 for PDI-EPD dimer (Table III-2, Table III-3 and Figure III-8).

Table III-3 OPV devices performance parameters and statistics for **PPDT2FBT: PDI-EPD dimer** active layer blend, cast from a 1:1 ratio at 20 mg/mL in o-xylene with various DPE concentrations.

Processing	Voc (V)	Jsc (mA/cm^2)	FF (%)	PCE (%)
0.0 % v/v DPE	1.00 (1.00)	5.0 (5.3)	37 (37)	1.9 (2.0)
0.25% v/v DPE	1.00 (1.00)	5.6 (5.7)	40 (40)	2.2 (2.3)
0.50% v/v DPE	1.00 (1.00)	6.0 (6.3)	41 (41)	2.5 (2.6)
0.75% v/v DPE	1.01 (1.01)	6.7 (6.6)	43 (44)	2.9 (3.0)
1.0% v/v DPE	1.00 (1.00)	5.6 (6.0)	41 (42)	2.3 (2.5)
3.0% v/v DPE	1.00 (1.01)	6.3 (6.7)	42 (41)	2.7 (2.8)
5.0% v/v DPE	1.01 (1.01)	6.7 (6.9)	44 (45)	3.0 (3.1)
8.0% v/v DPE	1.00 (1.00)	6.4 (6.5)	42 (43)	2.7 (2.8)
10% v/v DPE	0.91 (0.91)	7.7 (7.7)	44 (44)	3.1 (3.1)

Average (Best) device.

The use of solvent additive diphenyl ether (DPE) has been previously reported to promote aggregation and crystallization of PDI and *N*-PDI NFAs.[1,5] Hence, it was then implemented in the processing of the active layer blends, in order to evaluate its influence on PDIs self-assembly properties. Solvent additives are commonly known to drastically improve the PCE.[6,7] Through their interaction with the photoactive layer, they play major roles in affecting surface and bulk morphologies evolution of the BHJ blends.[8–11] This can lead to highly ordered domains, increased phase separation in the active layer and therefore more efficient charge extraction.[12]

PPDT2FBT: PDI dimer active layer blends exhibit complementary absorption profiles (Figure III-7). **PPDT2FBT** spans the absorption spectra from 350 to 750 nm with a maximum at ~651 nm and a higher energy band at ~600 nm also attributed to the polymer, while PDI dimers fill

expectedly the region from 450 to 600 nm. No significant difference is observed in the absorption bands or their intensities upon addition of DPE.

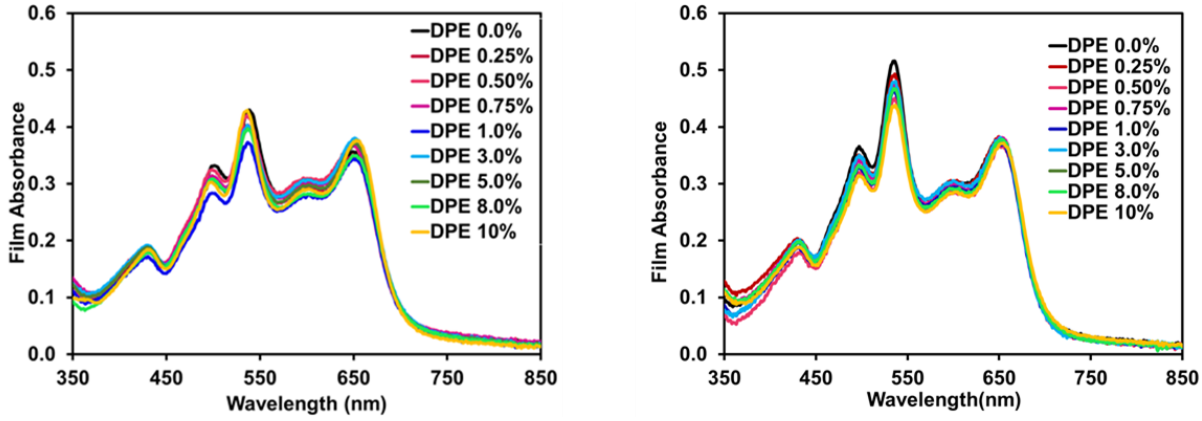

Figure III-7 Thin-film absorption profiles of the BHJ blends, **PPDT2FBT: PDI-Cy dimer** (left) and **PPDT2FBT: PDI-EPD dimer** (right).

The performances (Figure III-8) of **PPDT2FBT: PDI dimer** based devices were found to slightly increase upon increasing solvent additive values (0.25, 0.5, 0.75, 1.0, 3.0, 5.0, 8.0, 10.0 % v/v), in which PCEs for PDI-Cy dimer and PDI-EPD dimer reached up to 2.7% and 3.1%, respectively at 10.0% v/v DPE. This was accompanied by a consistent high open-circuit voltages (V_{OC}) around 1.00V and increase in fill factors (FF) reaching in both dimers 44% at 10% v/v DPE, in addition to the increase in short-circuit current (J_{SC}) values from 5.0 at 0.25 % to 6.1 at 10% v/v DPE for PDI-Cy dimer and 5.6 at 0.25 % to 7.7 at 10% v/v DPE for PDI-EPD dimer. Thin films absorption spectra of the active layer blends were also recorded without and with the solvent DPE additive with a varying range of concentration (0.25-10.0 %).

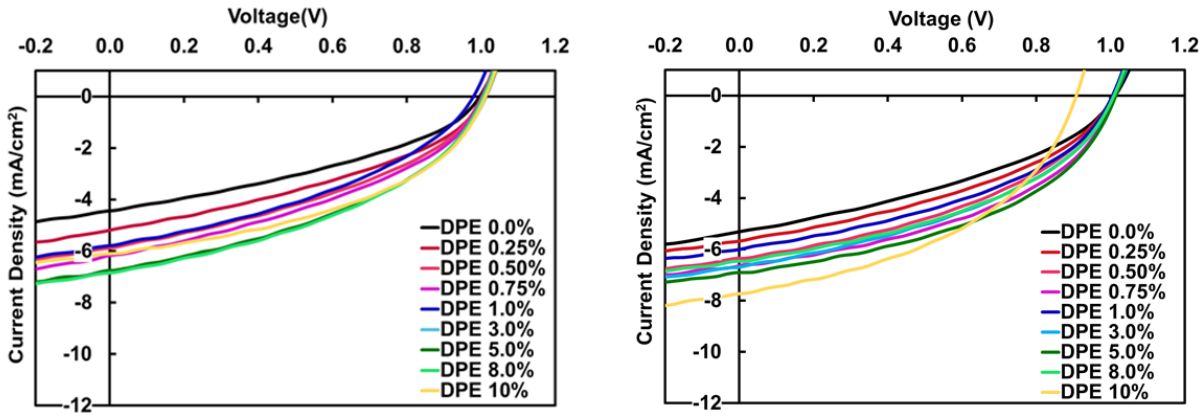

Figure III-8 J-V curves for the corresponding active layer blends, **PPDT2FBT: PDI-Cy dimer** (left) and **PPDT2FBT: PDI-EPD dimer** (right).

Moreover, optical properties of neat film of PDI-Cy dimer processed with and without DPE were also studied (Figure III-9). Film absorption spectra of the dimer **16** shows strong absorption in the visible region between 450 to 550 nm, characteristic of the π–π* electronic transition of PDI derivatives. A first peak with a maximum (λ_{max}) at ~540 nm corresponds to the 0–0 vibronic transition, and a weaker peak at ~500 nm which corresponds to 0–1 vibronic transition.

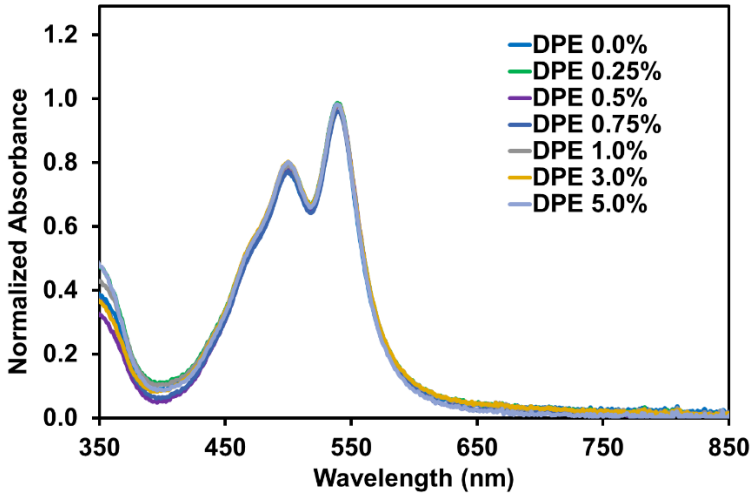

Figure III-9 Film absorption spectra of neat films of PDI-Cy-dimer.

The absorption profile of the neat films shows no significant change upon varying DPE additive concentration, this is also reflected on polarized optical microscopy (POM) and fluorescence microscopy (FM) images where no aggregation of the PDI is observed. Similarly, POM and FM images of neat films of PDI-EPD dimer show that DPE did not induce crystallization within the film. In contrast, processing films with another solvent additive, 1,8-diiodooctance (DIO) (3% v/v) induced aggregation within the films, for PDI-EPD dimer, distinct crystalline features are observed in POM images, and FM images that show their emission of red light, characteristic color emission for PDI chromophores. Whereas PDI-Cy dimer films show flower-like less ordered aggregates as shown by POM and FM images (Figure III-10).

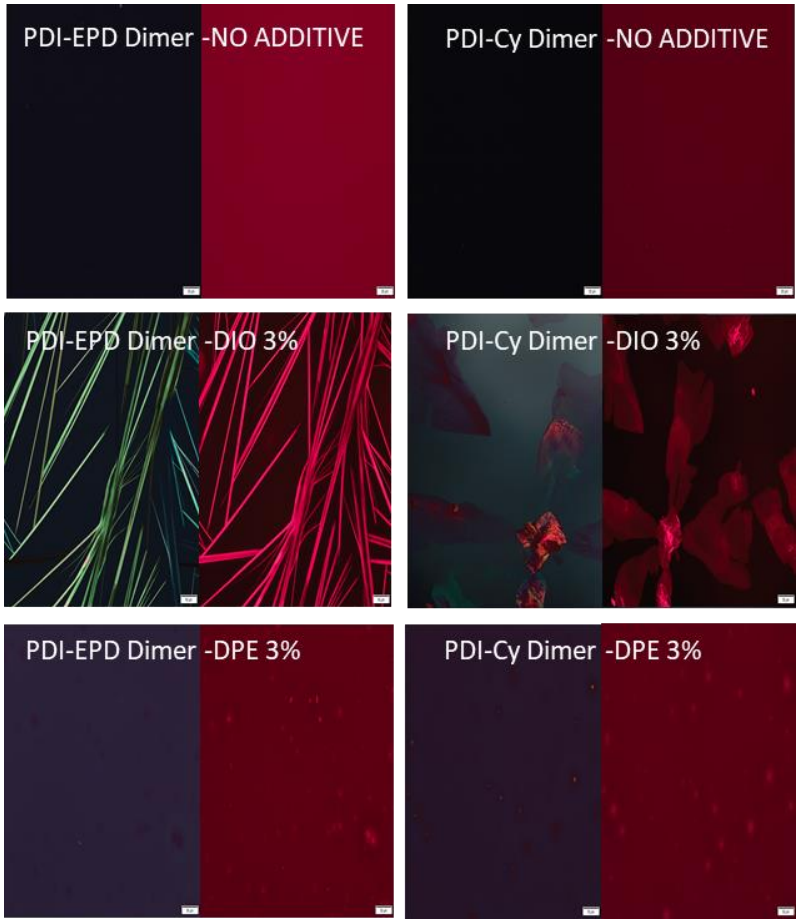

Figure III-10 POM and FM images of neat films of PDI-EPD dimer and PDI-Cy dimer spun cast from 10mg/ml solution in o-xylene without and with 3% of DPE or DIO.

The photovoltaic performance of **PPDT2FBT: PDI dimer** active layer blends were probed with different donor-acceptor ratio for optimization. Active layer BHJ blends were spin-cast in a similar manner, using also o-xylene, at 20 mg/mL concentrations and cast at 2000 rpm with D:A ratios 1:1, 1:2, 2:1, 2:3 and 3:2. The best donor-acceptor ratio was found to be with higher acceptor loadings, which is interesting, considering the cost of the donor and the ease of the preparation of the corresponding PDI acceptors. Following the optimized processing conditions, the best device efficiency was achieved with 2:3 donor-acceptor ratio having the highest PCEs, as a result of higher fill factor (FF) and short-circuit current (J_{SC}) in comparison with other ratios, accompanied by a high open-circuit voltages (V_{OC}). Compared to PDI-Cy dimer device efficiency that reached 2.2% PCE at 2:3 ratio, PDI-EPD dimer was a better performing cell which recorded higher FF (44% versus 39%) and Jsc (7.8 mA/cm^2 versus 5.6 mA/cm^2) with 3.5% PCE (Table III-4 and Table III-5).

Thin films absorption spectra of the corresponding active layer blends were also recorded. Both **PPDT2FBT: PDI-Cy dimer** and **PPDT2FBT: PDI-EPD dimer** absorption profile show an

increase in the intensity of the peaks attributed to the donor polymer, with the highest intensity related to 2:1 ratio, whereas a slight increase in the intensity of PDI absorption bands is observed which is more important in PDI-EPD dimer, with no significant difference between both analyzed spectra at different ratios.

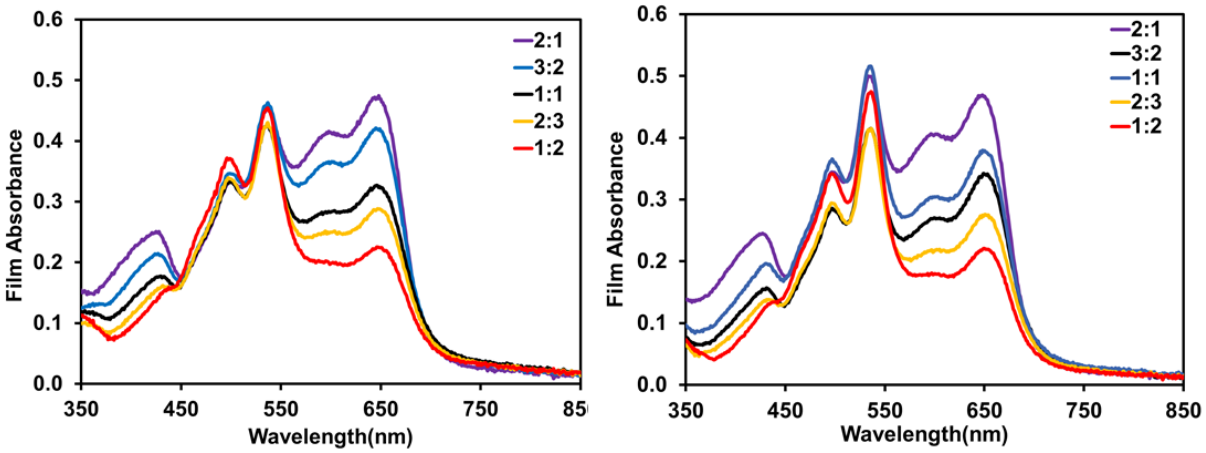

Figure III-11 Thin-film absorption profiles of the BHJ blends, **PPDT2FBT: PDI-Cy dimer** (left) and **PPDT2FBT: PDI-EPD dimer** (right).

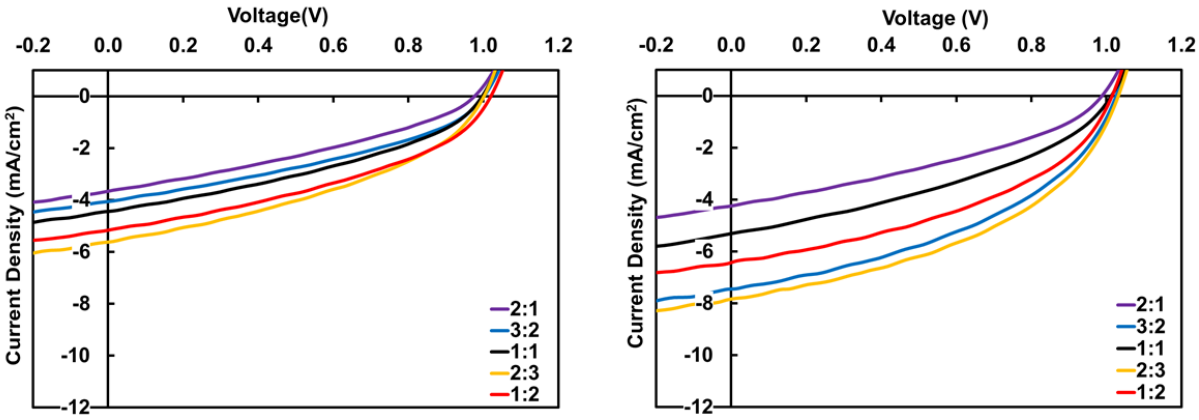

Figure III-12 J-V curves for the corresponding active layer blends, **PPDT2FBT: PDI-Cy dimer** (left) and **PPDT2FBT: PDI-EPD dimer** (right).

Table III-4 Optimization device parameters for organic solar cell devices of **PPDT2FBT: PDI-Cy dimer** active layer blend cast from 20 mg/mL solutions in o-xylene with various ratios.

Ratio	Voc (V)	Jsc (mA/cm^2)	FF (%)	PCE (%)
2:1	0.97 (0.97)	3.5 (3.7)	33 (33)	1.1 (1.2)
3:2	0.99 (1.00)	3.9 (4.0)	36 (36)	1.4 (1.5)
1:1	0.99 (1.00)	4.4 (4.6)	37 (37)	1.6 (1.7)
2:3	1.00 (1.00)	5.6 (5.6)	39 (39)	2.2 (2.2)
1:2	1.01 (1.02)	5.1 (5.2)	39 (39)	2.0 (2.0)

Average (Best) device.

Table III-5 Optimization device parameters for organic solar cell devices of **PPDT2FBT: PDI-EPD dimer** active layer blend cast from 20 mg/mL solutions in o-xylene with various ratios.

Ratio	Voc (V)	Jsc (mA/cm^2)	FF %	PCE %
2:1	0.99 (0.98)	4.0 (4.2)	35 (35)	1.4 (1.5)
3:2	1.01 (1.03)	7.4 (7.6)	42 (43)	3.1 (3.4)
1:1	1.00 (1.00)	6.0 (6.3)	41 (41)	2.5 (2.6)
2:3	1.02 (1.03)	6.8 (7.8)	43 (44)	3.0 (3.5)
1:2	1.01 (1.01)	6.4 (6.4)	42 (42)	2.7 (2.7)

Average (Best) device.

Analysis of the surface morphology of the active layers by atomic force microscopy (AFM) were also carried out, in which films were processed with and without solvent additives DPE, 1,8-diiodooctance (DIO) (Figure III-13). The study revealed non-uniform surfaces with a moderate increase in roughness for **PPDT2FBT: PDI-EPD dimer** active layers compared to non-additive processed films where the highest root-mean-square (RMS) roughness reached 3.7 nm when using 3% v/v DPE during film formation. In the case of **PPDT2FBT: PDI-Cy dimer**, non-additive processed films showed RMS of 2.5 nm that remained insignificantly changed upon using 3% v/v DPE or DIO during film formation, in which RMS of 2.6 nm was recorded.

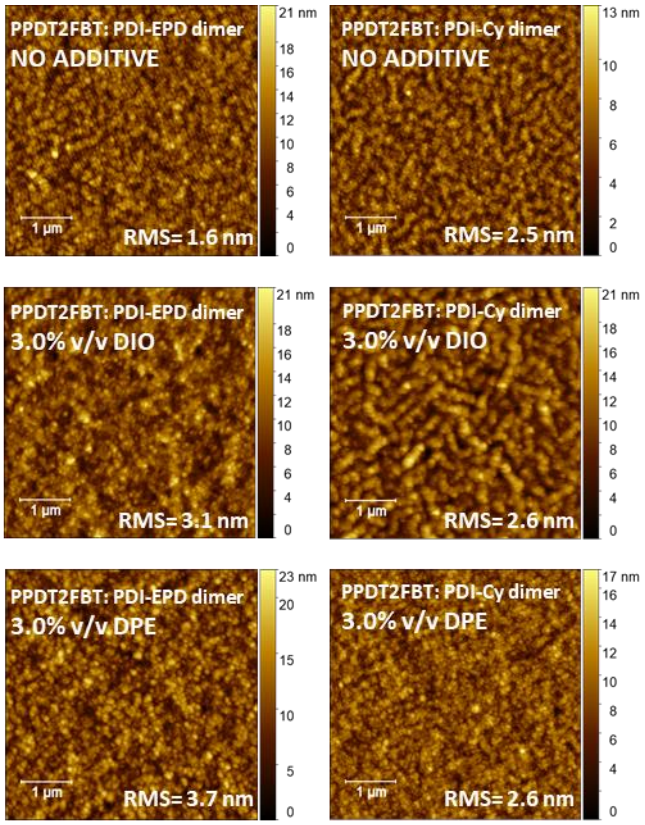

Figure III-13 AFM images of the active layer blends.**PPDT2FBT: PDI-EPD dimer** (left) and **PPDT2FBT: PDI-Cy dimer** (right) spun cast with and without 3.0% v/v DPE or DIO.

III.3 Conclusion

To investigate the application of PDIs in solar cells as powerful acceptors, we have prepared PDI-Cy dimer **16** in our laboratory and characterized it during an internship period at the University of Calgary in Calgary, AB. Consequently, we started studies on side chains engineering on the imide positions of PDI and compared the photovoltaic performance of PDI-Cy dimer **16** with PDI-EPD dimer using first as electron donor **PTB7-Th** in which the best PCEs reached for **PTB7-Th: PDI$_x$** active layer blends were 3.2% and 4.2%. We also investigated the photovoltaic performance of these dimers blended with another donor, which is **PPDT2FBT**. During the process of the active layer blends, increasing values of the solvent additive DPE were implemented, which reflected an increase in performances of **PPDT2FBT: PDI$_x$** based devices reaching up to 2.7% and 3.1% at 10.0% v/v DPE for PDI-Cy dimer and PDI-EPD dimer, respectively, accompanied by a consistent high V_{OC}, increase in FF and J_{SC} values.

Analysis of absorption profiles, polarized optical microscopy (POM) and fluorescence microscopy (FM) images of the films indicated a difference in the dimers when processed with DIO but not when possessed with DPE. AFM images showed that the surface morphology of the **PPDT2FBT: PDI-EPD dimer** active layer is more affected by the presence of solvent additives than **PPDT2FBT: PDI-Cy dimer**.

To optimize the processing conditions, **PPDT2FBT: PDI$_x$** active layer blends were probed with different donor-acceptor ratio. The results showed best performances at 2:3 donor-acceptor ratio in which an increase of FF and J_{SC}, accompanied by high V_{OC} resulted in PCEs of 2.2% and 3.5% for PDI-Cy dimer and PDI-EPD dimer, respectively.

III.4 References

[1] S. V. Dayneko, A. D. Hendsbee, G. C. Welch, *Small Methods* **2018**, *2*, 1800081.

[2] A. D. Hendsbee, J.-P. Sun, W. K. Law, H. Yan, I. G. Hill, D. M. Spasyuk, G. C. Welch, *Chem. Mater.* **2016**, *28*, 7098–7109.

[3] S. M. McAfee, J. M. Topple, I. G. Hill, G. C. Welch, *Journal of Materials Chemistry A* **2015**, *3*, 16393–16408.

[4] T. L. Nguyen, H. Choi, S.-J. Ko, M. A. Uddin, B. Walker, S. Yum, J.-E. Jeong, M. H. Yun, T. J. Shin, S. Hwang, et al., *Energy & Environmental Science* **2014**, *7*, 3040–3051.

[5] M. Li, J. Liu, X. Cao, K. Zhou, Q. Zhao, X. Yu, R. Xing, Y. Han, *Physical Chemistry Chemical Physics* **2014**, *16*, 26917–26928.

[6] Y. Zheng, T. Goh, P. Fan, W. Shi, J. Yu, A. D. Taylor, *ACS Appl. Mater. Interfaces* **2016**, *8*, 15724–15731.

[7] R. Lin, M. Wright, A. Uddin, *physica status solidi (a)* **2013**, *210*, 1785–1790.

[8] M.-S. Su, C.-Y. Kuo, M.-C. Yuan, U.-S. Jeng, C.-J. Su, K.-H. Wei, *Advanced Materials* **2011**, *23*, 3315–3319.

[9] A. Laventure, S. Stanzel, A.-J. Payne, B. H. Lessard, G. C. Welch, *Synthetic Metals* **2019**, *250*, 55–62.

[10] M. Li, L. Wang, J. Liu, K. Zhou, X. Yu, R. Xing, Y. Geng, Y. Han, *Physical Chemistry Chemical Physics* **2014**, *16*, 4528–4537.

[11] C. McDowell, M. Abdelsamie, M. F. Toney, G. C. Bazan, *Advanced Materials* **2018**, *30*, 1707114.

[12] H. Zhong, C.-H. Wu, C.-Z. Li, J. Carpenter, C.-C. Chueh, J.-Y. Chen, H. Ade, A. K.-Y. Jen, *Advanced Materials* **2016**, *28*, 951–958.

Chapter IV : Reactivity of amino-*bay* substituted PDI

IV.1 Preparation of amino-*bay* PDI

Among all the available reducing agents for the reduction of the nitro functional group on the PDI chromophore previously used and discussed was chosen the catalytic hydrogenation of compound **3** for its transformation to amino-PDI **17**, in which palladium on activated charcoal (Pd/C) was introduced into a sealed reaction system containing hydrogen gas. The reaction mixture was stirred at room temperature in DMF for 2h during which the reaction color turned from red to violet. After, the solvent was concentrated and the crude product was purified by using neutral alumina column chromatography. Further purification via precipitation from $CHCl_3$/petroleum ether gave after filtration compound **17** in 81% yield (Figure IV-1). The reaction was also carried out in THF, ethyl acetate and CH_2Cl_2, however, the product was only obtained when THF was employed as the solvent and with lower yields compared to the reactions done in DMF.

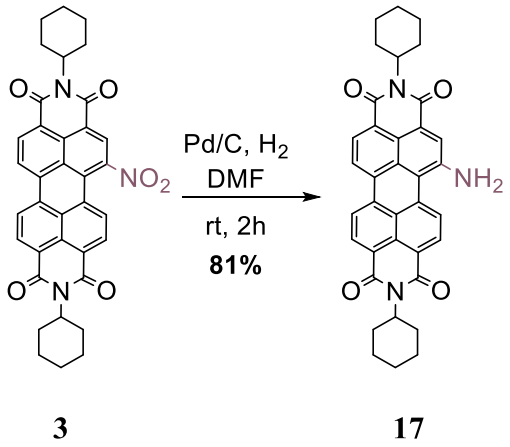

Figure IV-1 Reduction reaction of compound **3**.

Similar to mono-nitro PDI **3**, quantum chemical calculations were also performed for mono-amino PDI **17** using density functional theory (DFT) at the PBE0/6-311+G(2df,2pd) level which revealed that the HOMO is delocalized mainly on the amino group and the perylene core, as expected, while the LUMO is extended along the central perylene core to the bisimide groups (Figure IV-2). Going from mono-nitro PDI to PDI **17**, a decrease of the HOMO and LUMO energy levels is observed, -6.06 eV (*vs* -6.69 eV) and -3.40 eV (*vs* -3.90 eV) respectively, due to the electron-donating ability of the amino group.

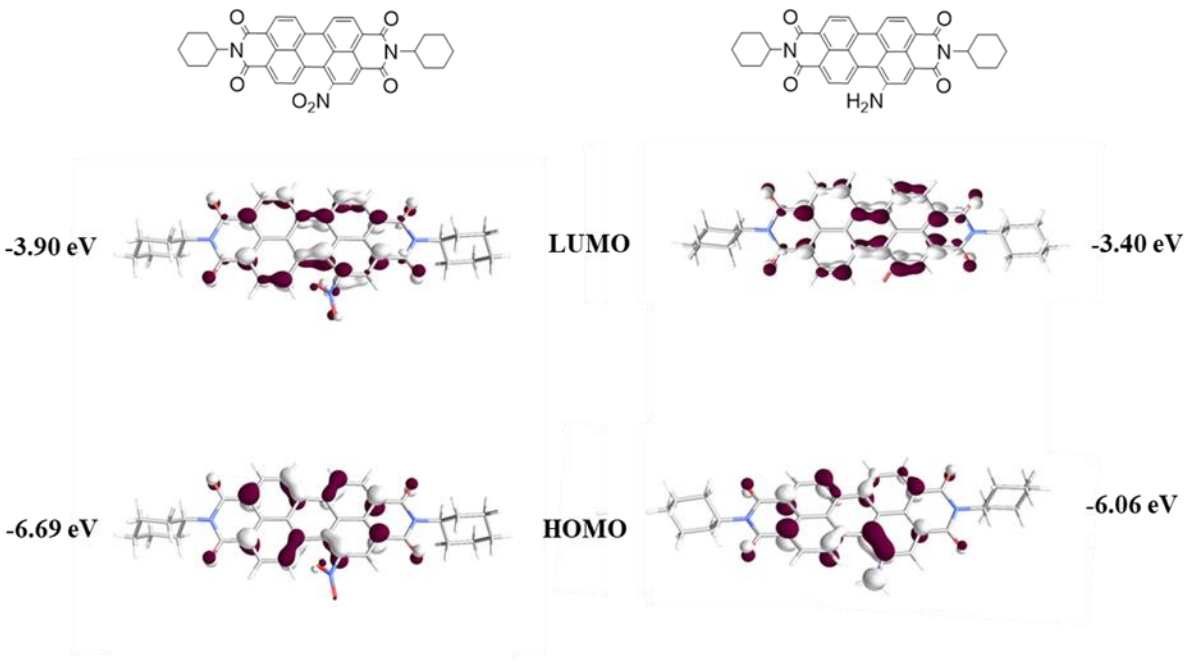

Figure IV-2 PBE0/6-311+G(2df,2pd) computed FOs of mono-nitro PDI **3** and mono-amino PDI **17**. HOMOs (bottom) and LUMOs (top).

IV.2 Diazonium salt chemistry

IV.2.1 Diazotization of PDI

IV.2.1.1 Preparation pathways

The reactivity of the mono-amino PDI was first investigated through the one pot synthesis of diazonium salt of PDI, in which the mono-nitro PDI was transformed into the mono-amino PDI following the catalytic hydrogenation procedure described above, using THF as solvent. The reaction mixture was stirred for 2h at room temperature before the addition of a mixture containing sodium nitrite, $NaNO_2$ (10 equivalents) and fluoroboric acid diethyl ether complex, $HBF_4 \cdot Et_2O$ (20 equivalents). The reaction mixture was stirred at 0°C for around 90 min, during which the reaction color turned from violet to dark brown. Precipitation and filtration using diethyl ether afforded the diazonium salt of PDI **18** in 90% yield (Figure IV-3). Arenediazonium salts are unstable at room temperature and should be used directly after their formation, however tetrafluoroborates are among the salts known to be stable at room temperature.[1] The product was allowed to be stored at low temperatures for a duration that did not exceed 24h before its use in the next step reactions, such as Sandmeyer reactions. Although this synthetic method proved to be effective to give the expected product, it was realized that this diazotization reaction carried out several times under the same conditions was suffering from reproducibility. Carrying

out the same reaction procedure with using water into the bargain to dissolve $NaNO_2$ before its addition followed by the addition of $HBF_4{\cdot}Et_2O$ at 0°C did not lead to the formation of the product wanted.

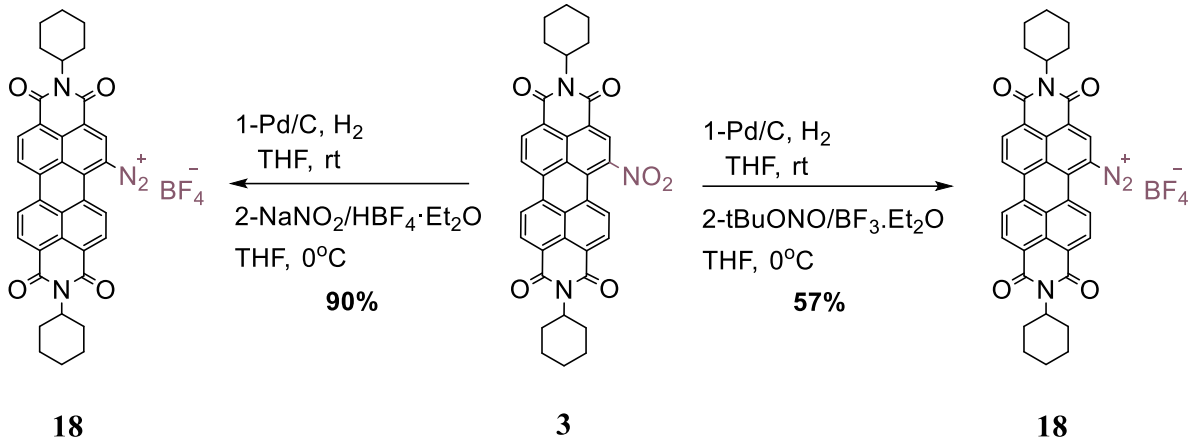

Figure IV-3 Diazotization reaction.

Moreover, replacing $NaNO_2$ and $HBF_4{\cdot}Et_2O$ with tert-butylnitrite, *t*BuONO (1.5 equivalents) and boron trifluoride etherate, $BF_3{\cdot}Et_2O$ (1.2 equivalents), was unsuccessful.[2] In this one-pot synthesis, $BF_3{\cdot}Et_2O$ was added to the reaction mixture containing amino-PDI followed by the addition of *t*BuONO dropwise at 0°C. The reaction was stopped after 30 min during which no color change was noticed. However, following the same procedure while increasing the equivalents of *t*BuONO and $BF_3.Et_2O$ to 10 equivalents and 20 equivalents, respectively, introduced a positive effect on the reaction. An instantaneous color change after the complete addition of *t*BuONO was observed and compound **18** was obtained after precipitation and filtration using diethyl ether in 57% yield (Figure IV-3). Despite the success of this method, complications were also noticed through the repetitive use of this procedure that was also suffering from reproducibility.

To overcome the intricacy of this procedure, diazotization was also performed on a mono-nitro PDI having ethylpropyl group on its imide position instead of cyclohexyl group. It is known that the PDI bearing ethylpropyl groups are more soluble than those with cyclohexyl groups at the *N*-imide positions. Hence, this would allow the study of the effect of solubility on the formation of the diazonium salt of the PDI and the reproducibility of the corresponding reaction. The mono-nitro PDI **20** was synthesized using CAN and HNO_3 in CH_2Cl_2 under ambient temperature and obtained after purification in 75% yield (Figure IV-4). The nitration reaction can also be carried out without the use of CAN,[3] as described before for PDI **3**. After, the conversion reaction of the mono-nitro PDI into the diazonium salt was carried out in one-pot synthesis, in

which the reduction reaction was performed using palladium on activated charcoal introduced into a sealed reaction system containing hydrogen gas. The reaction mixture was stirred in THF for 2h at room temperature before the addition of a mixture containing sodium nitrite, $NaNO_2$ (10 equivalents) and $HBF_4 \cdot Et_2O$ (20 equivalents). The reaction mixture was stirred at 0°C for around 90 min followed by precipitation and filtration using diethyl ether to afford diazonium salt of PDI **22** in 57% yield (Figure IV-4). The use of this procedure for the reformation of PDI **22** was also not successful, which indicates that the solubility was not the main reason behind the difficulty of such diazotization reaction.

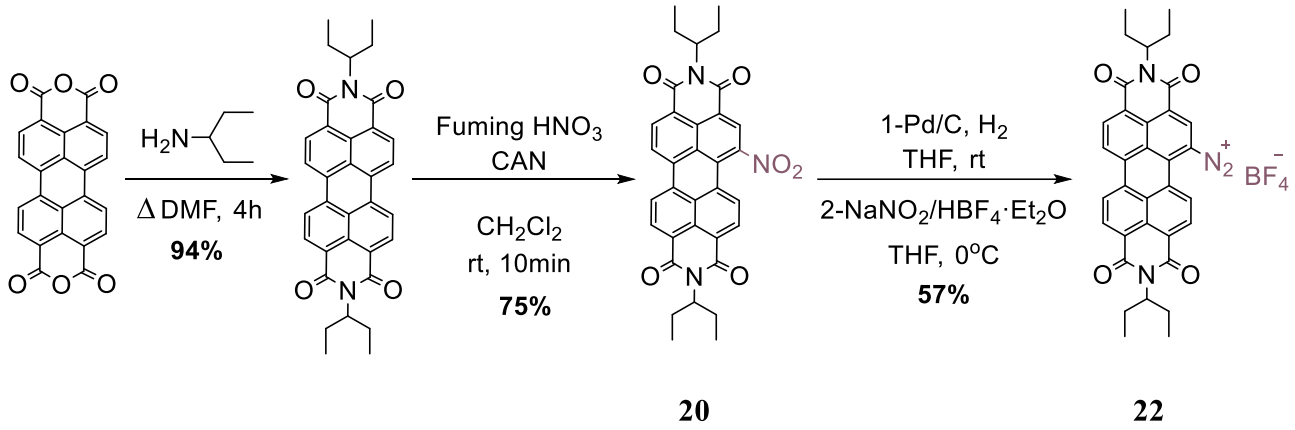

Figure IV-4 Diazotization reaction.

IV.2.2 Transformation of the diazonium salt

IV.2.2.1 Fluorination

IV.2.2.1.1 Balz–Schiemann reaction

IV.2.2.1.1.1 Thermal properties

The thermal properties of compound **22** were investigated by thermogravimetric analysis (TGA) and differential scanning calorimetry (DSC), as shown in Figure IV-5, in which the study demonstrates that weight loss of about 14.62% occurring at around 85-105°C, is in good agreement with the theoretical calculation of 15% that is most likely due to the fragmentation of $N_2^+BF_3^-$, and hence the molecule becomes mono-fluorinated. The DSC thermogram shows that fusion of the new formed compound occurs at 236°C which corresponds to its melting point. This study allows the knowledge of the temperature at which compound **22** is converted into mono-fluoro PDI following Balz–Schiemann reaction, where the aryl fluorides are prepared via thermal decomposition of the aryl diazonium salts through the replacement of the diazonium group by fluorine atom.

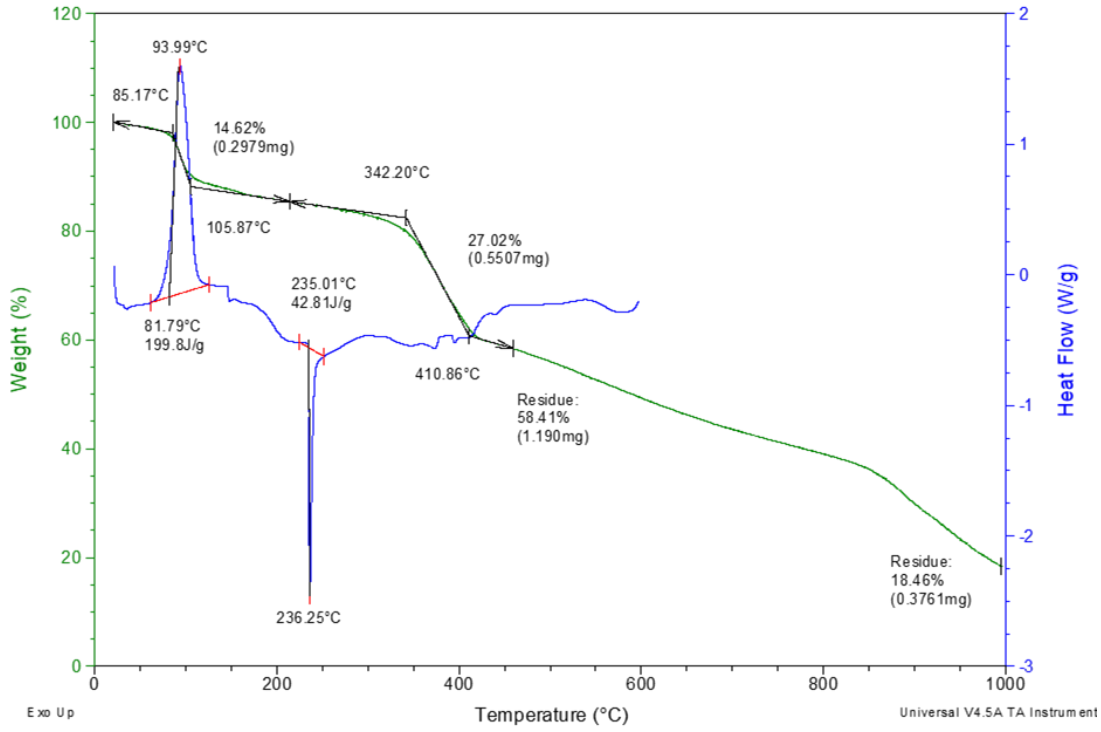

Figure IV-5 DSC-TGA analysis.

The fluorination reaction shown in Figure IV-6 was carried out at 235°C, in which the isolated diazonium salts of PDI **18** and **22** were heated under solvent-free conditions for 2h during which

the color of the violet solid turned to dark brown. After purification using silica gel column chromatography, the mono-*bay* fluoro PDI **23** and **24** were obtained as traces.

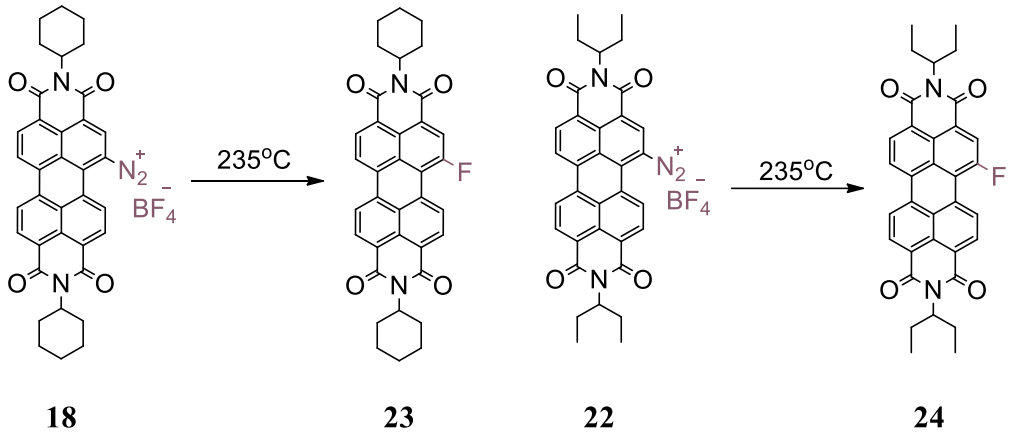

Figure IV-6 Fluorination reaction of the diazonium salts of PDI **18** and **22**.

IV.2.2.2 Iodination

The iodination reaction (Figure IV-7) of isolated diazonium salt from PDI **18** treated with KI or NaI in THF at room temperature was not successful. However, carrying out one-pot diazotization–iodination of mono-amino PDI gave successfully the mono-*bay i*odo PDI **25** after purification with silica gel column chromatography, despite the very low yields (< 8%). The one pot synthetic procedures for the preparation of PDI **25** starts with the reduction of the mono-nitro PDI **3**, followed by the simultaneous addition of $NaNO_2$, $HBF_4{\cdot}Et_2O$ and KI at -78°C, stirred for 24h. Another method used included the reduction of mono-nitro PDI **3**, followed by the diazotization using $NaNO_2$ and $HBF_4{\cdot}Et_2O$ (or *t*BuONO and $BF_3{\cdot}Et_2O$) at 0°C for 90 min after which KI was added and the reaction mixture was stirred at room temperature for additional 24h. It should be noted that hydro-dediazotization reaction could occur during the synthesis of PDI **25**, in which the diazonium group is replaced by a hydrogen atom through hydrogenolysis of the PDI diazonium salt leading to parent PDI **2** as by-product. Of the mechanisms proposed for the reductive dediazotization,[1,4,5] are the ionic pathway in which the aryl cations are generated and reduced by a hydride source, and the radical pathway, in which, aryl radicals are generated and undergo hydrogen atom abstraction from a reagent or a solvent, such as DMF, methanol, ethanol or THF.

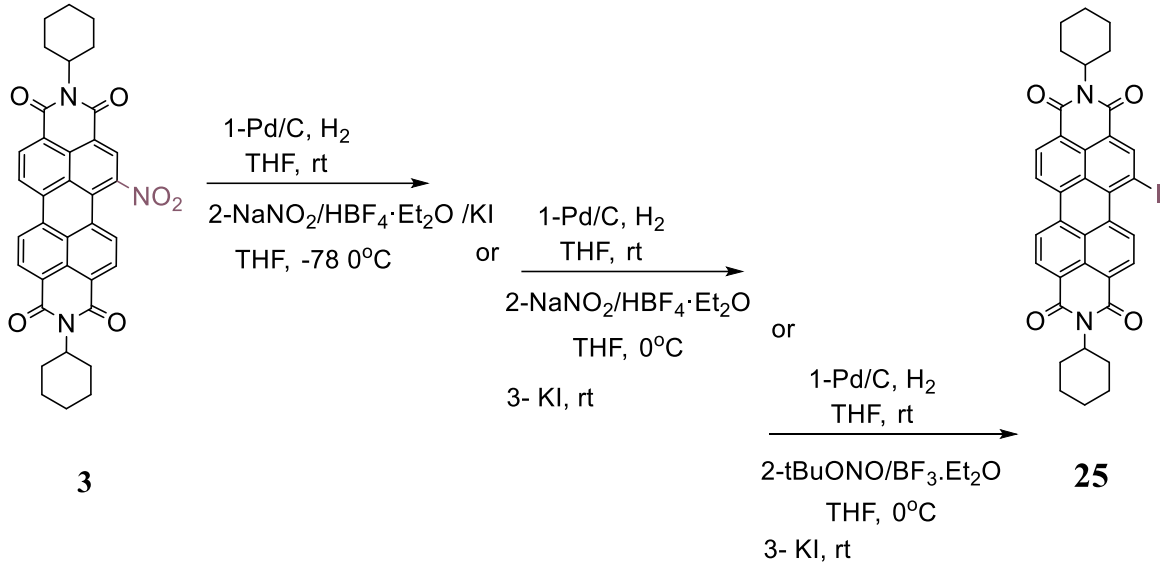

Figure IV-7 One-pot synthesis of mono-*bay* iodo PDI.

IV.2.2.3 Bromination

The one-pot synthesis of brominated PDI was carried out using modified literature procedure,[6] in which the reduction of the mono-nitro PDI **3** via the catalytic hydrogenation is followed by the addition of $NaNO_2$ dissolved in water and hydrobromic acid HBr at 0°C for the formation of the diazonium salt with Br^- as the counteranion. Addition of CuBr and HBr were necessary for the last bromination step carried out at room temperature for 24h. Compound **26** was obtained after purification by silica gel column chromatography in 10% yield (Figure IV-8).

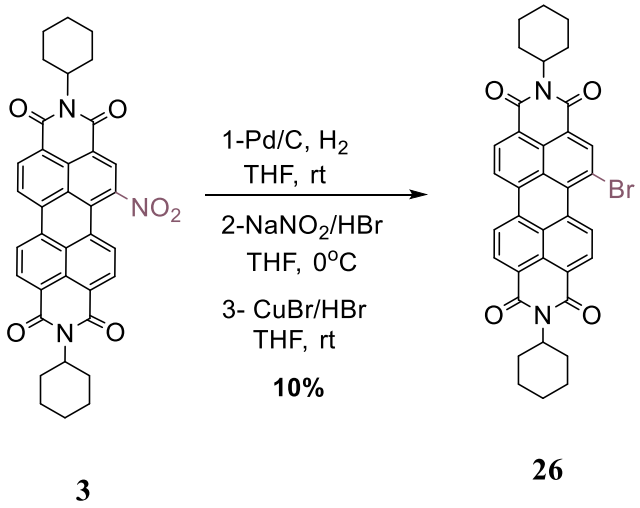

Figure IV-8 One-pot synthesis of mono-*bay* bromo PDI.

IV.3 Application to Pictet-Spengler reaction

IV.3.1 Objective

Study of the reactivity of mono amino-*bay* PDI **17** through the preparation of azabenz-annulated perylene derivatives following Pictet-Spengler reaction procedure accompanied by oxidative aromatization was applied. Pictet-Spengler reaction is known to be one of the most powerful reactions to prepare tetrahydroisoquinoline derivatives encountered in bioactive compounds and drugs. In addition to the synthesis of alkaloid scaffolds. While the reaction has been widely used in the synthesis of natural products and pharmaceutical drugs, we wanted to extend its investigation to the synthesis of organic materials based PDIs which is until recently limited to very few examples. The reaction requires an amino functional group and aldehyde. The mechanism is initiated by an iminium ion formation followed by an intramolecular electrophilic aromatic substitution of the aromatic system by the iminium ion. After annulation, an oxidative rearomatization takes place to generate the fully π-extended system. We aimed to extend the perylene core by introducing different donor and acceptor counterparts in order to study respectively the effect of these extending moieties on the optoelectronic properties and photovoltaic performance of PDIs.

IV.3.2 Synthesis of D-A systems

IV.3.2.1 TPA-PDIaza

Pictet-Spengler reaction was firstly investigated starting from mono amino-*bay* PDI **17** using triphenylamine (TPA) as the electron donor counterpart. Triphenylamine (TPA) is an excellent electron donor with good luminescence properties and hole-transporting capability, and its derivatives are widely used in opto- and electron-active materials.[7–10] The reaction between PDI **17** and 4-formylTPA (prepared from TPA using Vilsmeier-Haack reaction [11]) was carried out following the literature procedure,[12] in which, both starting materials were dissolved in DMF and treated with large excess of triflic acid as the catalyst. However, this procedure did not lead to the formation of the expected product. Repeating the same procedure under argon demonstrated the same result (Figure IV-9).

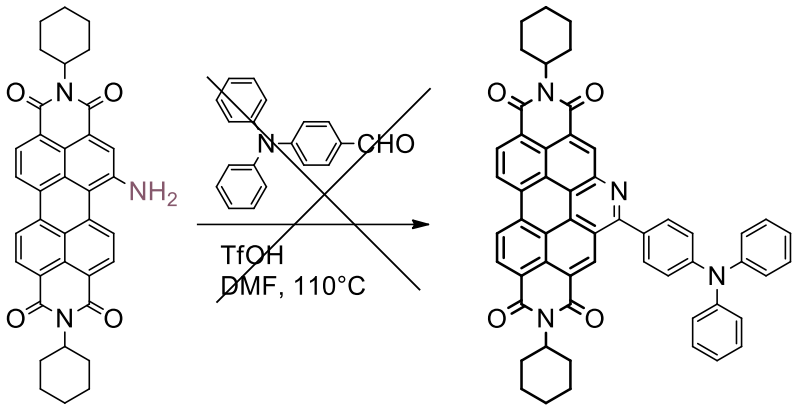

17

Figure IV-9 Attempts to synthesize PDI-TPA acceptor molecule.

An alternative effective method was developed using a slightly modified literature procedure,[13] in which PDI **17** and 4-formylTPA were treated with a large excess of triflic acid in dry DMF at 130°C under argon atmosphere in the presence of activated molecular sieves 3Å. Under these experimental conditions, the water formed during the reaction is trapped allowing the equilibrium of iminium ion formation to be shifted towards the product. In order to achieve the oxidative aromatization of the intermediate tetrahydroisoquinoline, argon was then replaced by pure oxygen and the reaction was refluxed for additional 24h. The general reaction mechanism is depicted in Figure IV-10.

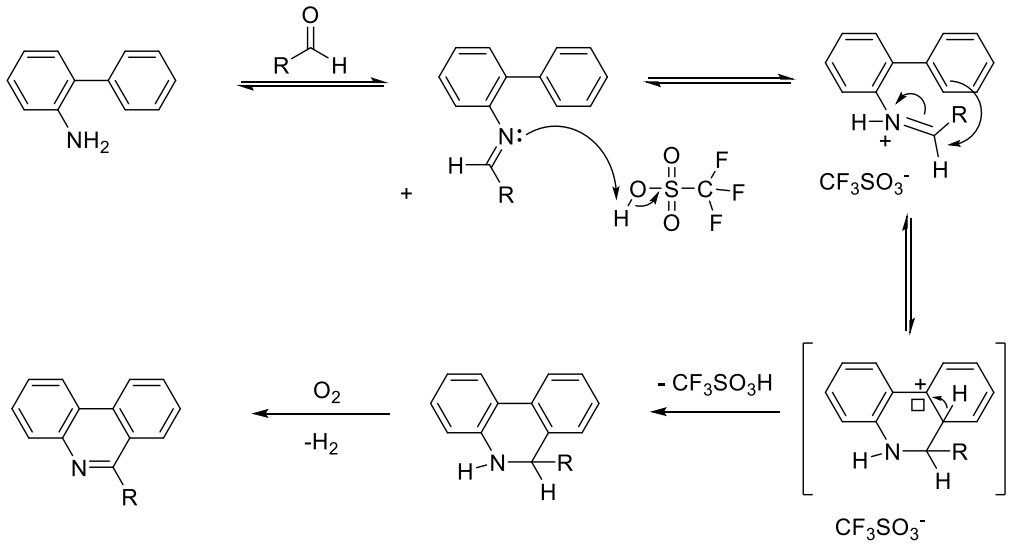

Figure IV-10 General reaction mechanism of Pictet-Spengler reaction followed by oxidative dehydrogenation.

After purification using silica gel column chromatography and precipitation, the product was obtained in 46% yield (Figure IV-11). It should be noted that replacing oxygen by DDQ for the

oxidative aromatization step was also used with which the reaction was also successful. However, to avoid additional by-products caused by introducing another molecule in the reaction system, the use of pure oxygen was preferred over DDQ for the optimized reaction conditions.

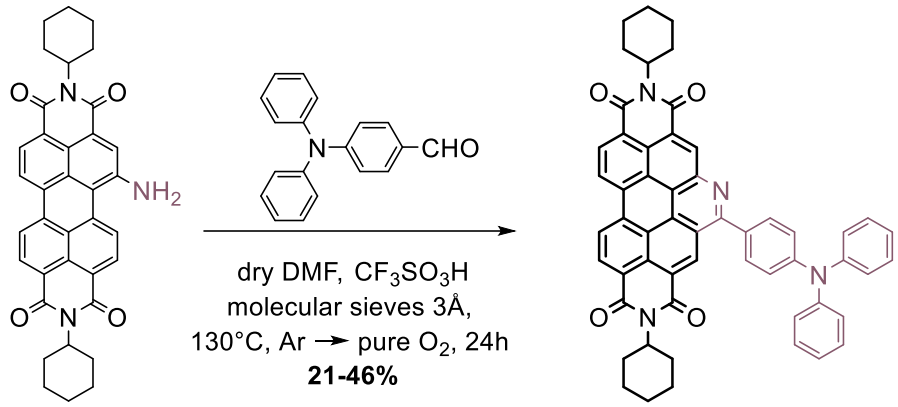

17 **27**

Figure IV-11 Synthesis of TPA-PDIaza **27**.

IV.3.2.2 Fluorene-PDIaza

The second electron donor counterpart was the fluorene grafted on the PDI chromophore (Figure IV-12). Fluorene is highly fluorescent chromophore and possesses high thermal and photochemical stability due to its rigid core. Fluorene and its derivatives are broadly used as electron donors.[14,15] The reaction between PDI **17** and the commercially available, 2-formylfluorene, was carried out following the optimized conditions described above, in which both starting materials were treated with a large excess of triflic acid in dry DMF at 130°C under argon atmosphere in the presence of activated molecular sieves 3Å. Argon was then replaced by pure oxygen and the reaction was refluxed for additional 24h to complete the formation of the product. Fluorene-PDIaza **28** was obtained in 35% yield after purification by column chromatography followed by precipitation. It was noted that the compound has poor solubility in most common organic solvents, such as CH_2Cl_2 and $CHCl_3$. The further decrease of solubility of this compound could be explained by the absence of solubilizing substituents at the **9** position of the fluorene chromophore (Figure IV-12).[16]

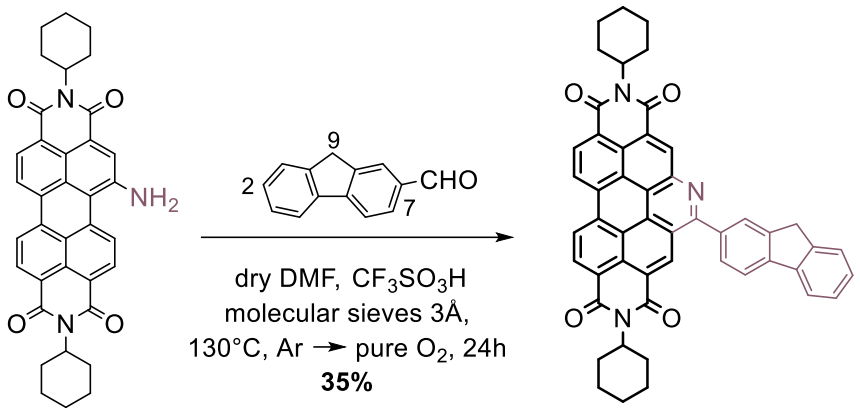

Figure IV-12 Synthesis of Fluorene-PDIaza **28**.

IV.3.3 Synthesis of A-A systems

IV.3.3.1 PDI-PDIaza

In order to investigate the effect of introducing another PDI system on the optoelectronic properties of the PDI chromophore, PDI **17** was reacted with PDI **5** through the same Pictet-Spengler protocol (Figure IV-13).

Figure IV-13 Synthesis of PDI-PDIaza **29**.

This reaction allowed us to study the reactivity of PDI **17** towards another PDI molecule bearing the aldehyde functional group. Both starting materials were treated with a large excess of triflic acid in dry DMF at 130°C under argon atmosphere in the presence of activated molecular sieves 3Å. Argon was then replaced by pure oxygen and the reaction was refluxed for additional 24h to achieve after purification by column chromatography and precipitation PDI-PDIaza **29** in

25% yield. The compound produced is asymmetrical due to the expected formation of N-heterocyclic unit during the course of the reaction.

IV.3.3.2 PMI-PDIaza

The last acceptor counterpart appended on the PDI moiety we describe here is the perylene-3,4-mono(dicarboximide) or PMI derivative, which is a weaker electron acceptor in comparison with PDI.[17] PMI-PDIaza **30** shown in Figure IV-14, was prepared from the reaction between PDI **17** and PMI (synthesized according to the literature procedure[17]) using large excess of triflic acid in dry DMF at 130°C under argon atmosphere in the presence of activated molecular sieves 3Å. Argon was then replaced by pure oxygen and the reaction was refluxed for additional 24h to afford the product in 41% yield after purification by silica gel column chromatography and precipitation. PMI-PDIaza **30** was best soluble in chlorobenzene in which it had very poor solubility in most other organic solvents, including THF, $CHCl_3$, DMF, CH_2Cl_2, xylene, CS_2, DMSO and MeTHF.

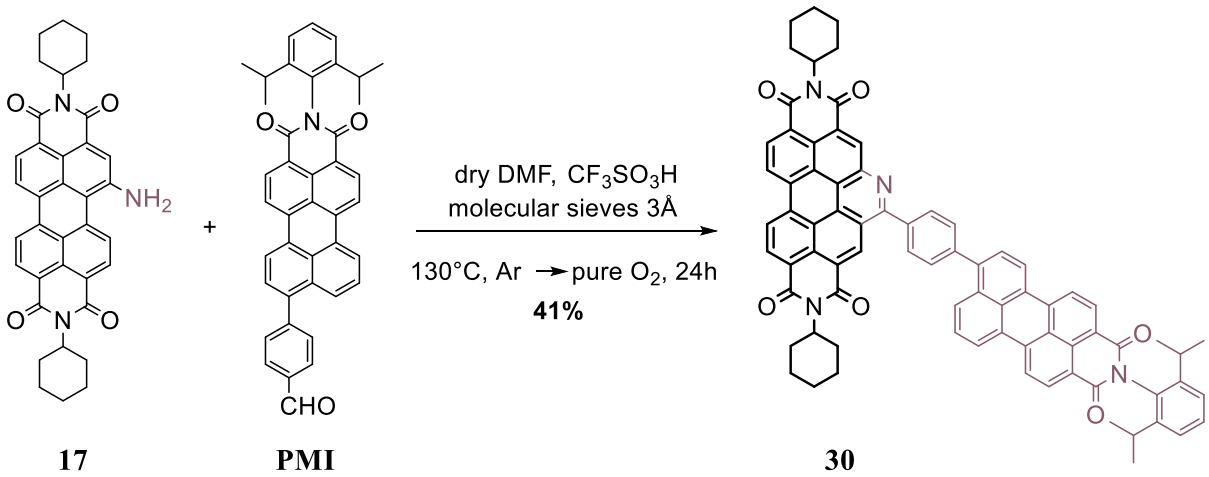

Figure IV-14 Synthesis of PMI-PDIaza **30**.

IV.3.4 Optical Properties

IV.3.4.1 D-A systems

The optical properties of PDI derivatives **27** and **28** have been analysed in diluted $CHCl_3$ solutions by UV–vis absorption (ca. 10^{-5} M), shown in Figure IV-15, and photoluminescence emission (ca. 10^{-6} M) spectroscopy (Figure IV-16). The UV–Vis spectrum of the unsubstituted parent PDI **2**, mono amino-*bay* PDI **17** and PDI-TPA **6** were also studied as references. PDI **2** exhibit the expected three strong absorption peaks between 400-530 nm. These peaks are characteristic of the π–π* electronic transition of the PDI core, whereas the UV–Vis spectrum of the mono-amino *bay* PDI **17** is dominated by a very broad, and nearly structureless, absorption band that spans a large part of the visible spectrum, between 400-650 nm. These broad bands are characteristic of PDI derivatives N-substituted at the *bay*-core positions, due to charge transfer absorption.[18]

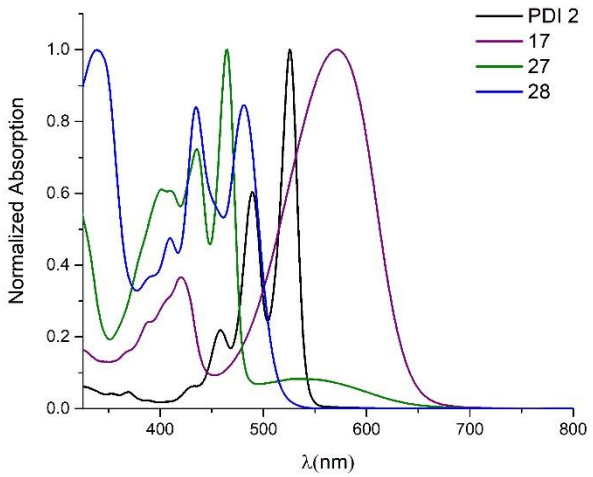

Figure IV-15 Normalized UV/vis absorption spectra of compounds **27**and **28** ($CHCl_3$, 298K).

Table IV-1 UV/vis absorption and emission data of compounds **27** and **28**.

Compound	$\lambda_{abs\ 1}^{max}$(nm)	$\varepsilon_1/10^4$($M^{-1}cm^{-1}$)	$\lambda_{abs\ 2}^{max}$(nm)	$\varepsilon_2/10^4$($M^{-1}cm^{-1}$)	λ_{em}^{max}(nm)	Φ_{fl}	$E_{onset}^{c}(eV)$	$E_0^d(eV)$
27	465	6.7	435	4.8	-	0.01[a]	1.75	-
28	481	8.2	434	8.2	553	0.36[b]	2.09	2.45

[a] Determined with Rhodamine 6G (Φ_{fl}= 0.94 in EtOH) and [b]Comarine 153 (Φ_{fl}= 0.38 in EtOH) as the standard.
[c] E_{onset}=1240/ λ_{onset}
[d] Determined by the intersection of the absorption and emission spectra.

Both UV-vis spectra of TPA-PDIaza **27** and Fluorene-PDIaza **28** show intense absorption in the visible region between 400 to 550 nm, with well-defined vibronic π–π* transition absorption bands with the maximum at 465 nm and 481 nm for TPA-PDIaza **27** and Fluorene-PDIaza **28**, respectively. An intramolecular charge transfer band (ICT) is observed for TPA-PDIaza **27** from 500 to 650 nm, with a maximum around 532 nm, data are summarized in Table IV-1. It should be noted that this ICT band is also observed for the TPA-PDI dyad **6**.

Both compounds **27** and **28** are blue-shifted relative to the corresponding parent compound PDI **2** (λ_{max}= 525 nm) as a reflection of the extended perylene core along the short molecular axis. In comparison with PDIaza **27**, the maximum absorption of Fluorene-PDIaza **28** is bathochromically shifted about 16 nm.

Regarding the photoluminescence properties, a quasi-total and partial quenching of fluorescence were observed for TPA-PDIaza **27** (Φ_{fl}=0.01) and Fluorene-PDIaza **28** (Φ_{fl}=0.36), respectively, suggesting an intramolecular energy/electron transfer interaction between the donor TPA or Fluorene to the acceptor PDIaza. It is noteworthy that TPA-PDIaza **6** does not show any emission. Figure IV-16 shows the emission spectra of both TPA-PDIaza **27** and Fluorene-PDIaza **28** (λ_{ex}= 434 nm).

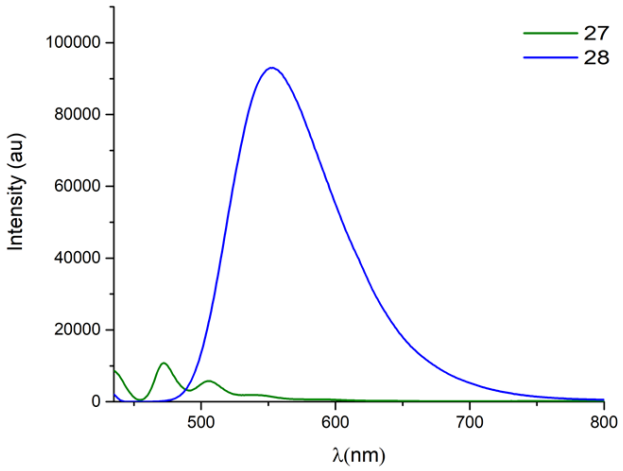

Figure IV-16 Emission spectra of compounds **27** and **28** ($CHCl_3$, 298K).

IV.3.4.2 A-A systems

The optical properties of PDI derivatives **29** and **30** have been analysed in diluted $CHCl_3$ or chlorobenzene solutions by UV–vis absorption (ca. 10^{-5} M) and photoluminescence emission

(ca. 10^{-6} M) spectroscopy together that of PDI **5**, PMI and PDI-azacoronene **31** for comparison, compounds structures are depicted in Figure IV-17. PDI-azacoronene **31**, in which benzene is appended on the N-heterocyclic unit, was prepared following the procedure described above, using PDI **17** and benzaldehyde in 34% yield.

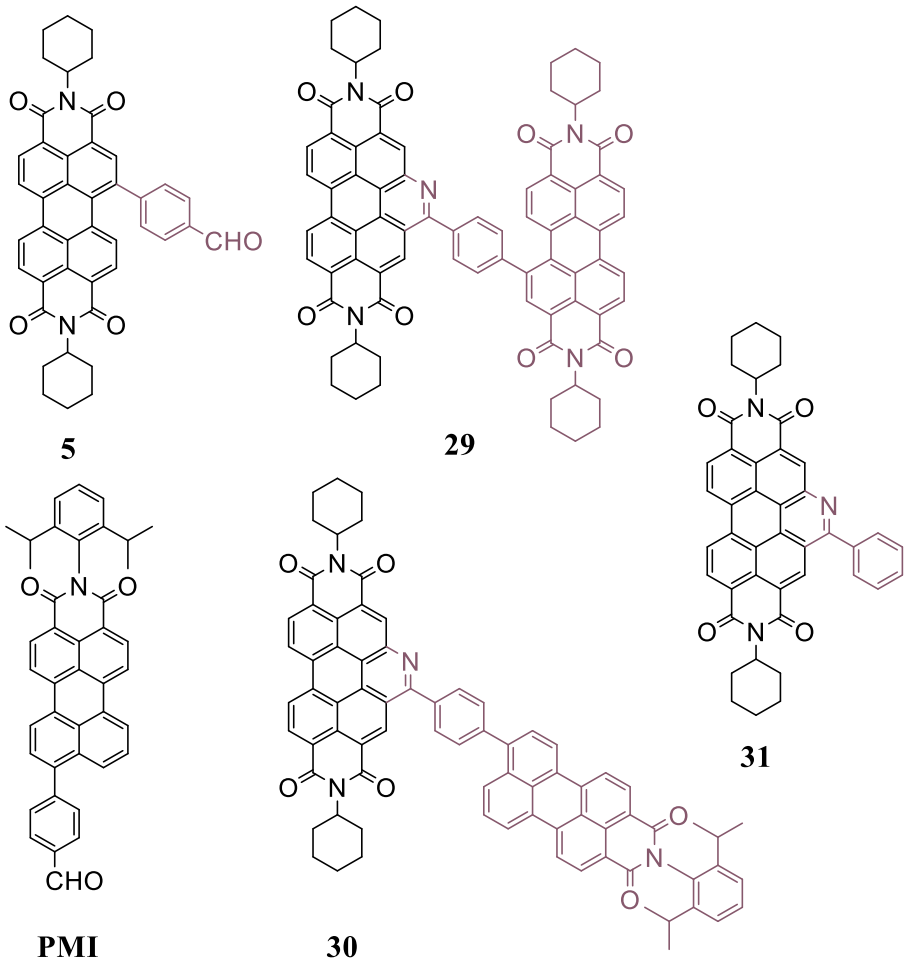

Figure IV-17 Chemical structures of **PMI**, PDI **5**, **29**, **30** and **31**.

PDI **5** shows strong absorption in the visible region between 400 to 550 nm, characteristic of the π–π* electronic transition of PDI derivatives, the strongest peak corresponding to 0-0 transition at 533 nm, a less intense peak at 498 nm corresponding to 0-1 electronic transition and the last shoulder-like, less defined peak at 465 nm, corresponding to 0-2 transition. PMI shows two absorption bands at 521 nm and 495 nm of equal intensities and a very broad shoulder band around 464 nm. These absorption bands correspond to 0-0, 0-1 and 0-2 vibronic transitions respectively. The UV-vis spectra of PDI-PDIaza **29** and PMI-PDIaza **30** are red-shifted relative to the corresponding PDI-azacoronene **31**, and exhibit extended coverage of the absorption from 400 to 600 nm. This could be explained by the linear combination of both PDI absorption spectra

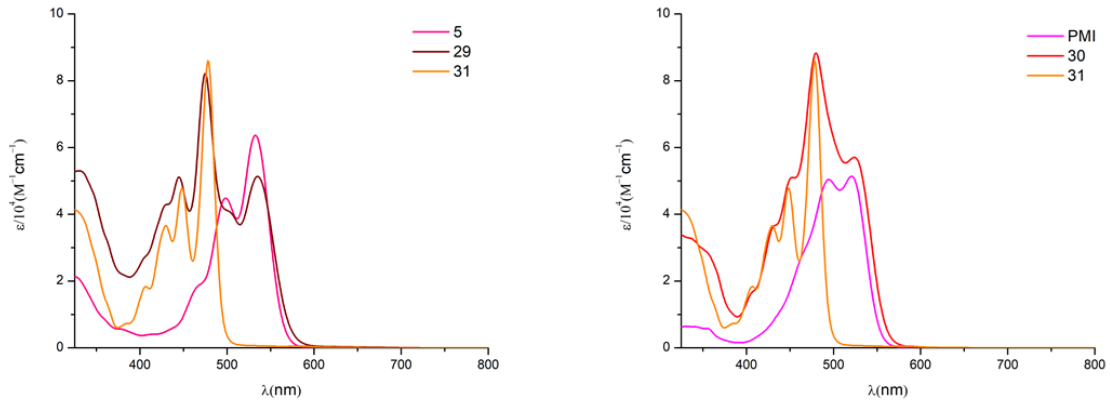

Figure IV-18 UV/vis absorption spectra of **PMI**, PDI **5**, **29** and **31** in $CHCl_3$, and chlorobenzene for **30** (298K).

for the asymmetrical PDI **29** and the presence of PMI core for PDI **30**, which is reflected by the superimposition of both absorption spectra on the sum of the absorption spectra of PDI and PDIaza for PDI **29** and PMI and PDIaza for PDI **30** (Figure IV-18). This suggest the absence of electronic coupling in the ground state between the accepting moieties of both compounds. In comparison with PMI-PDIaza **30**, the maximum absorption of PDI-PDIaza **29** is bathochromically shifted about 11 nm, data are summarized in Table IV-2.

Table IV-2 UV/vis absorption and emission data of **PMI**, PDI **5**, **29**, **30** and **31**.

Compound	$\lambda_{abs\,1}^{max}$(nm)	$\varepsilon_1/10^4$($M^{-1}cm^{-1}$)	$\lambda_{abs\,2}^{max}$(nm)	$\varepsilon_2/10^4$($M^{-1}cm^{-1}$)	λ_{em}^{max}(nm)	Φ_{fl}	$E_{onset}^{c}(eV)$	$E_0^d(eV)$
PDI 5	533	6.4	498	4.5	570	0.99[a]		2.25
PMI	521	5.1	495	5.0	596	0.82[a]		2.29
29	535	5.1	505	4.0	584	0.98[a]	2.04	2.23
30	524	5.7	480	8.8	-	0.19[a]	2.00	-
31	476	9.7	446	5.4	565	0.46[b]		2.56

[a] Determined with Rhodamine 101 (Φ_{fl}= 1 in MeOH) and [b]Comarine 153 (Φ_{fl}= 0.38 in EtOH) as the standard.
[c] E_{onset}=1240/ λ_{onset}
[d] Determined by the intersection of the absorption and emission spectra.

The fluorescence spectra (Figure IV-19) depict the same structure with a mirror image of the absorption spectrum for PDI-azacoronene **31** with a maximum emission peak at 565 nm (Φ_{fl}=0.46). PDI-PDIaza **29** emits strongly at 584 nm (Φ_{fl}=0.98), however, a significant quenching was observed (around 91-93% taking the emission quantum yield of PDI **5** or PMI **6** as the reference) for PMI-PDIaza dyad **30** (Φ_{fl}=0.19). This could arise from an energy or electron transfer between PDIaza and PMI units.

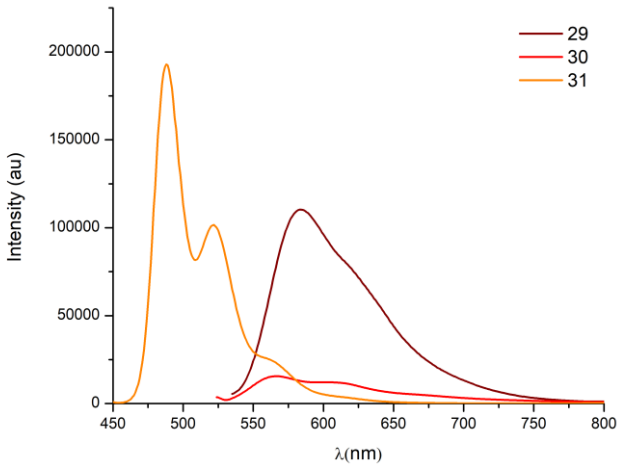

Figure IV-19 Emission spectra of compounds **29** (λ_{ex}=535 nm) and **31** (λ_{ex}=446nm) in $CHCl_3$ and **30** (λ_{ex}=524nm) in Chlorobenzene.

Thin films absorption spectra of compounds **27**, **28**, **29** and **30** were also recorded (Figure IV-20). Thin-films were prepared by spin-coating 0.5% wt/v solutions from $CHCl_3$ or chlorobenzene onto Corning glass micros slides. A pronounced difference in the spectra of the four compounds is observed, broadened and red-shifted relative to those of solution spectra. For TPA-PDIaza **27** and Fluorene-PDIaza **28**, observed a red shift in λ_{onset} of ~57 nm and ~80 nm respectively and an ICT still present for TPA-PDIaza **27**.

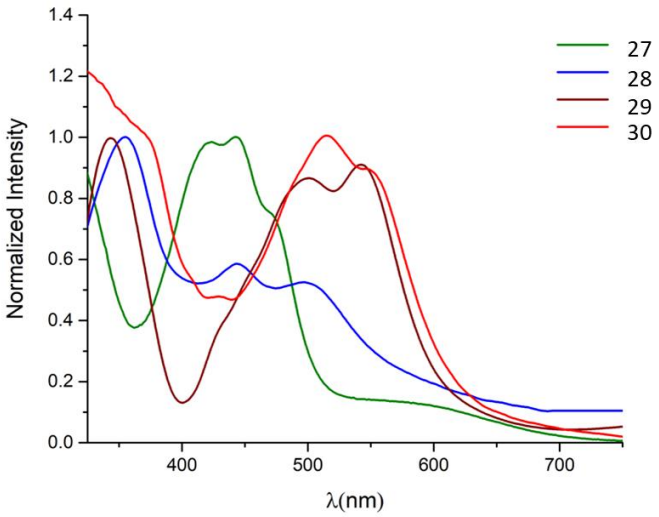

Figure IV-20 Film absorption spectra of compounds **27**, **28**, **29** and **30**.

The peaks corresponding to 0-1 transition in both compounds have the highest intensities, due to the aggregation of the PDI monomers. For PDI-PDIaza **29** and PMI-PDIaza **30**, observed a red shift in λ_{onset} of ~36 nm and ~58 nm respectively. The absorption complementarity of both PDI **5** and PMI units found in solution spectra for PDI-PDIaza **29** and PMI-PDIaza **30** respectively, is also observed in their thin films with an extended coverage from 400 to 650 nm.

IV.3.5 Electronic properties

IV.3.5.1 D-A systems

The electrochemical properties of TPA-PDIaza **27** and Fluorene-PDIaza **28** were investigated by cyclic voltammetry. Data are summarized in Table IV-3, in CH_2Cl_2 and in the presence of 0.1M Bu_4NPF_6 as supporting electrolyte.

Table IV-3 Redox potential values of **27** and **28** vs. Fc/Fc^+; Pt as a working electrode; Bu_4NPF_6 (0.1M), CH_2Cl_2, 1000 mV/s for **27**, 20 mV/s for **28**.

Compounds	E^1_{red}/V	E^2_{red}/V	E^1_{ox}/V	E^{LUMO}/eV[b]	E^{HOMO}/eV
27	-1.20	-1.43	+0.55	-3.60	-5.35[c]
28	- 1.49	- 1.72	+ 0.73[a]	- 3.31	- 5.40[c]/-5.76[d]

[a] Anodic potential oxidation wave. [b] E_{LUMO}= -(E^1_{red} + 4.8).
[c] $E_{HOMO} = E_{LUMO}-E_{onset}$. [d] $E_{HOMO} = E_{LUMO}-E_0$.

Considering the D-A systems, PDI derivatives show the expected two reversible one-electron reduction waves at E^1_{red} = – 1.20 V and E^2_{red} = – 1.43 V *vs* Fc/Fc^+ for TPA-PDIaza **27**, corresponding to the successive formation of $PDI^{\cdot-}$ and PDI^{2-}, respectively. A neat difference equal to ΔE = - 0.29V was observed for both reduction waves of Fluorene-PDIaza **28** (E^1_{red} = – 1.49 V and E^2_{red} = – 1.72 V *vs* Fc/Fc^+). This was attributed to the less donating power of the fluorene unit which was confirmed by comparison of the irreversible oxidation wave of fluorene at E^1_{ox} = + 0.73 V with the reversible oxidation wave of TPA at E^1_{ox} = + 0.55 V *vs* Fc/Fc^+ (Figure IV-21).

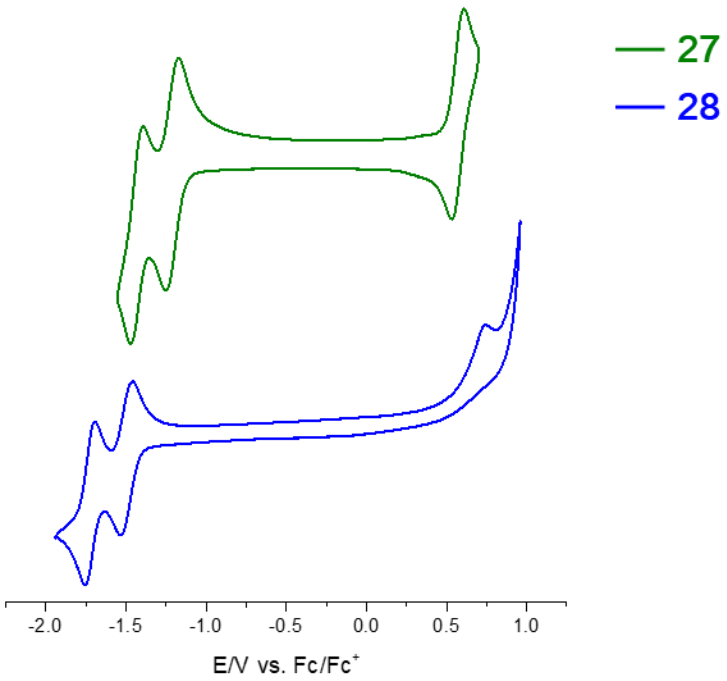

Figure IV-21 Cyclic voltammogram of **27** and **28**
(V vs Fc/Fc^+; Pt as a working electrode; Bu_4NPF_6 (0.1 M), CH_2Cl_2, 1000 mV/s for **27**, 20 mV/s for **28**).

IV.3.5.2 A-A systems

The electrochemical properties of PDI-PDIaza **29** and PMI-PDIaza **30** were analyzed by cyclic voltammetry (Figure IV-22) and deconvoluted cyclic voltammograms in CH_2Cl_2/Chlorobenzene (1:1) in the presence of 0.2M Bu_4NPF_6 as supporting electrolyte. Cyclic voltammetry of PDI **5**, PMI and PDI-azacoronene **31** to be used as references were also studied, data are summarized in Table IV-4. From PDI **5**, PDIaza **31** and the deconvoluted cyclic voltammograms, a clearer idea was introduced for assigning the electrochemical processes of PDI-PDIaza **29** (Figure IV-23).

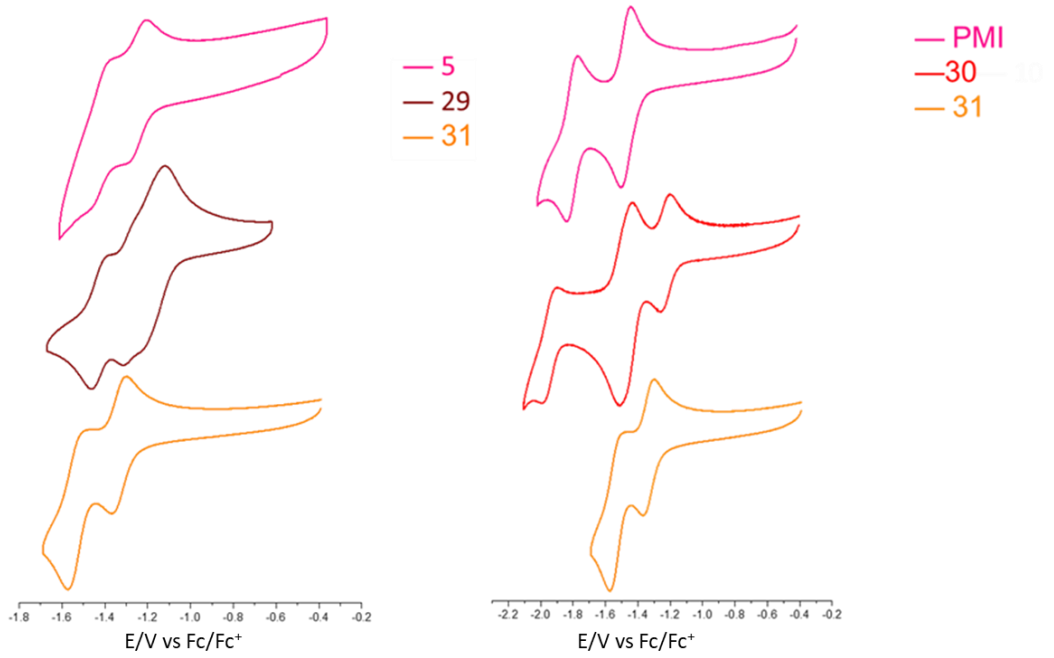

Figure IV-22 Cyclic voltammograms of **5, PMI**, and **29, 30** and **31** (V vs Fc/Fc^+; Pt as a working electrode; Bu_4NPF_6 (0.2 M), CH_2Cl_2/Chlorobenzene (1:1), 100 mV/s).

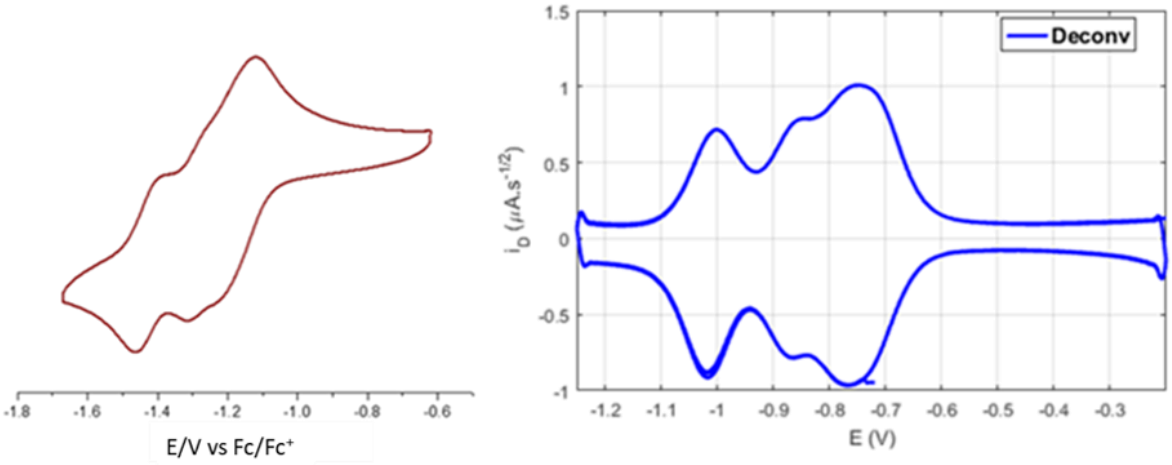

Figure IV-23 Cyclic voltammogram (CV) and deconvoluted CV of compound **29**.

Table IV-4 Redox potential values of **5**, **PMI**, **29**, **30** and **31** vs. Fc/Fc+; Pt as a working electrode; Bu_4NPF_6 (0.2M), CH_2Cl_2/Chlorobenzene (1:1), 100 mV/s).

Compounds	E^1_{red}/V	E^2_{red}/V	E^3_{red}/V	E^1_{ox}/V	E^{LUMO}/eV[b]	E^{HOMO}/eV
PDI 5	-1.23	-1.41			-3.57	-5.82[c]
PMI	-1.47	-1.80			-3.33	- 5.62[c]
29	-1.16	-1.26	-1.41		-3.64	-5.68[d]/-5.87[c]
30	-1.22	-1.45	-1.94		-3.58	-5.58[d]
31	-1.32	-1.57[a]			-3.48	-6.04[c]

[a] Cathodic potential reduction wave.[b] E_{LUMO}= -($E^1_{(red)}$+ 4.8).
[c] E_{HOMO}= E_{LUMO}- E_0.
[d] E_{HOMO}= E_{LUMO}- E_{onset}.

Moreover, the differential pulse voltammetry for PDI-PDIaza **29** is also illustrated in Figure IV-24. The first reduction process of PDI and that of PDIaza are overlapping leading to $PDI^{\cdot-}$-$PDIaza^{\cdot-}$ species. Following this two-electron process at E^1_{red} = – 1.16 V vs. Fc/Fc^+, were observed two one-electron reduction waves at – 1.26 and – 1.41 V corresponding to the generation of PDI^{2-}-$PDIaza^{\cdot-}$ and PDI^{2-}-$PDIaza^{2-}$ species, respectively.

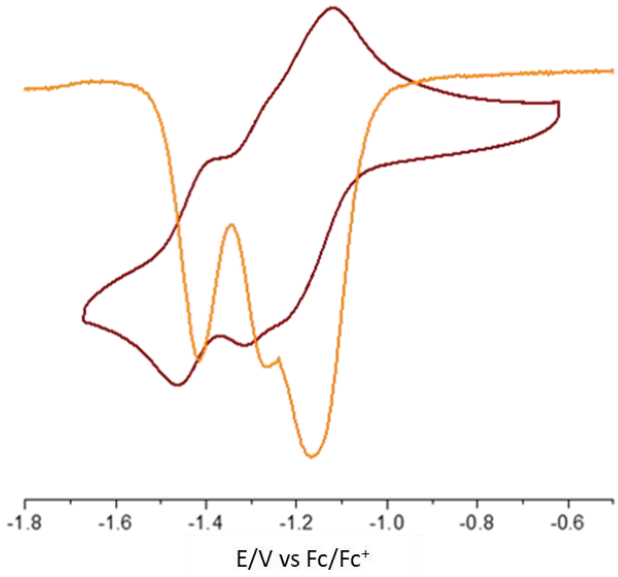

Figure IV-24 Cyclic voltammogram and differential pulse voltammetry of compound **29**.

With the aid of the deconvoluted cyclic voltammograms, Figure IV-25, and the references PMI and PDIaza **31**, the electrochemical processes of PMI-PDIaza **30** were assigned. The compound shows three reversible reduction waves with a first one-electron process at E^1_{red} = – 1.22 V *vs* Fc/Fc^+ corresponding to the formation of PMI-$PDIaza^{\cdot-}$ species. The second two-electron wave at E^2_{red} = – 1.45 V arises from the concomitant second reduction of PDIaza unit and the first

reduction of PMI leading to the $PMI^{\cdot-}$-$PDIaza^{2-}$ species. Finally, the last one-electron reduction wave at E^3_{red} = – 1.94 V corresponds to the PMI^{2-}-$PDIaza^{2-}$ species.

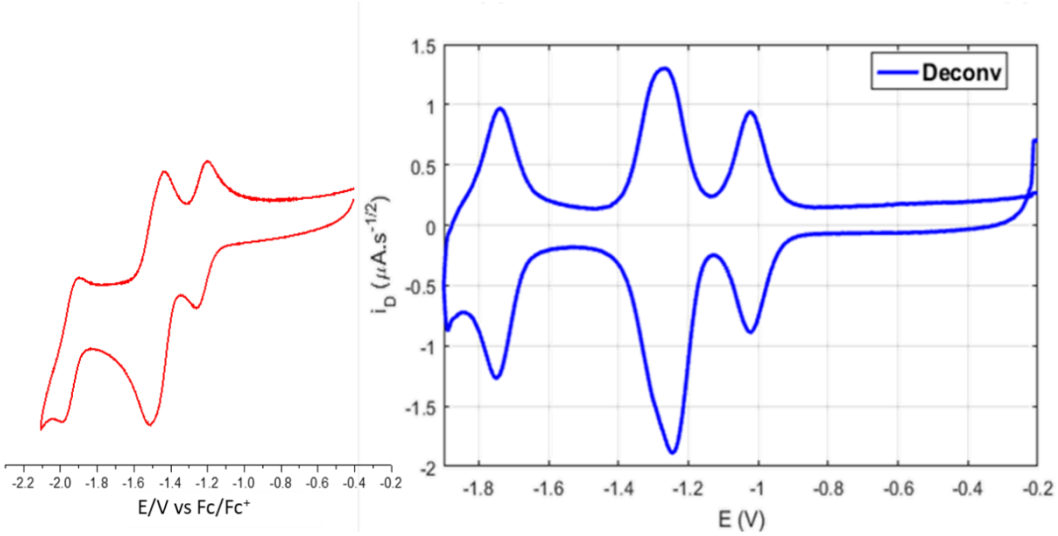

Figure IV-25 Cyclic voltammogram (CV) and deconvoluted CV of compound **30**.

IV.4 Solar cells application

TPA-PDIaza **27** and PMI-PDIaza **30** electron acceptor materials were used for the investigation in organic solar cells each blended with the donor **PTB7-Th**. BHJ solar cell devices were fabricated using the inverted device architecture (Glass/ITO/ZnO/BHJ/MoOx/Ag), where the active layer was cast from 10 mg/mL solutions in chlorobenzene with a1:1 w/w donor/acceptor ratio.

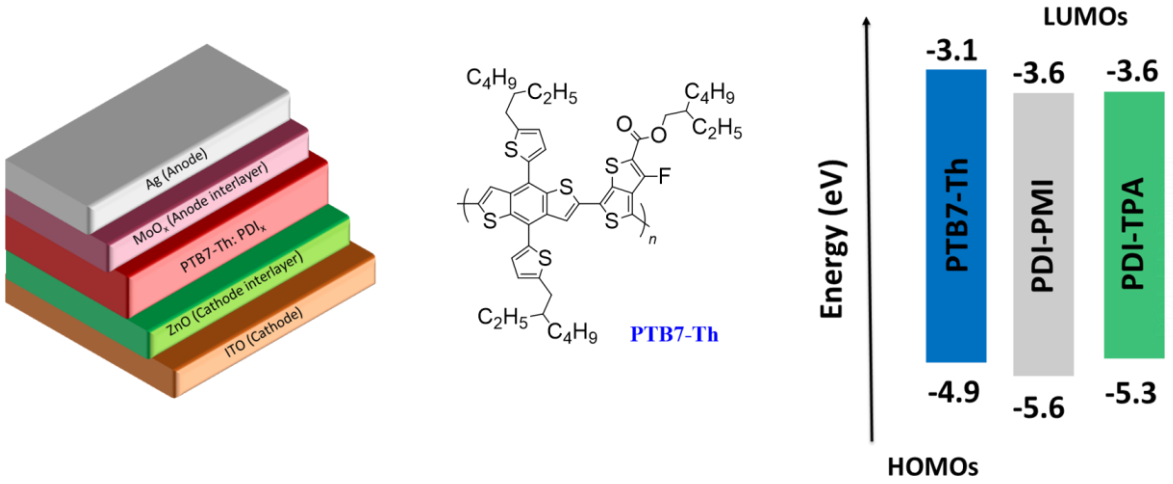

Figure IV-26 Device Architecture, chemical structure of **PTB7-Th** and energy level diagram of active layer materials.

The considered PMI-PDIaza **30** devices showed minimal photovoltaic response under these conditions. These devices resulted in a V_{OC} of approximately 0.67 V, but suffered from a low FF of 33% and very low J_{SC} leading to low 0.2% PCE. This could be explained by the completely asymmetric structure of the corresponding acceptor associated with no clear electron path and complex morphology, such properties are detrimental to OPV efficiencies. Compared to PMI-PDIaza **30**, devices of TPA-PDIaza **27** attained a relatively high V_{OC} of 0.92 V, indicating an appropriate energy level pairing of the materials. A FF of 38% and higher J_{SC} of 4.6 mA/cm^2 resulting in a PCE of 1.6% (Figure IV-27, Table IV-5).

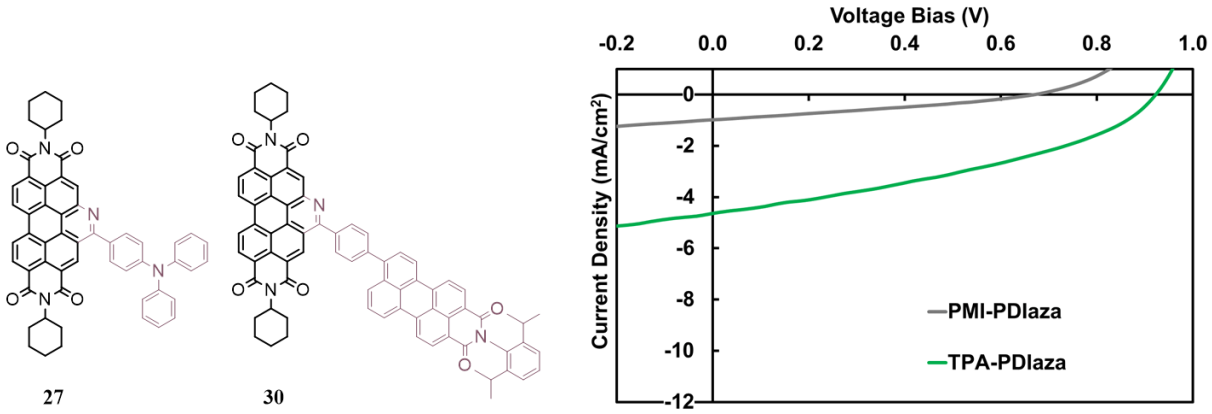

Figure IV-27 Chemical structure of the acceptors used. J-V curves for the active layer blends **PTB7-Th: TPA-PDIaza** and **PTB7-Th: PMI-PDIaza**.

Table IV-5 OPV devices performance parameters and statistics for **PPDT2FBT: PDI-EPD dimer** active layer blend, cast from a 1:1 ratio at 10 mg/mL in chlorobenzene.

Acceptor	Voc (V)	Jsc (mA/cm^2)	FF (%)	PCE (%)
TPA-PDIaza 27	0.90 (0.92)	4.6 (4.6)	36 (38)	1.5 (1.6)
PDI-PMIaza 30	0.58 (0.67)	1.0 (1.0)	28 (30)	0.2 (0.2)

Average (Best) device.

IV.5 Conclusion

In this chapter, we discussed the synthesis of mono-amino *bay* substituted PDI **17** and its successful purification using neutral alumina column chromatography. Starting from this compound, we aimed to establish the diazonium salt of PDI which was synthesized and characterized with two different N-imide groups (compounds **18** and **22**). Despite the successful synthesis made and discussed, the main drawbacks and intricacies associated with the diazotization including lack of reproducibility, in addition to the products obtained with low yields from subsequent substitution halogenation reactions, did not allow for further investigations on the chemistry of the diazonium salt.

Starting from mono-amino *bay* substituted PDI **17**, we prepared extended PDI-based azacoronene dyads with introduction of a donor or acceptor counterpart through a straightforward and versatile method known as Pictet-Spengler reaction followed by oxidative aromatization. Compounds TPA-PDIaza **27,** Fluorene-PDIaza **28,** PDI-PDIaza **29** and PMI-PDIaza **30** were obtained in moderate yields, and characterized by using ^{1}H, ^{13}C NMR and mass spectrometry (HRMS). Optical and electrochemical properties were studied using compound **5**, **PMI** and **31** as references.

We incorporated TPA-PDIaza **27** and PMI-PDIaza **30** in organic solar cells. The first study revealed the devices performances were respectively 1.6% and 0.2% PCE.

IV.6 References

[1] M. D. Threadgill, A. P. Gledhill, *Journal of the Chemical Society, Perkin Transactions 1* **1986**, *0*, 873–876.

[2] E. Touzé, F. Gohier, B. Daffos, P.-L. Taberna, C. Cougnon, *Electrochimica Acta* **2018**, *265*, 121–130.

[3] A. D. Hendsbee, J.-P. Sun, W. K. Law, H. Yan, I. G. Hill, D. M. Spasyuk, G. C. Welch, *Chem. Mater.* **2016**, *28*, 7098–7109.

[4] D. F. DeTar, T. Kosuge, *J. Am. Chem. Soc.* **1958**, *80*, 6072–6077.

[5] F. W. Wassmundt, W. F. Kiesman, *J. Org. Chem.* **1995**, *60*, 1713–1719.

[6] P. Swoboda, R. Saf, K. Hummel, F. Hofer, R. Czaputa, *Macromolecules* **1995**, *28*, 4255–4259.

[7] P. Blanchard, C. Malacrida, C. Cabanetos, J. Roncali, S. Ludwigs, *Polymer International* **2019**, *68*, 589–606.

[8] X. Liang, Q. Zhang, *Sci. China Mater.* **2017**, *60*, 1093–1101.

[9] C. Wang, B. Hu, J. Wang, J. Gao, G. Li, W.-W. Xiong, B. Zou, M. Suzuki, N. Aratani, H. Yamada, et al., *Chemistry – An Asian Journal* **2015**, *10*, 116–119.

[10] X. Yang, G. Zhou, W.-Y. Wong, *Chemical Society Reviews* **2015**, *44*, 8484–8575.

[11] G. Lai, X. R. Bu, J. Santos, E. A. Mintz, *Synlett* **1997**, *1997*, 1275–1276.

[12] L. Hao, W. Jiang, Z. Wang, *Tetrahedron* **2012**, *68*, 9234–9239.

[13] M. Schulze, M. Philipp, W. Waigel, D. Schmidt, F. Würthner, *The Journal of Organic Chemistry* **2016**, *81*, 8394–8405.

[14] A. Yella, R. Humphry-Baker, B. F. E. Curchod, N. Ashari Astani, J. Teuscher, L. E. Polander, S. Mathew, J.-E. Moser, I. Tavernelli, U. Rothlisberger, et al., *Chem. Mater.* **2013**, *25*, 2733–2739.

[15] J. Rodríguez-Romero, L. Aparicio-Ixta, M. Rodríguez, G. Ramos-Ortíz, J. L. Maldonado, A. Jiménez-Sánchez, N. Farfán, R. Santillan, *Dyes and Pigments* **2013**, *98*, 31–41.

[16] K. D. Belfield, A. R. Morales, B.-S. Kang, J. M. Hales, D. J. Hagan, E. W. Van Stryland, V. M. Chapela, J. Percino, *Chem. Mater.* **2004**, *16*, 4634–4641.

[17] J. Baffreau, L. Ordronneau, S. Leroy-Lhez, P. Hudhomme, *The Journal of Organic Chemistry* **2008**, *73*, 6142–6147.

[18] H.-Y. Tsai, K.-Y. Chen, *Dyes and Pigments* **2013**, *96*, 319–327.

General conclusion

The objectives of this thesis work concerned studies of the reactivity of mono-nitro PDI **3** and mono-amino PDI **17** as starting materials and development of their chemistry through different synthetic approaches. After the presentation of the state-of-the-art in terms of development in PDI functionalization in the first chapter, we have presented in the second chapter a modified Suzuki-Miyaura cross-coupling reaction and the original formation of a phosphinimine functionality starting from *bay*-substituted nitroPDI. The third chapter was devoted to the synthesis of a PDI dimer which was studied as a non-fullerene acceptor in organic solar cells. In the fourth chapter, we presented new developments from aminoPDI, with diazonium salt chemistry and Pictet-Spengler reaction to reach donor-acceptor and acceptor-acceptor dyads.

Concerning the reactivity of *bay*-substituted nitroPDI, we have demonstrated the possibility to carry out C-C coupling reactions, instead of using the corresponding bromo PDI derivative. Thus, from mono-nitro PDI **3**, we prepared a series of new PDI acceptors, compounds **4**, **5** and **6** that were obtained in higher yields compared to the previously reported results starting from mono-bromo PDI. Hence, with this straightforward methodology, we proved that our Suzuki-Miyaura coupling (SMC) method is advantageous, especially because the access to mono nitro PDI is much easier than that of the corresponding mono-bromo derivative.

We could use the aldehyde functionality of PDI derivative **4** to attach C_{60} through a Prato reaction to obtain PDI-C_{60} dyad **7** for which C_{60} is connected at the *bay* region of the PDI core. Attaching PDI chromophore to C_{60} yielded a visible light-harvesting dyad in which study of its optical and electrochemical properties using compound **3**, **4** and **8** as references revealed weak electronic interaction between C_{60} and PDI moieties in the dyad at the ground state. The quenching of the emission probably suggests the presence of a photo-induced energy transfer in solution from the photo-excited PDI chromophore to the electron-accepting fullerene unit.

Aiming to prepare di-carbazole based PDI through a Cadogan reductive cyclization using dinitro PDI **9**, we were surprised to isolate PDI derivative **10** bearing a phosphinimine functionality which was confirmed by X-ray single crystal analysis. Previously reported results showed that high temperature and excess of PPh_3 usually employed for such cyclisation reaction can also lead to the formation of phosphinimine functional groups, as it was the case for PDI **10**. However, analysis of the structure of PDI **10** obtained showed the presence of a hydroxyl group at the opposite *bay* region, corresponding to an unknown 2'-phosphinimine- 1,1'-biphenyl-2-ol type structure. We have proposed a mechanism to explain this original reaction. After studying the solvent effect on this reaction, we attempted to expand the scope by using the corresponding PDI derivatives in subsequent reactions such as aza-Wittig reactions, unfortunately without

satisfying results today. Study of the optical and electrochemical properties for PDI **10** suggested an intramolecular charge transfer (ICT) process for PDI **10**.

In the third chapter, we studied the influence of side chains on morphology and solar cell performances in collaboration with Dr. G. C. Welch research group at the University of Calgary, AB, Canada. We have synthesized the PDI dimer **16** functionalized with a different substituent at the imide *N*-positions, which is cyclohexyl group. The synthesis, carried out in our laboratory, starts from the reductive cyclisation of mono-nitro PDI, to obtain the *pyrrolic* nitrogen at the *bay* position of the PDI which was then alkylated to increase the forming PDI solubility. Bromination of PDI **14** and subsequent homocoupling reaction gave the dimer **16** that was then subjected for solar cell applications.

Inverted BHJ architecture was used for the fabrication of OPV devices and a comparative study of the photovoltaic performances between both PDI-Cy dimer **16** with PDI-EPD dimer was initiated with the standard electron donor polymer **PTB7-Th**. After, **PPDT2FBT** was used as one of the recent well-performing donor polymers with a variety of NFAs. Processing films with diphenyl ether (DPE) proved to enhance the devices performance in both dimers that reached up to 2.7% and 3.1% at 10.0% v/v DPE for PDI-Cy dimer and PDI-EPD dimer, respectively. Self-assembly of molecular materials in neat films were evaluated by POM and FM techniques that showed both dimers remained amorphous even after casting with DPE. This was in accordance with film absorption spectra of PDI-Cy dimer **16** that remained virtually unchanged upon varying DPE additive concentration. However, the results were considerably different when DIO was used instead as the processing additive where it showed to have a better organizing effect on PDI-EPD dimer than PDI-Cy dimer **16**. The results obtained with the techniques used showed that the self-assembly of PDI could not be evaluated properly in relation to OPV performance. The optimized processing conditions for **PPDT2FBT:PDI$_x$** active layer blends showed best device performances at 2:3 donor-acceptor ratio.

The last fourth chapter was devoted to the reaction of *bay* substituted mono-amino PDI. Access to diazonium salt of PDI via one pot syntheses were performed using two different N-imide groups in which PDI **18** and PDI **22** were obtained. However, the corresponding syntheses suffer from reproducibility to obtain the diazonium salts, despite different synthetic methods applied. Subsequent halogenations from the diazonium salts obtained have led to the expected products, such as mono-fluorinated PDI **23** or **24**, mono- iodinated PDI **25**, and mono- brominated PDI **26**, however, in very low yields. The poor responses of such study did not allow for further investigations on the chemistry of the diazonium salt.

After, we have concentrated our efforts to optimize reaction conditions utilizing Pictet-Spengler reaction method followed by oxidative aromatization. We could prepare extended azabenz-annulated perylene derivatives with the introduction of a donor or acceptor counterpart. Compounds TPA-PDIaza **27**, Fluorene-PDIaza **28**, PDI-PDIaza **29** and PMI-PDIaza **30** were obtained. This synthetic approach appears very promising for the preparation of different PDI-based dyads that requires amino and aldehyde functionalities. Study of the optical and electrochemical properties of the corresponding compounds showed the expected blue-shift in the absorption spectra for TPA-PDIaza **27**, Fluorene-PDIaza **28** compared to the parent PDI **2**. And a red-shift for PDI-PDIaza **29** and PMI-PDIaza **30** compared to PDI-azacoronene **31** due to the linear combination of both PDI absorption spectra with that of the acceptor counterpart. The quasi-total and partial quenching of fluorescence observed for TPA-PDIaza **27** and Fluorene-PDIaza **28** and PMI-PDIaza dyad **30** suggested either an intramolecular energy or electron transfer interaction between both moieties. The first study of TPA-PDIaza **27** and PMI-PDIaza dyad **30** in organic solar cells showed that the former gave better results paired with the donor **PTB7-Th** with 1.6% PCE.

Perspectives

We have demonstrated an alternative method for the classical SMC reaction through C-NO_2 bond functionalization. This reaction is of particular interest since mononitration of PDI is much more selective and easier to carry out compared to monobromination reaction. Moreover, nitration in aromatic series appears more interesting in terms of industrial developments compared to bromination conditions. Hence, expansion of such SMC chemistry would provide an effective replacement to be applied for the design and synthesis of new aromatic and heterocyclic systems useful for organic electronics.

The construction of PDI-C_{60} dyad **7** and the analysis of their optical and electrochemical properties highlight the significance of such acceptor-acceptor dyad. Follow-up work on this PDI-C_{60} dyad **7** to be used as singlet-oxygen photosensitizer or in organic photovoltaics should be addressed.

Concerning the phosphinimine chemistry, we have successfully obtained PDI **10** and PDI **12**. Better understanding of the formation and reactivity of these compounds is of great importance for further functionalization of the phosphinimine functional group on the PDI core.

With PDI-Cy dimer **16** and PDI-EPD dimer, we studied the impact of side chains on morphology and BHJ solar cell performance. More in depth extended studies and advanced characterizations on this topic are being carried out.

We have demonstrated the versatility of Pictet-Spengler reaction for the preparation of different PDI-based dyads. Future objectives concerning this chemistry are the extension of this synthetic strategy while targeting new electron acceptors for applications such as in OPV.

Experimental part

General

All reagents and **chemicals** from commercial sources were used without further purification. Commercial solvents were used without further purification. Column chromatography was performed with analytical-grade solvents using Aldrich silica gel (technical grade, pore size 60 Å, 40-63 µm particle size) and Acros aluminium oxide (Brockmann I, pore size 60 Å, 50-200 µm particle size). Flexible plates ALUGRAM® Xtra SIL G UV254 and ALUGRAM® ALOX N UV254 from MACHEREY-NAGEL were used for TLC.

NMR spectra were recorded with a Bruker AVANCE III 300 (^{1}H, 300 MHz and ^{13}C, 75 MHz, ^{19}F NMR, 283 MHz and ^{31}P, 122MHz) and Bruker AVANCE DRX 500 (^{1}H, 500 MHz and ^{13}C, 125 MHz). Chemical shifts are given in ppm and coupling constants J in Hz. Residual non-deuterated solvent was used as an internal standard.

MALDI-TOF (MS) spectra were performed on a Bruker Daltonics Biflex III using DCTB (trans-2-[3-(4-tert-Butylphenyl)-2-methyl-2-propenylidene]malononitrile) or DIT (dithranol) as matrix.

High resolution mass spectrometry (HRMS) was performed with a JEOL JMS-700 B/E using m-NBA (3-Nitrobenzyl alcohol) as matrix.

Elemental analysis was recorded on a Thermo Scientific Flash 2000.

UV-visible absorption spectra were recorded on a Shimadzu UV-1800 Spectrometer. Emission and excitation spectra were recorded on a Shimadzu RF-6000 Spectrofluorophotometer.

Thin-films were prepared by spin-coating 1% or 0.5% wt/v solutions from $CHCl_3$ or chlorobenzene onto Corning glass micros slides. Prior to use, glass slides were cleaned with soap and water, acetone and isopropanol, and followed by UV/ozone treatment using a Novascan UV/ozone cleaning system.

Electrochemical studies were recorded with bio-logic potentiostat SP-150 in a glove box. The working electrode is a platinum electrode, the counter electrode is a platinum wire and a silver wire as a pseudo-reference electrode.

HPLC analysis were performed on a Shimadzu CBM-20A controller equipped with a Buckyprep Waters (4.6 x 250 mm) column and a Shimadzu SPD-M20A photodiode array detector at 40°C.

TGA and **DSC** were performed with a TA Instruments Q500.

X-Ray Diffraction: Single crystals of the compounds were mounted on glass fibre loops using a viscous hydrocarbon oil to coat the crystal and then transferred directly to cold nitrogen stream for data collection. Data collection were mostly performed on an Agilent Supernova with CuKα (λ = 1.54184 Å). The structures were solved by direct methods with the SIR97 program and refined against all F2 values with the SHELXL-97 program using the WinGX graphical user interface.

Organic solar cell device fabrication, testing and characterization were performed in Gregory C. Welch laboratories, at the University of Calgary.

PTB7-Th polymer purchased from 1-Material, FBT polymer purchased from Brilliant Matters. The molecular material (PDI-EPD dimer) was synthetized in Gregory C. Welch laboratories following the procedure outlined in previously published literature.[1]

Solution preparation:

PTB7-Th-PDI_x solutions were prepared in air, from 10 mg/mL solutions of the single components, which were stirred for 2h before mixing in the required weight proportions.

PPDT2FBT-PDI_x solutions were prepared in air, from 20 mg/mL solutions of the single components, which were stirred for 2h before mixing in the required weight proportions. If applicable, DIO, DPE or CN were added to the solution in the desired v/v proportion. Final solutions were stirred for at least 1h before deposition.

ZnO precursor solutions were prepared following the sol-gel method proposed by Sun et al.,[2] 1 g of zinc acetate trihydrate, 0.280 mL of ethanolamine and 10.0 mL of 2-methoxy ethanol were mixed in air and stirred overnight at room temperature before use.

Film preparation: All studied films were prepared as follow: ITO-coated glass substrates were first cleaned by surfactant/water scrubbing, followed by sequentially ultra-sonicating in de-ionized water, acetone and isopropanol (10+ min each) before use. ITO substrates were then dried with pressurized air and UV-Ozone treated for 30 minutes. A ZnO precursor solution was spin-cast onto the ITO substrate at a speed of 4200 rpm for 55 s and then thermally annealed at 200 °C in air for 30 min. The organic layer was then cast at room temperature, in air, by spin-casting at 1000 or 2000 rpm for 50 s.

Optical Absorption Spectroscopy (UV/vis/near-IR): All absorption measurements were recorded using an Agilent Technologies Cary 60 UV-vis spectrometer at room temperature.

Optical Photoluminescence Spectroscopy: All measurements were recorded using an Agilent Technologies Cary Eclipse fluorescence spectrophotometer at room temperature.

Atomic force microscopy (AFM): AFM measurements were performed by using a TT-2 AFM in the tapping mode and WSxM software with a 0.01-0.025 Ohm/cm Sb (n) doped Si probe with a reflective back side aluminum coating.

Cyclic Voltammetry (CV): Electrochemical measurements were performed using a CH Instruments potentiostat in a standard three-electrode configuration equipped with a silver wire pseudo-reference, platinum wire counter electrode and glassy carbon working electrode. The

cyclic voltammetry experiments were performed in an anhydrous solution of CH_2Cl_2 with ~0.1 M tetrabutylammoniumhexafluorophosphate ($TBAPF_6$) supporting electrolyte. Samples were scanned at a rate of 100 mV/s following a dry N_2 purge to deoxygenate the solution. Solution CV measurements were carried out with a sample concentration of ~0.5 mg/mL in CH_2Cl_2. The HOMO and LUMO energy levels were estimated considering the energy level of Fc/Fc^+ with respect to the vacuum level:

$E^{HOMO} = [-(\ E^1_{ox}) - 4.8]$ and $E^{LUMO} = [-(\ E^1_{red}) - 4.8]$

Polarized Optical Microscopy: POM images were taken through an Olympus Optical Microscope (BX53) at 50x magnification and relative digital camera set-up.

Fluorescence Microscopy: FM images were taken with an Olympus Optical Microscope (BX53) at 50x magnification, equipped with a BX3-URA unit and a X-cite 120 LEDmini light source. A designated filter selectively allows green light to be transmitted to the sample, while red light sourced at the sample is selectively transmitted to the digital camera.

Solar Cells Fabrication: Solar cells were fabricated following the initial procedure for cleaning, ZnO deposition and organic layer deposition reported above. The fabricated films were then moved to an N_2 atmosphere glovebox overnight before evaporating MoO_x and Ag. MoO_x (10 nm) and Ag (100 nm) were thermally evaporated under high vacuum (10^{-5} torr).

Solar Cells Testing: Current density-voltage (J-V) characteristics were measured using a Keithley 2420 Source Measure Unit. Solar cell performance used an Air Mass 1.5 Global (AM 1.5G) Solar Simulator (Newport, Model 92251A-1000) with an irradiation intensity of 100 $mW.cm^{-2}$, which was measured by a calibrated silicon solar cell and a readout meter (Newport, Model 91150V).

Synthetic Procedures

Chapter II

N,N'-Dicyclohexylperylene-3,4:9,10-bis(dicarboximide)[3] 2

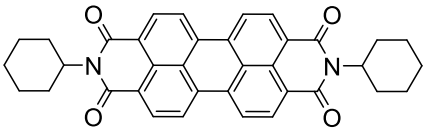

Red-purple Solid
$C_{36}H_{30}N_2O_4$
MW: 554.22

To a suspension of PTCDA (9.8 g, 25 mmol) in 200 mL of DMF, was added 15 mL of cyclohexylamine. The reaction mixture was refluxed using a heating mantle for 4h. After cooling, the solution was poured in a beaker. After addition of 150 mL HCl 1N, then 400 mL of MeOH, the precipitate was filtered on a Buchner. The precipitate was washed with methanol, then dried at 70°C under vacuum overnight, affording 13.56 g (yield = 98%) of compound **2** as a red-purple powder.

1-Nitro-*N,N'*-dicyclohexylperylene-3,4:9,10-bis(dicarboximide)[4,5] 3

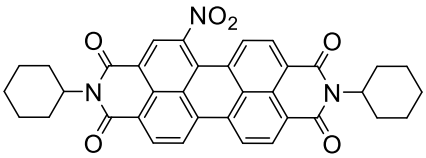

Red Solid
$C_{36}H_{29}N_3O_6$
MW: 599.21

To a solution of compound **2** (5.54 g, 10 mmol) in 500 mL anhydrous CH_2Cl_2 was added 10 mL fuming nitric acid. The reaction mixture was allowed to stir at 25°C for 20 min after which the TLC analysis indicated the complete conversion to the desired product and the reaction must be stopped before the appearance of dinitro derivative. The reaction was quenched by addition to 500 mL of water into a funnel. The organic phase was extracted, washed again two times with 500 mL of water, dried with $MgSO_4$ and concentrated. Two successive recrystallizations from CH_2Cl_2 and petroleum ether gave 5.55 g of compound **3** in 93% yield.

^{1}H NMR (300 MHz, $CDCl_3$): δ (ppm) = 8.74 (d, J = 8 Hz, 1H), 8.69-8.61 (m, 4H), 8.54 (d, J = 8 Hz, 1H), 8.15 (d, J = 8 Hz, 1H), 5.07-4.96 (m, 2H), 2.60-2.48 (m, 4H), 1.94-1.75 (m, 10H), 1.54-1.31 (m, 6H).

^{13}C NMR (75 MHz, $CDCl_3$): δ (ppm) = 163.6, 163.3, 163.2, 162.3, 147.7, 135.5, 132.9, 132.9, 131.4, 131.2, 129.4, 129.3, 129.0, 128.0, 127.5, 126.6, 126.5, 126.4, 125.5, 124.7, 124.6, 124.5, 124.1, 123.7, 54.6, 54.4, 53.6, 29.2, 29.2, 26.7, 26.6, 25.5, 25.4.

MS (MALDI-TOF negative mode): *m/z*: $C_{36}H_{29}N_3O_6$: 598 $[M]^-$, calcd: 599.

1-(3-Formyl)phenyl-*N,N'*-dicyclohexylperylene-3,4:9,10-bis(dicarboximide)[5] 4

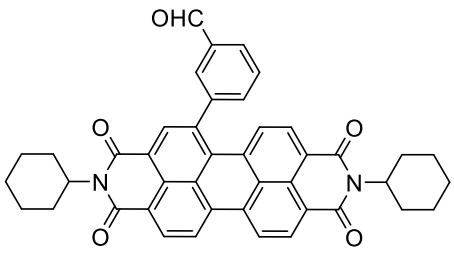

Purple Solid
$C_{43}H_{34}N_2O_5$
MW: 658.25

In a three-necked round-bottom flask, compound **3** (0.51 g, 0.85 mmol), K_3PO_4 (0.625 g, 2.95 mmol), 3-formylphenyl boronic acid (0.2 g, 1.33 mmol) and dry THF (75 mL) were added. The flask was then placed under controlled atmosphere by 3 vacuum / argon cycles while stirring. Then, the mixture was degassed by bubbling with argon for 1h before the addition of $Pd(PPh_3)_4$ (0.125 g, 0.108 mmol) quickly. After connecting the flask to a condenser, the reaction mixture was heated at 75°C for 48h under argon until the complete disappearance of compound **3** on TLC. The reaction mixture was allowed to cool to room temperature then the solvent was concentrated. The crude product was purified by silica gel column chromatography (eluent: CH_2Cl_2 then CH_2Cl_2/EtOAc 9/1). Recrystallization from CH_2Cl_2/petroleum ether gave after filtration 453 mg of compound **4** in 81% yield.

^{1}H NMR (300 MHz, $CDCl_3$): δ (ppm) = 10.08 (s, 1H), 8.69-8.54 (m, 4H), 8.50 (s, 1H), 8.07-8.01 (m, 3H), 7.73-7.68 (m, 3H), 5.08-4.94 (m, 2H), 2.63-2.45 (m, 4H), 1.90-1.71 (m, 10H), 1.55-1.35 (m, 6H).

^{13}C NMR (75 MHz, $CDCl_3$): δ (ppm) = 191.5, 163.9, 163.7, 143.8, 139.9, 138.3, 135.7, 134.8, 134.7, 134.2, 134.1, 132.6, 131.2, 131.2, 130.1, 130.1, 130.0, 129.9, 129.1, 129.0, 127.4, 123.9, 123.7, 123.2, 123.2,123.0, 54.3, 54.1, 29.2, 26.6, 25.5.

HRMS (EI+) *m/z*: calcd for $C_{43}H_{34}N_2O_5$: 658.2463; found: 658.2461.

1-(4-Formyl)phenyl-*N,N'*-dicyclohexylperylene-3,4:9,10-bis(dicarboximide)[5] 5

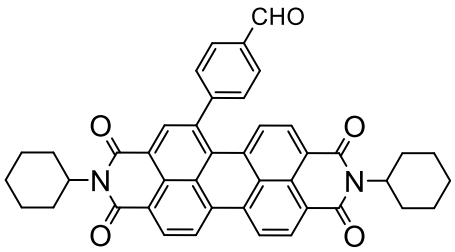

Purple Solid
$C_{43}H_{34}N_2O_5$
MW: 658.25

In a three-necked round-bottom flask, compound **3** (0.51 g, 0.85 mmol), K_3PO_4 (0.625 g, 2.95 mmol), 4-formylphenyl boronic acid (0.2 g, 1.33 mmol) and dry THF (75 mL) were added. The flask was then placed under controlled atmosphere by 3 vacuum / argon cycles while stirring. Then, the mixture was degassed by bubbling with argon for 1h before the addition of $Pd(PPh_3)_4$ (0.125 g, 0.108 mmol) quickly. After connecting the flask to a condenser, the reaction mixture

was heated at 75°C for 48h under argon until the complete disappearance of compound **3** on TLC. The reaction mixture was allowed to cool to room temperature then the solvent was concentrated. The crude product was purified by silica gel column chromatography (eluent: CH_2Cl_2). Recrystallization from CH_2Cl_2/petroleum ether gave after filtration 474 mg of compound **5** in 85% yield.

^{1}H NMR (500 MHz, $CDCl_3$): δ (ppm) = 10.14 (s, 1H), 8.67 (d, J = 8 Hz, 1H), 8.61 (d, J = 8 Hz, 1H), 8.58 (d, J = 8 Hz, 1H), 8.54 (d, J = 8 Hz, 1H), 8.48 (s, 1H), 8.06 (d, J = 8.2 Hz, 1H), 8.67 (d, J = 8.2 Hz, 2H), 7.68 (d, J = 8.2 Hz, 1H), 7.65 (d, J = 8.2 Hz, 2H), 5.05-4.96 (m, 2H); 2.58-2.48 (m, 4H), 1.93-1.88 (m, 4H), 1.79-1.71 (m, 6H), 1.52-1.28 (m, 6H).

^{13}C NMR (125MHz, $CDCl_3$): δ (ppm) = 191.5, 163.9, 163.7, 163.6, 148.9, 139.9, 136.2, 135.3, 134.8, 134.1, 133.9, 132.7, 132.62, 131.7, 131.3, 131.2, 130.3, 130.0, 129.6, 129.0, 128.6, 128.03, 127.4, 124.0, 123.8, 123.7, 123.3, 123.1, 123.0, 54.3, 54.1, 29.2, 29.2, 26.6, 25.6, 25.5, 22.7.

HRMS (EI+) *m/z*: calcd for $C_{43}H_{34}N_2O_5$: 658.2463; found: 658.2464.

1-(4-*N*,*N*-diphenylamino)phenyl-*N*,*N*'-dicyclohexylperylene-3,4:9,10 bis(dicarboximide)[5] 6

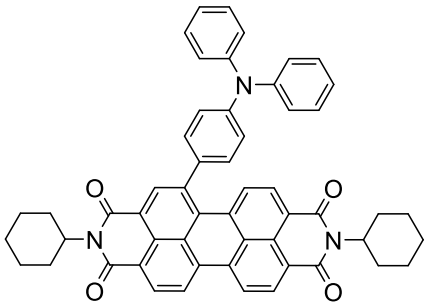

Dark Brown Solid
$C_{54}H_{43}N_3O_4$
MW: 797.33

In a Schlenk flask, compound **3** (0.15 g, 0.25 mmol), K_3PO_4 (0.13 g, 0.62 mmol), (4-(diphenylamino)phenyl)boronic acid (0.1 g, 0.37 mmol) and dry THF (30 mL) were added. The flask was then placed under controlled atmosphere by 3 vacuum / argon cycles while stirring. Then, the mixture was degassed by bubbling with argon for 30 min before the addition of $Pd(PPh_3)_4$ (0.03 g, 0.02 mmol) quickly. The flask was then sealed with cap and the reaction mixture was heated at 90°C for 48h until the complete disappearance of compound **3** on TLC. The reaction mixture was allowed to cool to room temperature then the solvent was concentrated. The crude product was purified by silica gel column chromatography using CH_2Cl_2- Petroleum ether (7:3) as eluent. Recrystallization from CH_2Cl_2/Petroleum ether gave after filtration 150 mg of compound **6** in 75% yield.

^{1}H NMR (300 MHz, $CDCl_3$): δ (ppm) = 8.64-8.50 (m, 5H), 8.22 (d, J = 8.2 Hz, 1H), 8.06 (d, J= 8.0, 1H), 7.38-7.29 (m, 6H), 7.22-7.08 (m, 8H), 5.09-4.97 (m, 2H); 2.62-2.50 (m, 4H), 1.93-1.73 (m, 10H), 1.54-1.33 (m, 6H).

^{13}C NMR (75MHz, $CDCl_3$): δ (ppm) = 164.1, 163.9, 148.6, 147.3, 141.7, 136.1, 135.6, 135.1, 134.7, 134.5, 132.2, 131.1, 130.7, 130.0, 129.7, 129.5, 129.1, 128.3, 128.2, 127.6, 125.2, 124.1, 123.9, 123.8, 123.7, 123.5, 122.8, 122.8, 122.6, 54.2, 54.0, 29.2, 26.7, 25.6, 22.8.

HRMS (EI+): calcd for $C_{54}H_{43}N_3O_4$: 797.3248; found: 797.3260.

Dyad PDI-C_{60} 7[5]

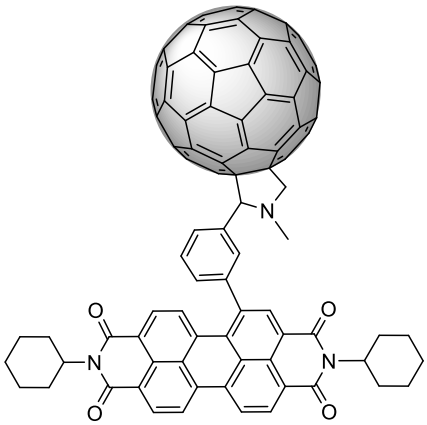

Red Solid
$C_{105}H_{39}N_3O_4$
MW: 1405.29

In a 250 mL round-bottom flask, C_{60} (164 mg, 0.22 mmol) was dissolved in o-DCB (70 mL) under vacuum, followed by the addition of sarcosine (27 mg, 0.30 mmol) and compound **4** (100 mg, 0.15 mmol). The flask was then placed under controlled atmosphere by 3 vacuum/ argon cycles while stirring. Then the reaction mixture was heated at 180°C under argon for 24h. The crude product was precipitated in methanol. After, purification by silica gel column chromatography (eluent: CS_2 then $CHCl_3$: Hexane 9:1) to afford 44 mg of **7** in 20% yield.

^{1}H NMR (300 MHz, $CDCl_3$): δ (ppm) = 8.67-8.53 (m, 5H), 8.10-7.34 (m, 6H), 5.07-5.00 (m, 2H), 4.96 (m, 1H (*CH*$_2$), 4.28 (m, 1H (*CH*$_2$)), 2.91-2.82(d, *J*= 2.9 Hz, 3H), 2.62-2.45 (m, 4H), 1.94-1.69 (m, 10H), 1.53-1.38 (m, 6H).

^{13}C NMR (125 MHz, $CDCl_3$): δ (ppm) = 163.8, 163.7, 156.0, 153.7, 153.1, 152.9, 147.4, 147.3, 146.3, 146.1, 146.0, 145.9, 145.9, 145.5, 145.3, 144.4, 142.7, 142.6,142.2, 142.1, 141.6, 140.2, 135.9, 135.6, 134.8, 134.4, 134.2, 130.8, 128.9, 128.5,128.0, 127.4, 124.0, 123.6, 123.4, 122.9, 122.8, 122.6, 70.1, 69.1, 54.1, 53.9, 41.3, 40.0, 36.0, 31.5, 29.2, 29.0, 27.6, 26.5, 26.5, 25.4, 25.4, 22.5, 22.5, 20.3, 18.1, 14.2, 13.9, 11.2, 0.92.

HRMS (FAB+): calcd for $C_{105}H_{39}N_3O_4$: 1405.2935 $[M]^+$, found: 1405.2936.

HPLC analysis: retention time: 9.58 min (eluent: toluene, flow rate: 1mL/min, wavelength: 320 nm).

1,6 and 1,7-Dinitro-*N,N'*-dicyclohexylperylene-3,4:9,10-bis(dicarboximide)[6] 9

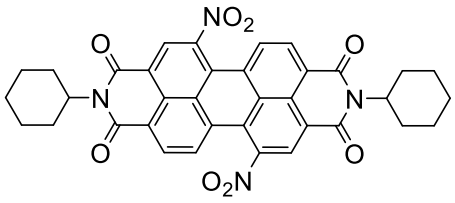

Red Solid
$C_{36}H_{28}N_4O_8$
MW: 644.19

To a solution of compound **2** (5.54 g, 10 mmol) in 500 mL anhydrous CH_2Cl_2 was added 10 mL fuming nitric acid. The reaction mixture was allowed to stir at 25°C for 24h after which the TLC analysis indicated the complete conversion to the desired product. The reaction was quenched by addition to 500 mL of water into a funnel. The organic phase was extracted, washed again two times with 500 mL of water, dried with $MgSO_4$ and concentrated. Two successive recrystallizations from CH_2Cl_2 and petroleum ether gave compound 5.7 g of **9** in 88% yield.

1,6-9 (55%): ^{1}H NMR (300 MHz, $CDCl_3$): δ (ppm) = 8.80 (s, 2H), 8.64 (d, *J* = 8.1 Hz, 2H), 8.31 (d, *J* = 8.1 Hz, 2H), 5.05-4.97 (m, 2H), 2.57-2.46 (m, 4H), 1.95-1.90 (m, 4H), 1.77-1.74 (m, 6H), 1.55-1.31 (m, 6H).

1,7-9 (45%): ^{1}H NMR (300 MHz, $CDCl_3$): δ (ppm) = 8.80 (s, 2H), 8.68 (d, *J* = 8.1 Hz, 2H), 8.29 (d, *J* = 8.1 Hz, 2H), 5.05-4.97 (m, 2H), 2.57-2.46 (m, 4H), 1.95-1.90 (m, 4H), 1.77-1.74 (m, 6H), 1.55-1.31 (m, 6H).

MS (MALDI-TOF negative mode): *m*/*z*: $C_{36}H_{28}N_4O_8$: 644.0 $[M]^-$, calcd: 644.2.

Compound 10 (1,6 and 1,7)

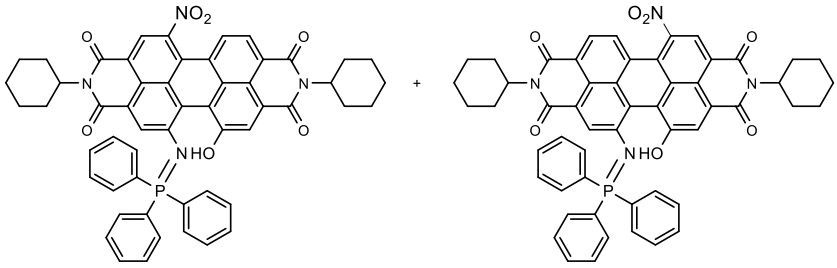

Green-blue Solid
$C_{54}H_{43}N_4O_7P$
MW: 890.92

In a 250 mL 3-necked round bottom flask, compound **9** (0.1 g, 0.15 mmol), PPh_3 (0.2 g, 0.93 mmol) and distilled THF (18 mL) were added. The flask was then placed under controlled atmosphere by 3 vacuum / argon cycles while stirring. After connecting the flask to a condenser, the reaction mixture was heated under reflux for 96h under argon. The reaction mixture was allowed to cool to room temperature then the solvent was concentrated. The crude product was purified by silica gel column chromatography (eluent: 100 % CH_2Cl_2 to collect the unreacted

dinitroPDI, then CH_2Cl_2/EtOAc 97:3 to collect the product). Recrystallization from CH_2Cl_2/petroleum ether gave after filtration 45 mg of compound **10** in 33% yield.

1,6-10 (60%): ^{1}H NMR (300 MHz, $CDCl_3$): δ (ppm) = 12.54 (s, 1H), 8.64 (s, 1H), 8.40 (s, 1H), 8.32 (d, *J* = 8.1 Hz, 1H), 8.08 (s, 1H), 7.90 (d, *J* = 8.1 Hz, 1H), 7.75-7.63 (m, 9H), 7.58-7.52 (m, 6H), 5.11- 4.86 (m, 2H), 2.65-2.40 (m, 4H), 1.94-1.77 (m, 7H), 1.69-1.65 (m, 3H), 1.50-1.31 (m, 6H).

^{31}P NMR (122 MHz, $CDCl_3$): δ (ppm) = 21.20 (s, 1P).

1,7-10 (40%)**:** ^{1}H NMR (300 MHz, $CDCl_3$): δ (ppm) = 12.54 (s, 1H), 8.61 (s, 1H), 8.40 (d, *J* = 8.1 Hz, 1H), 8.40 (s, 1H), 8.17 (d, *J* = 1.2 Hz, 1H), 8.10 (d, *J* = 6.9 Hz, 1H), 7.75-7.63 (m, 9H), 7.58-7.52 (m, 6H), 5.11- 4.86 (m, 2H), 2.65-2.40 (m, 4H), 1.94-1.77 (m, 7H), 1.69-1.65 (m, 3H), 1.50-1.31 (m, 6H).

^{31}P NMR (122 MHz, $CDCl_3$): δ (ppm) = 21.24 (s, 1P).

MS (MALDI-TOF negative mode): *m/z*: $C_{54}H_{43}N_4O_7P$: 890.2 $[M]^-$, calcd: 890.9

Compound 11

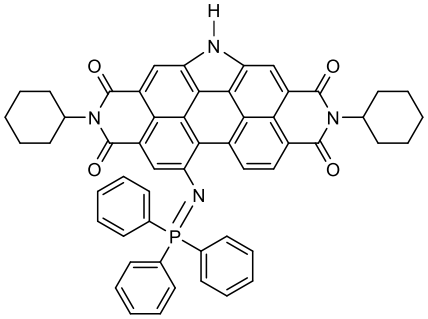

Purple Solid
$C_{54}H_{43}N_4O_4P$
MW: 842.30

In a 250 mL 3-necked round bottom flask, compound **9** (0.644 g, 1 mmol), PPh_3 (2.64 g, 10 mmol) and toluene (150 mL) were added. The reaction mixture was heated under reflux for 60h under argon. After, the reaction mixture was allowed to cool to room temperature then the solvent was concentrated. The crude product was purified by silica gel column chromatography (eluent: 100 % CH_2Cl_2, then CH_2Cl_2/EtOAc 95:5 to collect the product) first compound **10** (115 mg after recrystallization in CH_2Cl_2/petroleum ether, 13% yield), then compound **11**. Recrystallization from CH_2Cl_2/petroleum ether gave after filtration then 61 mg of compound **11** in 8% yield.

^{1}H NMR (500 MHz, $CDCl_3$): δ (ppm) = 10.33 (d, *J* = 8.3 Hz, 1H), 9.61 (s, 1H), 8.89 (s, 1H), 8.66 (d, *J* = 8.3 Hz, 1H), 8.53 (s, 1H), 8.02-7.95 (m, 7H), 7.66-7.58 (m, 9H), 5.30-4.98 (m, 2H), 2.79-2.50 (m, 4H), 1.92-1.74 (m, 10H), 1.56-1.35 (m, 6H).

^{31}P NMR (122 MHz, CDCl3): δ (ppm) = 9.81 (s, 1P).

^{13}C NMR (125 MHz, $CDCl_3$): δ (ppm) = 166.5, 166.3, 165.1, 164.9, 154.2, 136.1, 134.7, 133.0, 132.9, 132.8, 132.8, 132.4, 129.8, 129.5, 129.4, 129.0, 128.6, 127.1, 124.9, 124.8, 124.4, 124.3, 123.0, 122.9, 122.7, 122.5, 122.3, 121.4, 121.1, 119.9, 119.1, 117.7, 116.9, 113.3, 54.1, 54.0, 41.5, 41.2, 29.5, 29.5, 29.2, 27.0, 26.9, 25.9, 25.7, 22.8, 20.6, 19.6, 18.9, 14.5, 11.6.

MS (MALDI-TOF positive mode): *m/z*: $C_{54}H_{43}N_4O_4P$: 842.5 $[M]^+$, calcd: 842.30.

Compound 12

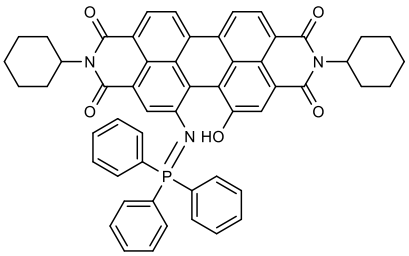

Purple Solid
$C_{54}H_{44}N_3O_5P$
MW: 845.92

In a 250 mL 3-necked round bottom flask, compound **3** (0.3 g, 0.52 mmol), PPh_3 (0.8 g, 3.12 mmol) and distilled THF (50 mL) were added. The flask was then placed under controlled atmosphere by 3 vacuum / argon cycles while stirring. After connecting the flask to a condenser, the reaction mixture was heated under reflux for 96h under argon. The reaction mixture was allowed to cool to room temperature then the solvent was concentrated. The crude product was purified by silica gel column chromatography (eluent: 100 % CH_2Cl_2 to collect the unreacted dinitroPDI, then CH_2Cl_2/EtOAc 97:3 to collect the product). Recrystallization from CH_2Cl_2/petroleum ether gave after filtration 126 mg of compound **12** in 30% yield.

^1H NMR (300 MHz, $CDCl_3$): δ (ppm) = 12.73 (s, 1H), 8.55 (s, 2H), 8.51 (d, *J* = 1.5 Hz, 2H), 8.41 (s, 1H), 8.09 (d, *J* = 1.3 Hz, 1H), 7.78-7.68 (m, 6H), 7.68-7.59 (m, 3H), 7.58-7.48 (m, 6H), 5.10 (m, 2H), 2.55 (m, 4H), 1.99-1.61 (m, 10H), 1.43 (m, 6H).

^{31}P NMR (122 MHz, $CDCl_3$): δ (ppm) = 20.28 (s, 1P).

MS (MALDI-TOF positive mode): *m/z*: $C_{54}H_{44}N_3O_5P$: 845,2 $[M]^+$, calcd: 845.92

Chapter III

Compound 13

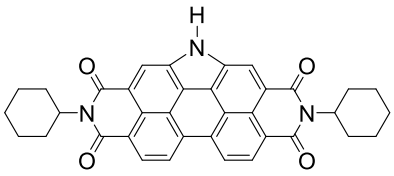

Dark Red Solid
$C_{36}H_{29}N_3O_4$
MW: 567.22

In a 20mL microwave vial, compound **3** (0.5 g, 0.83 mmol), PPh_3 (0.54 g, 2.07 mmol) and o-DCB (14 mL) were added. The vial was sealed with a Teflon cap and the reaction mixture was purged with argon for 30 min, followed by microwave heating at 180°C for 2 h. The reaction mixture was stirred in methanol for 1h. Filtration gave 1.3 g of compound **13** as dark red solid. The mass obtained corresponds to the addition of three successive reactions carried out on the same starting quantities. Due to solubility issues, it was preferred to do the reaction on small scales. Overall yield: 97%.

(MALDI-TOF negative mode): *m/z*: $C_{36}H_{29}N_3O_4$: 567.3 $[M]^-$, calcd: 567.2.

Compound 14

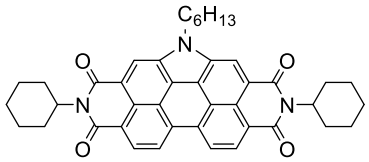

Red Solid
$C_{42}H_{41}N_3O_4$
MW: 651.31

In a 20ml microwave vial, compound **13** (0.5 g, 0.88 mmol) and potassium carbonate (0.25 g, 1.8 mmol) were added. The vial was sealed with a Teflon cap, followed by the addition of dry DMF (13 mL) and 1-bromo-hexane (0.3 g, 1.8mmol). The reaction mixture was purged with argon for 30 min, followed by microwave heating at 170°C for 1h. The reaction mixture was allowed to cool to room temperature and was extracted using water and CH_2Cl_2. The organic phase was collected and the solvent was concentrated. The crude product was purified by silica gel column chromatography (hexane to CH_2Cl_2 gradient, the product eluted at approximately 100% CH_2Cl_2). Recrystallization from CH_2Cl_2/methanol gave after filtration 1 g of compound **14** in 87% yield. The mass indicated is after two successive reactions of the same starting quantities.

^{1}H NMR (300 MHz, $CDCl_3$): δ (ppm) = 8.80 (s, 2H), 8.69 (s, 4H), 5.24-5.16 (m, 2H), 4.78-4.73 (t, 2H), 2.76-2.63 (m, 4H), 2.14-2.07 (m, 2H), 2.01-1.89 (m, 8H), 1.82-1.78 (m, 2H), 1.53-1.22 (m, 12H), 0.86-0.82 (t, 3H).

^{13}C NMR (75 MHz, $CDCl_3$): δ (ppm) = 165.6, 164.4, 134.7, 132.4, 127.6, 124.4, 123.7, 122.8, 122.2, 121.6, 119.3, 118.5, 54.5, 47.0, 31.6, 31.5, 29.5, 27.0, 26.9, 25.8, 22.6, 14.1.

(MALDI-TOF negative mode): *m/z*: $C_{42}H_{41}N_3O_4$: 651 $[M]^-$, calcd: 651.

Compound 15

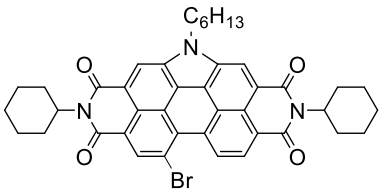

Dark Red Solid
$C_{42}H_{40}BrN_3O_4$
MW: 729.22

In a 100 ml Schlenk flask, compound **14** (0.6 g, 0.92 mmol), CH_2Cl_2 (55 mL) and Br_2 (approximately 5mL) were added. The reaction mixture was allowed to stir at room temperature for 4h at which time TLC analysis indicated the complete consumption of starting material. After the addition of an aqueous solution of $Na_2S_2O_3$, the reaction mixture was extracted using water and CH_2Cl_2. The organic phase was collected and the solvent was concentrated. The crude product was purified by silica gel column chromatography (100% CH_2Cl_2). Recrystallization from CH_2Cl_2/MeOH gave after filtration 440 mg of compound **15** in 65% yield.

^{1}H NMR (300 MHz, $CDCl_3$): δ (ppm) = 9.39 (d, *J* = 8.4 Hz, 1H), 8.67 (s, 1H), 8.64 (s, 1H), 8.60 (s, 1H), 8.42 (d, *J* = 8.4 Hz, 1H), 5.25-5.11 (m, 2H), 4.72-4.67 (t, 2H), 2.79-2.63 (m, 4H), 2.05-1.95 (m, 10H), 1.84 (d, J =11.8 Hz, 2H), 1.66-1.61 (m, 2H), 1.55-1.22 (m, 10H), 0.86-0.81 (t, 3H).

^{13}C NMR (125 MHz, $CDCl_3$): δ (ppm) = 165.2, 165.0, 163.9, 163.0, 134.0, 133.8, 133.8, 131.2, 129.4, 126.8, 126.5, 123.4, 122.7, 122.6, 122.5, 122.2, 122.1, 122.1, 121.2, 120.8, 117.8, 117.5, 117.4, 117.2, 54.7, 54.6, 46.8, 31.4, 31.4, 29.5, 29.5, 27.0, 26.9, 26.9, 25.8, 25.8, 22.6, 14.1.

(MALDI-TOF negative mode): *m*/*z*: $C_{42}H_{40}BrN_3O_4$: 729 [*M*]$^-$, calcd: 729.

PDI-Cy dimer 16

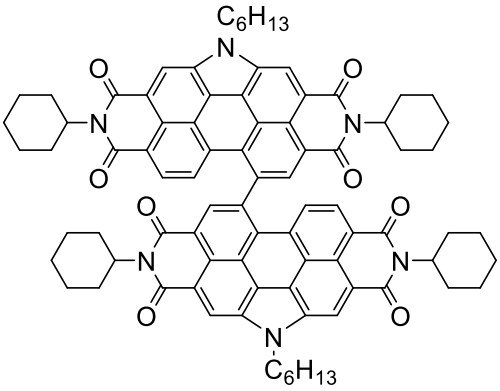

Red Solid
$C_{84}H_{80}N_6O_8$
MW: 1300.60

Compound **15** (0.4 g, 0.54 mmol), zinc dust (0.2 g, 3.29 mmol) and $Pd_2(dba)_3$ (0.1 g, 0.06 mmol) were brought inside the glove box and kept there for 1 night. All reagents were added together in a 100 mL Schlenk flask, followed by the addition of dry DMF (40 mL). The Schlenk was sealed and removed from the glove box. The reaction mixture was purged with argon for 10 min, after which it was heated at 103°C for 6 h at which time the reaction had turned a deep blue-purple and TLC analysis indicated the complete consumption of starting material. The reaction mixture was passed through a silica plug to remove solids from the reaction and the solvent was removed in vacuo. The crude product was purified by column chromatography (Al_2O_3, CH_2Cl_2). Recrystallization from $CHCl_2$/MeOH gave after filtration 150 mg of compound **16** in 21% yield.

^{1}H NMR (300 MHz, $CDCl_3$): δ (ppm) = 9.24 (s, 2H), 9.05 (s, 2H), 8.89 (s, 2H), 7.91 (d, *J* = 8.4 Hz, 2H), 7.55 (d, *J* = 8.4 Hz, 2H), 5.25-5.17 (m, 2H), 5.06-4.95 (m, 6H), 2.74-2.60 (m, 4H),

2.55-2.43 (m, 4H), 2.34-2.25 (m, 4H), 1.96-1.65 (m, 20H), 1.54-1.48 (m, 6H), 1.46-1.25 (m, 18 H), 0.93-0.88 (t, 6H).

^{13}C NMR (125MHz, $CDCl_3$): δ (ppm) = 165.8, 165.7, 164.2, 164.1, 141.0, 135.4, 135.1, 133.0, 130.4, 127.7, 126.9, 124.9, 124.6, 123.7, 123.6, 123.2, 123.0, 122.8, 122.2, 120.1, 119.9, 119.3, 118.7, 54.6, 54.2, 47.3, 31.8, 31.6, 29.5, 29.4, 29.3, 27.1, 26.8, 26.7, 25.7, 25.6, 22.7, 14.2.

HRMS (FAB+): calcd for $C_{84}H_{80}N_6O_8$: 1300.6033; found: 1300.6029.

Chapter IV

1-Amino-*N,N'*-dicyclohexylperylene-3,4:9,10-bis(dicarboximide)[7] 17

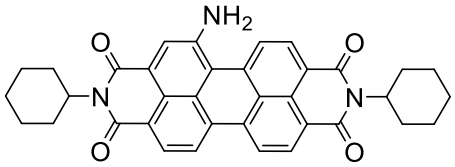

Violet Solid
$C_{36}H_{31}N_3O_4$
MW: 569.23

Compound **3** (0.2 g, 0.33 mmol), Pd/C and DMF (40 mL) were added in a 3-necked flask and degassed for 10 min by purging argon. Hydrogen was introduced into the sealed reaction system through a balloon, and the reaction was allowed to proceed at room temperature for 2h. After, the solvent was removed, and the product was purified by column chromatography (Al_2O_3, $CHCl_3$) Recrystallization from $CHCl_3$/petroleum ether gave after filtration 155 mg of compound **17** in 81% yield.

^{1}H NMR (300 MHz, $CDCl_3$): δ (ppm) = 8.82 (d, *J*= 8.2 Hz, 1H), 8.60 (d, *J*= 8.2 Hz, 2H), 8.48-8.40 (m, 3H), 8.10 (s, 1H), 5.13 (s, 2H), 5.07-4.96 (m, 2H), 2.65-2.49 (m, 4H), 1.95-1.74 (m, 10H), 1.51-1.37 (m, 6H).

(MALDI-TOF negative mode): *m/z*: $C_{36}H_{31}N_3O_4$: 569.3 $[M]^-$, calcd: 569.2.

N,N'-Dicyclohexylperylene-3,4:9,10-bis(dicarboximide) diazonium tetrafluoroborate 18

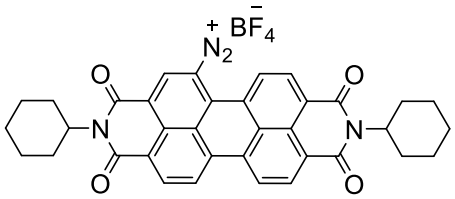

Violet Solid
$C_{36}H_{29}BF_4N_4O_4$
MW : 668.22

Procedure 1: Compound **3** (0.2 g, 0.33 mmol), Pd/C and THF (30 mL) were added in a 3-necked flask and degassed for 10 min by purging argon. Hydrogen was introduced into the sealed reaction system through a balloon, and the reaction was allowed to proceed at room temperature

for 2h. After, the reaction mixture was directly added to a mixture of $NaNO_2$ (0.22 g, 3.3 mmol) and $HBF_4 \cdot Et_2O$ (1mL, 6.7 mmol) at 0°C. The reaction was stirred at 0°C for 1h and 30 min, after which ether was poured into reaction solution to yield pure product. The resulting solid was filtered, washed by Et_2O and dried under vacuum to obtain 200 mg of compound **18** in 90% yield. The product was sealed and stored at low temperature for 24h before further use.

Procedure 2: Compound **3** (0.2 g, 0.33 mmol), Pd/C and THF (30 mL) were added to a 3-necked flask and degassed for 10 min by purging argon. Hydrogen was introduced into the sealed reaction system through a balloon, and the reaction was allowed to proceed at room temperature for 2h. After, the reaction mixture was cooled to 0°C and $BF_3C_4H_{10}O$ (0.8 mL, 6.7 mmol) was added, followed by the addition of tBuONO (0.4 mL, 3.3mmol). After 30 min, ether was poured into reaction solution to yield pure product, the resulting solid was filtered, washed by Et_2O and dried under vacuum to obtain 134 mg of compound **18** in 57% yield. The product was sealed and stored at low temperature for 24h before further use.

^{19}F NMR (283 MHz, $CDCl_3$) δ (ppm) = -153.97 (s, 1F).

N,N'-Bis(ethylpropyl)perylene-3,4:9,10- bis(dicarboximide) diazonium tetrafluoroborate 22

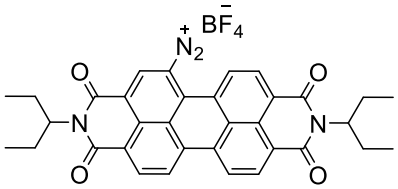

Violet Solid
$C_{34}H_{29}BF_4N_4O_4$
MW : 644.22

Compound **20** (0.2 g, 0.34 mmol), Pd/C and THF (30 mL) were added in a 3-necked flask and degassed for 10 min by purging argon. Hydrogen was introduced into the sealed reaction system through a balloon, and the reaction was allowed to proceed at room temperature for 2h. After, the reaction mixture was directly added to a mixture of $NaNO_2$ (0.23g, 3.4 mmol) and $HBF_4 \cdot Et_2O$ (1mL, 6.8 mmol) at 0°C. The reaction was stirred at 0°C for 1h and 30 min, after which ether was poured into reaction solution to yield pure product. The resulting solid was filtered, washed by ether and dried under vacuum to obtain 135 mg of compound **22** in 57% yield. The product was sealed and stored at low temperature for 24h before further use.

1-Fluoro- *N,N'*-dicyclohexyl perylene-3,4:9,10-tetracarboxylic diimide 23

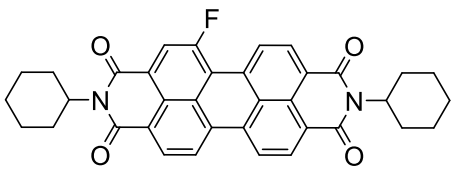

Red Solid
$C_{36}H_{29}FN_2O_4$
MW: 572.21

Compound **18** (50 mg, 0.07 mmol) was allowed to heat without a solvent at 235°C for 2h, during which the color turned from violet to brown. The crude product was purified by silica gel column chromatography (eluent: CH_2Cl_2: Petroleum ether, 9:1) giving compound **23** in a low yield.

^{1}H NMR (300 MHz, $CDCl_3$): δ (ppm) = 9.00-8.96 (m, 1H), 8.67-8.59 (m, 5H), 8.40 (d, *J* = 13.7 Hz, 1H), 5.06-4.97 (m, 2H), 2.60-2.53 (m, 4H), 1.81-1.73 (m, 10H), 1.56-1.37 (m, 6H).

^{19}F NMR (283 MHz, $CDCl_3$) δ (ppm) = -102.14 (s, 1F).

(MALDI-TOF negative mode): *m*/*z*: $C_{36}H_{29}FN_2O_4$: 571.6 $[M]^-$, calcd: 572.2.

1-Fluoro-*N,N'*-bis(ethylpropyl)perylene-3,4:9,10- bis(dicarboximide) 24

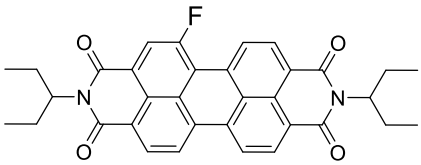

Red Solid
$C_{34}H_{29}FN_2O_4$
MW 548.21

Compound **22** (0.1g, 0.15 mmol) was allowed to heat without a solvent at 235°C for 2h, during which the color turned from violet to brown. The crude product was purified by silica gel column chromatography (eluent: CH_2Cl_2: Petroleum ether, 9:1) giving compound **24** in a low yield.

^{1}H NMR (300 MHz, $CDCl_3$): δ (ppm) = 9.02-8.97 (m, 1H), 8.69-8.59 (m, 5H), 8.43 (d, *J* = 13.7Hz, 1H), 5.12-5.00 (m, 5H), 2.35-2.18 (m, 4H), 2.02-1.88 (m, 4H), 0.96-0.91 (m, 12H).

^{19}F NMR (283 MHz, $CDCl_3$) δ (ppm) = -102.19 (s, 1F).

MALDI-TOF (negative mode): *m*/*z*: $C_{34}H_{29}FN_2O_4$: 547.6 $[M]^-$, calcd: 548.2.

1-Iodo-*N,N'*-dicyclohexylperylene-3,4:9,10-bis(dicarboximide) 25

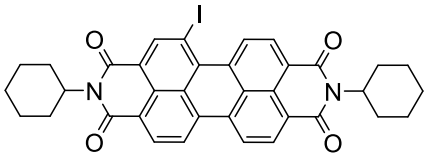

Red solid
$C_{36}H_{29}IN_2O_4$
MW: 680.12

Procedure 1: Compound **3** (0.2 g, 0.33 mmol), Pd/C and THF (30 mL) were added to a 3-necked flask and degassed for 10 min by purging argon. Hydrogen was introduced into the sealed reaction system through a balloon, and the reaction was allowed to proceed at room temperature for 2h. After, the reaction mixture was cooled down to -78°C then $NaNO_2$ (0.22g, 3.3 mmol), $HBF_4{\cdot}Et_2O$ (1 mL, 6.6 mmol) and KI (0.54 g, 3.3 mmol) were added. The reaction was kept stirring for 24h. The crude product was purified by silica gel column chromatography (eluent: CH_2Cl_2) giving compound **25** in a low yield.

Procedure 2: Compound **3** (0.2 g, 0.33 mmol), Pd/C and THF (30 mL) were added to a 3-neck flask and degassed for 10 min by purging argon. Hydrogen was introduced into the sealed reaction system through a balloon, and the reaction was allowed to proceed at room temperature for 2h. After, the reaction mixture was cooled down to 0°C then $BF_3C_4H_{10}O$ (0.8 mL, 6.7 mmol) and tBuONO (0.4 mL, 3.3mmol) were added. The reaction was allowed to stir for 1hr and 30 min at 0°C before the addition of KI (0.54 g, 3.3 mmol). After 24h, the reaction was quenched by the addition of H_2O and the organic phase was extracted. The crude product was purified by silica gel column chromatography (eluent: CH_2Cl_2) giving compound **25** in a low yield.

^{1}H NMR (300 MHz, $CDCl_3$): δ (ppm) = 9.71 (d, *J* = 8.2 Hz,1H), 9.18 (s, 1H), 8.67-8.63 (m, 3H), 8.56-8.50 (m, 2H), 5.10-4.96 (m, 2H), 2.64-2.48 (m, 4H), 1.94-1.74 (m, 10H), 1.50-1.32 (m, 6H).

MALDI-TOF (negative mode): *m*/*z*: $C_{36}H_{29}IN_2O_4$: 680 $[M]^-$, calcd: 680.

1-Bromo- *N,N'*-dicyclohexyl perylene-3,4:9,10-tetracarboxylic diimide 26

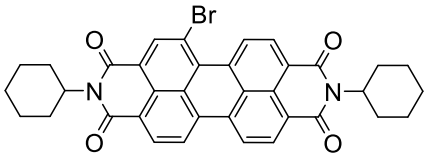

Red Solid
$C_{36}H_{29}BrN_2O_4$
MW: 632.13

Compound **3** (0.2 g, 0.33 mmol), Pd/C and THF (30 mL) were added in a 3-necked flask and degassed for 10 min by purging argon. Hydrogen was introduced into the sealed reaction system through a balloon, and the reaction was allowed to proceed at room temperature for 2h. After, the reaction mixture was cooled down to 0°C then HBr (33%, 38 µL, 0.66 mmol) and $NaNO_2$ (23 mg, 0.33 mmol) dissolved in water (1.5 mL) were added. The reaction was allowed to stir for 1hr at 0°C before the addition of CuBr (54.43 mg, 0.38 mmol) and HBr (33%, 49 µL, 0.84 mmol). After stirring for 24h, the reaction was quenched by the addition of H_2O and the organic phase was extracted using CH_2Cl_2. The crude product was purified by silica gel column chromatography (eluent: CH_2Cl_2) giving 22 mg compound **26** in 10% yield.

^{1}H NMR (300 MHz, $CDCl_3$): δ (ppm) = 9.79 (d, *J* = 8.2 Hz, 1H), 8.90 (s, 1H), 8.69-8.64 (m, 3H), 8.60 (m, 2H), 5.08-4.99 (m, 2H), 2.60-2.52 (m, 4H), 1.95-1.76 (m, 10H), 1.50-1.42 (m, 6H).

(MALDI-TOF negative mode): *m*/*z*: $C_{36}H_{29}BrN_2O_4$: 632.0 $[M]^-$, calcd: 632.1.

TPA-PDIaza dyad 27

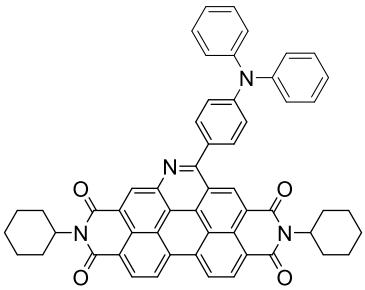

Green Solid
$C_{55}H_{42}N_4O_4$
MW: 822.32

Compound **17** (0.2 g, 0.35 mmol), 4-(diphenylamino)benzaldehyde (0.6 g, 2.1mmol) and activated molecular sieves (3Å) where placed in a Schlenk flask, then dry DMF (30 mL) was added. The mixture was degassed by bubbling with argon for 30 min before the addition of triflic acid (0.3 mL, 3.5mmol), the reaction mixture was stirred at 130°C under argon atmosphere for around 3h. Subsequently, the inert atmosphere was replaced by atmospheric oxygen and DDQ (80 mg, 0.35mmol) was added while heating. After stirring for 24h, the reaction mixture was quenched by addition of water and neutralized with 15% NaOH aqueous solution. The organic phase was extracted, washed again two times with water and brine, dried with $MgSO_4$ and concentrated. The crude product was purified by silica gel column chromatography (eluent: $CHCl_3$: Petroleum ether 9:1). Recrystallization from $CHCl_3$/petroleum ether gave after filtration 133 mg of compound **27** in 46% yield.

^{1}H NMR (500 MHz, CDCl): δ (ppm)= 9.32 (s, 1H), 9.11 (s, 1H), 8.71 (d, J= 8.1 Hz, 1H), 8.66 (d, J= 8.0 Hz, 1H), 8.60-8.57 (m, 2H), 7.80 (d, J= 8.4 Hz, 2H), 7.42-7.33 (m, 10H), 7.19-7.17 (t, 2H), 5.14-5.09 (m, 2H), 2.69-2.60 (m, 4H), 2.02-1.95 (m, 8H), 1.82 (d, J=12.5 Hz, 2H), 1.57-1.52 (m, 4H), 1.47-1.38 (m, 2H).

^{13}C NMR (125 MHz, $CDCl_3$) δ (ppm) = 163.7, 163.6, 163.4, 160.4, 149.8, 147.2, 143.9, 134.2, 133.2, 132.2, 132.2, 131.4, 130.6, 130.2, 129.8, 128.6, 128.4, 127.4, 126.0, 125.8, 125.6, 124.2, 123.5, 123.2, 123.0, 122.6, 122.1, 122.0, 121.9, 121.1, 117.2, 77.4, 54.7, 54.6, 31.1, 29.3, 26.8, 25.7, 25.7.

HRMS (FAB+): calcd for $C_{55}H_{42}N_4O_4$: 822.3201; found: 822.3219.

Fluorene-PDIaza dyad 28

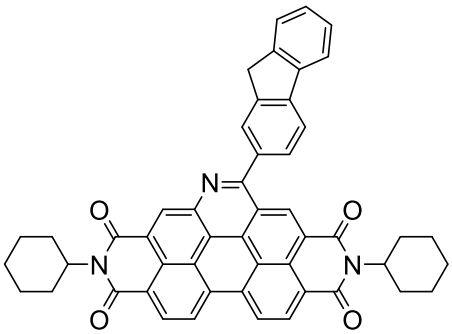

Orange Solid
$C_{50}H_{37}N_3O_4$
MW: 743.28

Compound **17** (0.15 g, 0.26 mmol), fluorene-2-carboxaldehyde (0.3 g, 1.6 mmol) and activated molecular sieves (3Å) where placed in a Schlenk flask, then dry DMF (30 mL) was added. The mixture was degassed by bubbling with argon for 30 min before the addition of triflic acid (0.23 mL, 2.6 mmol), the reaction mixture was stirred at 130°C under argon atmosphere for around 3h. Subsequently, the inert atmosphere was replaced by pure oxygen, and the reaction mixture was heated after under reflux for 24h. Then, the mixture was quenched by addition with water and neutralized with 15% NaOH aqueous solution. The organic phase was extracted, washed again two times with water and brine, dried with $MgSO_4$ and concentrated. The crude product was purified by silica gel column chromatography (eluent: $CHCl_3$: Petroleum ether 9:1). Recrystallization from $CHCl_3$/MeOH gave after filtration 70 mg of compound **28** in 35% yield.

^{1}H NMR ($CDCl_3$, 300 MHz): δ (ppm) = 9.61 (s, 1H), 9.60 (s, 1H), 9.28-9.24 (m, 2H), 9.13 -9.06 (m, 2H), 8.22 (m, 1H), 8.12 (d, J= 7.8 Hz, 1H), 7.97-7.93 (m, 2H), 7.65 (d, J= 7.7, 1H), 7.51-7.39 (m, 2H), 5.22-5.10 (m, 2H), 4.16 (s, 2H), 2.73-2.55 (m, 4H), 2.02-1.73 (m, 10H), 1.51-1.40 (m, 6H).

HRMS (FAB+): calcd for $C_{50}H_{37}N_3O_4$: 743.2779; found: 743.2784.

PDI-PDIaza dyad 29

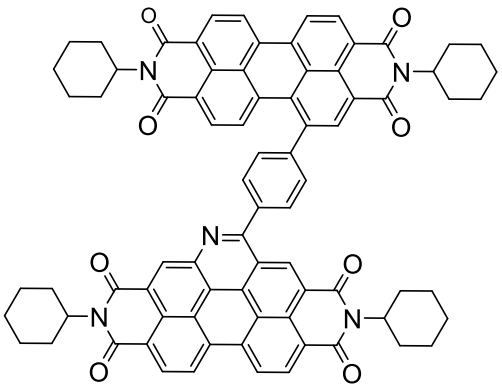

Dark Red Solid
$C_{79}H_{61}N_5O_8$
MW: 1207.45

Compound **17** (0.15 g, 0.26 mmol), compound **5** (0.17 g, 0.26 mmol) and activated molecular sieves (3Å) where placed in a Schlenk flask, then dry DMF (45 mL) was added. The mixture was degassed by bubbling with argon for 30 min before the addition of triflic acid (0.23 mL, 2.6 mmol), the reaction mixture was stirred at 140°C under argon atmosphere for around 3h. Subsequently, the inert atmosphere was replaced by pure oxygen, and the reaction mixture was heated after under reflux for 24h. Then, the mixture was quenched by addition with water and neutralized with 15% NaOH aqueous solution. The organic phase was extracted, washed again two times with water and brine, dried with $MgSO_4$ and concentrated. The crude product was purified by column chromatography (Al_2O_3, $CHCl_3$). Recrystallization from $CHCl_3$/EtOAc gave after filtration 80 mg of compound **29** in 25% yield.

^{1}H NMR (500 MHz, $CDCl_3$): δ (ppm) = 9.64 (s, 1H), 9.62 (s, 1H), 9.31 (dd, J=8.3 Hz, 2H), 9.15 (d, J= 8.2 Hz, 1H), 9.10 (d, J= 8.2 Hz, 1 H), 8.74-8.71 (m, 2H), 8.67-8.65 (m, 2H), 8.62 (d, J= 8.1 Hz, 1H), 8.47 (d, J=8.2 Hz, 1H), 8.24 (d, J= 8.3 Hz, 1H), 8.18 (d, J= 8.1 Hz, 2 H), 7.89 (d,

J= 8.1 Hz, 2H), 5.11-5.06 (m, 2H), 5.03-4.97 (m, 2H), 2.73-2.64 (m, 4H), 2.62-2.49 (m, 4H), 2.00-1.69 (m, 20H), 1.52-1.37 (m, 12H).

HRMS (MALDI): calcd for $C_{79}H_{61}N_5O_8$: 1207.4520; found: 1207.4520.

PMI-PDIaza dyad 30

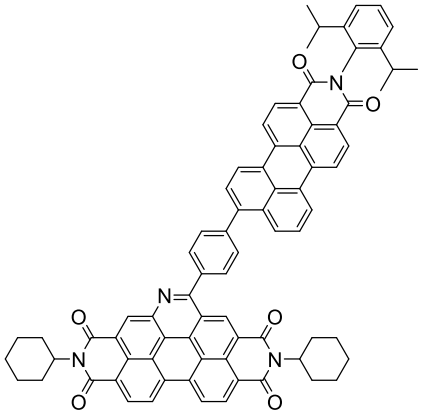

Dark Red Solid
$C_{77}H_{58}N_4O_6$
MW: 1134.44

Compound **17** (0.1 g, 0.17 mmol), PMI derivative (0.1 g, 0.17 mmol) and activated molecular sieves (3Å) where placed in a Schlenk flask, then dry DMF (30 mL) was added. The mixture was degassed by bubbling with argon for 30 min before the addition of triflic acid (0.15 mL, 1.75 mmol), the reaction mixture was stirred at 140°C under argon atmosphere for around 3h. Subsequently, the inert atmosphere was replaced by pure oxygen, and the reaction mixture was heated after under reflux for 24h. Then, the mixture was quenched by addition with water and neutralized with 15% NaOH aqueous solution. The organic phase was extracted, washed again two times with water and brine, dried with $MgSO_4$ and concentrated. The crude product was purified by column chromatography (Al_2O_3, $CHCl_3$). Recrystallization from $CHCl_3$/petroleum ether gave after filtration 80 mg of compound **30** in 41% yield.

^{1}H NMR (500 MHz, $CDCl_3$): δ (ppm) = 9.60 (s, 1H), 9.57 (s, 1H), 9.02-8.93 (m, 4H), 8.55 (d, J= 7.3Hz, 1H), 8.49-8.47 (m, 1H), 8.15-7.98 (m, 7H), 7.89 (d, J= 7.8Hz, 2H), 7.63 (d, J=7.7 Hz, 1H), 7.56-7.53 (t, 1H), 7.47 (s, 1H), 7.41 (d, J=8.0 Hz, 2H), 5.25-5.19 (m, 2H), 2.94-2.88 (m, 2H), 2.76-2.69 (m, 4H), 2.06-1.94 (m, 7H), 1.87-1.80 (m, 3H), 1.51 (m, 4H), 1.48-1.41 (m, 2H), 1.33-1.24 (m, 12H).

HRMS (FAB+): calcd for $C_{77}H_{58}N_4O_6$: 1134.4351; found: 1134.4363.

Compound 31

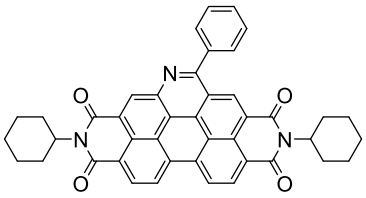

Orange Solid
$C_{43}H_{33}N_3O_4$
MW: 655.25

Compound **17** (0.2 g, 0.35 mmol), benzaldehyde (0.2 g, 2.1mmol) and activated molecular sieves (3Å) where placed in a Schlenk flask, then dry DMF (30 mL) was added. The mixture was degassed by bubbling with argon for 30 min before the addition of triflic acid (0.3 mL, 3.5 mmol), the reaction mixture was stirred at 130°C under argon atmosphere for around 3h. Subsequently, the inert atmosphere was replaced by pure oxygen, and the reaction mixture was heated after under reflux for 24h. Then, the mixture was quenched by addition with water and neutralized with 15% NaOH aqueous solution. The organic phase was extracted, washed again two times with water and brine, dried with $MgSO_4$ and concentrated. The crude product was purified by silica gel column chromatography (eluent: $CHCl_3$: MeOH 99:1). Recrystallization from $CHCl_3$/petroleum ether gave after filtration 79 mg of compound **31** in 34% yield.

^{1}H NMR (500 MHz, $CDCl_3$): δ (ppm) = 9.51 (s, 1H), 9.50 (s, 1H), 9.16-9.14 (m, 2H), 9.04 (d, J= 8.2 Hz, 1H), 8.99 (d, J= 8.1 Hz, 1H), 7.99-7.97 (m, 2H), 7.76-7.68 (m, 3H), 5.20-5.10 (m, 2H), 2.71-2.59 (m, 4H), 1.98-1.77 (m, 10H), 1.55-1.33 (m, 6H).

^{13}C NMR ($CDCl_3$,125 MHz) δ (ppm) = 167.5, 167.3, 167.3, 167.2, 164.8, 147.8, 141.7, 138.2, 137.5, 135.9, 135.9, 134.3, 134.2, 133.3, 132.7, 132.6, 132.6, 131.4, 129.8, 129.8, 127.5, 127.2, 127.1, 126.8, 126.3, 126.2, 126.0, 125.3, 121.9, 121.9, 58.0, 32.7, 32.7, 30.1, 29.0.

HRMS (FAB+): calcd for $C_{43}H_{33}N_3O_4$: 655.2466; found: 655.2464.

1-Pyrrolidinyl-*N,N'*-dicyclohexyl perylene-3,4:9,10-tetracarboxylic diimide[8,9] 32

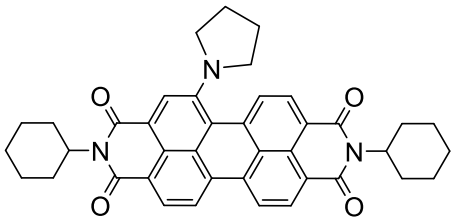

Green Solid
$C_{40}H_{37}N_3O_4$
MW: 623.28

In a 50 mL round bottom flask, compound **3** (0.1 g, 0.17 mmol) and pyrrolidine (7 mL) were added. The flask was then placed under controlled atmosphere by 3 vacuum / argon cycles while stirring. The reaction was allowed to proceed at room temperature for 72h. After, the solvent

was removed and the product was purified by silica gel column chromatography (eluent: $CHCl_3$: Et_3N 99:1) to give 21 mg of compound **32** in 20% yield.

^1H NMR (300 MHz, $CDCl_3$): δ (ppm) = 8.65-8.61 (m, 2H), 8.52-8.43 (m, 4H), 7.56 (d, *J* = 8.0 Hz, 1H), 5.13-5.00 (m, 2H), 3.78 (m, 2H), 2.79 (m, 2H), 2.66-2.51 (m, 4H), 2.12-1.98 (m, 4H), 1.94-1.75 (m, 10H), 1.50-1.37 (m, 6H).

(MALDI-TOF positive mode): *m*/*z*: $C_{40}H_{37}N_3O_4$: 623.7 $[M]^+$, calcd: 623.3.

1-Nitro-7-bromo-*N,N'*-dicyclohexylperylene-3,4:9,10-bis(dicarboximide) 33

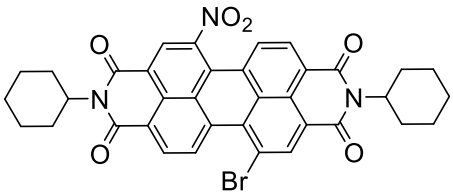

Dark red Solid
$C_{36}H_{28}BrN_3O_6$
MW: 677.12

In a Schlenk flask, compound **3** (0.1 g, 0.16 mmol) and concentrated H_2SO_4 (1 mL) were added. The reaction mixture was stirred at 60°C before the addition of NBS (30 mg, 0.2 mmol). After 20 min stirring, TLC analysis indicated the complete consumption of starting material. The mixture was then poured into ice to precipitate the solid. After filtration, the crude product was purified by silica gel column chromatography (eluent: $CHCl_3$: Hexane 7:3) to give 6 mg of compound **33** in 5% yield.

^1H NMR (300 MHz, $CDCl_3$,): δ (ppm) = 9.67 (dd, *J* = 8.2, 1.6 Hz, 1H), 8.92 (s, 1H), 8.79-8.71 (m, 2H), 8.58 (dd, *J* = 8.1, 1.4 Hz, 1H), 8.22-8.15 (m, 1H), 5.07-4.95 (m, 2H), 2.56-2.46 (m, 4H), 1.94-1.90 (m, 4H), 1.77-1.73 (m, 6H), 1.49-1.40 (m, 6H).

(MALDI-TOF negative mode): *m*/*z*: $C_{36}H_{28}BrN_3O_6$: 676.8 $[M]^-$, calcd: 677.1.

References:

[1] S. V. Dayneko, A. D. Hendsbee, G. C. Welch, *Small Methods* **2018**, *2*, 1800081.

[2] Y. Sun, J. H. Seo, C. J. Takacs, J. Seifter, A. J. Heeger, *Advanced Materials* **2011**, *23*, 1679–1683.

[3] Y.-S. Ma, C.-H. Wang, Y.-J. Zhao, Y. Yu, C.-X. Han, X.-J. Qiu, Z. Shi, *Supramolecular Chemistry* **2007**, *19*, 141–149.

[4] K.-Y. Chen, T.-C. Fang, M.-J. Chang, *Dyes and Pigments* **2012**, *92*, 517–523.

[5] R. El-Berjawi, P. Hudhomme, *Dyes and Pigments* **2018**, *159*, 551–556.

[6] K.-Y. Chen, T. J. Chow, *Tetrahedron Letters* **2010**, *51*, 5959–5963.

[7] P. Singh, K. Kumar, G. Bhargava, S. Kumar, *Journal of Materials Chemistry C* **2016**, *4*, 2488–2497.

[8] X. Kong, J. Gao, T. Ma, M. Wang, A. Zhang, Z. Shi, Y. Wei, *Dyes and Pigments* **2012**, *95*, 450–454.

[9] Y. Zhao, M. R. Wasielewski, *Tetrahedron Letters* **1999**, *40*, 7047–7050.

Crystallographic data

1-(3-Formyl)phenyl-*N,N'*-dicyclohexylperylene-3,4:9,10-bis(dicarboximide) 4

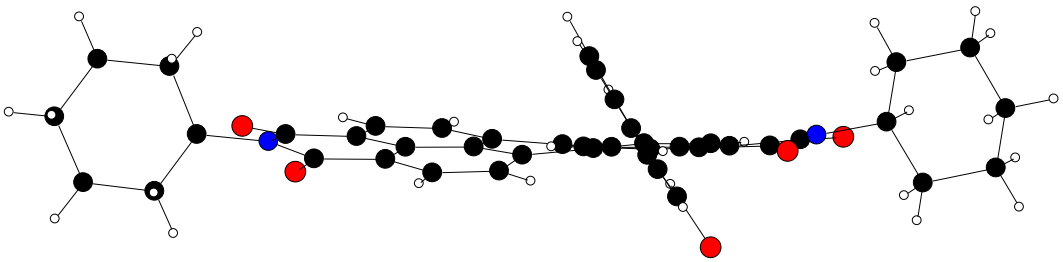

Empirical formula	$C_{43}H_{34}N_2O_5$
Formula weight	658.72
Temperature	150.0(1) K
Wavelength	1.54184 A
Crystal system, space group	Monoclinic, P 21/c
Unit cell dimensions	a = 13.2466(12) A alpha = 90 deg
	b = 16.6516(16) A beta = 96.209(8) deg.
	c = 14.3469(14) A gamma = 90 deg.
Volume	3146.0(5) A^3
Z, Calculated density	4, 1.391 Mg/m^3
Absorption coefficient	0.732 mm^-1
F(000)	1384
Crystal size	0.096 x 0.065 x 0.049 mm
Theta range for data collection	3.356 to 73.107 deg.
Limiting indices	-15<=h<=16, -19<=k<=19, -17<=l<=12
Reflections collected / unique	9537
Completeness to theta = 72.000	98.3 %
Absorption correction	Semi-empirical from equivalents
Max. and min. transmission	1.00000 and 0.91268
Refinement method	Full-matrix least-squares on F^2
Data / restraints / parameters	9537 / 0 / 452
Goodness-of-fit on F^2	0.807
Final R indices [I>2sigma(I)]	R1 = 0.0597, wR2 = 0.1437 [4345 Fo]
R indices (all data)	R1 = 0.1162, wR2 = 0.1614
Largest diff. peak and hole	0.427 and -0.300 e.A^-3

Compound 1,6-10

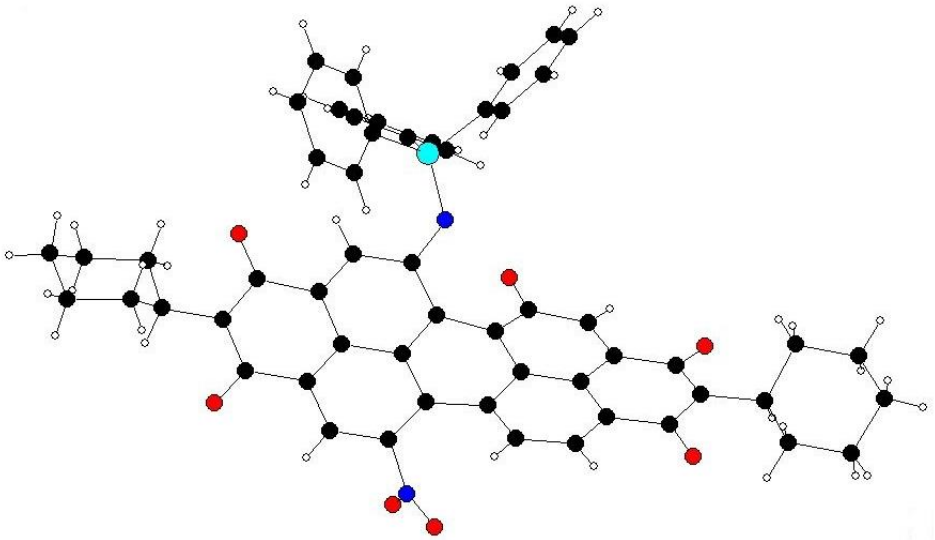

Empirical formula	$C_{54}H_{43}N_4O_7P$
Formula weight	890.9
Temperature	120.0(1) K
Wavelength	1.54184 A
Crystal system, space group	Triclinic, P -1
Unit cell dimensions	a = 15.4915(9) A alpha = 64.787(7) deg.
	b = 16.9656(11) A beta = 88.202(6) deg.
	c = 18.9059(15) A gamma = 73.271(6) deg.
Volume	4281.3(6) A^3
Z, Calculated density	2, 1.382 Mg/m^3
Absorption coefficient	1.082 mm^-1
F(000)	1864
Crystal size	0.3 x 0.072 x 0.036 mm
Theta range for data collection	2.598 to 73.154 deg.
Limiting indices	-19<=h<=17, -20<=k<=19, -21<=l<=23
Reflections collected / unique	27236 / 16275 [R(int) = 0.0421]
Completeness to theta = 72.000	98.6 %
Absorption correction	Semi-empirical from equivalents
Max. and min. transmission	1.0000 and 0.68187
Refinement method	Full-matrix least-squares on F^2
Data / restraints / parameters	16275 / 0 / 1191
Goodness-of-fit on F^2	1.043
Final R indices [I>2sigma(I)]	R1 = 0.0655, wR2 = 0.1698 [11658 Fo]
R indices (all data)	R1 = 0.0913, wR2 = 0.1924
Largest diff. peak and hole	0.604 and -0.566 e.A^-3

UNIVERSITE MATIERE BRETAGNE MOLECULES LOIRE ET MATERIAUX

université angers

Titre : Construction et caractérisation de nouveaux pérylènediimides basés sur des assemblages moléculaires dérivés des groupements nitro ou amino de composés substitués en position "bay".

Mots clés : pérylènediimide, synthèse organique, groupement nitro, groupement amino, photovoltaïque organique, accepteur d'électrons.

Résumé : Les dérivés de pérylènediimide (PDI) font partie des accepteurs d'électrons les plus performants. Leur squelette rigide lié à un système π aromatique étendu, des propriétés optiques et électroniques remarquables et une bonne stabilité chimique et thermique en font de bons candidats comme matériaux de type-n avec de nombreuses applications, en particulier dans le domaine du photovoltaïque organique. Ce travail étudie la réactivité de dérivés pérylènediimides en position « *bay* » pour la synthèse et la caractérisation de nouveaux systèmes accepteurs originaux dont certains seront utilisés comme matériaux dans des cellules solaires organiques. Dans la première partie de cette thèse, une procédure alternative à la réaction de couplage type Suzuki-Miyaura a été développée pour la synthèse de dérivés PDI à partir du composé possédant un groupement nitro en position « *bay* ». Une dyade associant le PDI au fullerène C_{60} a ensuite été étudiée. Dans une seconde partie, l'étude s'est portée sur la synthèse et la caractérisation de nouveaux dimères de PDI et leurs utilisations comme matériaux dans des cellules solaires organiques. Dans le dernier chapitre, des recherches ont été menées sur la réactivité d'un PDI possédant un groupement amino en position « bay », d'abord via la chimie des sels de diazonium, puis dans la synthèse d'azacoronènes pour former de nouvelles dyades à base de PDI. Ces nouveaux composés ont fait l'objet d'études préliminaires comme nouveaux matériaux accepteurs pour des applications en photovoltaïque.

Title : Construction and characterizations of new perylenediimide based molecular assemblies derived from nitro or amino bay-substituted derivatives

Keywords : Perylenediimides, organic synthesis, nitro group, amino group, organic photovoltaics, electron acceptor.

Abstract : Among the powerful organic electron acceptors are those based on perylenediimide derivatives. Their rigid planar backbone and extended π-conjugation with outstanding optical and electronic properties, chemical and thermal stabilities allowed them to be potentially useful as n-type materials in applications such as organic photovoltaic cells (OPVs). This dissertation describes the study of perylenediimide reactivity at the *bay* region for the synthesis and characterizations of new original acceptor systems. Some of them were applied in organic solar cells. In the first part of this thesis, an alternative procedure to conventional Suzuki-Miyaura coupling method was developed for the synthesis of PDI derivatives starting from mono-nitro PDI. From this was targeted the construction of PDI-C_{60} dyad. In the second part, synthesis and characterizations of PDI dimer and its application in organic solar cells are discussed. In the last part, investigations on the reactivity of mono-amino PDI are described via the chemistry of the diazonium salt or through the synthesis of PDI-based azacoronene dyads. Preliminary studies of some of these acceptors in organic solar cells are also presented.